VNIVERSITAT DE VALÈNCIA

Understanding the molecular causes of muscle atrophy in myotonic dystrophy type 1

Doctoral Program in Physiology

Doctoral Thesis

Nerea Moreno Cervera

September 2024

Directed by:

Prof. Dr. Rubén D. Artero Allepuz

Dr. Ariadna Bargiela Schönbrunn

Tutored by:

Prof. Dr. Francisco Dasí Fernández

Universidad de Valencia
Departamento de Genética

D**. Rubén D. Artero Allepuz,** Catedrático del Dpto. de Genética de la Universidad de Valencia.

Dña. **Ariadna Bargiela Schönbrunn**, Doctora en Biotecnología e Investigadora Postdoctoral en el Instituto de Investigación Sanitaria La Fe de Valencia.

CERTIFICAN:

Que la presente memoria, titulada "Understanding the molecular causes of muscle atrophy in myotonic dystrophy type 1", corresponde al trabajo realizado bajo su dirección por Dña. Nerea Moreno Cervera, para su presentación como Tesis Doctoral en el Programa de Doctorado en Fisiología de la Universidad de Valencia.

Y para que conste firman el presente certificado en Valencia, a 23 de septiembre de 2024.

RUBEN DARIO| ARTERO| ALLEPUZ

Digitally signed by RUBEN DARIO| ARTERO|ALLEPUZ
Date: 2024.09.24 09:05:16 +02'00'

Fdo. Dr. Rubén D. Artero Allepuz

BARGIELA SCHONBRUN N ARIADNA - 20902796M

Firmado digitalmente por BARGIELA SCHONBRUNN ARIADNA - 20902796M
Fecha: 2024.09.24 09:25:47 +02'00'

Fd. Dra. Ariadna Bargiela Schönbrunn

AGRADECIMIENTOS

En primer lugar, gracias a mis director@s de tesis por darme esta oportunidad. Aprender que significa la investigación me ha permitido crecer profesional y personalmente, llenándome de buenos recueros, algunos agridulces, pero sobre todo de momentos con mi gente. Gracias a todas las personas que me habéis acompañado en este camino.

Fany, aún recuerdo llegar mi primer día de prácticas, después de varias reuniones olvidadas, pensando "¿dónde me estoy metiendo?" y acabar encontrándote a ti. Gracias por haber sido mi mayor apoyo y mi mami científica desde el primer momento. Ese día, el papi científico Piotr también estaba ahí para acogerme y hacerlo más fácil, gracias Konickechy.

Gracias a María por ser mi hermana y compañera de equipo, por tus consejos y por nuestras fumadas que a veces acababan en buenas ideas. Águeda, gracias por animar las tardes en el laboratorio con tus locuras y tu intensidad, pero sobre todo por tu valentía. A Ire por ser una increíble compañera de camino y avisarme cuando había que hacer papeleo, al final nuestras cagadas son las mejores anécdotas. Naty, llegaste en un momento difícil pero tu cercanía y empatía hizo que conectáramos de inmediato.

A l@s más peques gracias por el aire fresco. A Andrea por su espontaneidad que hace que todo sea más divertido. A Alicia por ser un amor y llenarnos un poco de positivismo. A Anna por mostrarse tal y como es siempre. También a mis chicos de las juervezas Diego y Marc, gracias a todxs por estar ahí.

A todas las personas que han pasado o han llegado ahora al labo: Mouli, Anna, Angela, Raquel, Poyatos, Ana, Jorge … gracias por compartir parte de vuestro viaje conmigo.

También me gustaría agradecer al PAS, Jota, Mª Ángeles y Fede que hacen que el día a día en el departamento sea mucho más llevadero, y gracias a lxs compis de CBP por las risas en las cervezas y las fiestas de navidad.

Gracias a mis amig@s por hacer que tenga esta red de cuidados tan bonita. A mis Pájaras, por acompañarme en los inicios en la universidad. Gracias por todos los momentos compartidos, estoy muy orgullosa de cada una de vosotras. A mis Samuráis por ser uno de mis pilares fundamentales, en especial a la Resistencia, que ha vivido muy de cerca todos mis colapsos y han estado siempre dándome aliento y ánimo para continuar. A May por crecer a mi lado y no irte nunca.

Agradecer especialmente a Alicia N., que llegó en un momento muy turbulento para ayudarme a poner límites y aprender a entenderme. Sin ella esto no habría acabado igual.

A Víctor por ser un maravilloso compañero de vida e intentar ayudarme siempre, incluso cuando no puede. Gracias por ser mi recarga de batería.

Por último, gracias a toda mi familia, sin ellos no estaría hoy aquí. Pero quiero hacer especial mención a mi madre por su apoyo incondicional y por enseñarme a relativizar los problemas con una actitud siempre positiva. A mi padre por enseñarme el valor de la constancia, el trabajo duro y la superación. A mis hermanos, Noe y Dani, por ser mi refugio y mi mayor regalo. Y a mis abuelos, por ser las raíces y el comienzo de todo. Os quiero.

En general, gracias a todas las personas que se han tomado el tiempo para escucharme aunque no entendieran del todo lo que les estaba contando.

Equivocarse forma parte de avanzar.

RESUMEN

La distrofia miotónica tipo 1 (DM1), también conocida como distrofia miotónica de Steinert, es la distrofia muscular más común en adultos. Es considerada un trastorno genético raro y se estima que la prevalencia global es de 1 en 8000 individuos, aunque puede variar entre diferentes poblaciones debido a factores genéticos y ambientales. La causa genética subyacente consiste en la expansión anormal del triplete CTG en la región no traducida (3'-UTR) de los transcritos mutantes del gen *DM1 protein kinase* (*DMPK,* Entrez 1760), localizado en la región cromosómica 19q13.3. En un individuo sano, el número de repeticiones de este triplete puede oscilar entre 5 y 37 unidades, mientras que en el caso de personas afectadas por la DM1 este número sobrepasa las 50 repeticiones. En los casos más severos el número de copias puede llegar a miles, lo que está directamente relacionado con una aparición más temprana de la enfermedad y con síntomas más graves. Este fenómeno genético, en el que la gravedad de la enfermedad aumenta con cada generación debido al incremento en el número de repeticiones, se conoce como anticipación.

La DM1 se trata de una enfermedad multisistémica con una gran variabilidad en el espectro clínico que presentan los diferentes pacientes. Entre las principales manifestaciones que cursan con la DM1 se incluyen la afectación del sistema nervioso, respiratorio, ocular, endocrino, sexual, y digestivo, entre otros. No obstante, los síntomas más estudiados, por su contribución a la mortalidad y la morbilidad de los pacientes, son aquellos relacionados con el sistema muscular. En estos pacientes los síntomas se manifiestan como debilidad (miopatía), rigidez muscular (miotonía) y pérdida de masa muscular (atrofia). De entre las diversas manifestaciones, la degeneración y la atrofia muscular son las características más debilitantes, ya que provocan limitaciones severas en la movilidad de los pacientes afectando significativamente su capacidad para realizar actividades diarias, además de que puede llegar a comprometer la función respiratoria.

La patogénesis de la DM1 ha sido ampliamente estudiada y la hipótesis más aceptada para explicar cómo las expansiones de repeticiones de CUG provocan las manifestaciones clínicas observadas se basa en un mecanismo de ganancia de función tóxica. Los transcritos mutantes del gen *DMPK* que contienen estas expansiones forman estructuras secundarias en forma de horquillas caracterizadas por desapareamientos U - U en el ARN de doble cadena. Los transcritos anómalos se acumulan en el núcleo de las células afectadas, dando lugar a la formación de unas estructuras visibles al microscopio llamadas foci ribonucleares. Estos foci secuestran diversas proteínas de unión a ARN impidiendo que lleven a cabo sus funciones normales. Entre las proteínas secuestradas, la más importante es Muscleblind-like splicing regulator 1 (MBNL1), una proteína esencial para la regulación del *splicing* alternativo, un proceso fundamental en la maduración del ARN mensajero. En la DM1, MBNL1 queda secuestrado en los foci ribonucleares, lo que impide su función y provoca la inclusión anormal de exones alternativos en muchos de sus transcritos diana, lo que genera un patrón alterado de *splicing*. Este fenómeno, conocido como espliceopatía, es uno de los marcadores moleculares distintivos de la DM1, y fue en esta enfermedad donde se acuñó por primera vez este término.

Adicionalmente, los síntomas de la DM1 también están vinculados con una proteína que actúa regulando el *splicing* de forma antagónica con MBNL1: CUGBP Elav-like family member 1 (CELF1). Mientras que MBNL1 es secuestrada en los foci ribonucleares y no puede cumplir con su función, CELF1 está hiperactivada en los pacientes con DM1.Concretamente, el aumento de función de CELF1 se debe a su hiperfosforilación mediada por la proteína quinasa C (PKC), lo que estabiliza esta proteína dentro del núcleo celular y exacerba la disfunción en el *splicing* alternativo. Este desequilibrio entre ambas proteínas afecta gravemente el proceso de maduración del ARN y en lugar de producirse el cambio normal de un patrón de *splicing* fetal a uno adulto, las células de los pacientes con DM1 continúan expresando isoformas proteicas fetales en los tejidos adultos. Además, esta alteración en la expresión de isoformas fetales está directamente relacionada con

algunos de los síntomas más característicos de la enfermedad, como la miotonía, la atrofia muscular y otros efectos multisistémicos.

Sin embargo, a pesar de los avances en la comprensión del papel de MBNL1 y CELF1, ni sus defectos funcionales ni las alteraciones del *splicing* explican la totalidad de los síntomas de la DM1, como es el caso de la debilidad y la pérdida de masa muscular. En los últimos años diferentes estudios han puesto de manifiesto la excesiva actividad autofágica en DM1 y cómo esta ruta podría estar contribuyendo a la atrofia muscular de los pacientes. La autofagia y el sistema de ubiquitina-proteasoma (UPS) son procesos celulares esenciales para mantener la homeostasis muscular. La autofagia es un proceso celular crucial para la degradación y reciclaje de componentes celulares dañados o no funcionales, mientras que el sistema UPS es responsable de la degradación de proteínas. En condiciones normales, ambos sistemas están finalmente equilibrados y regulados por vías de señalización como la IGF1 /AKT/ mTOR, que promueven la síntesis de proteínas e inhiben su degradación. Sin embargo, en la DM1 se observa una sobreactivación patológica de estos procesos, cuyo desequilibrio y desregulación afectan negativamente a el crecimiento y la regeneración muscular. Por tanto, la modulación de la autofagia y del UPS constituye una posible estrategia terapéutica para mitigar la disfunción muscular y mejorar los fenotipos asociados con DM1.

Un descubrimiento clave en la regulación de la autofagia en la DM1 es el papel del microARN miR-7, que actúa como un represor de la autofagia. En particular, se ha confirmado que miR-7 está subexpresado en varios modelos celulares de la enfermedad y en biopsias de pacientes. Además, la biogénesis de este miRNA está regulada por un complejo formado por las proteínas Musashi RNA binding protein 2 (MSI2) y Hu antigen R (HuR), que forman un heterodímero que se une al pri-miR-7 para impedir su procesamiento a pre-miR-7. Posteriormente se descubrió que la causa de los bajos niveles de miR-7 es la sobreexpresión de la proteína MSI2. Estudios independientes reportaron que la variación de los niveles de HuR no conduce a un cambio de expresión de miR-7, ya que esta proteína estaría implicada

en lo que es el reconocimiento del sitio de unión al pri-miR-7. Además, estudios anteriores han demostrado que reducir la actividad autofágica mediante la modulación del eje MSI2>miR-7>autofagia rescata fenotipos típicos de la DM1 en modelos celulares. Esta modulación se llevó a cabo en distintos puntos del eje, utilizando tanto miméticos de miR-7 (agomiR-7) como la inhibición de MSI2 mediante nucleótidos antisentido (ASOs) o pequeñas moléculas, lo que, en conjunto, resultó en una disminución de MSI2 y un aumento significativo de la expresión de miR-7. Estos hallazgos sugieren que intervenir en esta vía reguladora podría tener el potencial de revertir la degeneración muscular *in vivo*.

Teniendo en cuenta estos antecedentes se plantearon los objetivos de esta tesis doctoral, que se centran en profundizar y entender mejor el funcionamiento del eje MSI2 >miR-7 > autofagia y cómo su modulación puede influir en la atrofia muscular observada en la DM1. Para ello, la tesis se encuentra estructurada en tres capítulos, cada uno de los cuales aborda un aspecto específico relacionado con este eje. A lo largo de los capítulos, se desentrañan los mecanismos moleculares subyacentes a la desregulación del MSI2 >miR-7>autofagia y se exploran posibles estrategias terapéuticas para mitigar los fenotipos musculares asociados con la DM1.

CAPÍTULO 1: MSI2 AUMENTA LA DISFUNCIÓN MUSCULAR EN UN MODELO DE RATÓN CON DISTROFIA MIOTÓNICA TIPO 1.

En el primer capítulo de esta tesis se aborda en profundidad el papel de la proteína MSI2 en la regulación de la autofagia y su implicación en la patogénesis de la DM1 empleando el modelo murino conocido como HSA^{LR}. Además, los resultados mostrados en este capítulo se detallan en el artículo “Msi2 enhances muscle dysfunction in a myotonic dystrophy type 1 mouse model”, publicado en octubre de 2023 en la revista Biomedical Journal y del que soy coautora.

El ratón HSA^{LR} es uno de los modelos ampliamente reconocidos en la investigación relacionada con la DM1 debido a su capacidad para replicar algunas de las características moleculares de la enfermedad, tales como la presencia de foci

ribonucleares, el secuestro de MBNL1 o las alteraciones en el *splicing* alternativo de transcritos musculares. A pesar de ello, este modelo no reproduce el característico fenotipo atrófico que se observa en los pacientes. Durante el desarrollo de nuestro estudio identificamos en primer lugar la ausencia de la activación excesiva de la vía autofágica que ocurre en DM1. A su vez, tampoco detectamos una reducción significativa en los niveles de miR-7 ni una sobreexpresión de la proteína Msi2 en estos ratones. En consecuencia, propusimos la hipótesis de que la sobreexpresión de MSI2, proteína que ejerce un efecto inhibidor sobre miR-7, podría ser un factor determinante para que el modelo murino HSA^{LR} reproduzca el fenotipo atrófico *in vivo*.

Para evaluar esta hipótesis, diseñamos un experimento en el que se inyectaron ratones neonatos P2 - P3 con virus adenoasociados recombinantes (AAV) que nos permitían sobreexpresar MSI2 bajo el control del promotor de la Desmina humana (hDES). El promotor hDES se seleccionó por su especificidad para dirigir la expresión del gen de interés al musculo, lo que nos permitió focalizar la sobreexpresión de MSI2 en el tejido muscular. Como grupo control utilizamos ratones neonatos inyectados paralelamente, pero con adenoasociados que expresaban el promotor hDES sin el transgén MSI2, de forma que pudiéramos comparar los efectos específicos de la sobreexpresión de MSI2. Tras un periodo de 21 días de desarrollo postnatal, los ratones fueron destetados y a los 41 días de edad se sacrificaron para recolectar los tejidos de interés. Posteriormente, se realizaron diferentes análisis moleculares e histológicos para evaluar los cambios producidos a nivel celular y tisular. Durante este período también se llevó a cabo un estudio funcional en el cual se midió la fuerza de las extremidades anteriores.

Los resultados obtenidos mostraron de forma concluyente que la sobreexpresión de MSI2 induce un aumento del flujo autofágico, lo que quedó evidenciado por una mayor expresión de proteínas implicadas en la regulación de la autofagia como LC3, p62 y ATG7. Este incremento autofágico se tradujo además en un empeoramiento de los fenotipos histopatológicos, como una mayor aparición de núcleos centrales

y una disminución del área de las fibras musculares, lo que era indicativo de daño muscular. Además, los ratones con sobreexpresión de MSI2 presentaron una disminución de la fuerza en las patas delanteras, que fue notablemente inferior a la observada en los ratones control inyectados con el AAV sin MSI2. Estos datos demuestran que la sobreexpresión de MSI2 no solo incrementa la actividad autofágica, sino que también agrava los defectos musculares reproduciendo de manera más precisa las alteraciones musculares de la DM1.

Por otra parte, los análisis mediante western blots revelaron que estos cambios no dependían de alteraciones en los niveles de las proteínas Mbnl1, Mbnl2 y Celf1, que permanecieron sin cambios significativos tras la sobreexpresión de MSI2. Estos hallazgos fueron particularmente reveladores, ya que demuestran que la disfunción muscular provocada por la sobreexpresión de MSI2 ocurre de manera independiente de los mecanismos de patogénesis regulados por estos tres factores clave para la DM1.

Por lo tanto, los datos moleculares, histológicos y funcionales obtenidos en el modelo HSA^{LR} con la sobreexpresión nos llevan a concluir que MSI2 desempeña un papel fundamental en la atrofia y la disfunción muscular asociada a la DM1. La sobreexpresión de esta proteína en el modelo murino HSA^{LR} reproduce varios de los rasgos patológicos, lo que implica que MSI2 podría ser un objetivo terapéutico relevante para mitigar los efectos musculares de la DM1. Además, estos resultados subrayan la importancia de la autofagia como un mecanismo clave en la progresión de la enfermedad, abriendo nuevas vías para el desarrollo de estrategias terapéuticas dirigidas a modular esta vía celular.

CAPÍTULO 2: EL SECUESTRO DE MIR-107 POR LAS REPETICIONES CUG ACTIVA EL EJE PATOGÉNICO MSI2/MIR-7 EN LA DISTROFIA MIOTÓNICA.

El segundo capítulo de esta tesis se centra en investigar las bases moleculares que explican la sobreexpresión de MSI2 en el contexto de la DM1 enfocándose en el papel clave de miR-107. Los resultados presentados en este capítulo están siendo

revisados para su publicación en un artículo del que soy coautora ("miR-107 sequestration by cug repeats triggers the msi2/mir-7 pathogenesis axis in myotonic dystrophy") para la revista Molecular Therapy Nucleic Acids.

MiR-107 es un microRNA que ha sido identificado como un represor de la expresión de MSI2. Asimismo, este miRNA pertenece a la familia miR-15/miR-107, la cual está altamente conservada entre especies y que está caracteriza por contener una región semilla (AGCAGCA) que presenta complementariedad con las repeticiones CUG. Las predicciones bioinformáticas sugieren que esa complementariedad podría implicar la unión de miR-107 a las expansiones de *DMPK,* así como la potencial regulación de *DMPK* por este miRNA. Por lo tanto, la hipótesis planteada en este capítulo es que la sobreexpresión de MSI2 podría deberse al secuestro de miR-107 en las repeticiones de los transcritos mutantes de *DMPK*. De esta forma, la función de miR-107 quedaría inhibida, lo que conduciría a la desrepresión de MSI2 y del resto de sus dianas.

Con el propósito de confirmar esta hipótesis, en primer lugar, analizamos bioinformáticamente la expresión de las dianas validadas de miR-107 en dos bases de datos en diferentes muestras de DM1. En general, se observó que muchas de estas dianas presentaban una regulación al alza, lo que nos indicaba una pérdida en la función de miR-107. Esta observación apoyaba la idea de que miR-107 no estaba ejerciendo su función reguladora debido al posible secuestro por las expansiones CUG. Además, el análisis de los niveles de expresión de miR-107 en muestras de DM1 reveló una reducción significativa en mioblastos inmortalizados derivados de pacientes diferenciados durante 7 días, así como una tendencia a su disminución en biopsias musculares, en comparación con controles sanos. A su vez también observamos un cambio en la localización subcelular de miR-107, con un aumento significativo de la fracción nuclear del miRNA en comparación con la fracción citoplasmática, lo que provocaría la falta de función de miR-107 en este compartimento y apoyaría la idea de que miR-107 se encuentra secuestrado en el núcleo al unirse a los transcritos de *DMPK*.

Para investigar más a fondo la hipótesis del secuestro de mir-107 utilizamos diversos enfoques experimentales que nos permitieron estudiar la interacción entre miR-107 y las expansiones CUG. Los resultados de los ensayos *in vitro*, que incluyen el EMSA (*Electrophoretic Mobility Shift Assay*) y el DSF (*differential scanning fluorimetry),* demostraron que miR-107 se une de forma complementaria y directa a las secuencias CUG. Por otra parte, los ensayos de luciferasa se llevaron a cabo cotransfectando durante 72 y 96 horas en células HEK plásmidos conteniendo las expansiones CUG y la luciferasa con y sin el mimético de miR-107 (agomir-107). El análisis de los datos obtenidos reveló que además de la unión, miR-107 actuaba regulando la expresión de *DMPK*. En consecuencia de la unión directa de miR-107 a las repeticiones, nos planteamos que podía existir una potencial competencia del miRNA con MBNL1 por los sitios de unión en las expansiones CUG de los transcritos mutantes. Esto se hace evidente al estudiar el efecto de tratar células DM1 con el agomiR-107, ya que se produjo una reducción de los foci ribonucleares y una menor colocalización de estos con MBNL1 comparado con las células sin tratar.

Finalmente, también estudiamos la modulación del eje MSI2>miR-7>autofagia mediante la adicción del mimético de miR-107 en dos modelos celulares de DM1 para ver su efecto en los fenotipos típicamente relacionados con la DM1. Los resultados evidenciaron que la regulación de este eje con el tratamiento con agomir-107 recupera los niveles alterados de MSI2 y miR-7. Por consiguiente, el flujo autofágico se vio disminuido, en este caso medido a través de la cuantificación de las proteínas ATG4, ATG7 y p62 así como mediante la tinción LysoTracker. Además, se observó una mejora en el índice de fusión y el diámetro de las células diferenciadas, que fue cuantificado utilizando tinciones de Desmina, un marcador específico de la diferenciación muscular.

En definitiva, los experimentos realizados confirmaron el secuestro de miR-107 en las expansiones CUG de los transcritos de *DMPK* y pusieron de manifiesto el mecanismo que explica la sobreexpresión de MSI2 y su efecto en la activación patológica del eje MSI2>miR-7>autofagia en la DM1.

CAPÍTULO 3: EL POTENCIAL TERAPÉUTICO DE LA SUPLEMENTACIÓN DE ÁCIDO OLÉICO EN MODELOS CELULARES MUSCULARES DE DISTROFIA MIOTÓNICA.

Por último, el tercer capítulo de la tesis aborda la modulación del eje MSI2>miR-7>autofagia mediante el uso de ácido oleico (OA). Los resultados que se detallan en este capítulo han sido ya publicados en el artículo titulado "Therapeutic Potential of Oleic Acid Supplementation in Myotonic Dystrophy Muscle Cell Models", en la revista *Biological Research* en mayo de 2024, y del cual soy primera autora.

El OA es un ácido graso monoinsaturado (18:1 cis - 9) que ha sido identificado como un regulador alostérico de la actividad de la proteína MSI2. Concretamente, el OA tiene la capacidad de modular la biogénesis de miR-7 al unirse a MSI2 y evitar la formación del complejo MSI2 - HuR - pri-mir-7, de forma que se impide su maduración a pre-miR-7.

Inicialmente en este capítulo evaluamos los niveles endógenos de este ácido graso y estudiamos su potencial terapéutico en modelos *in vitro*. En primer lugar, los estudios realizados demostraron que hay una reducción de los niveles de OA en diferentes modelos celulares de DM1 diferenciados durante 7 días (fibroblastos inmortalizados transdiferenciados, mioblastos inmortalizados y dos líneas de fibroblastos primarios transdiferenciados), una deficiencia que además estaría contribuyendo a la desregulación del eje MSI2 >miR-7 >autofagia.

Los experimentos en modelos celulares de la enfermedad demostraron que tras la suplementación con OA durante 24 horas se consiguieron revertir algunos de los fenotipos relacionados con la enfermedad. Los resultados derivados del tratamiento con OA en los dos modelos *in vitro* utilizados dieron lugar a un aumento en la expresión de miR-7 y de sus dianas, pero sin alterar la expresión de MSI2. Es decir, el OA actúa aguas debajo de MIS2 y su suplementación no reduce la sobreexpresión de MSI2 que ocurre en la DM1. No obstante, al conseguir aumentar la actividad de miR-7, se observó una reducción de la actividad autofágica, cuantificada en este caso a través de la tinción con Lysotracker y la detección por

inmunofluorescencia de la proteína LC3-II, un marcador clave en la formación de autofagosomas. La inhibición de la autofagia tras el tratamiento con OA fue también confirmada con la detección de las proteínas LC3, ATG4 y P62 mediante western blots. Por otra parte, la suplementación con OA en los cuatro modelos celulares de la enfermedad diferenciados durante 7 días produjo un incremento en el índice de fusión y el diámetro, lo sugiere que el OA facilita la recuperación de la capacidad celular para diferenciarse y organizarse en estructuras musculares funcionales en comparación con las células DM1 no tratadas.

Con el objetivo de comprobar la especificidad del mecanismo de acción del OA en la inhibición del complejo MSI2 - HuR - pri-mir-7, comparamos los resultados obtenidos del tratamiento con OA con su isómero trans, el ácido elaídico (EA). A diferencia de lo que ocurría con el OA, el EA no produjo ningún efecto en los modelos de DM1 ya que no actúa como un regulador alostérico de MSI2. En este caso, los niveles de miR-7 se mantuvieron invariables, así como sus dianas y otras proteínas relacionadas con la autofagia. Además, el EA también fue incapaz de mejorar la diferenciación de las células tratadas. Estos datos refuerzan la idea de que los resultados observados con el tratamiento de OA dependen de su capacidad para modular la actividad de MSI2 en la biogénesis de miR-7 de forma específica.

Por último, en este capítulo también intentamos profundizar en los mecanismos bioquímicos que explican la reducción de los niveles de OA en las células de DM1. En concreto, pudimos identificar una deficiencia en la enzima estearoil-CoA desaturasa (SCD1), responsable de convertir el ácido esteárico en ácido oleico, en las muestras de DM1. Además, los niveles de proteína SCD1 se correlacionaban de forma positiva ($r = 0.74$, $p = 0.03$) con la cantidad de ácido oleico presente en las muestras. No obstante, con el fin de corroborar la implicación de SCD1 en la deficiencia de OA decidimos tratar las células DM1 con un agonista del receptor LXR, que se encarga de regular positivamente la expresión de SCD1. Los resultados demostraron que la activación de esta vía es capaz de aumentar los niveles de OA en las células DM1. Esto sugiere que la desregulación de SCD1 contribuye de

manera significativa a la reducción de la síntesis de ácido oleico en el contexto de la enfermedad, lo que explicaría los bajos niveles observados en las muestras de DM1.

En conjunto el análisis de los datos de este capítulo revela el potencial terapéutico del OA en el contexto de la DM1, actuando en la regulación de la biogénesis de miR-7 y la autofagia a través de MSI2. Además, se destaca la especificidad de unión del OA a MSI2 diferenciándolo del EA, un ácido graso de misma composición, pero diferente estructura. A lo largo del estudio, también se identifica una posible nueva diana terapéutica, la enzima SCD1, cuya activación mejora la deficiencia de OA en los modelos celulares. Por otra parte, los bajos niveles de SCD1 también podrían estar relacionados con la desregulación de otras vías metabólicas debido a su papel central en la conversión de ácidos grasos saturados en insaturados, un proceso esencial para mantener la fluidez de las membranas celulares y regular múltiples procesos metabólicos. Todo esto subraya la importancia de continuar investigando la función de SCD1 en el contexto de la DM1, ya que su modulación podría abrir nuevas oportunidades terapéuticas relacionadas con la parte metabólica de la enfermedad.

En conclusión, los resultados obtenidos en esta tesis permiten extraer diversas conclusiones que contribuyen a una mejor comprensión de los mecanismos responsables de la atrofia muscular en la DM1. En primer lugar, uno de los hallazgos más relevantes es el papel central de la proteína MSI2, que ha demostrado ser una reguladora clave tanto de la autofagia como de la atrofia muscular en modelos experimentales de DM1. En particular, hemos determinado que la sobreexpresión de MSI2 está directamente relacionada con el secuestro del microRNA miR-107 por las expansiones CUG en los transcritos mutantes de *DMPK*. Esta retención nuclear de miR-107 altera su distribución celular normal, interfiriendo con su capacidad para regular la expresión de genes diana de manera post-transcripcional en el

citoplasma. Así, hemos conseguido definir un eje regulador más amplio que involucra a miR-107, MSI2 y miR-7, el cual contribuye a explicar los mecanismos moleculares subyacentes a la atrofia muscular observada en la DM1, y que ofrece nuevos puntos de intervención terapéutica. Además, hemos podido concluir que el eje miR-107>MSI2>miR-7>autofagia actúa de forma independiente a las proteínas MBNL1 y CELF1. Esto sugiere que existen mecanismos paralelos que estarían contribuyendo a la patogénesis de la DM1, subrayando una vez más la complejidad de esta enfermedad.

Por otro lado, este estudio ha identificado por primera vez un deterioro en el metabolismo del ácido oleico en los modelos celulares de DM1, originado al menos parcialmente por una disminución en la enzima SCD1. Este déficit metabólico se presenta como un factor adicional que contribuye a la patogénesis de la enfermedad, ya que la reducción en los niveles de ácido oleico actúa de manera sinérgica con la sobreexpresión de MSI2, exacerbando la alteración del eje MSI2>miR-7>autofagia. Este hallazgo refuerza la idea de que los desequilibrios metabólicos podrían ser una pieza clave en la comprensión de la DM1 y sugiere que el metabolismo lipídico podría representar una nueva diana terapéutica para esta patología.

En conjunto, los hallazgos de la tesis doctoral proporcionan una comprensión más detallada de los mecanismos moleculares subyacentes a la patogénesis de la DM1 y abren nuevas vías de investigación para el desarrollo de estrategias terapéuticas innovadoras dirigidas a regular procesos clave como la autofagia y el metabolismo de los ácidos grasos.

INDEX

INTRODUCTION

1. MYOTONIC DYSTROPHY TYPE 1: CLINICAL PRESENTATION

Myotonic dystrophy type 1 (DM1), also known as Steinert's disease (DM1; OMIM #160900), is an autosomal dominant neuromuscular disorder described for the first time in 1909 (Steinert et al., 1909).

DM1 represents a rare yet clinically significant neuromuscular disorder characterized by variable clinical expressivity and penetrance. Despite its rarity, DM1 stands as the most predominant form of muscular dystrophy affecting adults. Prevalence estimates 1 in 2,100 people carrying the mutation to 1 in 8,000 individuals manifesting the disease (Ashizawa et al., 2018; Johnson et al., 2021). However, the reported prevalence exhibits notable variability attributed to subclinical presentations and demographic disparities among study cohorts. On a global scale, prevalence rates exhibit a nuanced landscape, averaging approximately 9.3 cases per 100,000 individuals (Liao et al., 2022), as derived from a comprehensive meta-analysis. Interestingly, a comparison of pooled estimated prevalence for DM1 between different continents indicated that DM1 was more prevalent in Europe than in other continents. Specifically, the overall prevalence of DM1 per 100.000 was estimated as 12.25 cases (95% CI: 7.50-18.06) in Europe and 3.61 cases (95% CI: 0.58-9.09) in other continents (Asia and Oceania) (Liao et al., 2022). This disparity underscores the regional variability in DM1 prevalence and highlights the need for further investigation into underlying factors contributing to geographical differences in disease burden.

1.1. Genetic basis of DM1 pathogenesis.

The seminal breakthrough in DM1 research came in 1992 when Brook et al. (Brook et al., 1992) identified the genetic mutation responsible for the disorder, a CTG trinucleotide repeat expansion in the 3' untranslated region of the *DM protein kinase* (*DMPK)* gene on chromosome 19q13.3. This discovery revolutionized the understanding of DM1 by providing a molecular framework for its pathogenesis,

which later gave rise to RNA-mediated toxicity mechanisms that contribute to the development of this disease.

While unaffected individuals typically harbor between 5 and 35 CTG repeats in the *DMPK* gene, DM1 patients exhibit an expanded number of repeats, often surpassing 50 and, in severe cases, reaching into the thousands (Ashizawa & Sarkar, 2011; Pavićević et al., 2013). This pathological expansion tends to increase in successive generations due to germinal instability and is the underlying cause of the clinical phenomenon known as genetic anticipation. Thus, individuals with a higher number of repeats tend to experience earlier onset and more severe symptoms (Harley et al., 1992). Despite established genotype-phenotype correlations, significant variability exists even among individuals with similar repeat lengths, suggesting other modifying factors play a role in disease manifestation. Environmental factors, epigenetic modifications, and additional genetic elements may influence the clinical variability observed in DM1 (Visconti et al., 2023). Importantly, somatic or mitotic instability of the CTG repeats has been shown to contribute to the phenotypic variability in DM1 (Martorell et al., 2004; Meola & Cardani, 2015). Somatic instability is reflected by high levels of somatic mosaicism, with heterogeneity in the number of repeats between and within tissues of the same individual, which tends to increase over the lifetime of the affected person (Higham et al., 2012; Morales et al., 2012). Additionally, the expanded CTG repeats in DM1 are sometimes interrupted by other sequences, and these interruptions have been found to modify disease presentation (Santoro et al., 2017). Together, these factors help explain the significant clinical variability observed in DM1 patients, even among those with similar repeat lengths.

1.2. Clinical manifestations and histopathological aspects.

DM1 is a highly variable multisystem disorder, with clinical manifestations largely influenced by the number of CTG repeats in the *DMPK* gene. The disease is categorized into five subtypes based on age of onset:

Congenital DM1: this subtype represents the most severe form, typically presenting at birth at least 1,000 repeats. Newborns exhibit significant hypotonia, respiratory distress, and feeding difficulties. Facial diplegia and arthrogryposis are common in these infants, who, in addition, often suffer from profound and persistent cognitive impairment. The neonatal period is particularly critical, with a 30% rate of mortality due to respiratory complications (Echenne & Bassez, 2013).

Infantile DM1: Symptoms manifest before the age of 10, primarily impacting psychomotor development. Affected children may display learning disabilities and behavioural issues, along with mild myopathic features. These early signs often lead to delayed milestones and require early intervention and support (Antonio et al., 2016).

Juvenile DM1: Onset occurs between 10 and 18 years of age, with common features including myotonia, muscle weakness, and significant cognitive and behavioural difficulties. School performance is often adversely affected, and social interaction challenges are frequent, needing tailored educational and psychological support (Antonio et al., 2016).

Adult DM1: This is the most prevalent and studied form of DM1, typically manifesting between the ages of 20 and 40. Patients present a wide range of symptoms, mostly muscular, like myotonia, muscle weakness, and atrophy. Other symptoms can include cataracts, cardiac arrhythmias, and endocrine abnormalities like insulin resistance. The onset of symptoms in adulthood often leads to progressive physical disability and a reduced life expectancy, mainly due to respiratory and cardiac complications (Antonio et al., 2016).

Late-onset DM1: Symptoms appear after the age of 50 and are generally mild. Patients could experience cataracts and mild myotonia, with muscle weakness and other systemic features being less pronounced compared to earlier-onset forms (Antonio et al., 2016).

Despite the prevalence of muscle symptoms, DM1 is a multisystemic disorder with a wide spectrum of clinical manifestations (Fig. I-1). The muscular symptoms of DM1 primarily manifest as progressive muscle weakness, myotonia, and muscle stiffness, predominantly affecting distal muscles such as those in the hands and feet (Meola, 2013; Thornton, 2014). This leads to challenges in fine motor tasks and foot drop, impacting daily activities. The myotonia, characterized by delayed muscle relaxation after contraction, significantly affects the quality of life of individuals with DM1. Furthermore, respiratory muscle involvement can result in respiratory failure (Rossi et al., 2019). However, DM1 affects various organs beyond the neuromuscular system.

Cardiovascular complications are a significant concern in DM1, with cardiac arrhythmias being common. Patients with DM1 are at an increased risk of conduction defects and sudden cardiac death, often necessitating regular cardiac monitoring and interventions to manage these risks (Bhakta et al., 2004; Lau et al., 2015).

Respiratory dysfunction is the leading cause of mortality in DM1, particularly in the congenital form (Mathieu et al., 1999). The multifactorial etiology of respiratory dysfunction includes peripheral respiratory muscle atrophy, central respiratory drive impairment, upper airway muscle dysfunction leading to obstructive sleep apnea, and increased susceptibility to pulmonary infections (Poussel et al., 2015; Sansone et al., 2015). Mortality rates from respiratory failure, especially in congenital DM1, range between 51% and 76% (Rossi et al., 2019).

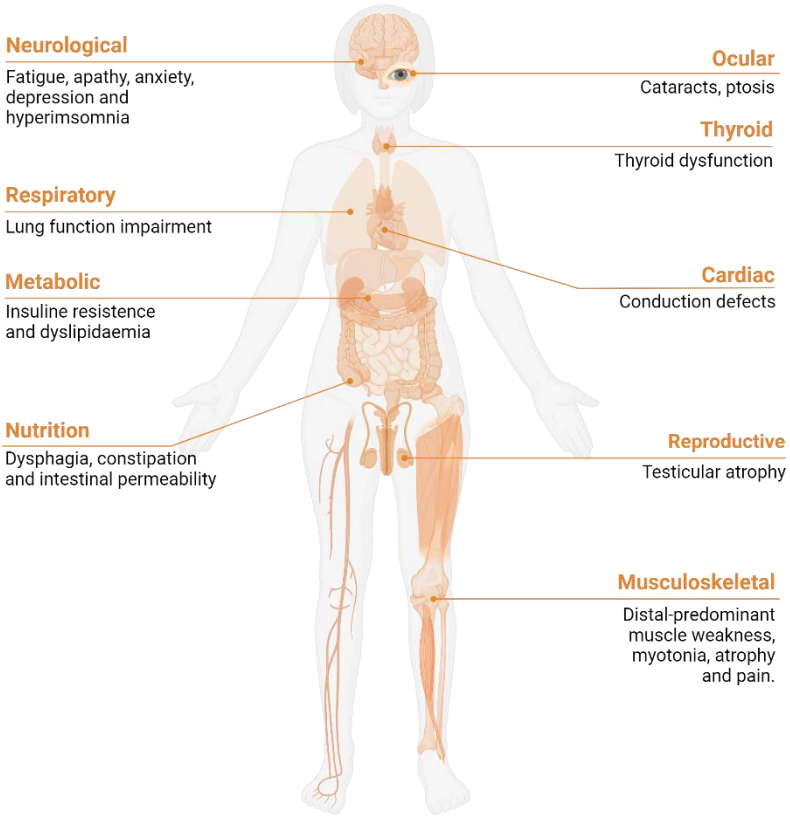

Fig. I-1. DM1 clinical manifestations. Beyond muscle involvement, DM1 presents with a diverse range of clinical manifestations affecting neurological, ocular, thyroid, cardiac, respiratory, metabolic, reproductive, nutritional, and musculoskeletal systems. These widespread symptoms underscore the complexity of DM1 and its impact on multiple organs and tissues. Figure created with BioRender.com.

Other characteristics include endocrine abnormalities (Vujnic et al., 2015) and neurological manifestations, including cognitive impairment, depression, anxiety, and excessive daytime sleepiness (Meola, 2014). In adulthood, ocular manifestations commonly include cataracts that require surgical intervention. Other ocular issues like ptosis and external ophthalmoplegia can also impact visual function (García-Cruz et al., 2023; Ikeda et al., 2016). Constipation is the most

prevalent digestive symptom and may require dietary adjustments, but severe cases may need enteral feeding support because of dysphagia, altered intestinal permeability, and other motility problems, contributing to nutritional deficiencies and affecting quality of life (Perna et al., 2020).

Histopathologically, DM1 is characterized by several distinct features in muscle biopsies, including the presence of central nuclei, increased fibrosis, and atrophy of type 1 muscle fibers. These fibers, also known as slow-twitch oxidative fibers, are characterized by their ability to contract slowly and maintain contraction for an extended period. Muscle tissue often exhibits ring fibers and nuclear inclusions, indicating regenerative attempts within the muscle. Additionally, there is a notable increase in connective tissue and fat replacement within the muscles, along with variability in muscle fiber diameter and irregular shapes of myonuclei from the earliest stages of the disease (Garibaldi et al., 2022; Viegas et al., 2022; Vihola et al., 2003). As the disease progresses, other histopathological features become more prominent, including the presence of nuclear pyknotic clumps, fiber breakage, vacuoles within the fibers, sarcoplasmic masses, and disorganization of Z bands and sarcomere structures (Meola & Cardani, 2015; Pisani et al., 2008; Thomas et al., 2018; Thornton, 2014; Vihola et al., 2003).

2. SKELETAL MUSCLE FORMATION AND COMPOSITION

The skeletal muscle is a highly specialized tissue that comprises approximately 40% of the total body mass in humans, making it one of the largest systems in the body. It is essential for motion, posture maintenance, and metabolic regulation (Frontera & Ochala, 2015).

Skeletal muscle's primary function is to generate force and produce movement through contraction facilitated by its unique structure and composition. Muscle contraction is driven by the interaction of actin and myosin filaments within the myofibrils, orchestrated by the sliding filament theory. Low-level contraction, known as muscle tone, also plays a crucial role in maintaining posture and stabilizing joints

(Huxley, 1975; Mitsui & Ohshima, 2012). However, beyond movement, skeletal muscles are involved in thermogenesis, aiding in the maintenance of body temperature through shivering thermogenesis and acting as a metabolic reservoir influencing systemic metabolism and energy homeostasis (Frontera & Ochala, 2015).

2.1. Morphology and principal components.

Vertebrate skeletal muscle is composed of muscle fibers, connective tissue, blood vessels, and nerves. Each muscle fiber is a multinucleated cell formed by the fusion of myoblasts during development and muscle homeostasis. The muscle fibers are bundled into fascicles, which are encased in connective tissue layers (Fig. I-2). The endomysium surrounds individual fibers, the perimysium encases fascicles, and the epimysium covers the entire muscle (Frontera & Ochala, 2015; Mukund & Subramaniam, 2020). This hierarchical organization supports both the structural integrity and functional capacity of muscles.

The contractile units of muscle fibers are the sarcomeres, which contain the thick and thin filaments of myosin and actin, respectively. The alignment of these filaments creates the characteristic striated appearance of skeletal muscle. Sarcomeres are delineated by Z-discs, which anchor the actin filaments and provide structural support (Frontera & Ochala, 2015; Mukund & Subramaniam, 2020). The sarcoplasmic reticulum and transverse tubules facilitate the rapid transmission of action potentials and calcium release, essential for coordinated muscle contraction (Hubbard, 1973).

Muscle contraction is regulated by the nervous system through motoneurons that release acetylcholine at the neuromuscular junction, triggering an action potential in the muscle fiber (Anglister et al., 1985). This action potential propagates along the sarcolemma and T-tubules, releasing calcium from the sarcoplasmic reticulum and subsequent muscle contraction (Hubbard, 1973).

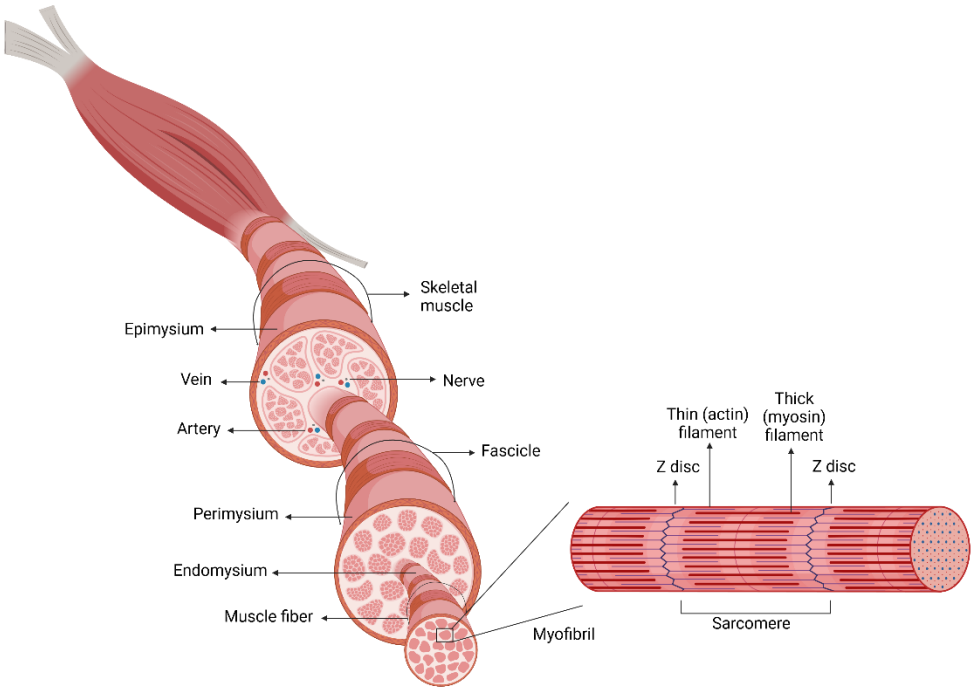

Fig. I-2. Skeletal muscle macrostructure. Skeletal muscle is structured into three distinct concentric layers, each defined by a specific connective tissue sheath. The outermost layer, known as the epimysium, encases the entire muscle. Within the muscle, bundles of muscle cells, referred to as fascicles, are wrapped in another connective tissue layer called the perimysium. Each individual muscle fiber is further enclosed by the endomysium. These connective tissue layers integrate to maintain the muscle's integrity and form tendons that connect muscles to bones. The muscle structure also includes myofibrils, which are organized into sarcomeres. The sarcomeres contain Z discs, thin filaments (actin), and thick filaments (myosin). Additionally, veins, arteries, and nerves are present to support muscle function. Figure created with BioRender.com.

2.2. Normal myogenesis and muscle differentiation.

Myogenesis is the process by which skeletal muscle is formed and involves a complex interplay of molecular signals to guide the proliferation, differentiation, and maturation of muscle progenitor cells. This intricate process is regulated by a

network of transcription factors, signalling pathways, and epigenetic modifications that ensure the proper formation and maintenance of muscle tissue.

Embryonic myogenesis begins with the formation of somites from the paraxial mesoderm, which then differentiate into the dermomyotome and sclerotome. Muscle progenitor cells arise from the dermomyotome and express *Pax3* and *Pax7*, crucial transcription factors for early myogenic specification (Bareja et al., 2014). These cells then upregulate *Myf5* and *MyoD*, essential myogenic regulatory factors (MRFs) that drive the commitment to the muscle lineage (Koike et al., 2022; Lima & Relaix, 2021).

Adult muscle regeneration is mediated by satellite cells, which are quiescent muscle stem cells located beneath the basal lamina of muscle fibers. Upon muscle injury, these cells activate, proliferate, and differentiate into myoblasts that fuse to form new myofibers or repair damaged ones (Careccia et al., 2023). This process recapitulates many aspects of embryonic myogenesis but involves additional regulatory mechanisms to adapt to the adult muscle environment. The myogenic differentiation program is governed by a hierarchical gene expression network. At the top of this hierarchy are MRFs, including *MyoD*, *Myf5*, *myogenin*, and *MRF4*, which sequentially regulate the progression of myogenic differentiation. *MyoD* and *Myf5* are involved in the early stages of myogenic commitment, while *myogenin* and *MRF4* are essential for the later stages of differentiation and myofiber maturation (Bareja et al., 2014; Koike et al., 2022; Zammit & Beauchamp, 2001).

Satellite cell activation is tightly regulated by a network of intrinsic factors, including *Pax7*, which is essential for satellite cell maintenance and self-renewal. The upregulation of MRFs such as *MyoD* and *Myf5* upon activation drives the myogenic differentiation program (Bentzinger et al., 2010; Zammit & Beauchamp, 2001). Notably, the interplay between Notch and Wnt signaling pathways is crucial in this context. Notch signaling maintains the quiescence of satellite cells, while its

downregulation upon muscle injury promotes Wnt signaling activation and satellite cell proliferation and differentiation (Geetha-Loganathan et al., 2008).

During differentiation, myoblasts exit the cell cycle, align, and fuse to form multinucleated myotubes, which then mature into muscle fibers that are capable of contraction. The balance between myoblast proliferation and differentiation is crucial for proper muscle formation and regeneration. This equilibrium ensures that there are enough precursor cells to proliferate and replace damaged muscle tissue while allowing for differentiation into mature muscle fibers (Careccia et al., 2023).

Growth factors and cytokines play significant roles in regulating muscle homeostasis. Insulin-like Growth Factor 1 (IGF-1) plays a dual role by promoting both myoblast proliferation and differentiation, depending on the context and concentration (Yoshida & Delafontaine, 2020). IGF-1 activates the PI3K/Akt pathway, which enhances cell survival and proliferation while also promoting the expression of MRFs like *MyoD* and *myogenin* to facilitate differentiation (Yu et al., 2015). For instance, studies have shown that IGF-1 stimulates muscle cell proliferation during early myogenesis while also aiding differentiation at later stagesthrough upregulation of *MyoD* and *myogenin* (Forini, Ewton, y Coolican 1996; Yoshida y Delafontaine 2020). Fibroblast Growth Factors (FGFs), particularly FGF2, are well-known for their role in stimulating myoblast proliferation while inhibiting differentiation. FGFs achieve this by activating the MAPK/ERK signalling pathway, which promotes cell cycle progression and proliferation while suppressing the expression of differentiation markers, which guarantees that there is a sufficient pool of proliferating myoblasts available for muscle growth and repair (Delfini et al., 2009; Florini & Magri, 1989; Kurogoushi et al., 2021).

Metabolic regulation is another crucial aspect. Anabolic processes are crucial for muscle growth and involve the synthesis of proteins, leading to muscle hypertrophy (McCarthy & Esser, 2010). Key anabolic signals include IGF-1 and mTOR, which promote protein synthesis and muscle growth. mTOR is activated by nutrients,

growth factors, and mechanical load, driving anabolic processes in myoblasts and myofibers. Studies have shown that activation of the mTOR pathway is critical for muscle hypertrophy and can prevent muscle atrophy, underscoring its role in maintaining muscle mass (Barclay et al., 2019; Maltzahn et al., 2011). Conversely, catabolic pathways break down molecules to provide energy and remove damaged components. Myostatin, a member of the TGF-β family, is a potent inhibitor of muscle growth, promoting protein degradation and suppressing anabolic pathways. Myostatin inhibits the Akt/mTOR pathway and upregulates components of the ubiquitin-proteasome system, leading to muscle protein breakdown (X. Q. Lan et al., 2024; McPherron et al., 1997; Morissette et al., 2009).

3. PATHWAY DYSREGULATION IN DM1 MUSCLE: MECHANISMS AND IMPLICATIONS

The expanded CUG repeats in the *DMPK* mRNA are known to be the primary pathogenic trigger in DM1 because of the sequestration and disruption of RNA-binding protein's functions. In the nucleus, the mRNA containing CUG expansions forms double-stranded RNA (dsRNA) structures with U-U mismatches capable of binding and sequestering dsRNA binding proteins. Consequently, large ribonuclear aggregates, also known as ribonuclear foci, are formed (Michalowski et al., 1999; Miller et al., 2000; Mooers et al., 2005; B. Tian et al., 2000). These expansions could interfere protein function by its binding, including the regulation of alternative splicing, transcription, translation, polyadenylation, miRNA biogenesis, mRNA stability, and intracellular mRNA localization (Batra et al., 2014; Ebralidze et al., 2004; Kalsotra et al., 2008; J. E. Lee & Cooper, 2009). As a result, these proteins are no longer present in their corresponding subcellular locations, leading to altered function.

3.1. MBNL and CELF proteins.

One of the key mechanisms by which CUG repeat expansions exert their pathogenic effects is through the sequestration of the Muscleblind family (MBNL) of proteins,

evolutionarily conserved RNA-binding proteins (RNPs) that play a crucial role in regulating alternative splicing during development and in adult tissues. They were discovered in *Drosophila* (Artero et al., 1998; Begemann et al., 1997), where the *muscleblind* (*mbl*) gene generates different isoforms through alternative splicing (Begemann et al., 1997). In contrast, humans and mice have three Muscleblind homologs: *MBNL1 (Muscleblind-like splicing regulator 1), MBNL2 (Muscleblind-like splicing regulator 2)*, and *MBNL3 (Muscleblind-like splicing regulator 3)*. In human and mouse tissues, the expression patterns of *MBNL1* and *MBNL2* exhibit substantial overlap, being detected in a variety of adult tissues, including skeletal muscle, heart, brain, intestine, liver, lung, kidney, and placenta. In contrast, the expression of *MBNL3* is more restricted, primarily observed during embryonic development in the placenta and transiently in adult skeletal muscle, specifically in the context of muscle regeneration following injury. This expression pattern suggests a degree of functional redundancy among the MBNL1 and 2 proteins playing more prominent roles in adult tissues (Fardaei et al., 2002; Kanadia et al., 2003; Miller et al., 2000).

MBNL proteins contain conserved CCCH-type zinc finger (ZnF) motifs in their N-terminal region, responsible for binding to RNA hairpin structures containing pyrimidine mismatches (Hale et al., 2018; Irion, 2012; Miller et al., 2000; Oddo et al., 2016; Vicente-Crespo et al., 2008). MBNL1 interacts with RNA through four ZnFs that fold into two compact tandem domains (ZF1-2 and ZF3-4) (Teplova & Patel, 2008), binding to YGCY motifs in the pre-mRNA, which are also necessary for its splicing factor activity (Goers et al., 2010). Another highly conserved region in Muscleblind proteins is the KRAEK motif located in the C-terminal region, which is required for their proper nuclear localization (Fernandez-Costa and Artero 2010; Kino et al. 2015; Vicente-Crespo et al. 2008). The inclusion of a similar KRAEK-containing exon 5 in the MBNL1 mRNA is regulated by MBNL1 itself, demonstrating an autoregulatory mechanism coupling nuclear localization and alternative splicing control (Gates et al., 2011).

In addition to the sequestration of MBNL, DM1 is also characterized by the upregulation of another family of RNA-binding proteins, the CELF (CUGBP Elav-like family) proteins. In DM1, the CELF1 (also known as CUGBP1) protein is hyperphosphorylated because of its hyperphosphorylation by protein kinase C (PKC), leading to CELF1 stabilization (Kuyumcu-Martinez et al., 2007; Salisbury et al., 2008; Timchenko, 2013). Recent research has further elucidated the complex regulation of CELF1. Protein kinase B, also known as AKT, has been implicated in regulating CELF1 by influencing its subcellular localization. AKT inhibits glycogen synthase kinase 3 beta (GSK3β), which stabilizes the repressive form of CELF1, whereas PKC contributes to CELF1 misregulation through hyperphosphorylation, affecting its localization and function (Ozimski et al., 2021).

CELF1 and the MBNL proteins have antagonistic roles in regulating alternative splicing, with CELF1 generally promoting the generation of fetal splice isoforms, while MBNL proteins favour the inclusion of exons that results in adult splice isoforms (E. T. Wang et al., 2015). The imbalance between MBNL and CELF1 activities is a key driver of the splicing dysregulation observed in DM1 muscle (Du et al., 2010; Ho et al., 2004; Lin et al., 2006). The disruption of the MBNL-CELF balance leads to the misregulation of alternative splicing of numerous transcripts involved in muscle structure and function. Recent studies have also confirmed that 34 splicing events in DM1 patients exhibit inclusion patterns typically seen in the fetal stage of development (Degener et al. 2022). For example, the alternative splicing of the cardiac troponin T (cTNT) transcript is dysregulated in DM1, with MBNL1 repressing the inclusion of exon 5, while CELF1 promotes its inclusion (Ho et al., 2004). This imbalance results in the persistence of the fetal isoform of *cTNT* in adult DM1 muscle, contributing to the cardiac abnormalities observed in the disease (Ho et al., 2004, 2005).

The dysregulation of alternative splicing in DM1, known as spliceopathy, directly links the muscular symptoms with myotonia, muscle weakness, and insulin resistance. Myotonia has been associated with errors in the processing of exon 7a

of the *chloride channel type 1 gene (CLCN1*), leading to the inclusion of a premature stop codon and the production of a non-functional truncated protein (Charlet-B et al., 2002; Mankodi et al., 2002). The altered splicing of exon 22 in the ATP2A1 (SERCA1) gene can also affect intracellular Ca2+ signalling and sarcolemmal excitability in DM1 and DM2 myotubes, potentially influencing myotonia (Santoro et al., 2014). Muscle weakness in DM1 has been correlated with the skipping of exon 11 in the mature transcripts of the *Amphiphysin 2* (*BIN1*) gene in skeletal muscle, which is directly associated with disease severity and altered T-tubule network organization (Fugier et al., 2011). Defects in the processing of exon 29 in *calcium channel voltage-dependent* transcripts (*CACNA1s*) have also been linked to muscle weakness in DM1 (Santoro et al., 2014; Tang et al., 2012). Cisco et al (2024) studied the combined effect of two missplicing using a mouse model with forced skipping of exon 29 in the *CaV1.1 calcium channel* combined with the loss of *ClC-1 chloride channel*. This combination showed a markedly reduced lifespan, myotonia, weakness, and impairment of mobility and respiration, suggesting that Ca2+/Cl- bi-channelopathy contributes significantly to muscle impairment in DM1 (Cisco et al., 2024).

Additionally, the regulation of alternative splicing of CELF1 itself is significantly altered in DM1. The splicing of the 5' UTR of CELF1 mRNA produces isoforms that vary in their N-terminal domain lengths, and this splicing is efficiently regulated during development and tissue differentiation but disrupted in DM1 skeletal muscles (Kajdasz et al., 2022).

In addition to their role in alternative splicing regulation, MBNL proteins have also been implicated in the control of polyadenylation, mRNA stability, and microRNA biogenesis (Batra et al., 2014; Fernandez-Costa et al., 2013; Rau et al., 2011). The sequestration of MBNL proteins by CUG repeat expansions can lead to the dysregulation of these additional post-transcriptional processes, further contributing to the complex molecular pathogenesis of DM1. Recent findings have shown that MBNL proteins form motile and anchored granules in neurons and

myoblasts, associating selectively with kinesins through their domains, suggesting a motor-RBP specificity code and its perturbation led to widespread mRNA mis-localization (Hildebrandt et al., 2023).

The development of DM1 animal models, including transgenic mice expressing CUG repeat expansions and *Mbnl1* knockout mice, has been instrumental in elucidating the central role of MBNL protein sequestration in the disease. These models demonstrated that loss of MBNL function is a critical driver of the DM1 phenotype as *Mbnl1* knockout mice recapitulate many of the key features of the disease, such as myotonia, muscle wasting, and cardiac abnormalities (Dixon et al., 2015; Du et al., 2010; Kanadia et al., 2003). Conversely, the loss of function of *Mbl* (MBNL 1-3 orthologue in *Drosophila)* causes defects in muscle junctions and the disorganization of the sarcomeres, while the overexpression of MblC isoform in *Drosophila* models of DM1 has been shown to partially rescue the muscle atrophy, cardiac defects, and rough eye phenotypes (Artero et al., 1998; Bargiela et al., 2015).

Recent studies have further reinforced the importance of MBNL proteins in DM1 pathogenesis. (Merien et al., 2021) revealed that MBNL1 and 2 proteins are crucial for late myogenic maturation during human myogenesis and its depletion in human-induced pluripotent stem cells (hiPSCs) led to the manifestation of key features of DM1. Additionally, a functional neuromuscular model combining DM1 and MBNL knock-out hiPSCs-derived motor neurons and healthy skeletal muscle cells revealed presynaptic defects affecting the formation or stability of the neuromuscular junction at an early developmental stage (Tahraoui-Bories et al., 2023). However, studies on *Mbnl1* and *Mbnl2* knockout mice showed no obvious deleterious effects on muscle regeneration or satellite cell numbers, suggesting that additional factors beyond spliceopathy associated with *MBNL* loss are likely involved in the defects seen in skeletal muscle regeneration in DM1 (Yadava et al., 2024).

In summary, the dysregulation of RNA-binding protein pathways, particularly the sequestration of MBNL proteins and the upregulated function of CELF1, is a central mechanism underlying the multisystemic pathology of DM1.

3.2. MSI2>miR-7 axis.

Musashi RNA-binding protein 2 (MSI2) is a critical post-transcriptional regulator that influences various cellular processes, including stem cell maintenance, differentiation, and signalling pathways (Duggimpudi et al., 2018; P. Jiang et al., 2023; X. Jiang et al., 2019; R. Wang et al., 2024; Zhong et al., 2024). MSI2 belongs to the Musashi family of RNA-binding proteins, characterized by its two N-terminal RNA recognition motifs (RRMs), which facilitate specific binding to target mRNAs (L. Lan et al., 2020). These interactions occur primarily through consensus sequences within the 3' UTRs of target mRNAs, impacting their stability and translation efficiency (Bennett et al., 2016; Nguyen et al., 2020).

MSI2 is produced in multiple isoforms through alternative splicing, which enables it to perform various functions in different cellular contexts (L. Lan et al., 2020; M. Li, Li, et al., 2020; MacNicol et al., 2017). MSI2 is ubiquitously expressed but is particularly abundant in stem cells and certain cancers, where it plays critical roles in cell fate determination, proliferation, and differentiation (Nguyen et al., 2020; Siddall et al., 2006). In stem cells, MSI2 helps maintain pluripotency by regulating the balance between self-renewal and differentiation (Wuebben et al., 2012). However, MSI2 also interacts with several other key proteins and pathways. For example, it regulates IL-6 signalling by promoting the degradation of the IL6ST mRNA (Duggimpudi et al., 2018). Despite the efforts investigating MSI2 in cancers, the expression of MSI2 remains controversial, being overexpressed or downregulated in different cancers. However, recent studies correlated a high MSI2 expression with poor prognosis and aggressive tumour (L. Jiang et al., 2022; Kudinov et al., 2017; M. Li, Li, et al., 2020; P. Wei et al., 2019; Zhong et al., 2024).

Specifically, in DM1, MSI2 is overexpressed, and independent reports have identified MSI2 as a regulator of miR-7 biogenesis in brain cells. miR-7 is a microRNA that plays crucial roles in various cellular processes, including cell differentiation, tumour progression, and stress responses (Choudhury et al., 2013; Lyu et al., 2023; Ma et al., 2022; Zacharjasz et al., 2024). MSI2, along with Hu antigen R (HuR), binds to the conserved terminal loop of pri-miR-7-1, a well known regulation site for miRNAs biogenesis (Michlewski & Cáceres, 2019), to stabilize the immature form of miR-7 and preventing its maturation (Fig. I-3) (Choudhury et al., 2013). This interaction is critical in DM1, where the overexpression of MSI2 leads to reduced levels of mature miR-7, thereby disrupting normal cellular functions (Sabater-Arcis et al., 2021).

The downregulation of miR-7 in DM1 has profound implications for muscle function. miR-7 is involved in the regulation of autophagy, a cellular degradation pathway that is hyperactivated in DM1 muscle cells (Sabater-Arcis et al., 2020). miR-7 inhibition de-represses its target genes, which include key autophagy regulators that lead to increased autophagic activity, contributing to muscle atrophy and weakness observed in DM1 model flies (Fernandez-Costa et al., 2013; Gu et al., 2017). In fact, the observed miR-7's mechanism of action in improving atrophy-related phenotypes is independent of MBNL1.

Recent studies have underscored the potential therapeutic implications of targeting the MSI2-miR-7 axis in DM1. Strategies aimed at reducing MSI2 expression or modulating its activity could restore normal miR-7 levels and improve muscle function. For instance, antisense oligonucleotides (ASOs) designed to specifically target *MSI2* mRNA have shown promise *in vitro* models, leading to a reduction in MSI2 levels and partial rescue of miR-7 levels. Additionally, small molecules like Ro 08-2750 that disrupts the MSI2-HuR complex interaction with pri-miR-7 could offer a novel approach to modulate miR-7 levels and alleviate muscle pathology in DM1 (Sabater-Arcis et al., 2021).

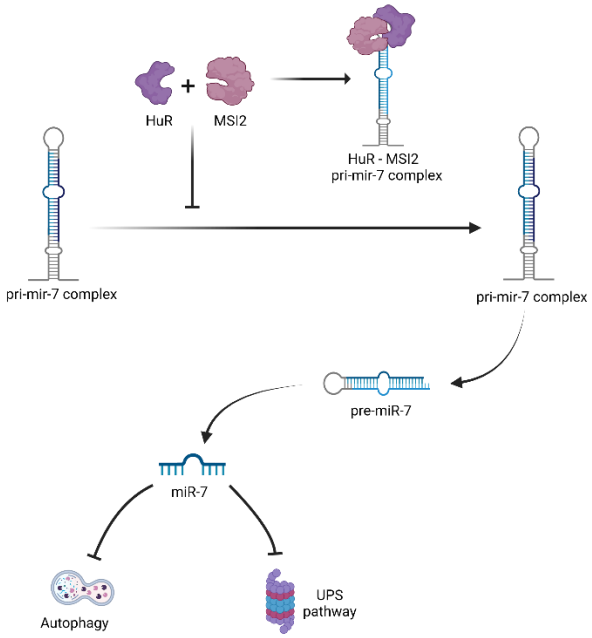

Fig I-3. Inhibition of miR-7 biogenesis. The biogenesis of miR-7 is regulated by the proteins MSI2 and HuR. These proteins inhibit the processing of pri-miR-7 into pre-miR-7 by forming a complex with pri-miR-7, the pri-miR-7-MSI2-HuR complex. Consequently, without conversion to pre-miR-7, the miRNA biogenesis pathway is halted, preventing the formation of mature miR-7. This inhibition impacts the regulatory functions of miR-7, including its role in suppressing autophagy and the ubiquitin-proteasome system (UPS). Figure created with BioRender.com

3.3. Ubiquitin proteasome system and autophagy.

The UPS and autophagy are two crucial cellular processes that work in the same direction to maintain muscle homeostasis by degrading misfolded proteins and damaged organelles. In normal conditions, the UPS and autophagy operate in a balanced manner, ensuring that the degradation of proteins and organelles is matched by the synthesis of new proteins and organelles. This balance is maintained through the regulation of various signalling pathways, including the IGF1/AKT/mTOR pathway, which promotes protein synthesis and inhibits the

degradation of proteins (Y. Li et al., 2022; Stitt et al., 2004; Yoshida & Delafontaine, 2020).

The UPS pathway is a complex process that involves the covalent attachment of ubiquitin to target proteins, followed by their degradation by the proteasome. In muscle cells, the UPS pathway is activated in response to various signals, including the lack of IGF1, which leads to the dephosphorylation of FOXO and its translocation to the nucleus, where it activates the transcription of atrogenes such as *TRIM63, MuRF1, FBXO32,* and *Atrogin-1*. These atrogenes promote the activity of the UPS, leading to the degradation of muscle proteins and the development of muscle atrophy (K. Chen et al., 2022; Sandri et al., 2004; Stitt et al., 2004).

The dysregulation of the UPS has been observed in the skeletal muscles of transgenic animal models of DM1. For example, overactivated UPS was confirmed in the DMSXL mouse model of DM1 (Huguet et al., 2012). The pathological activation of the UPS in DM1 leads to the excessive degradation of essential muscle proteins, contributing to the development of muscle atrophy and weakness. Furthermore, studies have reported the aberrant activation of signalling pathways, such as the AMP-activated protein kinase (AMPK) and the TWEAK/Fn14 axis, in the skeletal muscles and cardiac tissue of DM1 animal models and in samples obtained from DM1 patients (Brockhoff et al., 2017).

Conversely, autophagy is a critical cellular process that maintains homeostasis by degrading and recycling damaged organelles, misfolded proteins, and other cellular debris through the lysosomal pathway. This mechanism is essential for cellular health and function, allowing cells to survive under stress conditions and adapt to nutrient deprivation (Franco-Romero & Sandri, 2021; Klionsky et al., 2021). This process involves the formation of double-membrane vesicles known as autophagosomes that engulf cytoplasmic components and deliver them to lysosomes for degradation. It is regulated by a group of autophagy-related (ATG)

proteins that orchestrate the various stages of autophagosome formation (Y. P. Yang et al., 2005).

In DM1, autophagy is excessively activated. This activation correlated with the size of CTG expansion in DM1 primary myoblast (Loro et al., 2010) Studies in a *Drosophila* model of DM1 showed significantly reduced mean area of indirect flight muscles (IFM), concomitantly with an activation of apoptosis and autophagy. Consequently, genetic inhibition of both processes was sufficient to ameliorate the atrophic phenotype (Bargiela et al., 2015). Furthermore, analysis in biopsies of DM1 patients and myoblast revealed an increased expression of genes associated with autophagy, detecting an almost two-fold increase in the expression of the gene *ATG4A* (Fernandez-Costa et al. 2013).

Recent studies have shown that autophagic activity is elevated in skeletal muscle satellite cells (SSCs) from DM1 patients, has been proposed reduces their proliferative capacity. This reduction in SSC proliferation is crucial as these cells drive muscle regeneration. In this case, MBNL1 plays a significant role, as research has demonstrated that MBNL1 overexpression in SSCs from DM1 patients enhances their proliferative capacity by inhibiting autophagy through the mTOR pathway (K. Y. Song et al., 2020). Furthermore, Hu et al. identified a new autophagy-related biomarker called DAPK1 that correlated with the progression of DM1 (Hu et al., 2022).

The roles of UPS and autophagy in muscle pathology are intricate and multifaceted. While these processes are essential for clearing damaged proteins and organelles, their dysregulation can lead to muscle degradation, atrophy, and apoptosis (Klionsky et al., 2021; Y. Li et al., 2022). In DM1, abnormal autophagy impairs myogenic differentiation, exacerbating muscle symptoms. Studies have demonstrated that restoring normal autophagy levels through miR-7 overexpression can rescue muscle phenotypes in DM1 models (Sabater-Arcis et al., 2020). Hyperactivation of autophagy in DM1 is partly due to the repression of miR-7

biogenesis by the overexpression of MSI2. Thus, silencing MSI2 has been shown to reduce autophagy levels and improve disease-related phenotypes (Sabater-Arcis et al., 2021).

All these findings highlight the critical role of hyperactivated autophagy in DM1 pathogenesis, suggesting that targeting autophagy pathways could be a promising therapeutic approach to mitigate muscle dysfunction and improve related phenotypes. In DM1, strategies to modulate autophagy and UPS pathways could rescue atrophy and muscle regeneration and counteract the progressive muscle deterioration associated with the disease.

4. ROLE OF MICRORNAS IN DM1

miRNAs are a class of small, non-coding RNA molecules, typically 20-24 nucleotides in length, that play pivotal roles in the post-transcriptional regulation of gene expression. miRNAs function by binding to complementary sequences on target mRNAs, leading to either mRNA degradation or inhibition of translation, thus this type or regulation is predominantly negative (Fukunaga, 2023).

The primary function of miRNAs is to modulate gene expression, thereby influencing a wide array of cellular activities by regulating the stability and translation of mRNAs. For instance, miRNAs are essential in the development and maintenance of tissues by ensuring that genes are expressed at appropriate levels and timepoints. Dysregulation of miRNAs has been implicated in numerous diseases (Roy et al., 2022; Urbańska et al., 2022; Venneri & Passantino, 2023).

4.1. Biogenesis and functions of miRNAs.

The biogenesis of miRNAs is a highly regulated process that begins in the cell nucleus and is completed in the cytoplasm. Most miRNAs follow the canonical pathway of biogenesis, but it is important to note that non-canonical pathways also exist. These alternative pathways involve variations in the processing steps and can

bypass certain components of the canonical machinery, adding an extra layer of complexity to miRNA regulation (Creugny et al., 2018).

In the canonical pathway (Fig. I-4), biogenesis starts with the transcription of miRNA genes by RNA polymerase II, which produces a primary miRNA transcript (pri-miRNA). These pri-miRNAs are characterized by a stem-loop structure and may be several kilobases long (Ha & Kim, 2014). The pri-miRNA undergoes cleavage by a complex comprising the RNase III enzyme Drosha and its cofactor DGCR8 (DiGeorge syndrome critical region 8). This cleavage produces a precursor miRNA (pre-miRNA) of approximately 70 nucleotides in length (Denli et al., 2004).

The pre-miRNA is then exported from the nucleus to the cytoplasm by Exportin-5, a nuclear transport receptor, in a Ran-GTP-dependent manner (Okada et al., 2009). Once in the cytoplasm, the pre-miRNA is further processed by another RNase III enzyme, Dicer, which cleaves the pre-miRNA near the terminal loop to generate a miRNA duplex (~22 nucleotides) (Denli et al., 2004; H. Zhang et al., 2004). This duplex consists of the mature miRNA strand (guide strand) and the complementary strand (passenger strand).

The mature miRNA is then incorporated into the RNA-induced silencing complex (RISC), where it is guided by the Argonaute (Ago) protein, a key component of RISC. The guide strand of the miRNA duplex is preferentially retained in the RISC, while the passenger strand is usually degraded. The miRNA-loaded RISC can then bind to complementary sequences in the UTR of target mRNAs, leading to translational repression or mRNA degradation (Gregory et al., 2005; Ha & Kim, 2014; Okada et al., 2009). This interaction is facilitated by the seed region of the miRNA, typically nucleotides 2-7 at the 5' end, which is crucial for target recognition (Renna et al., 2017; Savkur et al., 2001).

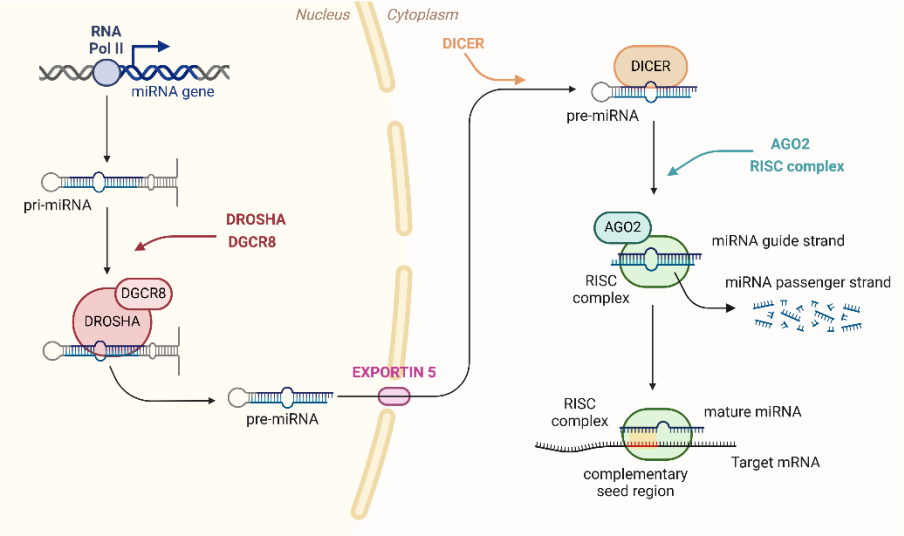

Fig I-4. Canonical miRNA biogenesis pathway. miRNAs are transcribed as precursor transcripts called pri-miRNAs, which are initially processed in the nucleus by Drosha and DGCR8. The pre-miRNAs are then exported to the cytoplasm via Exportin 5. Once in the cytoplasm, they undergo further processing by Dicer, resulting in a double-stranded miRNA. This double-stranded miRNA is subsequently incorporated into the RNA-induced silencing complex (RISC) and Argonaute 2 to produce the mature miRNA. Then the mature miRNA is guided by the RISC complex to bind to its target mRNA transcripts through its seed region, thereby inhibiting their expression. Figure created with Biorender.com.

This process is also regulated by several RBPs that bind to the conserved terminal loop (TL) of their target pri-miRNAs, such as MSI2 inhibiting miR-7 biogenesis. The TL serves as a critical site of interaction where RNA-binding proteins (RBPs) can either enhance or inhibit the processing of pri-miRNAs by enzymes such as Drosha and Dicer (Michlewski & Cáceres, 2019). This dynamic interplay between different proteins and the TL of pri-miRNAs highlights a sophisticated regulatory network that ensures the proper temporal and spatial expression of miRNAs.

4.2. miRNAs involved in DM1 muscle pathogenesis.

Several studies have identified myomiRs, such as miR-1, miR-133a/b, miR-206, miR-208a/b, miR-499, and miR-486 dysregulated in DM1 myotubes and skeletal muscle

biopsies from patients. These miRNAs are predominantly expressed in skeletal muscle and play essential roles in muscle differentiation, growth, and response to stress (Koehorst et al., 2020).

Gambardella *et al.* initially reported miR-206 was found to be upregulated in DM1 muscle biopsies and that this miRNA is localized in central nuclei and nuclear clusters, hallmark features of DM1 histopathology (Gambardella et al., 2010).

Further studies demonstrated the downregulation of miR-29b/c and miR-33 also showed that miR-335 and miR-1 are overexpressed in DM1 muscle biopsies compared to healthy controls. In fact, they found that predicted targets of miR-1 and miR-29b/c involved in muscle development (MEF2a, MET, GATA6, and HAND2), arrhythmia (KCNE1, KCNJ2, CALM2), splicing (SFRS9), and atrophy (DAG1, DIABLO, RET, TRIM63, TGFB3) were significantly upregulated in DM1 patients (Perbellini et al., 2011).

miR-206 overexpression was corroborated by subsequent studies, indicating a robust pattern specific to DM1 muscle pathology (Fritegotto et al., 2017). In addition to miR-206, Fritegotto *et al.* identified significant downregulation of miR-1 and miR-133a/b in DM1 muscle biopsies, miR-1 upregulation was also confirmed in independent research (Ambrose et al., 2017). miR-1 and miR-133a/b are crucial for muscle differentiation and function, and their decreased levels likely contribute to the muscle dysfunction observed in DM1. However, in contrast to Fritegotto *et al.*, Ambrose *et al.,* saw the upregulation of miR-133a in this case in patient's blood. Likewise, miR-29b and miR-33a were significantly upregulated in blood, while mR-29c was significantly downregulated in the DM1 skeletal muscles.

The dysregulation of miR-208a/b and miR-499, which are primarily expressed in cardiac muscle, contribute to cardiac complications such as arrhythmias and cardiomyopathy (Koehorst et al., 2020). miR-486, which is downregulated in DM1 affects muscle growth and maintenance by targeting genes such as *PAX3, PAX7, or MSTN*. By targeting *PTEN, FOXO1*, and *MSTN*, this miRNA also promotes hypertrophy

and overall skeletal muscle growth, but the decreased levels of miR-486 contribute to muscle wasting and weakness in DM1 (Small et al., 2010; Yedigaryan & Sampaolesi, 2021).

The dysregulation of some miRNAs in DM1 is related to the dysregulation of MBNL proteins. For example, MBNL1 sequestration in the ribonuclear foci inhibits miR-1 maturation and leads to its downregulation (Rau et al., 2011). Recently Soudi et al confirmed that in *Drosophila* DM1 mbnl sequestration stabilizes Bru3 causing the inefficient processing of pre-dmiR-1 and destabilization of mature dmiR-1. Consequently, the level of dmiR-1 is decreased, while the level of its target Mp is elevated. This imbalance results in an enlarged heart, negatively impacting contractility and causing disorganization of the myofibrils in the heart tubes producing dilated cardiomyopathy (DCM) in *Drosophila*, a phenotype associated with DM1 (Souidi et al., 2023).

Recent studies further elucidated the complex role between MBNL1/2 and miRNAs in DM1 pathology. Cerro-Herreros *et al*. discovered two miRNAs upregulated in DM1, miR-23b and miR-218, which regulate MBNL1/2 translation. In fact, targeting these miRNAs with antagomiRs in *in vitro* and *in vivo* models has shown potential in rescuing MBNL protein levels and ameliorating DM1 phenotypes (Cerro-Herreros et al., 2018, 2020, 2021).

Notably, there is a downregulation of miR-322 and miR-503 during myoblast differentiation, and their overexpression was reported to rescue myoblast differentiation defects and repress ribonuclear foci formation in a DM1 cell model. Overexpression of these miRNAs leads to the upregulation of myogenic markers and the inhibition of CELF1, a critical factor in DM1 pathology, thereby restoring normal myotube formation and correcting dysregulated alternative splicing patterns (Y. Li et al., 2022; Shen et al., 2020). Similarly, miR-206 and miR-148a were reported to play a crucial role in DM1 by directly targeting the non-CUG repeat region of the *DMPK* 3'UTR, influencing muscle differentiation and regeneration processes. Additionally,

miR-15b/16, members of the mir-15/107 family also targets *DMPK* regions associated with DM1, the expanded repeats, due to the conserved seed region conserved in this family which is complementary to the CUG repeats. Koscianska et al. demonstrated that miR-15b/16 can significantly down-regulate DMPK and that the repression efficiency increased with the length of the repeated CUG sequence(Koscianska et al., 2015).

Furthermore, Fernandez-Costa *et al*. identified downregulated three conserved miRNAs in the *Drosophila* DM1 model: miR-1, miR-7, and miR-10. The alteration of these miRNAs affects the expression of their target genes. Particularly, some of miR-7 targets like *CTSB*, *ATG4A* and *VCL* were overexpressed in the fly model. These genes are involved in protein degradation, autophagy, and cytoskeletal dynamics, processes that are disrupted in DM1 muscle pathology (Bargiela et al., 2015; Fernandez-Costa et al., 2013).

5. METABOLIC ALTERATIONS IN DM1

Patients with DM1 exhibit a range of metabolic disturbances, most notably an increased prevalence of metabolic syndrome. This includes hypertriglyceridemia, low levels of high-density lipoprotein (HDL), cholesterol, hypertension, central obesity, and hyperglycaemia (Stojanovic et al., 2010; Vujnic et al., 2015). Furthermore, studies described that DM1 patients frequently suffer from insulin resistance, which exacerbates these metabolic issues. Abnormal splicing of the *insulin receptor* gene (INSR) has been identified as a contributing factor to insulin resistance in DM1 patients. This splicing alteration leads to the predominance of the fetal INSR isoform, which is less responsive to insulin, thereby impairing glucose metabolism (Renna et al., 2017, 2019; Savkur et al., 2001). IGF-1 signalling impairment also modulates the PI3K/Akt/mTOR pathway and reduces protein synthesis and muscle growth, which in turn contributes to the reduced anabolic activity observed in DM1 and influences the balance between myoblast proliferation and differentiation. (Barclay et al. 2019; Yoshida y Delafontaine 2020)

Independent studies reported that DM1 patients have impaired oxidative phosphorylation, reduced ATP production, and increased accumulation of reactive oxygen species (ROS). These mitochondrial defects are evident in both muscle tissues and fibroblasts derived from DM1 patients. Furthermore, studies using magnetic resonance spectroscopy revealed significant abnormalities in brain and muscle oxidative metabolism in DM1 patients (García-Puga et al., 2020; Gramegna et al., 2018).

The combined effects of these metabolic alterations significantly impact the quality of life and overall health of DM1 patients. These metabolic issues are part of the disease pathology and necessitate comprehensive management strategies to mitigate their impact on DM1 patients.

5.1. Fatty acids metabolism in DM1.

Lipid metabolism is profoundly affected in DM1, which includes disruptions in lipid profiles, fatty acid composition in cellular membranes, and regulatory mechanisms governing lipid metabolism.

Dyslipidaemia is associated with the dysfunction of lipin proteins, which play a crucial role in lipid metabolism, including the regulation of triacylglycerol levels and lipid signalling pathways (Mateus et al., 2021). Lipins are phosphatidate phosphatase enzymes involved in lipid metabolism and signalling pathways. Alterations in lipin function have been linked to the metabolic syndrome observed in DM1, suggesting that targeting lipin proteins could offer therapeutic potential for managing metabolic complications in DM1 patients (Mateus et al., 2021).

Furthermore, increased visceral fat accumulation has been documented, indicating a propensity for central obesity, which exacerbates insulin resistance and other metabolic disorders (Takada, 2018).

Adiponectin, a hormone with beneficial effects on lipid and glucose metabolism, is found reduced in DM1 patients. Notably, there is a selective reduction in high

molecular weight (HMW) adiponectin oligomers, which are crucial for its insulin-sensitizing effects. This reduction correlates with increased insulin resistance and metabolic complications in DM1 (Daniele et al., 2011).

Another significant aspect is that DM1 patients are at a higher risk of developing non-alcoholic fatty liver disease (NAFLD) due to their metabolic profile. A study on the clinical characteristics of metabolically associated fatty liver disease (MAFLD) in DM1 patients found a significant prevalence of liver disease, highlighting the severe metabolic impact of DM1 on hepatic function (Miele et al., 2021). Moreover, in an inducible liver-specific mouse model of DM1, the expression of toxic CUG-repeat RNA caused hepatic steatosis, inflammation, and necrosis, indicating a direct impact of DM1 on liver metabolism. This model also demonstrated impaired drug metabolism and increased susceptibility to hepatotoxicity, further underscoring the metabolic vulnerabilities in DM1 (Dewald et al., 2021).

6. EXPERIMENTAL MODELS IN DM1 RESEARCH

Understanding and treating diseases at a molecular level necessitates robust and reliable models. Both *in vitro* and *in vivo* models serve as essential tools to elucidate the pathophysiology of diseases and to test potential therapeutic compounds.

6.1. *In vitro* models.

Among the models used in this study are the immortalized myoblast and the immortalized transdifferentiated fibroblast, both from Dr. Denis Furling's laboratory (Institut de Myologie, Paris, France). These cells were obtained from primary cells isolated from skeletal muscle or skin biopsies of an 11-year-old female donor expressing 1,300 CTG repeats and from a 25-year-old non-DM1 donor used as control (Arandel et al., 2017). For myoblast and fibroblast immortalization, cells were transduced to express the human telomerase steadily (hTERT) and the additional inhibition of the p16 pathway by the overexpression of CDK4. The *hTERT* gene is responsible for immortalizing the cells by maintaining telomere length, while

the *CDK4* gene helps to regulate cell proliferation. Thus, the cell lines have a potentially unlimited number of divisions while maintaining the disease characteristics. These disease model cells exhibit key DM1 features such as RNA foci, splicing defects, and impaired cell fusion, making them valuable for drug testing and mechanistic studies (Arandel et al., 2017). Furthermore, clonal selection leads to homogeneous cell cultures, which provide more consistent and reproducible results. Additionally, the immortalized fibroblast can be transdifferentiated in myotubes via the myogenic factor *MyoD*, as they were stably transduced to express the *MyoD* gene in a doxycycline-inducible manner. This approach allows fibroblasts, which are easier to obtain and manipulate than myoblasts, to enter the myogenic program and form myotubes, mimicking muscle tissue.

As removing CTG repeats in DM1 phenotypes has been considered a possible therapeutic approach. The CRISPR/Cas9 gene editing system has been used to explore this aspect and demonstrating its potential to address the pathogenic mechanism in DM1. For instance, Agtmaal *et al.* employed this system for the transduction of the immortalized myoblast (Arandel et al., 2017) with a lentiviral vector expressing a guide RNA (gRNA) to target the CTG repeats in the *DMPK* gene and a Cas9 enzyme to excise the repeats. The removal of the repeats normalizes the myogenic capacity, the nucleoplasmic distribution, and the dysfunctional interaction RNPs with *DMPK* transcripts. Importantly, the results confirmed the secuences lost do not have a known biological effect in DM1 locus but further research is needed to prove the safety of CRISPR-Cas9 technology for recovering DM-related phenotypes (Agtmaal et al., 2017). Similarly, Dastidar *et al.* applied this technique in DM1 patient-specific induced pluripotent stem cells, DM1-iPSC-derived myogenic cells, and DM1 patient-specific myoblasts. They designed a dual gRNA-based strategy to efficiently excise the CTG-repeat expansion. This excision resulted in the disappearance of ribonuclear foci and restored the normal intracellular localization of muscleblind-like splicing regulator 1 (MBNL1), leading to the normalization of the SERCA1 splicing pattern (Dastidar et al., 2018).

Nevertheless, future works need to assess off-target effects induced by CRISPR/Cas9 to ensure the safety and efficacy of this gene-editing approach.

Beyond the described cell lines, several other *in vitro* models have been developed. Induced pluripotent stem cells (iPSCs) derived from DM1 patients provide a versatile platform to study early developmental stages and differentiate into various cell types (Y. Gao et al., 2016; Ueki et al., 2017).

Muscle primary cells derived from DM1 patients are also a valuable tool for investigation, as they facilitate the study of the dissease in different genetic backgrounds. However, they have limited proliferation, and the availability of primary cells is limited due to the need for muscle biopsies, which are invasive and difficult to obtain (Bigot et al., 2009). Additionally, the variability in culture conditions and replicative senescence of primary cells can lead to experimental variability between different samples (Hintze et al., 2021). In this case, primary fibroblasts are more common due to their relative accessibility and ease of manipulation in culture, in contrast to myoblasts.

Three-dimensional (3D) tissue models have also emerged, offering a more physiologically relevant environment compared to traditional 2D cultures. These 3D models, derived from patient fibroblasts transdifferentiated into myotubes, recapitulate the architecture and functional properties of muscle tissue, providing a new system for studying DM1 and testing therapeutic compounds. The 3D models enable the formation of aligned muscle fibers and the establishment of a more complex extracellular matrix, mimicking the *in vivo* environment more closely than 2D models. Additionally, these models can replicate key pathological features of myotonic dystrophy type 1, such as abnormal splicing patterns, ribonuclear foci and impaired fusion capability (Fernández-Garibay et al., 2021).

6.2. *In vivo* models.

Over the past two decades, a diverse range of animal models has been developed to investigate the pathophysiological mechanisms of DM1. These models include the nematode *Caenorhabditis elegans* (K. Y. Chen et al., 2007), the fruit fly *Drosophila melanogaster* (García-López et al., 2011; Haro et al., 2006; Picchio et al., 2013), the zebrafish *Danio rerio* (Todd et al., 2014) and the mouse *Mus musculus,* which has a large number of different models.

In this study we used one of the most common and well-characterized murine model of DM1: the HSA^{LR} mouse (Mankodi et al., 2000). This transgenic model involves the insertion of approximately 250 CTG repeats in the 3'UTR of the human *alpha-1 actin* gene (*ACTA1*) in an FVB/NJ mouse background. It provided the first evidence that these expansions, even in the absence of the *DMPK* gene context, were sufficient to cause DM1. The expression of *ACTA1* is specific to skeletal muscule, so transcripts with CUG expansions in the 3' UTR of *ACTA1* reproduce typical physiological and molecular features of muscle disorders. These include myotonica, myopathy, and molecular alterations such as Mbnl sequestration, splicing defects, and ribonuclear foci. However, this model has some limitations as it does not exhibit some of the typical features od DM1 such as hyperactivated autophagy, muscle atrophy o the expression of the expansions beyond the muscle. Despite these limitations, this model has provided valuable insights into the molecular mechanisms underlying skeletal muscle dysfunction in DM1 and has been widely used in testing therapeutic strategies.

Several other mouse models have been developed to study DM1, including the EpA960 (Orengo et al., 2008; G. S. Wang et al., 2007; P. Y. Wang et al., 2017), DMSXL (Huguet et al., 2012; Seznec et al., 2000), TREDT960I (Morriss et al., 2018), DMPK-GFP-(CTG) (Mahadevan et al., 2006), DM200 (Mahadevan et al., 2006; Yadava et al., 2020, 2021) and EDM1, which is a model of early-induction DM1 (Gladman et al., 2013). Recent advancements include the triple heterozygous mutant DM1 mouse model (DSM-TKO), which replicates most adult onset of DM1 phenotypes, and the quadruple mutant DM1 mouse model (DSMD-QKO) that also mimic symptoms of

the most severe form of DM1, including hypotonia, respiratory problems and developmental delay (Yin et al., 2020). These models were used to investigate different therapeutic strategies and to study the molecular pathogenesis of the disease in various tissues, including skeletal muscle, the heart, and the central nervous system.

OBJECTIVES

DM1 is a genetic disorder characterized by progressive muscle wasting and weakness. Among the various symptoms, muscle atrophy is one of the most debilitating, leading to severe mobility issues, respiratory complications and significant functional difficulties. Understanding the molecular mechanisms that contribute to muscle atrophy in DM1 is crucial for developing effective therapeutic strategies.

Autophagy, a cellular degradation process, was identified as a key contributor to muscle atrophy in DM1. The hyperactivation of this cellular process leads to excessive muscle breakdown, exacerbating the atrophic phenotype. Building on the established observation that miR-7 is downregulated in DM1, leading to the activation of the pro-catabolic autophagy pathway in cellular models of the disease, our overarching goal was to investigate mechanistic details of how the MSI2>miR-7>autophagy axis worked, including how it operates in vivo in DM1 muscles and the ultimate reason for the upregulation of MSI2 levels. To this end, the specific objectives of this thesis were:

Objective 1: Investigate the effects of MSI2 levels on skeletal muscles *in vivo*.

Objective 2: Uncover the underlying reasons for the upregulation of MSI2 in the disease.

Objective 3: Evaluate the impact of oleic acid, a known allosteric regulator of MSI2 activity, on miR-7 levels.

RESULTS

CHAPTER 1:

MSI2 ENHANCES MUSCLE DYSFUNCTION IN A MYOTONIC DYSTROPHY TYPE 1 MOUSE MODEL

Published on October 2023 DOI:10.1016/j.bj.2023.100667

1.1. BACKGROUND

Myotonic dystrophy type 1 (DM1; OMIM #160900) is the most common muscular dystrophy in adults, with a worldwide disease prevalence between 1/8,000 and 1/3,000 (Ashizawa et al., 2018), although a recent newborn screening program reported a higher frequency of the mutant allele (1/2,100 ref). DM1 is an autosomal dominant disease originating from the pathogenic expansion (>50) of the CTG trinucleotide microsatellite in the 3´-untranslated region of the *DM1 protein kinase* (*DMPK*) gene (Brook et al., 1992). Consequently, mutant RNA carrying expanded CUG repeat becomes toxic by forming ribonuclear foci comprising secondary structures able to sequester RNA-binding proteins of the Muscleblind Like Splicing Regulator (MBNL) family (Yuan et al., 2007). MBNL1 plays a crucial role in regulating alternative splicing and polyadenylation sites in transcripts during development, causing a transition from fetal to adult patterns in muscle, while MBNL2 likely has a similar role in the brain (Batra et al., 2014; Konieczny et al., 2014). In contrast, Mbnl3 deficit was linked to age-associated pathologies observed in myotonic dystrophy (Choi et al., 2016). While MBNLs are deprived of their normal function, the CUGBP Elav-Like Family Member 1 (CELF1) becomes activated and regulates splicing antagonizing MBNL activity (E. T. Wang et al., 2015). This leads to a downstream cascade of mis-splicing events caused by MBNL sequestration and CELF activation, resulting in the maintenance of fetal splicing patterns in adult tissue for several critical muscle transcripts (Fernandez-Costa et al., 2011). Consequently, some DM1 symptoms originate from expressing inappropriate muscle protein isoforms. For instance, myotonia and insulin resistance are linked to defects in *CLCN1* (Wheeler et al., 2007) and *INSR* (Savkur et al., 2001) regulation of inclusion of alternative exons, respectively, while heart conduction defects and cardiac arrhythmias are associated with *SCN5A* mis-splicing (Pang et al., 2018).

DM1 patients show multisystemic symptoms, although the most consistent feature is diseased muscles, known as myopathy, including progressive muscle wasting (atrophy), especially with a distal pattern, difficulty when relaxing a contracted

muscle (myotonia), neuromuscular respiratory insufficiency, and dysphagia (Thornton, 2014). Globally, all these symptoms contribute to muscle dysfunction, leading to reduced strength and endurance and thus to physical disability.

Multiple factors have been proposed to explain muscle loss, including AKT-GSK3β (C. Wei et al., 2018), TWEAK/Fn14 (Yadava et al., 2015), AMPK/mTORC1 (Brockhoff et al., 2017), and PKC (Kuyumcu-Martinez et al., 2007) pathways (Ozimski et al., 2021). Additionally, during the last few years, the pathological contribution of increased autophagy has gained relevance as a possible cause contributing to the imbalance of protein synthesis and degradation, leading to muscle atrophy. Briefly, in a *Drosophila* model of the disease, hyperactivation of autophagy was confirmed concomitantly with reduced area of indirect flight muscles and reduced survival and motor capacity of model flies (Bargiela et al., 2015). Genetic and chemical rescue of the pathway was sufficient to ameliorate molecular, histological, and functional phenotypes in *Drosophila*, murine and cellular models (Bargiela et al., 2019; Sabater-Arcis et al., 2020). Dysregulation of autophagy linked to the alteration of molecular markers of muscle atrophy was also confirmed in DM1 muscle cells (Bargiela et al., 2015; Loro et al., 2010). Additionally, a murine model that inducibly expresses 960 CUG shows histological alterations and muscle wasting (Morriss et al., 2018). A proteomic analysis of these DM1 model mouse muscle samples confirmed increased expression of proteins involved in autophagy, thus suggesting an imbalance between anabolic and catabolic pathways that regulate muscle maintenance.

Musashi homolog 2 (MSI2) is an RNA-binding protein member of the Musashi gene family, characterized by its function as an alternative splicing factor (Matalkah et al., 2022), mRNA translational regulator (Cragle et al., 2019), and a cancer-driver gene in some tumors, including breast, brain, colon, lung, liver, pancreas, or leukemia (Kudinov et al., 2017). Its function in these tumors relates to mRNA translation and stability (Cragle et al., 2019). In addition, Msi2 maintains stem cell self-renewal and promotes oncogenesis by enhancing cell proliferation (Kudinov et al., 2017). We

have recently demonstrated that MSI2 levels are increased in DM1 myoblasts and biopsy samples. Using different silencing strategies targeting MSI2, we observed that miR-7, whose biogenesis is inhibited by MSI2-HuR complex (Choudhury et al., 2013), was enhanced, and atrophy-related phenotypes were restored in different DM1cell models (Sabater-Arcis et al., 2021). Besides, it was demonstrated that miR-7 levels are reduced in human muscle biopsies and DM1 myotubes. Downregulation of miR-7 in control myotubes leads to DM1-like phenotypes, while restoration of normal miRNA levels in DM1 cells inhibits excessive autophagy (Sabater-Arcis et al., 2020). Interestingly, miR-7 was described as a critical inhibitor of the autophagic pathway through the up-regulation of the mTOR signaling and direct translational repression of key autophagy genes, namely *ATG7, ULK2,* and *ATG4A* (Gu et al., 2017). Additionally, miR-7 biogenesis is regulated by MSI2 and Hu antigen R (HuR). MSI2 binds through HuR to the conserved terminal loop of *pri-miR-7-1*, stabilizing the precursor miRNA and reducing the mature form (Choudhury et al., 2013).

Pivotal in DM1 research was the demonstration that human skeletal actin (HSA)-driven expression of long repeat (LR) CUG RNA *in vivo* (HSA^{LR} mice), independently of *DMPK* sequences, develop many characteristic DM1 symptoms, including myotonia, centrally located nuclei and variable muscle fiber size, and aberrant alternative splicing (Mankodi et al., 2000). However, these mice do not show a clear and consistent muscle atrophy phenotype. To demonstrate the involvement of specific proteins in the pathogenic mechanism of the disease, Li et al. 2020 recently used HSA^{LR} mice to overexpress Hnrnpa1 using recombinant adeno-associated viruses (rAAV). Hnrnpa1 was sufficient to boost DM1-like spliceopathy, thus demonstrating the pathogenic role of this protein in a DM1 context (M. Li, Zhuang, et al., 2020). In a similar approach, independent authors promoted Staufen1 overexpression using rAAV, which was sufficient to enhance progressive muscle wasting in this murine model (Crawford Parks et al., 2020).

We have previously observed that miR-7 levels in the skeletal muscle of HSA^{LR} do not differ from those in control mice (Sabater-Arcis et al., 2020). Building off our *in vitro*

results, we proposed that *in vivo* levels of Msi2 were critical to the muscle atrophy phenotype, potentially explaining HSA^{LR} failure to show overt muscle degeneration. Therefore, if miR-7 biogenesis is inhibited by Msi2 overexpression, reduced levels of the mature miR-7 will release repression of several autophagy-related genes, enhancing muscle catabolism beyond normal homeostasis and leading to muscle degradation. Considering this hypothesis, we report the results of overexpressing murine Msi2 in HSA^{LR} mice skeletal muscle and provide experimental evidence indicating the involvement of Msi2 to the muscle wasting phenotype in DM1.

1.2. MATERIAL AND METHODS

RNA extraction and reverse transcription-quantitative PCR (RT-qPCR)

Total RNA from murine muscles was isolated using the miRNeasy Mini Kit (Qiagen, Germantown, Maryland, CA, USA, 217004). One microgram of RNA was digested with DNase I (Invitrogen, Carlsbad, CA, USA, 18068015) and reverse-transcribed with SuperScript II (Invitrogen, Carlsbad, CA, USA, 18064014) using random hexanucleotides (Sigma-Aldrich, San Luis, Missouri, USA, 11277081001). Mean of *Gtf2b, Hprt1,* and *Gapdh* expression were used as endogenous controls. 500 ng of mouse tissue cDNA was used as the template for RT-qPCR using miRCURY LNA SYBR® Green PCR Kit (Qiagen, Germantown, Maryland, USA, 1477.6). The primers used were: *Gapdh* (fwd ATCAACGGGAAGCCCATCAC; rev CTTCCACAATGCCAAAGTTGT), *Gtf2b* (fwd ATGGCGGACAGAATCAACCTCC; rev ACAAGCAGAGGCTATCGCGTCA)*; Hprt1* (fwd GTTGGATACAGGCCAGACTTTGT; rev CACAGGACTAGAACACCTGC); *Msi2* (fwd CAGCCGAAAGAAGTCATGTTCCC; rev CCTCTGCCATAGGTTGCCACAA); *Mrf4* (fwd ATCAGCTACATTGAGCGTCTACA; rev CCTGGAATGATCCGAAACACTTG); *Mstn* (fwd CTCAGACCCGTCAAGACTCC; rev CTCTGCCAAATCAATACCAGTGCC); *Atg4a* (fwd CAGTCTCCACAGCGGATGAGTA; rev GTGTGATGGGTGCTTCTGAACC); *Atg7* (fwd GACCGGTCTTACCCTGCTC; rev TGTGGTTGCTTGCTTCAGAC); *P21* (fwd TCGCTGTCTTGCACTCTGGTGT; rev CCAATCTGCGCTTGGAGTGATAG); *Pax7* (fwd GAGCACTCGGCTAATCGAAC; rev

CCGTGTTTCTCATGGTTGTG); Tgfbr1 (fwd TGCTCCAAACCACAGAGTAGGC; rev CCCAGAACACTAAGCCCATTGC); *Atrogin1* (fwd CTCTGTACCATGCCGTTCCT; rev GGCTGCTGAACAGATTCTCC); *Trim63* (fwd ACCTGCTGGTGGAAAACATC; rev AGGAGCAAGTAGGCACCTCA); *Foxo1* (fwd GAGAGCTCAGCCGAGAAGAG; rev CTCCCTCTGGATTGAGCATC); *Foxo3a* (fwd CAGGCTCCTCACTGTATTCAGCTA; rev CATTGAACATGTCCAGGTCCAA); *Nanoluc* (fwd GGGAGGTGTGTCCAGTTTGT; rev TTCACCGCTCAGGACAATCC); *HSA* (fwd ACGGGTGCGTGGTGTCTC; rev GGTCAGGATACCTCTCTTGCT). miRNA expression in murine muscles was quantified using specific miRCURY™-locked nucleic acid microRNA PCR primers (Qiagen, Germantown, Maryland, CA, USA, 339306) and was normalized to U1 snRNA. All procedures followed the corresponding manufacturer's recommendations. Expression levels were measured using an Applied Biosystems Quant Studio 5 Time PCR System. Expression relative to the endogenous gene and control group was calculated using the $2^{-\Delta\Delta Ct}$ method.

Western blotting

For total protein extraction, quadriceps and gastrocnemius mouse muscles were homogenized in RIPA buffer (Fisher Scientific, Waltham, Massachusetts, USA, 10230544) supplemented with protease and phosphatase inhibitor cocktails (Roche Applied Science, Indianapolis, IN, USA, 4906837001). Total protein was quantified using a BCA assay kit (Thermo Scientific Pierce, Grand Island, NY, USA, 10741395) following the manufacturer´s instructions. For specific protein detections, 20 µg of total protein were denatured for 5 min at 100 °C, electrophoresed on 12-15% SDS-PAGE gels, and transferred onto 0.45 µm nitrocellulose membranes (Cytiva, Little Chalfont, UK, GE10600002). Membranes were blocked with blocking solution [5% non-fat dried milk in PBS-T (8 mM Na2HPO4, 150 mM NaCl, 2 mM KH2PO4, 3 mM KCl, 0.05% Tween 20, pH 7.4)] for 1 h at RT. Membranes were incubated overnight with blocking solution at 4 °C with the corresponding primary antibody: goat horseradish peroxidase (HRP)-conjugated anti-GAPDH (1:3500, Santa Cruz, Dallas, Texas, sc-365062), rabbit anti-ATG4A (1:1000, 108322), rabbit anti-LC3B (1:3000,

51520), rabbit anti-MSI2 antibody (1:1000, EP1305Y) or mouse anti-P62 (1:1000, 65416), all these from Abcam, Cambridge, UK. All primary antibodies, except anti-GAPDH were detected using goat HRP-conjugated anti-rabbit-IgG (1 h, 1:3500, Sigma-Aldrich, San Luis, Missouri, USA, A0545) or goat HRP-conjugated anti-mouse-IgG (1:5000, Sigma-Aldrich, San Luis, Missouri, USA, B7264) incubated for 1 h at RT. Images were acquired with an Amersham ImageQuant 800 and were quantified using ImageJ software (NIH).

Jess Simple Western system

V5-tag and Msi2 protein were quantified by automated Simple Western assays using the Jess system (ProteinSimple; Bio-Techne, Minneapolis, Minnesota, USA) following the manufacturer´s recommendations. A final concentration of 0.4 mg/mL for V5, and 1.8 mg/mL for Msi2, of gastrocnemius or quadriceps muscle protein extract was mixed with 5× master mix, heated at 95 °C for 5 min and kept on ice. 12–230 kDa Jess/Wes Separation Module (cat#SM-W004) was used, and 4 µl of each sample was loaded for 9 s. The incubation time of the primary and the secondary antibodies was 30 min. Rabbit anti-V5-Tag (Cell Signalling, Danvers, Massachusetts, USA, D3H8Q) was used at 1:20 dilution, and anti-Msi2 (Abcam, Cambridge, UK, 76148) at 1:250. Ready to use HRP-conjugated anti-rabbit antibody module (cat. #DM-001) was used as the secondary antibody. Msi2 antibody was prepared in antibody diluent 2 solution, and mouse anti-V5-Tag was prepared in 5% BSA. The RePlex Module was used to remove primary and secondary antibodies in a RePlex assay with total protein determination in a single run (cat. #RP-001). Total protein quantification was performed using the total protein detection module for chemiluminescence (cat. #DM-TP01).

rAAV generation

Gene synthesis, cloning, and production of rAAV vectors were carried out by the Viral Vector Production Unit from Universitat Autònoma de Barcelona (Barcelona, Spain). The construct designed for overexpressing isoform 4 of murine Msi2

(NP_001350124.1) was rAAV9-hDES-mMsi2-V5-T2A-Nanoluc. rAAV9-hDES-Nanoluc was used as a control. hDES refers to a human DESMIN promoter suitable for achieving gene expression in skeletal muscle (Pacak et al., 2008). The hDES-mMsi2-V5-T2A-Nanoluc construct was cloned into a pAAV plasmid containing the ITRs of the AAV9 genome. The resulting plasmid pAAV-hDES-mMsi2-V5-T2A-Nanoluc was used for AAV9 particle packaging. The sequence and description of the construct are shown in Supplementary Fig. 1. To generate the empty control rAAV9-hDES-Nanoluc, *Bam*HI restriction sites were used to remove mMsi2-V5-T2A. All construct detail requests can be addressed to the corresponding author.

Animal experimentation and rAAV administration

Homozygous transgenic HSA^{LR} (Mankodi et al., 2000) mice were provided by Prof. C. Thornton (University of Rochester Medical Center, Rochester, NY, USA). Mice with the same genetic background (Friend Virus B; FVB) obtained from The Jackson Laboratory were used as controls. For systemic expression, P2-P3 HSA^{LR} male pups were injected once in the temporal vein with 35 µl of rAAV diluted in PBS using a 31G insulin needle. 15 mice received rAAV9-hDES-mMsi2-V5-T2A-Nanoluc (Msi2) and 10 rAAV9-hDES-Nanoluc (hDES). In both cases, 5×10^{11} vg were administered per animal. FVB (n=8) and HSA^{LR} (n=8) mice of the same age were injected with PBS 1x as controls. Mice were sacrificed six weeks after injection, and quadriceps and gastrocnemius were harvested. Each muscle was divided into three parts, two were snap-frozen in liquid nitrogen for protein and RNA isolation, and the third was frozen in isopentane for histological analyses. Body weight was monitored weekly since they were weaned on day 21. For Msi2 and autophagic markers analyses, FVB and HSA^{LR} males of 1.5 and 4.5 months old were sacrificed, and quadriceps and gastrocnemius were harvested.

Forelimb grip strength test

The forelimb grip strength was measured on day 21 and before sacrifice, as previously described (Bargiela et al., 2019).

Histological analysis of mouse muscle samples

To quantify muscle fiber CSA, 10 µm-sections from gastrocnemius and quadriceps were obtained with a Leica CM 1510S cryostat. For muscle fiber CSA quantification, muscle sections were washed with PBS 1x and immunostained with Wheat Germ Agglutinin, Alexa Fluor™ 488 Conjugate (1:400, Biotium, Fremont, California, USA, 29022-1) for 20 min, washed three times with PBS 1x and finally mounted with VECTASHIELD® mounting medium containing DAPI (Vector Laboratories, London, UK, H-1200-10) to detect the nuclei. Images were taken in an LSM800 confocal microscope (Zeiss, Stuttgart, Germany) at 400x magnification. Around 5000 fibers were analyzed in each condition using Zeiss analysis software (ZEN).

Sections were stained with hematoxylin-eosin (H&E) and mounted with DPX (Sigma-Aldrich, San Luis, Missouri, USA, 06522) according to standard procedures to quantify central nuclei in muscle fibers. Images were taken at 100× magnification with a Leica DM2500 microscope. For central nuclei quantification, 500 fibers were analyzed in each mouse using ImageJ software (NIH).

In vivo bioluminescence imaging

Mice infected with Msi2 (n=4) or hDES, as control, (n=4) rAAV9, or administered PBS (n=3), as previously described, were injected intraperitoneally with 100 µl of 3.5 mM fluorofurimazine (Promega, Madison, Wisconsin, USA, CS320501) before sacrifice. Mice were anesthetized with isoflurane and 10 min post substrate injection, the animals were imaged every 5 min for 25 min at the IVIS Lumina X5 (Perkin Elmer, Waltham, Massachusetts, USA). Data analysis was performed by drawing regions of interest in the images taken at the peak of bioluminescence emission.

Modelization of the muscle fibers' cross-sectional area

A generalized linear mixed model (GLMM;(Pacak et al., 2008)) was fitted to the CSA of muscle fibers. Since this experiment consists of repeated measurements of subjects, a random effect term for each mouse was included in the model. Msi2-

infected groups were considered as the fixed-effects parameter. Moreover, the CSA data of muscle fibers have a skewness that deviates from the normal distribution; for this reason, it was assumed a gamma distribution for the response variable and a logarithmic link function so that the logarithm of the mean CSA is linearly connected to the predictors in the model. As the ultimate purpose was to evaluate the difference in muscle fiber area of each treatment group with respect to hDES, three hypothesis tests were performed on the basis of the coefficients of the GLMM model.

Blood assays

When animals were sacrificed, the blood was collected by cardiac puncture exsanguination, and the samples were analyzed by Laboratorios Montoro Botella (Valencia, Spain). White blood cell differential count (basophils, segmented cells, stab cells, eosinophils, and lymphocytes) and biochemistry parameters (creatinine, total cholesterol, glucose, triglycerides, amylase, alkaline phosphatase, alanine aminotransferase, aspartate aminotransferase, and total bilirubin) were analyzed in the different experimental conditions.

Statistical analyses

In all molecular studies, for comparison of mean data, all parameters were assumed to follow a normal distribution. The samples were compared using an unpaired *t*-test ($\alpha = 0.05$), applying Welch's correction when necessary or multiple Student´s t-test with Holm-Sidak correction for multiple comparisons. Sample size (n) is included in the captions.

The white blood differential cell count statistical analyses were performed by applying multivariate analysis of variance (MANOVA) with Tukey HSD post hoc test.

Two-tailed Binomial test ($\alpha = 0.05$) was used to compare the number of parameters with significant differences and no significant differences between PBS and hDES.

1.3. RESULTS

1.3.1. HSA^{LR} model mice do not reproduce the alteration of the MSI2-miR-7-autophagy axis described in DM1 patients.

Considering previously reported data (Bargiela et al., 2019; Sabater-Arcis et al., 2021), we hypothesized that dysregulation of the MSI2-miR-7-autophagy axis contributes to an imbalance between the synthesis and degradation of muscle proteins, thus leading to muscle atrophy and dysfunction. We first tested this hypothesis with the HSA^{LR} murine model of disease expressing 250 CTG repeats, which is widely used as it reproduces relevant disease phenotypes such as myotonia, centrally located nuclei in muscle fibers suggestive of an incomplete maturation of type 1 fibers in a DM1 context (Pisani et al., 2008), and alternative splicing defects (Crawford Parks et al., 2020; Mankodi et al., 2000) but shows weak or no muscle atrophy phenotypes (Crawford Parks et al., 2020; Mankodi et al., 2000). Therefore, Msi2 levels were analyzed in the quadriceps and gastrocnemius of age-matched HSA^{LR} and FVB controls of 1.5 and 4.5 months. The results showed that both protein and transcript Msi2 levels were similar among control and model mice independently of age (Fig R-1 A-C). Two Msi2 immunoreactive bands corresponding to Msi2 isoforms (31 and 35 kDa) were revealed by western blotting (Fig. R-1 A), whereas only one was detected by Jess Simple Western (Fig. R-1 B) due to the different composition of gels in capillaries, which makes the technique, although more precise and sensitive, with less resolution. Similar results were observed for miR-7 expression (Fig. R-1 D).

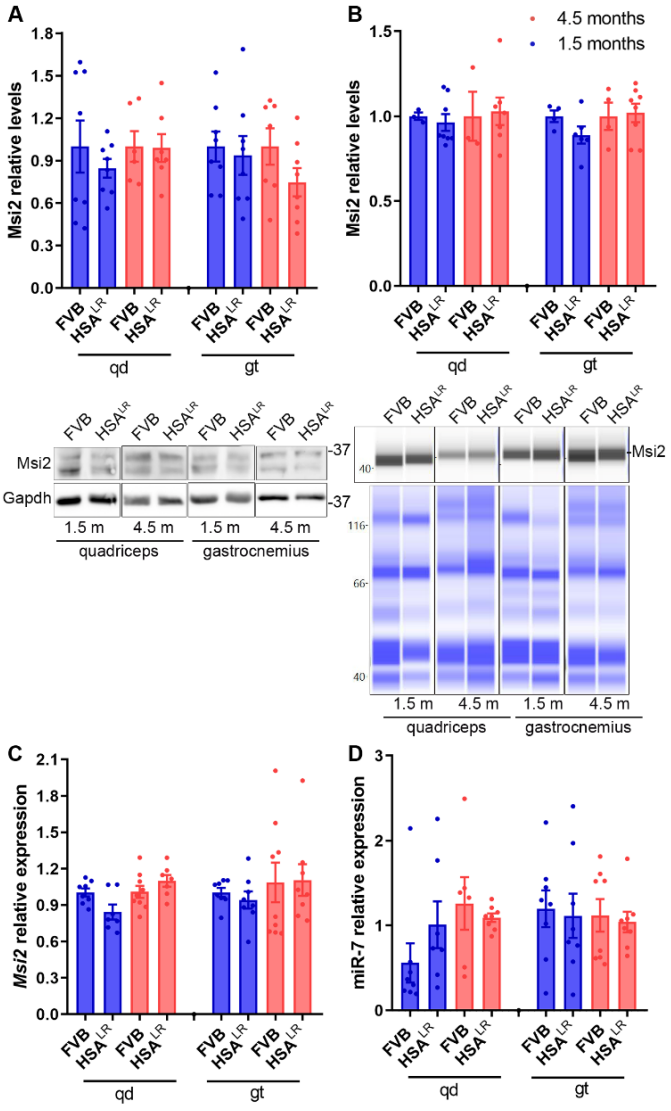
A
Msi2 relative levels
1.8
1.5
1.2
0.9
0.6
0.3
0.0
FVB
HSA LR
qd
gt
B
4.5 months
1.5 months
Msi2 relative levels
1.5
1.0
0.5
0.0
Msi2
Gapdh
37
1.5 m
4.5 m
quadriceps
gastrocnemius
116
66
40
C
Msi2 relative expression
2.1
1.8
1.5
1.2
0.9
0.6
0.3
0.0
D
miR-7 relative expression
3
2
1
0

Fig. R-1. Msi2 and miR-7 expressions were normal in HSA^{LR} model mice. (A) Quantification and representative western blots of total Msi2 in protein extracts obtained from control (FVB, n=6-8) and DM1 model mice (HSALR, n=6-8) at 1.5 (blue bars) and 4.5 (red bars) months of age. Determination was performed in the quadriceps (qd) and gastrocnemius (gt). Gapdh was used as an endogenous control. Molecular weight sizes are given in kDa. (B) Relative Msi2 protein was quantified using Jess Simple Western technology in the same samples as in (a). A representative lane view shows the bands (upper panel) observed. Msi2 signal was normalized to total protein (lower panel). (C) Quantification by RT-qPCR of the relative expression of c Msi2 (n=6-8) and (D)miR-7 (n=6-8) in the same samples as in a. miR-7 quantification was relative to endogenous U1. Msi2 was referenced to Gtf2b, Gapdh, and Hprt1 expression. At least three independent experiments were carried out, and three technical replicates were performed from each biological sample in b and d. The bar graphs show the mean ± SEM; no significant differences were detected between FVB and HSA^{LR} according to multiple Student´s t-test with Holm-Sidak correction for multiple comparisons.

Finally, it was confirmed that the model mice also did not reproduce the hyperactivated autophagy found in patients (Ozimski et al., 2021) by quantifying the levels of Atg7, which is a direct target of miR-7 (Gu et al., 2017), the LC3II/LC3I ratio and P62 proteins (Fig.R-2).

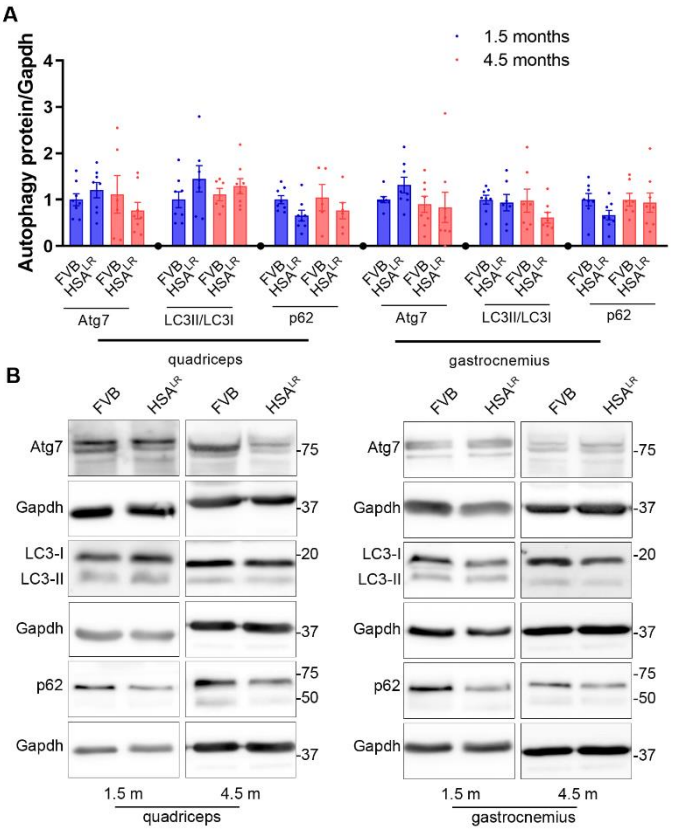

Figure R-2. HSA^{LR} mice do not reproduce excessive autophagy in skeletal muscle. (A) Quantification and (B) representative blots, with indication of molecular weight sizes to the right in kDa, of the immunodetection of total Msi2, LC3II/LC3I ratio, and total P62 protein in protein extracts obtained from control (FVB, n=6-8) and DM1 model mice (HSA^{LR}, n=6-8) at 1.5 (blue bars) and, 4.5 (red bars) months of age. Quantification was carried out in quadriceps and gastrocnemius. Gapdh was used as an endogenous control. The bar graphs show the mean ± SEM; no significant differences were detected between FVB and HSA^{LR} according to multiple Student´s t-test with Holm-Sidak correction for multiple comparisons.

1.3.2. rAAV-infected mice overexpress murine Msi2 in the skeletal muscle.

To demonstrate that Msi2 overexpression was sufficient to enhance disease-related muscle phenotypes, we overexpressed Msi2 in HSA^{LR} model mice. For that purpose, we generated recombinant adeno-associated virus (rAAV) particles encoding Msi2 under the control of the human DESMIN promoter (Fig. R-3). The recombinant adeno-associated viral serotype 9 (rAAV9) pseudotype was selected to ensure a broad and sustained expression of the transgene in skeletal muscle after intravenous injection (Muraine et al., 2020). Specifically, murine *Msi2* isoform 4 was chosen as it contains all described exons and its sequence is identical to the canonical isoform of MSI2 in humans.

Msi2 was fused to the V5 tag for subsequent immunodetection. Nanoluciferase (Nanoluc) reporter was also included, separated from Msi2 by a T2A linker, which induces ribosomal skipping during translation (Lewis et al., 2015), allowing both Msi2 and Nanoluc proteins to be synthesized from one transcript with two ORFs. This construct is hereafter referred to as Msi2. As a control, a similar construct was generated containing only Nanoluc controlled by the human DESMIN promoter. We will refer to this construct as hDES. We thus injected Msi2 or hDES rAAV9 in the temporal vein of P2-P3 HSA^{LR} pups and collected samples six weeks post-infection (Fig. R-4 A). As a procedural control, model mice were treated with PBS 1X.

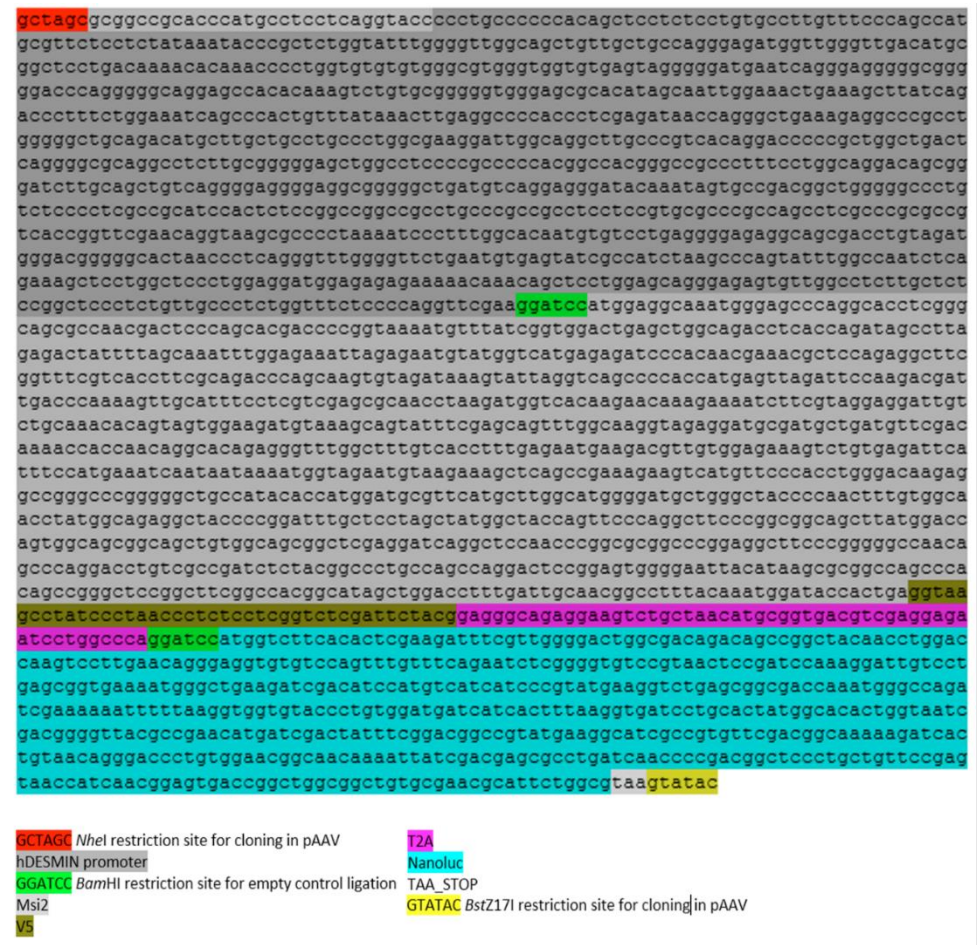

Fig. R-3. Sequence and description of the individual sequence elements used to generate the rAAV9-hDES-mMsi2-V5-T2A-Nanoluc construct.

Prior to euthanasia, the Nanoluc substrate, fluorofurimazine, was injected to generate bright bioluminescent imaging. This experiment confirmed that the transgene was expressed in skeletal muscle in hDES and Msi2-infected mice. As expected, no signal was detected in mice injected with PBS (Fig. R-4 B). The brightness generated by bioluminescence was quantified over time at 5-minute intervals, and no differences were detected between hDES and Msi2, confirming that rAAV expression was similar in both experimental groups (Fig. R-4 C).

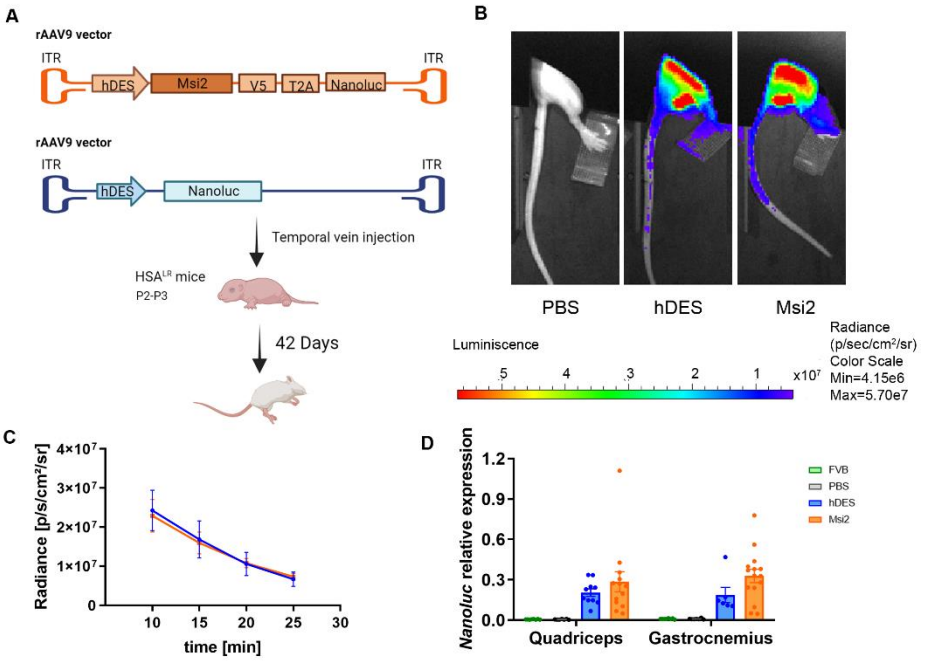

Fig. R-4. rAAV9 targets HSA^{LR} skeletal muscle. (A) Experimental design. Recombinant AAV serotype 9 expressing Msi2 (upper) and control constructs (lower) were injected intravenously in P2-P3 HSA^{LR} male pups. 42 days post-injection, mice were sacrificed, and quadriceps and gastrocnemius muscles were dissected. hDES: Human DESMIN promoter; mMsi2: murine Msi2 isoform 4; V5: V5-tag; Nanoluc: *nanoluc* transgene; ITR: inverted terminal repeat sequences of 145 bp in length. T2A: Linker to allow both Msi2 and Nanoluc expression under the control of the hDES promoter. (B) *In vivo* imaging after subcutaneous administration in HSA^{LR} mice treated with PBS (n=3), or rAAV9-hDES (n=4) or rAAV9-Msi2 (n=4). (C) Quantification of total maximum flux in Radiance of fluorofurimazine after intraperitoneal administration in Msi2 and hDES-treated mice. (D) Quantification by RT-qPCR of *Nanoluc* transgene expression in quadriceps and gastrocnemius of control mice (FVB, n=8), or HSA^{LR} treated with vehicle (PBS, n=8), rAAV9-hDES (n=10), or rAAV9-Msi2 (n=15) viruses. *Nanoluc* was normalized to *Gtf2b, Gapdh,* and *Hprt1* expression. At least three biological replicates were carried out in (C) and (D), and three technical replicates were performed from each biological sample in (D). Bars show the mean ± SEM. No significant differences were detected between hDES and Msi2 according to Student´s t-test.

These results were confirmed by quantification of *Nanoluc* transcripts in quadriceps

and gastrocnemius that evidenced similar expression of the reporter in both hDES and Msi2 groups (Fig. R-4 D). Blood serum was extracted from all experimental groups for biochemical analyses and white blood cell count. Importantly, no differences were observed in any of the parameters analyzed between the PBS and hDES groups, which rules out a deleterious effect linked to rAAV infection *per se*. Alkaline phosphatase (AP), alanine aminotransferase (ALT), aspartate aminotransferase (AST), and bilirubin levels are part of the biochemical determinations aimed at detecting hepatic affections (Lala et al., 2024). When comparing hDES vs. Msi2, it was observed that AP and bilirubin were increased in Msi2-transduced animals, ALT remained unchanged, while AST was decreased. Low levels of this enzyme are associated with vitamin B6 deficiency (ONO et al., 1995). Overall, the results suggest that Msi2 overexpression damages the liver, although the reduction in AST would require further testing before confirming liver disease. Additionally, it is important to note that AP levels have been shown to correlate positively with low muscle mass and have been proposed as a predictive marker of sarcopenia (J. H. Lee et al., 2021), while independent studies performed in patients with type 2 diabetes suggested a positive correlation between bilirubin levels and decreased skeletal muscle mass (Inoguchi et al., 2022). Finally, no significant changes were detected among the groups of interest in the white blood cell counts.

1.3.3. rAAV9-infected muscles express functional Msi2 protein.

Once confirmed that AAV targeted the skeletal muscles in infected model mice, we addressed Msi2 levels in the quadriceps and gastrocnemius six weeks after treatment. It was confirmed that Msi2 remained stable in model mice treated with PBS when compared to controls (FVB). Additionally, data showed that protein expression increased by about 2-fold in quadriceps and 4-fold in gastrocnemius compared to model mice infected with empty rAAV (hDES). These differences were also significant at the mRNA level (Fig. R-5 A-C). Unlike what was observed in other DM1 models or patients, we detected decreased *Msi2* transcripts in the quadriceps of model mice.

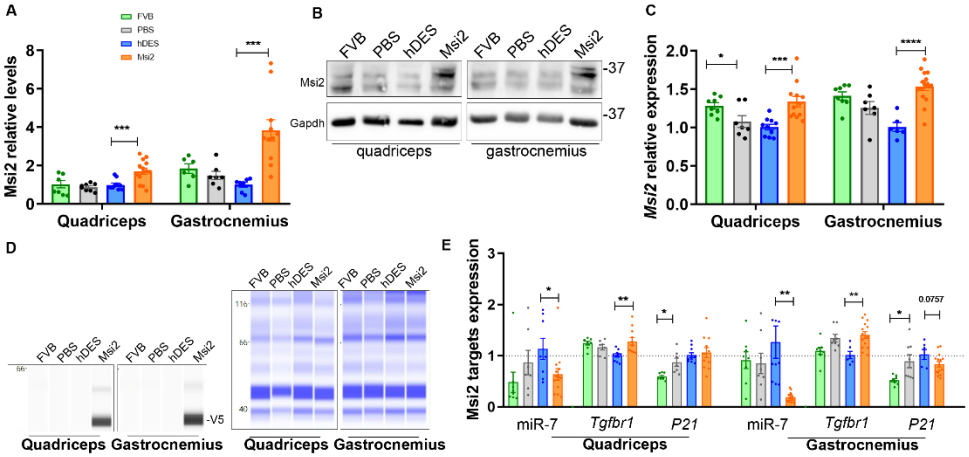

Fig. R-5. Msi2 is overexpressed in skeletal muscle upon rAAV9 infection. (A,B) Western blotting quantification and representative blots of Msi2 levels in quadriceps and gastrocnemius from control and neonate DM1 model mice injected with PBS (FVB and PBS), rAAV9-hDES or rAAV9-Msi2. Protein levels were normalized to Gapdh. (C) Quantification by RT-qPCR of the relative expression of *Msi2* in the same experimental groups as in a,b. (D) V5 protein was detected using Jess Simple Western technology. A representative lane view shows the bands immunodetected with an anti-V5 antibody (left panel) and total protein (right panel) used for internal normalization. (E) Msi2 targets: miR-7, *Tgfbr1*, and *P21* in the indicated biological groups. miR-7 quantification was normalized to endogenous *U1* levels and *Msi2, Tgfbr1*, and *P21,* were normalized to mean of *Gtf2b, Gapdh* and *Hprt1* expression. In all cases, relative levels were normalized to hDES samples. P values were calculated using Student´s t-test. In all cases comparisons were FVB vs. PBS and hDES vs. Msi2. Plots represent mean ± SEM. ∗p < 0.05, ∗∗p < 0.01, ∗∗∗p < 0.001, and ∗∗∗∗p < 0.0001. FVB (n=8), HSA^{LR} PBS (n=8), HSA^{LR} rAAV9-hDES (n=6-10) and HSA^{LR} rAAV9-Msi2 (n=13-15).

Overall, we observed that there were no significant differences between the PBS and hDES groups, so in this and subsequent experiments, the effect of Msi2 overexpression will be assessed by comparing Msi2 vs. hDES. Furthermore, after performing an overall analysis of the results obtained for the different parameters between the PBS and hDES groups, we confirmed that there was a significantly greater number of unchanged parameters between both conditions (p=0.0009 quadriceps; p=0.0041 gastrocnemius), thus supporting the conclusion that non-

specific effects by hDES were minoritarian. V5-tagged (rAAV-derived) Msi2 was immunodetected using Jess Simple Western technology (Fig. R-5 D), making Msi2-V5 expression in infected muscle fibers conspicuous.

Once overexpression was confirmed in Msi2-transduced mice, the protein's functionality was assessed by evaluating the expression of three MSI2 direct targets. We confirmed a 1.4-fold and 12-fold reduction in miR-7 levels in quadriceps and gastrocnemius, respectively, compared to the group treated with the empty vector, hDES (Choudhury et al., 2013). Additionally, we quantified *Tgfbr1* levels, as it was demonstrated to be regulated by MSI2 (Park et al., 2014) and also *P21* (also known as *Cdkn1a*), which, in contrast to *TGFBR1*, is inhibited by MSI2 (Zhou et al., 2020). *Tgfbr1* levels increased between 30 and 40% in both analyzed muscles, while *P21* levels remained unchanged upon sustained Msi2 expression (Fig. R-5 e).

The expression of the *HSA*^{LR} transgene was quantified in all animals involved in the experiment, denoting a great variability between muscles and animals (Fig. R-6). Notably, expression variability was much more evident in gastrocnemius, where differences between hDES and Msi2 groups were statistically significant.

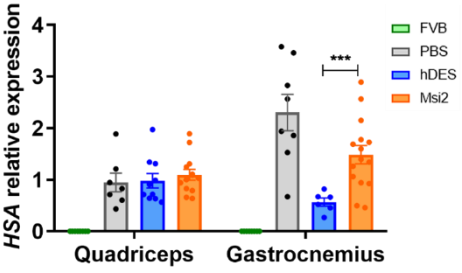

Fig. R-6. Msi2 overexpression does not affect *HSA* transgene expression. Quantification of the *HSA* transgene by RT-qPCR ($2^{-\Delta Ct}$) in quadriceps and gastrocnemius from control and P2-P3 DM1 model mice injected (i.v) with PBS (FVB and PBS, respectively), rAAV9-hDES-Nanoluc (hDES) or rAAV9-hDES-Msi2(V4)-V5-T2A-Nanoluc (Msi2). P values were calculated using Student´s t-test. Plots represent mean ± SEM, ***p < 0.001. FVB (n=8), HSA^{LR} PBS (n=8), HSA^{LR} rAAV9-hDES (n=6-10) and HSA^{LR} rAAV9-Msi2 (n=13-15).

1.3.4. Sustained Msi2 overexpression promotes autophagy independently of Mbnl, Celf1, and Hnrnpa1 proteins.

We analyzed by RT-qPCR the expression of genes related to autophagy, myogenesis, and muscle atrophy and differentiation (Fig. R-7 A-I). Globally, we observed that these markers were not impaired in HSA^{LR} model mice. These results partially explain the limited muscle dysfunction in HSA^{LR} mice. These data were fully consistent with previous works in which HSA^{LR} mice do not reproduce the pathological increase in autophagy reported in patients and different DM1 models (Bargiela et al., 2015; Morriss et al., 2018; Sabater-Arcis et al., 2021). However, upon Msi2 overexpression in skeletal muscle, we observed dysregulation of Atg4, Atg7, Atrogin 1, Mrf4, and LC3II/LC3I in both analyzed muscles, indicating that Msi2 was sufficient to change muscle gene expression towards disease-like patterns. However, the effect of Msi2 overexpression on other analysed markers was milder as dysregulation was detected in one of the two analyzed muscles. An exception was *Mstn*, which, besides being the only one of 9 genes altered in one of the muscles, did not change upon Msi2 overexpression (Fig. R-7 I). Consistently with our initial hypothesis, increased Msi2 expression in model mice was sufficient to activate autophagic flux as determined by the LC3II/LC3I ratio (Klionsky et al., 2016) (Fig. R-7 J,M). Additionally, we assessed levels of P62, a scaffold protein that carries cargoes committed to lysosomal degradation to the autophagosome. Increased autophagic activity leads to P62 reduction as it is removed by autophagy itself (Klionsky et al., 2016). A decrease in gastrocnemius of almost half was observed in model mice injected with rAAV-Msi2 compared to those treated with control construct hDES. However, no significant effect was detected in the quadriceps where, in fact, significantly lower P62 levels were detected (Fig. R-7 K,N). Finally, ATG7 levels were evaluated. This protein promotes phagophore growth by means of ATG8 lipidation through its E1-like enzymatic activity during the elongation and maturation steps of degradative autophagy (Klionsky et al., 2016). We observed in quadriceps from Msi2 infected mice an almost 2-fold increase in the expression of Atg7 when compared to the hDES group (Fig. R-7 L,O). Conversely, no effect was detected in gastrocnemius.

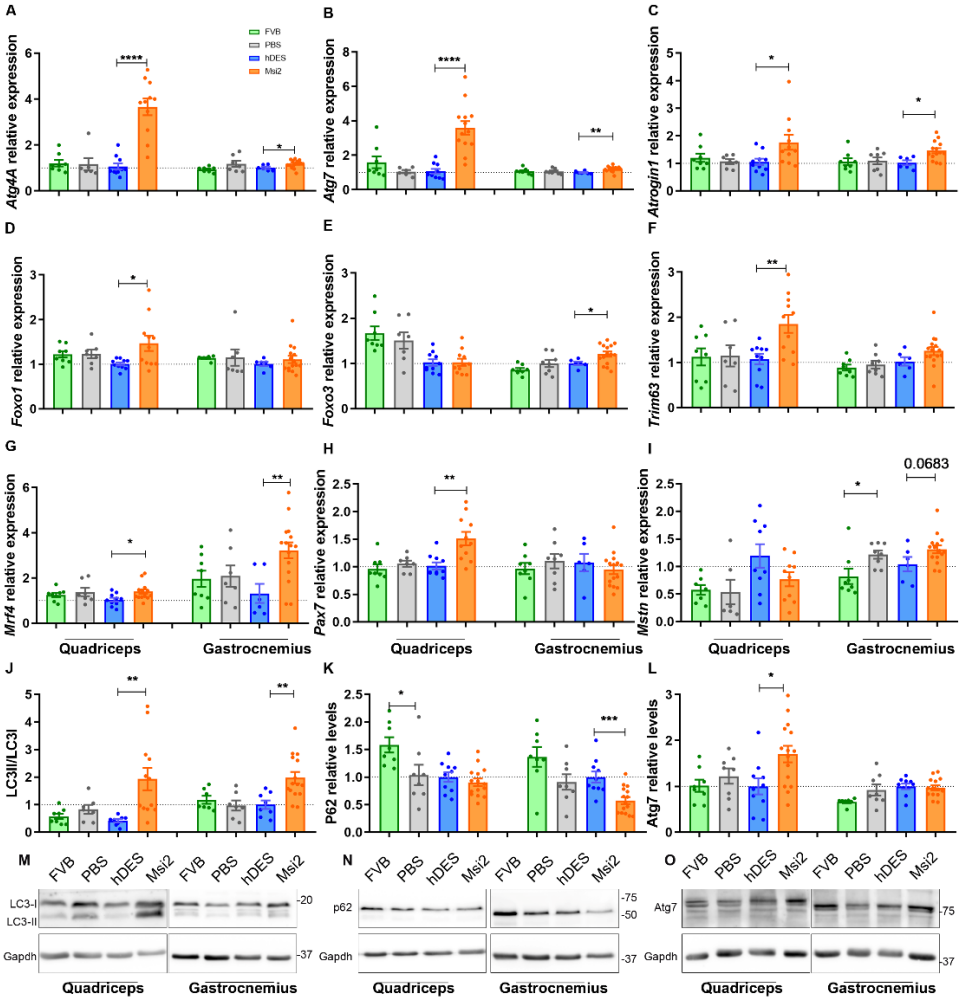

Fig. R-7. Msi2-overexpressing mice show altered muscle homeostasis gene expression. (A-I) Quantification by RT-qPCR ($2^{-\Delta\Delta Ct}$) of the indicated genes in samples obtained from quadriceps or gastrocnemius from control and model mice treated with PBS (FVB and PBS, respectively), rAAV9-hDES or with rAAV9-Msi2. All values are relative to hDES in each muscle (dashed line). Gene's expression is normalized to mean of *Gapdh*, *Gtf2b,* and *Hprt1* expression. (J-O) Relative quantification and representative western blots, with indication of molecular weight sizes to the right in kDa of the LC3-II/LC3-I ratio, P62, and Atg7 protein in protein extracts obtained from the same biological groups as in (A-J). Gapdh was used as an endogenous control. Plots represent mean ± SEM. ∗p < 0.05, ∗∗p < 0.01, ∗∗∗p < 0.001, and ∗∗∗∗p < 0.0001 according to Student´s t-test. In all cases comparisons were FVB vs. PBS and hDES vs. Msi2. FVB (n=8), HSA^{LR} PBS (n=8), HSA^{LR} rAAV9-hDES (n=6-10) and HSA^{LR} rAAV9-Msi2 (n=13-15).

To investigate whether Msi2 may contribute to the DM1 pathophysiology through already described splicing factors involved in the pathogenic mechanism of the disease, the levels of Mbnl1, Mbnl2, Celf1, and Hnrnpa1 were assessed upon AAV infection (Fig. R-8). Notably, no effect was detected upon Msi2 modulation in the total protein levels of none of the splicing factors compared to hDES controls, thus suggesting that the atrophy-promoting gene expression changes generated by increased Msi2 expression is independent of Mbnl, Celf1, and Hnrnpa1 protein level changes. In contrast, the results suggest that increased Msi2 expression's effects are mediated by the induction of proteins/genes involved in the ubiquitin-proteasome system and/or autophagy.

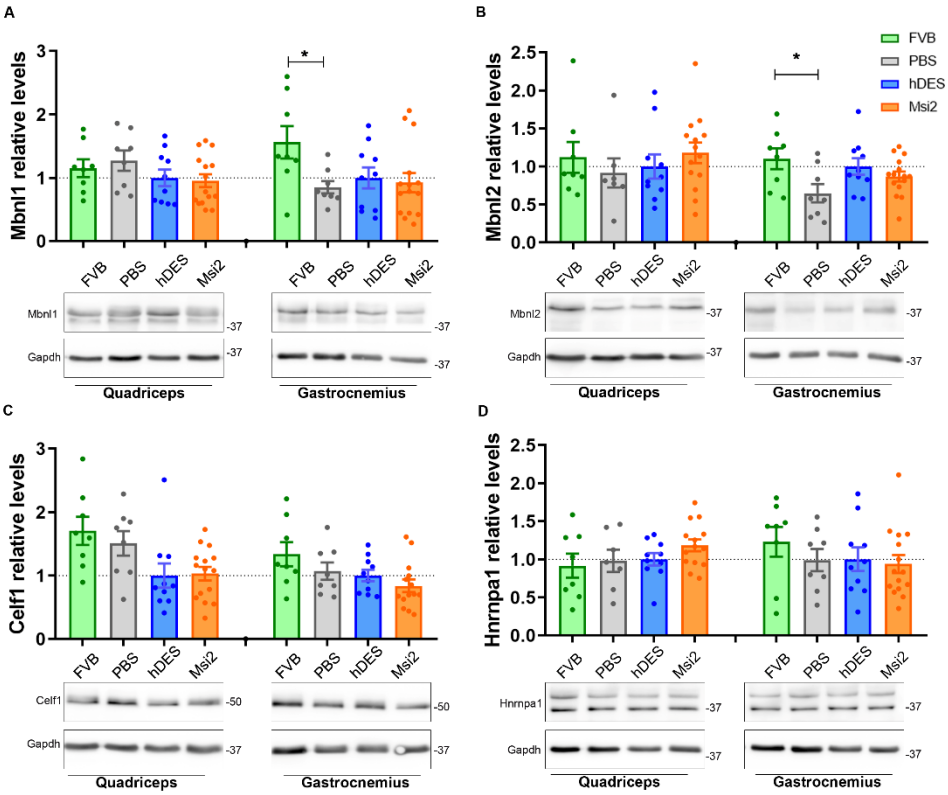

Fig. R-8. DM1 altered splicing factors remain unchanged upon rAAV-Msi2 overexpression. Relative protein expression levels in quadriceps and gastrocnemius of (A) Mbnl1, (B) Mbnl2, (C) Celf1, and (D) Hnrnpa1 in FVB and HSA^{LR} treated with PBS as vehicle or HSA^{LR} injected with empty rAAV9 as control (hDES) or rAAV9 expressing Msi2 (Msi2). Data was relative to hDES. Gapdh was the endogenous control. Plots represent mean ± SEM. No significant differences were detected according to Student´s t-test. In all cases comparisons were FVB vs. PBS and hDES vs. Msi2. FVB (n=8), HSA^{LR} PBS (n=8), HSA^{LR} rAAV9-hDES (n=6-10) and HSA^{LR} rAAV9-Msi2 (n=13-15).

1.3.5. Increased Msi2 expression causes myopathy in HSA^{LR} skeletal muscle and alters muscle histology.

After weaning, we functionally characterized the impact of Msi2 overexpression in a DM1 context. The body weight of the mice was measured at four time-points prior to euthanasia. The results showed no differences in weight between the model mice and the FVB controls, nor when comparing the Msi2-overexpressing mice with their hDES control (Fig. R-9 A).

Foreleg strength was measured and ratioed to each mouse's weight at 21 days old and prior to sacrifice. The results showed that at the first studied time point, there were no differences between different groups. These results are in line with those published by Wei et *al.* 2018, where authors reported that young HSA^{LR} mice of 1 month of age did not display grip weakness (C. Wei et al., 2018). However, in 42-day-old mice, a significant decrease in grip strength was observed in individuals infected with rAAV expressing Msi2 compared to those infected with empty rAAV as a control. Furthermore, since no differences in weight were observed at this age, the possibility that the lower relative strength of Msi2-overexpressing mice was due to lower body mass is ruled out (Fig. R-9 B). Strikingly, HSA^{LR} model mice at the indicated age showed more grip strength than FVB controls, contrary to what we observed at 4.5 months of age (Bargiela et al., 2019). Remarkably, we observed a significant negative correlation between Msi2 levels and foreleg force in quadriceps ($r= -0.57$, $p=0.04$) and gastrocnemius ($r= -0.56$, $p=0.03$) from mice overexpressing Msi2, highlighting

the relevance of Msi2 dysregulation contribution to the muscle phenotype (Fig. R-9 C).

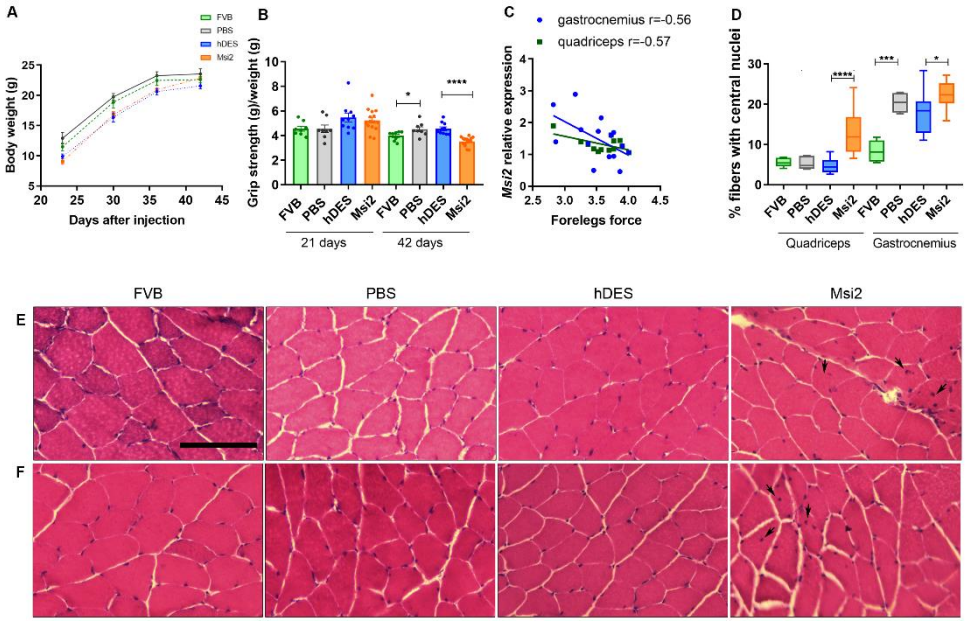

Fig. R-9. Msi2 overexpression enhances DM1-like phenotypes in HSA^{LR} mice. (A) Body weight measured at the indicated time points after the injection of age-matched controls and P2-P3 DM1 model mice treated with PBS (FVB and PBS, respectively), rAAV9-hDES, or rAAV9-Msi2. (B) Mice grip strength was normalized to body weight at the indicated intermediate time point and before the sacrifice in the same biological groups described in a. Plots represent mean±SEM. (C) Pearson's correlation between Msi2 relative expression and grip strength measured in rAAV9-Msi2 mice (D) Analysis of the percentage of muscle fibers with central nuclei in quadriceps and gastrocnemius of the indicated experimental condition. The boxplots show the median with the interquartile range with the minimum and maximum values. Representative hematoxylin and eosin staining of (E) quadriceps and (F) gastrocnemius from all experimental groups. Arrows point to examples of centrally located nuclei in muscle fibers. Scale bar=100 μm. $*p < 0.05$, $**p < 0.01$, $***p < 0.001$, and $****p < 0.0001$ according to Student´s t-test. In all cases comparisons were FVB vs. PBS and hDES vs. Msi2; FVB (n=8), HSA^{LR}PBS (n=8), HSA^{LR} rAAV9-hDES (n=10) and HSA^{LR} rAAV9-Msi2 (n=15).

Hematoxylin and eosin staining was performed on quadriceps and gastrocnemius cross-sections. The overexpression of Msi2 in adult DM1 skeletal muscle supports

the idea that it negatively impacts muscle histology (Fig. R-9 D-F). Indeed, quadriceps and gastrocnemius muscles from these mice displayed a significantly higher percentage of central nucleation of ~3 and 1.25 fold, respectively, compared with hDES, which is consistent with histological features of skeletal muscle biopsy in DM1 (Vihola et al., 2003). Notably, there were no histopathological features at this age in the quadriceps other than occasional central nuclei.

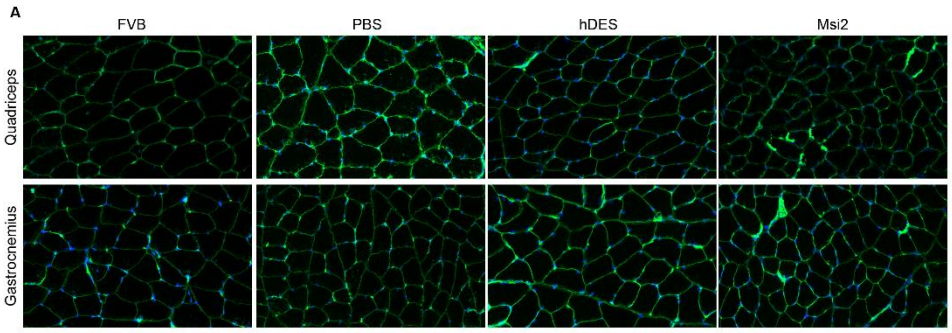

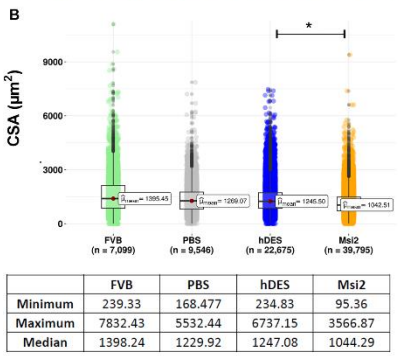

	FVB	PBS	hDES	Msi2
Minimum	239.33	168.477	234.83	95.36
Maximum	7832.43	5532.44	6737.15	3566.87
Median	1398.24	1229.92	1247.08	1044.29

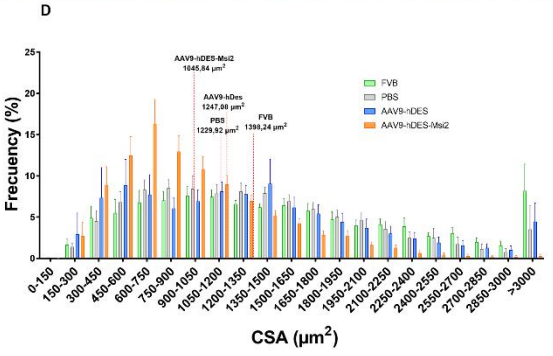

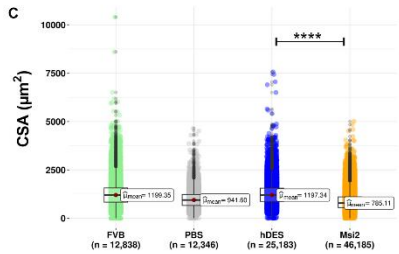

	FVB	PBS	hDES	Msi2
Minimum	228.65	156.08	195.44	90.15
Maximum	6465.51	4585.4	5703.65	3673.40
Median	1202.98	942.88	1197.61	785.34

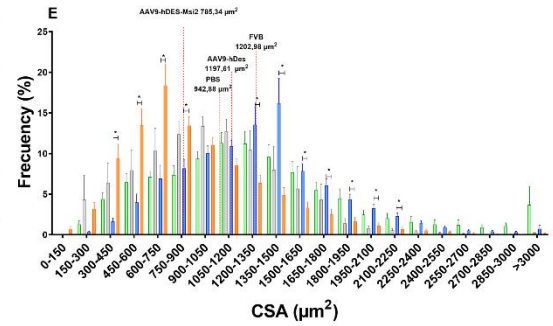

Fig. R-10 Msi2 overexpression reduces area of muscular fibers. (A) Representative confocal images of WGA-stained (green) quadriceps and gastrocnemius sections from control and DM1 model mice treated with PBS (FVB and PBS, respectively) or DM1 mice injected with rAAV9-hDES or rAAV9-Msi2. Nuclei were counterstained with DAPI (blue). Scale bar=50 μm. Quantification of the CSA of fibers from (B) quadriceps and (C) gastrocnemius muscles in the indicated biological groups. Tables indicate the minimum, maximum, and median values (in μm^2) of the area of the fibers in the indicated conditions. (C) quadriceps and (D) gastrocnemius fiber CSA (μm^2) displayed as a frequency distribution (% of total) of the same biological groups as in b, c. Values above the vertical dashed lines indicate the median area of each biological condition. Plots represent mean ± SEM. $*p < 0.05$, and $****p < 0.0001$ according to multiple Student´s t-test. In all cases comparisons were FVB vs. PBS and hDES vs. Msi2; FVB (n=6), HSA^{LR}, PBS (n=8), HSA^{LR} rAAV9-hDES (n=9) and HSA^{LR} rAAV9-Msi2 (n=13-14). The number of fibers analyzed (n) in each condition is shown in (B) and (C).

Additionally, WGA staining was performed in quadriceps and gastrocnemius sections from all the experimental groups to stain the plasma membrane necessary to measure muscle fibers' cross-sectional area (CSA) (Fig. R-10 A-C). No differences were detected between the CSA of control mice (FVB) and disease model mice (PBS), reinforcing the weak myopathic phenotype of the HSA^{LR} model. Sustained Msi2 overexpression led to a significant 20 and 30% decrease in CSA in quadriceps and gastrocnemius, respectively (Fig. R-10 B,C).

In agreement with these data, the frequency distribution of CSA showed an increased frequency of smaller fibers in mice overexpressing Msi2 concomitant with a decreased frequency of larger fibers when compared to DM1 model mice infected with the empty vector (Fig. R-10 D,E).

With this information, we performed a generalized linear mixed model assuming a gamma distribution of the area of the fibers (Fig. R-11). In this model, the logarithm of the mean of the fiber area is linearly adjusted to each treatment. The model also takes into account the different areas that have been measured in the same mouse. Therefore, a random effect associated with the mouse is also considered. No significant differences were detected in the fibers area of the quadriceps, although

a clear tendency to a reduction was observed in Msi2-expressing mice when compared to hDES (p=0.054; Table R-1 A). However, in gastrocnemius, a 30% reduction in the fibers´ area was detected (p<0.00001; Table R-1 B) concomitantly with decreased mean of the CSA.

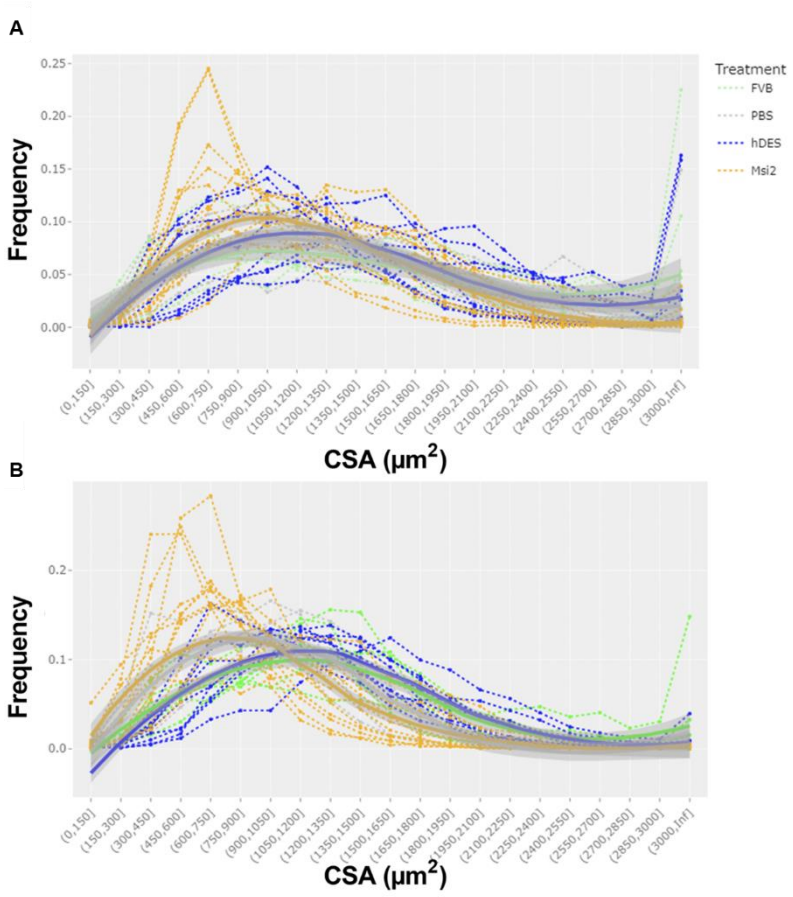

Fig. R-11. Msi2 overexpression leads to an increased frequency of smaller fibers. Distribution of myofibers size in (A) quadriceps and (B) gastrocnemius muscles of control and DM1 model mice treated with PBS (FVB and PBS, respectively) or DM1 mice injected with rAAV9-hDES-NAnoluc (hDES) or rAAV9-hDES-Msi2(V4)-V5)-T2A-Nanoluc (Msi2) FVB (n=6), HSA^{LR} PBS (n=8), HSA^{LR} AAV9-hDES (n=9) and HSA^{LR} AAV9-hDES-Msi2 (n=13-14).

A

Contrast <chr>	Estimation <dbl>	Estimated error <dbl>	Ratio <dbl>	Estimated error <dbl>	P value <dbl>
PBS - DES	-0.03721095	0.12302578	0.9634729	0.11853200	0.76229787
MSI - DES	-0.18500503	0.09612852	0.8311001	0.07989242	0.05428451
FVB - DES	0.08386255	0.11730871	1.0874794	0.12757081	0.47467848
MSI - PBS	-0.14779408	0.11547784	0.8626087	0.09961219	0.20059860
FVB - PBS	0.12107350	0.13339400	1.1287079	0.15056285	0.36406936

B

Contrast <chr>	Estimation <dbl>	Estimated error <dbl>	Ratio <dbl>	Estimated error <dbl>	P value <dbl>
PBS - DES	-0.26331121	0.10769759	0.7685027	0.08276588	0.01448871
MSI - DES	-0.35793357	0.07963391	0.6991195	0.05567362	0.00000697
FVB - DES	0.02652979	0.09635710	1.0268848	0.09894764	0.78306441
MSI - PBS	-0.09462236	0.10193525	0.9097164	0.09273217	0.35327299
FVB - PBS	0.28984100	0.11568718	1.3362150	0.15458295	0.01223180

Table R-1. Data obtained from the generalized linear mixed model (GLMM). GLMM for (A) quadriceps and (B) gastrocnemius**.** Estimation is the result of the pairwise comparisons of the mean muscle fiber areas for each treatment group extracted from the GLMM in the logarithmic scale and its estimated error in the following column. The ratio is the pairwise comparison of the estimation transformed into ratios as well as its error. The last column shows the p-value of the comparisons.

Altogether, our results show that sustained expression of Msi2 in an HSA^{LR} background is sufficient to boost functional and histological phenotypes that suggest increased myopathy.

1.4. DISCUSSION

Myotonic dystrophy type 1 is a multisystemic disease with multiple characteristic symptoms at molecular (insulin resistance, alternative splicing defects, or calcium homeostasis dysregulation), histological (fiber size variability and central nucleation), and functional levels (myotonia, muscle weakness, and atrophy) (Ozimski et al., 2021). The murine model HSA^{LR} displays myotonia and muscle

weakness, centrally located nuclei in muscle fibers, and alternative splicing impairment (Mankodi et al., 2000, 2002). However, its muscle atrophy phenotype is weak or absent, as reported here and independent studies (Bargiela et al., 2023; Crawford Parks et al., 2020).

Available data support that the increase in autophagy in DM1 contributes to the imbalance between protein synthesis and degradation, leading to the atrophic phenotype. Specifically, we hypothesize that the disease-associated upregulation of MSI2 leads to a defect in miR-7 biogenesis (Sabater-Arcis et al., 2020, 2021). This fact results in the derepression of autophagy mediated by the miR-7 decreased repressor activity on its targets, including ATG4, ATG7, and ULK2 (Gu et al., 2017). In this work, we described that Msi2 protein levels remain unaltered in model mice concomitantly with control-like levels of autophagy activation state. However, in DM1 myotubes and DM1-patient's biopsies, miR-7 and MSI2 dysregulation were confirmed concurrently with evident markers of muscle atrophy and increased protein degradation (Sabater-Arcis et al., 2020, 2021).

By means of AAV infection, we discovered that sustained overexpression of murine Msi2 promotes a progressive myopathy characterized by molecular, histological, and functional deficits. Overall, we report that the overexpression of Msi2 in HSA^{LR} skeletal muscles exacerbates dystrophic and atrophic features by inhibiting miR-7 biogenesis concomitantly with the activation of proteins and genes involved in the autophagic pathway. Thereby, Msi2 overexpressing mice recapitulate several histological abnormalities observed in the inducible CUG-960 model mice characterized by an overt muscle wasting phenotype accompanied by disruption of the balance between catabolic and anabolic pathways, including autophagy (Morriss et al., 2018). Furthermore, despite the variability observed, the data obtained indicate that overexpression of Msi2 in HSA^{LR} muscle induces significant histological modifications, characterized by smaller myofibers and increased central nucleation, leading to functional phenotypes such as weakened strength. At the molecular level, these phenotypes are accompanied by an increase of the

autophagic activity marked by an increase of ATG7 and LC3-II/LC3-I ratio and decreased P62 accompanied by an induction of atrogenes expression. These results agree with previous reports demonstrating the involvement of AMPK/mTORC1 deregulation in DM1 muscle pathophysiology in HSALR mice under fasting conditions and in aged individuals (Brockhoff et al., 2017). Msi2 enhanced muscle dysfunction in the HSA^{LR} mouse model, but the extent to which these phenotypes might be overexpression-only effects vs. DM1-dependent MSI2 overexpression effects could not be investigated because of lack of a Msi2 overexpression condition in the FVB genetic background.

Our results indicate that the pathological effect of Msi2 overexpression is independent of RNA-binding proteins well-known to be involved in disease pathogenesis, such as MBNL, CELF1, and HNRNPA1 (M. Li, Zhuang, et al., 2020). These results are in line with those previously published, evidencing that miR-7 (whose biogenesis is directly regulated by MSI2) supplementation in DM1 muscle cells restored DM1-like phenotypes in an MBNL-independent manner (Sabater-Arcis et al., 2020). However, in our previous work, we observed that targeting MSI2 through ASO gapmers in DM1 myotubes was sufficient to increase MBNL1 levels significantly (Sabater-Arcis et al., 2021), while in the current MSI2 upregulation was not sufficient to reduce MBNL1 levels *in vivo*. This suggests that either other factors contribute to the regulation of MBNL1 or that the levels of MSI2 overexpression achieved in our experiments are not high enough to reach autophagy levels that would have a significant impact on Mbnl1 degradation as it was reported that MBNL proteins were removed in an autophagy-dependent manner (Bargiela et al., 2019). These results explain that HSA^{LR} model mice do reproduce the splicing defects characteristic of the disease and the phenotypes associated with these alterations but, in contrast, lack myopathy because catabolic degradation of proteins is insufficient to induce muscle waste. Furthermore, results generated *in vitro* and *in vivo* models of the disease showed that CELF1 remains unchanged after both up- (Fig. R-8 C) and down-modulation of MSI2 (Sabater-Arcis et al., 2021). These data suggest that the MSI2>miR-7>autophagy axis contributes to the muscle atrophy phenotype

independently of the GSK3β/CELF1 pathway, which is dysregulated in DM1 and associated with muscle dysfunction (C. Wei et al., 2018). Increased CELF1 and HNRNPA1 are reported to exacerbate muscle dysfunction-related phenotypes in DM1 (M. Li, Zhuang, et al., 2020; Ward et al., 2010). However, both proteins remained stable after MSI2 modulation. Taken together, it is possible that if all three factors contribute independently/additively to the atrophic phenotype, the worsening observed in rAAV9-Msi2-infected HSA^{LR} mice is not as potent as it might be if Celf1 and Hnrnpa1 expression were simultaneously promoted.

A certain degree of variability in Msi2 overexpression can be observed in muscle tissues and, consequently, in analyzed phenotypes (Fig. R-5 E and R-7). Variability in the levels of the overexpressed protein and downstream effects are in line with those reported by Li et al. 2020(M. Li, Zhuang, et al., 2020), where the authors used rAAV9 to overexpress the splicing regulatory factor HNRNPA1 and observed variability in the results among the analysed muscles, including gastrocnemius, and quadriceps. The authors noted that transduced FVB control mice exhibited similar variability in protein expression across muscles compared to transduced HSALR mice. This variability suggests that rAAV-mediated overexpression fluctuates inherently between muscles and among individuals. Notably, rAAV9 demonstrates preferences for specific myofiber types, potentially influencing mosaic transduction patterns in skeletal muscle (Riaz et al., 2015). In this regard, it has been confirmed that HSA^{LR} mice exhibit impaired myofiber-type distribution compared to unaffected controls (Brockhoff et al., 2017). This fact will likely favor heterogeneity in AAV infection, resulting in a wider dispersion of the values obtained for the different parameters studied. Additionally, Fig. R-6 shows the considerable variability of the levels of CTG repeat-expressing transgene in HSA^{LR} model mice. Specifically, a significantly lower HSA^{LR} transgene expression in gastrocnemius in hDES mice suggests this muscle could be less sensitive to Msi2 levels because less toxic RNA is expressed. Consequently, we hypothesize that despite the higher Msi2 overexpression in gastrocnemius muscles, the lower additive effects by toxic RNA levels lead to somewhat reduced overall overexpression phenotypes. In contrast, in

quadriceps, where Msi2 levels relative to negative control hDES are lower than in gastrocnemius (1.7-fold vs. 3.8-fold, respectively), the opposite is true for toxic RNA amounts (Fig. R-5). Therefore, gene expression fluctuations stemming from the AAV overexpression method and the *HSA* transgene likely contribute to the variability observed in the results between muscles and animals. Overall, this issue has been addressed by conducting experiments with a sufficiently large number of individuals. A higher expression of Msi2 was detected in gastrocnemius concomitantly with a stronger reduction of miR-7 and CSA of the muscle fibers (Fig. R-5 and R-10). These results again support the association of MSI2 with the atrophic phenotype in a pathological context. We observed a negative correlation between force and Msi2 levels in mice injected with rAAV-Msi2 (Fig. R-9 c). Interestingly, we have reported a similar relationship between MSI2 and ankle dorsiflexion strength in DM1 patients (Sabater-Arcis et al., 2021). Morriss et al. 2018 characterized muscle atrophy in CUG_{960} mice, and as with HSA^{LR} overexpressing Msi2, the difference in muscle fiber size was more evident in smaller muscle fibers and the gastrocnemius than in the quadriceps (Morriss et al., 2018). However, our results suggest that more factors contribute to this phenomenon as, overall, the enhancement of DM1-like was globally significant, but the potentiation of the pathological phenotypes was variable. It is also possible that further overexpression is necessary to induce stronger phenotypes.

In summary, our findings furnish compelling *in vivo* evidence demonstrating the association of levels of Msi2 overexpression with the progressive muscle degeneration observed in DM1. Thus, we propose a new axis: MSI2>miR-7>autophagy that contributes to the muscle atrophy phenotype together with other signaling cascades that were reported to contribute to DM1 muscle atrophy, including AKT/ GSK3β (C. Wei et al., 2018), TWEAK/Fn14 (Yadava et al., 2015), AMPK (Brockhoff et al., 2017), or PKC (Kuyumcu-Martinez et al., 2007). Altogether, the MSI2>miR-7>autophagy axis could be explored as a novel target for therapeutic intervention.

CHAPTER 2:

MIR-107 SEQUESTRATION BY CUG REPEATS TRIGGERS THE MSI2/MIR-7 PATHOGENESIS AXIS IN MYOTONIC DYSTROPHY.

2.1. BACKGROUND

Myotonic dystrophy type 1 (DM1) is an autosomal dominant genetic disorder characterized by a broad spectrum of multisystem manifestations. These encompass myotonia, muscle weakness, cardiac abnormalities, and cognitive deficits (André et al., 2018; Bartolomé et al., 2022; Hamel, 2022). The disease arises from the expansion of unstable trinucleotide (CTG) repeats in the 3' untranslated region (3' UTR) of the *DM1 protein kinase gene* (*DMPK*) (Brook et al., 1992). The expanded CUG repeats initiate a pathological cascade by sequestering RNA-binding proteins from the Muscleblind-Like Splicing Regulator (MBNL) family. MBNL1 and MBNL2 proteins play a crucial role in post-transcriptional regulation, including alternative splicing, polyadenylation, miRNA biogenesis, and mRNA stability (Holt et al., 2009; Taylor et al., 2018). In addition, the pathophysiology of DM1 is enhanced by dysregulation of CUGBP Elav-like family member 1 (CELF1), a splicing factor antagonistic to MBNL that is stabilized in DM1 due to its hyperphosphorylation by protein kinase C (Cox et al., 2020). Altogether, MBNL sequestration by ribonuclear foci and CELF1 stabilization contribute to alternative splicing disruption (Chau & Kalsotra, 2015; Holt et al., 2007; Konieczny et al., 2014). Dysfunctional autophagy and ubiquitin-proteasome activity, coupled with AMPK downregulation, disruption of the AKT/FOXO signalling pathway and GSK3β activation, further contribute to the muscle pathology characteristic in DM1 patients (Ozimski et al., 2021).

MicroRNAs are a class of small non-coding RNAs critical for post-transcriptional gene regulation. These molecules bind to the 3' UTR of target mRNAs, thereby modulating their stability and translation (O'Brien et al., 2018; Saliminejad et al., 2019). Recent research has underscored the pivotal role of microRNA-mediated post-transcriptional regulation in shaping the molecular landscape of DM1. Notably, miR-23b and miR-218 negatively regulate MBNL1 and 2 protein synthesis (Cerro-Herreros et al., 2018, 2020, 2021), miR-206 is involved in muscle maturation (W. Dong et al., 2019), miR-16 colocalizes with *DMPK* ribonuclear foci (Koscianska et al., 2015), and miR-322/-503 with a seed region complementary to CUG repeats, was

proved to directly and specifically target the expanded CUG repeats in the DM1 cells. Ectopic expression of miR-322/-503 in DM1 muscle cells leads to significant improvements in myoblast differentiation and repression of ribonuclear foci formation and aberrant alternative splicing (Shen et al., 2020).

In recent years, autophagy, the cellular process responsible for degrading and recycling cellular components, has emerged as a critical pathway implicated in muscular disorders and has highlighted its importance in maintaining muscle homeostasis and addressing atrophy-related pathways in DM1 (Bargiela et al., 2015, 2019; Franco-Romero & Sandri, 2021; Ozimski et al., 2021; Sabater-Arcis et al., 2020). miR-7 is a repressor of autophagy (Gu et al., 2017) and its biogenesis is regulated by Musashi homolog 2 (MSI2) and HuR antigen (HuR). MSI2, an RNA-binding protein, binds through HuR to the terminal loop of pri-mir-7-1, inhibiting the biosynthesis of the mature form of the miRNA (Choudhury et al., 2013; Kumar et al., 2017). MSI2 is an alternative splicing factor and mRNA translational and stability regulator (Cragle et al., 2019; Matalkah et al., 2022). In DM1, the increased expression of MSI2 triggers the MSI2>miR-7>autophagy axis, contributing to dysregulated autophagy and muscular atrophy in DM1 (Sabater-Arcis et al., 2021, 2023). Notably, MSI2 is upregulated in DM1 muscle cells and biopsies, and upon restoration of its levels, a rescue was observed in miR-7 and atrophy-related gene expression within the UPS system autophagy markers (Sabater-Arcis et al., 2021). Additionally, experimental induction of DM1-like phenotypes was observed upon AAV-mediated overexpression of murine Msi2 in skeletal muscle in neonatal HSA^{LR} mice. This overexpression prompted autophagic flux, altered the expression of critical autophagy proteins, and led to increased central nuclei, diminished myofiber area, and compromised muscle strength (Sabater-Arcis et al., 2023).

MSI2 is directly regulated by miR-107 (P. Dong et al., 2017). Indeed, the miRNA family of miR-107, which consists of miR-15/-107/-16, has garnered attention due to its potential implications in DM1. Earlier research has evidenced that *DMPK* is directly

regulated by miR-206, miR-148a, and miR-16. Thus, other miR-107 family members may also modulate the disease pathology (Koscianska et al., 2015).

This study aimed to elucidate the causes leading to MSI2 overexpression in DM1. We hypothesized that it could be due to miR-107 sequestration by the expanded CUG repeats in the *DMPK* mutant transcripts. Thus, miR-107 would be deprived of its normal regulatory function, leading to the derepression of MSI2 in a DM1 context. Understanding the regulatory interplay between mutant *DMPK*, miR-107, and MSI2 is vital in understanding the autophagic dysregulation and resultant muscle atrophy observed in DM1.

2.2. MATERIALS AND METHODS

miR-107 targets analyses

Available transcriptomics analyses of immortalized control and DM1 TDMs (Arandel et al., 2017, p. 20) of 4 and 8 days of differentiation (Bargiela et al., 2019; Overby et al., 2023) were reanalyzed. These data have been deposited in the Gene Expression Omnibus database (accession nº. GSE173359 and GSE128844). Differential gene expression (DEG) analysis was performed using the R package edgeR with the cut points of a log2 fold change of 1 and an adjusted p-value under 0.05. Then, the DEGs were searched for potential hsa-miR-107 targets using the gene-target database mirTarbase (Hsu et al., 2011; Huang et al., 2022). A similar DEG and miR-107 target analysis was performed in the control and DM1 patient's tibialis biopsies RNAseq data available at DMseq.org (E. T. Wang et al., 2019), with the same cutting points used for the cell culture.

Cell culture and transfection

TDM and immortalized myoblast were obtained from the Institute of Myology, Paris (Arandel et al., 2017). Cells were cultured as previously described (Arandel et al., 2017; Sabater-Arcis et al., 2020). Moreover, three different immortalized CRISPR-edited myoblast lines (derived from the DM1 immortalized myoblast) were also

used: 4F9 (2,600 CTG) as CRISPR control, 3B1Δ/Δ and 4A3Δ/Δ, having the deletion of CTG in both alleles (Agtmaal et al., 2017). Cells were transfected after 4 days in differentiation medium (MDM) with agomiR-107 using Lipofectamine RNAiMAX transfection reagent (Invitrogen; Spain) following the manufacturer's recommendations to final concentrations ranging from 0.25 to 1000 nM depending on the experiment. After 48 h, the medium containing the agomiR was replaced by fresh MDM. HEK 293T cells were cultured as described in (Koscianska et al., 2015).

Oligonucleotides

Oligonucleotides used where:

miR-107 sense strand: 5'-AGCAGCAUUGUACAGGGCUAUCA-3'

miR-107 antisense strand:

5'-$_{m}$U*$_{m}$G*$_{m}$A$_{m}$U$_{m}$A$_{m}$G$_{m}$C$_{m}$C$_{m}$C$_{m}$U$_{m}$G$_{m}$U$_{m}$A$_{m}$C$_{m}$A$_{m}$A$_{m}$U$_{m}$G$_{m}$C$_{m}$U*$_{m}$G*$_{m}$C*$_{m}$U*-3'-chol,

where "m" denotes 2'-Ome RNA, * phosphorothioate internucleoside linkages, and "chol" denotes a cholesterol group.

The hybridization of both strands was made by mixing them in equal concentrations. The mix was heated to 95 °C for 2 min and slowly cooled to room temperature.

Control RNA (cRNA) for EMSA assay was:

5'-UUCUCCGAACUUCUGACUUUG-3' (cRNA).

The oligonucleotides were synthesized by Biomers (Ulm, Germany).

Cell fraction, miRNA isolation, and RNA-seq bioinformatics analyses

Immortalized DM1 and CNT myoblast (Arandel et al., 2017) differentiated for 5 to 8 days, were harvested for RNA isolation, and were fractioned into nucleus and cytoplasms using a PARIS kit (Invitrogen) until the step in which both sub-cellular fractions were separated, followed by subsequently miRNAs isolation using

miRNeasy Mini Kit (Qiagen; Hilden, Germany). miRNA-enriched RNA was sent to the Oxford Genomics Centre for sequencing. For miRNA sequencing, cDNA libraries were prepared using a TruSeq Small RNA Library Preparation Kit (Illumina) following the manufacturer's instructions. Sequencing was performed using rapid mode in a HiSeq 2500 System (Illumina).

The total RNA was ribodepleted, and this fraction was converted to cDNA. A second strand cDNA synthesis incorporated dUTP. Then, the cDNA was end-repaired, A-tailed, and adapter-ligated. Prior to amplification, samples underwent uridine digestion, and prepared libraries were size-selected, multiplexed, and quality-checked before sequencing. Pair-end sequencing was performed in a HiSeq 4000 System (Illumina).

Single-end reads from the miRNA library were cleaned from adaptors using Trimmomatic (Bolger et al., 2014), and quality was checked with the FastQC application to remove those reads with low-quality values from the dataset (Phred score threshold below 20). Follow-up analyses were computed through webserver sRNAtoolbox (Aparicio-Puerta et al., 2022), including reads assembling, reads mapping on human GRCh38_p12 reference genome, reads annotation based on miRBase reference database, and reads count. Differential expression analyses were carried out in DEseq2. These data have been deposited in the Gene Expression Omnibus (GEO) database (accession nº. GSE262164).

Toxicity assay

DM1 TDMs were seeded in 96-well plates with 1.0×10^4 cells per well. Cells were transfected with increasing agomiR-107 concentrations (from 1 nM to 1 μM) per quadruplicate. To measure cell viability, 20 μl of MTS/PMS (CellTiter 96® AQueous Non-Radioactive Cell Proliferation Assay, Promega; Madison, WI, USA) was added to each well after 7 days of differentiation. The mix contained 100 μl of MDM and was incubated for 4 h at 37ºC in a humidified chamber with 5% CO2. Absorbance at 490 nm was measured using an Infinite 200 PRO plate reader (Tecan Life Sciences;

Männedorf, Switzerland). Data were transformed to a survival percentage relative to cells not exposed to agomiR, which was considered 100% viability. TC_{50} was obtained using the least-squares non-linear regression model.

Luciferase reporter assay

HEK293 cells were seeded at 60,000 cells per well in p24 plates. After 24 h, cells were transfected with 0.5 µg/ml of the pmiR-GLO plasmid containing varying CTG repeat numbers (0, 5, 44, 53, and 72) and agomiR at a concentration of 100 nM. Additionally, to eliminate CTG repeats and establish a negative control, the pmiR-GLO plasmid with 72 CUG repeats was digested with *Dra*I and *Xba*I restriction enzymes and subsequently purified. Cells were harvested at 72 and 96 h following the Dual-Luciferase® Reporter Assay System protocol (E1960, Promega; Madison, WI, USA). Luciferase activity was measured using a plate reader (Tecan 200 Infinity Pro) with technical quadruplicates. Analysis was performed by normalizing firefly luciferase activity to *Renilla* luciferase.

Electrophoretic Mobility Shift Assays (EMSA)

The mixtures of RNA (CUG_{20}) and miR-107 or cRNA at different ratios in Tris buffer (Tris 10 mM, NaCl 100 mM, pH 7.4) were incubated for 1 h at RT and loaded onto a native 16% polyacrylamide mini-gel in 1X TBE. The gels were run for 90 min at 120 V and stained with Sybr Green (1:100). The bands were displayed and quantified with a G800 BIORAD™ densitometer and analysis software. The concentration of CUG_{20} was confirmed by UV-Vis, considering the extinction coefficient provided by the manufacturer. Prior to the experiments, CUG_{20} RNA was denatured at 95 °C for 10 min and was left cool to room temperature overnight to form secondary structures.

RNA isolation and RT-qPCR

We seeded $1x10^6$ cells per replicate in Petri plates. RNA was isolated using the miRNeasy mini kit (QIAGEN; Hilden, Germany) according to the manufacturer's instructions. 1 µg of RNA was digested with DNase I (Invitrogen) and reverse-

transcribed with SuperScript II (Invitrogen) using random hexanucleotides. RT-qPCR was performed using 5× HOT FIREPol EvaGreen qPCR mix plus (ROX) (Solis BioDyne) and the following primers: GAPDH (fwd CATCTTCCAGGAGCGAGATC; rev GTTCACACCCATGACGAACAT), GPI (fwd CAGGGCATCATCTGGGACAT; rev TCTTAGCCAGCTGCTTTCCC) and MSI2 (fwd GCAGACCTCACCAGATAGCCTT; rev AAGCCTCTGGAGCGTTTCGTAG). *DMPK* (FAM-labeled probe) quantification was normalized by *GAPDH* (MAX-labeled probes). The sequence of primers and probe (acquired from Integrated DNA Technologies, Leuven, Belgium) for *DMPK* quantification were: fwd AGCCTGAGCCGGGAGATG; rev GCGTAGTTGACTGGCGAAGTT; and probe AGGCCATCCGCACGGACAACC and primers for *GAPDH* were: fwd CAACGGATTTGGTCGTATTGG; rev TGATGGCAACAATATCCACTTTACC; and probe CGCCTGGTCACCAGGGCTGCT. miR-7 and miR-107 expressions were quantified using specific miRCURY™-locked nucleic acid microRNA PCR primers (Exiqon). Relative gene expression was normalized to U1 or U6 small nuclear RNAs (snRNAs). mRNA and miRNA levels were assessed with Applied Biosystems QuantStudio 5 and 3 Real-Time PCR Systems and quantification used the delta-delta Ct method ($2^{-\Delta\Delta Ct}$).

Western blot

To extract total protein, 1 × 10^6 cells were sonicated in radioimmunoprecipitation assay (RIPA) buffer supplemented with protease and phosphatase inhibitor cocktails (Roche Applied Science). The total protein content was quantified spectrophotometrically at 562 nm using the Pierce™ BCA protein assay kit (Thermo Fisher Scientific; Grand Island, NY, USA) with Bovine Serum Albumin (BSA) as the protein standard. Subsequently, 20-30 µg of protein samples underwent denaturation at 100 °C for 5 min, followed by electrophoresis on 12% SDS-PAGE gels and transfer onto 0.45 µm nitrocellulose membranes (GE Healthcare). All the primary antibodies were used with 5% non-fat dried milk in PBS-T (PBS 1X containing 0.05% Tween 20) as blocking buffer except for ATG7, which needs to be blocked with 5% BSA in PBS-T (PBS 1X containing 0.05% Tween 20). The antibodies comprised

rabbit anti-ATG4A (1:1,000, D62C10, Cell Signaling Technology; Danvers, MA, USA), rabbit anti-MSI2 antibody (1:1,000, EP1305Y; Abcam; Cambridge, UK), rabbit anti-ATG7 (1:1,000, D12B11, Cell Signaling Technology; Danvers, MA, USA), mouse anti-SQSTM1 (1:1,000, 2C11 Abcam), and mouse anti-DMPK (1:200, MANDM5 5G12; DSHB). Blocking of the membranes was performed by immersion in a solution of 5% non-fat dried milk in PBS-T (0.05% Tween 20) for 1 h, except for the ATG7 antibody, which underwent incubation in 5% BSA. The membranes were incubated overnight at 4ºC in a 5% blocking solution containing primary antibodies at appropriate dilutions. The visualization of immunoreactive bands was achieved using the Signal™ West Pico PLUS Chemiluminescent Substrate (Thermo Fisher Scientific; Grand Island, NY, USA), and subsequent imaging was performed using an Amersham ImageQuant 800 system (GE Healthcare; Pittsburgh, PA, USA). Quantitative analysis of the obtained images was conducted using ImageJ (NIH) software.

Differential Scanning Fluorimetry (DSF)

For the DSF analysis (T. Wu et al., 2023), we utilized the StepOnePlus Real-Time PCR (Life Technologies) along with the melting curve software. The sample volume for each run was 50 µl. In this experiment, we incorporated the RiboGreen dye at a final concentration of 300 nM. Additionally, we employed synthetic double-stranded CUG RNA (CUG_{20}) and CGA RNA (CGA_{20}) as an unstructured control, both acquired at IDT (Integrated DNA Technologies, Leuven, Belgium) and used at a final concentration of 600 nM. To maintain the integrity of the RNA, we used a sodium cacodylate buffer with a pH of 6.5. The study encompassed 17 concentrations (ranging from 0.25 nM to 1 µM) of the miR-107 sense strand with technical triplicates.

Ribonuclear foci and MBNL1 detection

Fibroblasts were seeded into 96 and 24-well plates, and after agomiR-107 treatment, cells were fixed in 4% PFA for 15 min at room temperature (RT), followed by washes in 1× PBS. Foci detection was made as described in (Sabater-Arcis et al., 2020) using an IN-cell analyzer 2200 imaging system. In *situ* detection of CUG

repeats and MBNL1 immunofluorescence was performed in 24-well plates. A permeabilization step with PBS-T (0.3% Triton X-100) was followed by a blocking step for 30 min using a blocking buffer composed of PBS-T supplemented with 1% normal goat serum. Anti-MBNL1 antibody (1:100, MB1a(4A8), DSHB) and incubated overnight at 4°C followed by three washes with PBS-T 1X 0.3% Triton. A highly cross-absorbed anti-mouse secondary antibody Alexa Fluor™ Plus 488 (Thermo Fisher Scientific; Grand Island, NY, USA) was then applied at a dilution of 1:100 and incubated for 1.5 h at RT. Cells were washed with SSC UltraPure™ buffer diluted 2x (Thermo Fisher Scientific; Grand Island, NY, USA) supplemented with 30% formamide for 10 min at RT. Subsequently, Cy3-(CAG)7-Cy3 labeled probe, diluted at 1:100, was added to cells in hybridization buffer (8 ml Formamide, 2 ml SSC UltraPure™ 20X, 4 ml BSA 1% in PBS, 2 g Dextran Sulfate, 2 ml tRNA (10 mg/ml), 2 ml Vanadil Complex, 2 ml Herring Sperm) and incubated in a humid chamber at 37 °C for 2 h. Afterward, a double wash with 2x dilution of SSC UltraPure™ (Thermo Fisher Scientific; Grand Island, NY, USA) with 30% formamide at 45 °C for 15 min each was performed, followed by a triple wash with filtered PBS 1X for 10 min each at RT. Finally, samples were mounted using VECTASHIELD medium containing DAPI (Vector Laboratories; London, UK) and imaged in an LSM 800 confocal microscope (Zeiss; Jena, Germany). MBNL1 and foci colocalization were quantified using ZEN, a Zeiss software analysis tool.

Immunofluorescence methods.

To carry out immunodetection of Desmin, TDMs and immortalized myoblast were seeded in 24-well plates, treated with agomiR-107, and differentiated for 7 days. Cells were fixed with 4% PFA for 15 min at RT and were processed using mouse anti-DESMIN (1:50, D33, Abcam; Cambridge, UK), biotin-conjugated anti-mouse-IgG (1:200, Sigma-Aldrich, St. Louis, MO, USA) and streptavidin-FITC (1:200, Vector). Images were taken with an LSM800 confocal microscope (Zeiss, Jena, Germany). The fusion index was defined as the percentage of nuclei within myotubes (>2 myonuclei) out of the total number of nuclei in each condition. Myotube diameters

were measured at 5 points along the entire tube. Quantification was performed using ImageJ software (NIH).

For LysoTracker staining, a 24-well plate was seeded, and a miR-107 mimic was used (100 and 300 μM) to treat cells. Samples were incubated with 100 nM LysoTracker RED-DND99 (Invitrogen, Madrid, Spain) at 37 °C for 30 min. After two washes with warmed PBS, cells were fixed with 4% PFA for 15 min, followed by additional washes in 1× PBS. Subsequently, cells were mounted using Vectashield (Vector Laboratories, London, UK) containing 2 μg/mL DAPI. Micrographs were acquired using an LSM800 confocal microscope (Zeiss, Jena, Germany).

Statistical analyses

In all molecular studies, for comparison of mean data, all parameters were assumed to follow a normal distribution. The experiments with two conditions were compared using a Student's t-test ($\alpha = 0.05$), applying Welch's correction when necessary. For comparisons of more conditions, one-way ANOVA ($\alpha = 0.05$) and Tukey's HSD post hoc test were employed when necessary. Two-way ANOVA ($\alpha = 0.05$) was used to compare the differences when there are two variables, followed by Tukey's multiple comparison test.

2.3. RESULTS

2.3.1. miR-107 function is depleted in DM1.

Considering previous works (W. Dong et al., 2019; Koscianska et al., 2015; Shen et al., 2020) and bioinformatics predictions in miRWalk (Sticht et al., 2018) and TarBase-v9.0 (Skoufos et al., 2024) (score 0.92 and 0.95, respectively), we hypothesized that miR-107 could base pair the expanded CUG repeats in the 3´UTR of *DMPK* (Fig. R-23 A). Therefore, miR-107 targets, including MSI2, would be derepressed. By resorting to RNAseq data from DM1 biopsies (E. T. Wang et al., 2019) and from transdifferentiated myotubes derived from immortalized fibroblasts (TDM) (Bargiela et al., 2019; Cerro-Herreros et al., 2021) we evaluated the status of

miR-107 predicted targets by differential gene expression. The results showed that in DM1 TDMs differentiated for 4 days, the number of up and downregulated miR-107 targets was similar (Fig. R-23 B). However, the number of upregulated miR-107 targets was 2.5 and 5.25 times higher than those downregulated compared to control-derived samples in TDM differentiated for 8 days and in patient´s biopsies, respectively (Fig. R-12 C,D). Overall, these results reinforced our hypothesis about a deficit in miR-107 repressor activity in a DM1 context.

A prediction from miR-107 sequestration is a significant accumulation of this miRNA in the nuclear fraction of DM1 myoblasts. Thus, we studied the distribution of miR-107 between the nucleus and the cytoplasm in control and DM1 immortalized myoblasts (Fig. R-12 E,F). Interestingly, in healthy controls, miR-107 was preferentially detected in the cytoplasm (58.3%, p=0.0006) as expected for a functional miRNA. In the case of DM1 cells, there was a change in the distribution pattern as the nuclear fraction of the miRNA was significantly higher than the cytoplasmic one (54.9% p=0.0489). These results were further supported when comparing miR-107 expression levels in the nucleus from CNT and DM1 myoblasts. We observed a statistically significant 1.3-fold increase of miR-107 in DM1 nuclei compared to the same fraction in CNT myoblasts (p-value=0.0058). These data reinforced our hypothesis of miR-107 accumulation in the DM1 nuclei due to expanded CUG repeats.

To find out if, besides detecting an impaired subcellular distribution, there were differences in miR-107 total levels, we analyzed miR-107 expression in 4 and 7-day-differentiated TDMs, immortalized myoblasts, and muscle biopsies from DM1 patients. While no differences in expression were detected between CNT and DM1 TDMs, this difference became significant in myoblasts with a reduction to half the expression in DM1 compared to controls. Finally, a borderline significant reduction in miR-107 levels was observed in muscle biopsies (p-value=0.06) (Fig. R-12 G-I). Collectively, these findings support a concomitant reduction in global miR-107 levels and a change in the subcellular localization of miR-107 in the presence of

mutant *DMPK,* possibly due to its sequestration by CUG repeats, a fact that is reinforced by the upregulation of miR-107 predicted targets in DM1 samples.

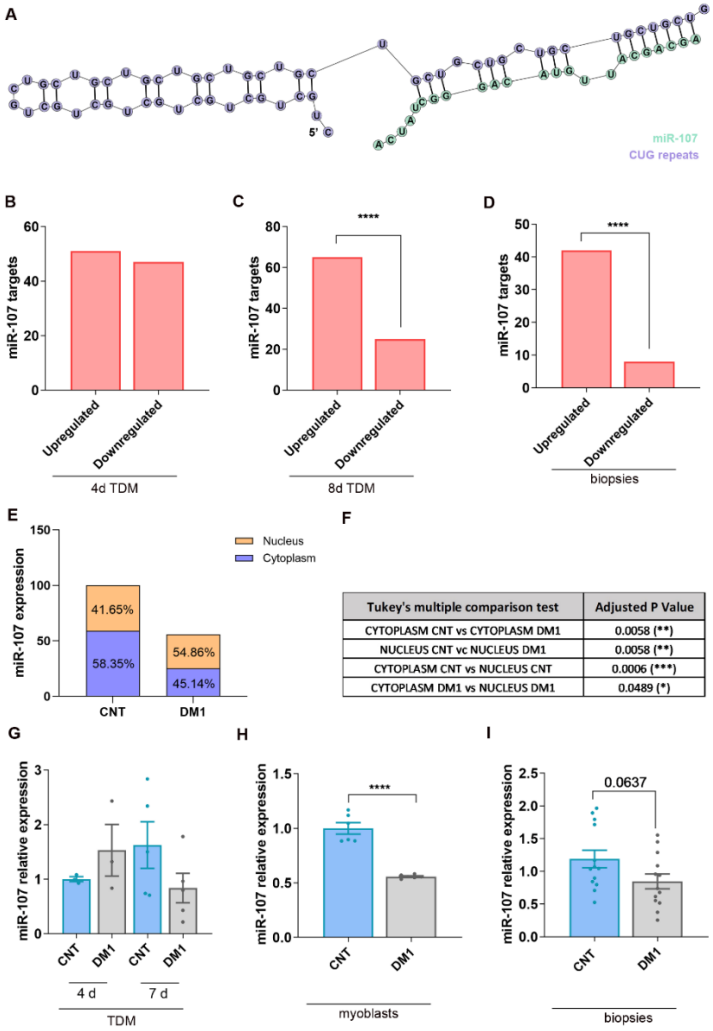

Fig. R-12. miR-107 dysregulation in DM1. (A) Illustration depicting the complementarity between miR-107 and 20 CUG triplets. (B-D) Representation of the number of upregulated and downregulated miR-107 targets in DM1 TDM differentiated over 4 or 8 days and in patient biopsies. (E) Proportional expression of miR-107 in nucleus and cytoplasm in healthy immortalized myoblasts versus DM1 cells. (F) Data show the adjusted p-value of miR-107 comparative expression across different cellular compartments and conditions (healthy or diseased). (G-I) Quantification of miR-107 relative levels in TDMs at 4 (n=3) and 7 (n=5) days of differentiation and biopsies (n=14) by RT-qPCR and immortalized myoblasts (n=5) by RNAseq. The bar graphs show mean±S.E.M. except for the proportions (E). *P<0.05, ***P<0.001, **** P<0.0001 according to Student's t-test or one-way ANOVA test with post hoc tests when necessary.

2.3.2. miR-107 directly targeted CUG repeats.

We observed changes in the subcellular localization of miR-107 under pathological conditions and the derepression of its targets, suggesting direct binding of miRNA to CUG repeats and its functional deficit, respectively. To further investigate if miR-107 interaction with expanded CUG repeats leads to *DMPK* repression, we performed a luciferase reporter assay to study the interaction of miR-107 and CUG repeats fused to the luciferase reporter gene (Koscianska et al., 2015). Briefly, we transfected reporter constructs carrying 5, 44, 53, and 72 CTG triplets, the latter two falling within the pathogenic range in DM1, fused to firefly luciferase in HEK293 cells and miR-107 mimic. A reduction in firefly luciferase induced by miRNA binding to the repeats indicates that *DMPK* is targeted by miR-107 and that this miRNA regulates its translation. A vector without CTG repeats (VTC) was used as a control.

When comparing co-transfecting the CUG reporters with agomiR-107 to the transfection with the construct carrying the CTG repeats (red vs. gray bars), a significant reduction in luciferase activity was observed at both 72 h (Fig. R-13 A) and 96 h (Fig. R-13 B), denoting the ability of miR-107 to reduce reporter expression (asterisks in brackets). Moreover, comparing VTC transfected with agomiR versus the co-transfection with luciferase sensors expressing different CUGs lengths (red bars) revealed a reduction in luciferase (asterisk above the bars), suggesting again

the regulation of *DMPK* by miR-107. At 72 h (Fig. R-13 A), the decrease in luminescence was around 30%, except for CUG_{53} (50% reduction). Meanwhile, at 96 h (Fig. R-13 B), the miRNA effect was more pronounced, generally reducing luciferase expression by 50%.

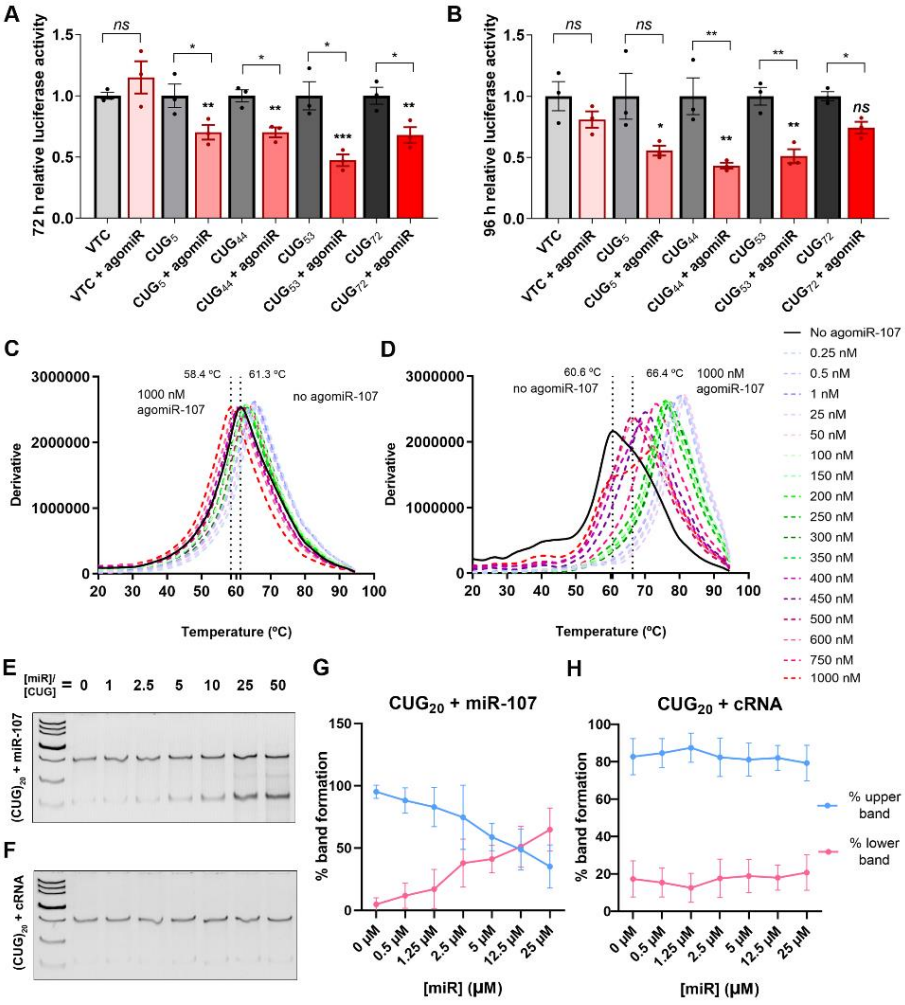

Fig. R-13. miR-107 represses *DMPK* expression and directly binds CUG repeats. Relative luciferase activity quantified after 72 (A) or 96 h (B) of co-transfection of reporter constructs carrying 5, 44, 53, 72 or 0 (denoted as VTC) CTG repeats and 100 nM miR-107 mimic in HEK293 cells. Asterisks above the bars represent the comparison of that condition with VTC + agomiR, while asterisks in the brackets indicate comparisons of each condition with the corresponding without the miR-107 mimic. The firefly luciferase activity was normalized to Renilla luciferase. (C,D) Normalized fluorescence intensity of RiboGreen fluorescence versus temperature at different miR-107 concentrations with CUG20 (C) or CGA20 as a control (D). The bar graphs show mean±S.E.M. calculated from three independent experiments. Representative EMSA blots of CUG20 with increasing concentrations of miR-107 (E) or control RNA (cRNA) (F). Quantification of the percentage of each band in EMSAs combining CUG20 probe, and miR-107 mimic (G) or cRNA control (H). The results presented in EMSA assay are the average of three (G) and two (H) independent experiments. *P<0.05, **P<0.01, according to Student's t-test or one-way ANOVA test with post hoc tests when necessary.

2.3.3. Mutant *DMPK* sequester miR-107 depriving it of its normal function

Luciferase reporter assays suggest that miR-107 can recognize CUG repeats and repress protein production through RNA-induced silencing complexes (RISC). However, in the nucleus, miR-107 could recognize and bind CUG repeats directly and not require any specific protein. To test this possibility, we studied the interaction between CUGs and miR-107 *in vitro*. Since differential Scanning Fluorimetry (DSF) has proven to be a powerful tool for investigating *in vitro* interactions between biomolecules (K. Gao et al., 2020, p. 202; Uniewicz et al., 2010) we performed a conventional DSF assay to test miR-107 interaction with CUG repeats. The experiment involved varying concentrations of agomiR-107 (ranging from 0.5 to 1000 nM) while keeping constant the concentration of the CUG_{20} repeats probe (600 nM). CGA_{20} probe, sharing structural similarities with the CUG repeats (Galka-Marciniak et al., 2012), was used as a control to address the possibility that miR-107 recognized a secondary structure instead of a complementary sequence. Interestingly, while at concentrations above 400 nM of miR-107 the melting temperature (Tm) of double-stranded CUG_{20} showed a notable reduction (Fig. R-13 C), which indicates destabilization of the secondary structure, the CGA_{20} probe

behaved the opposite even at low concentrations of miR-107 (Fig. R-13 D). To quantify the affinity of the miR-107 for CUG_{20}, we conducted an electrophoretic mobility shift assay (EMSA) with a constant concentration of CUG_{20} RNA and increasing concentrations of miR-107 (Fig. R-13 E-H) and their technical controls. We observed two bands corresponding to CUG_{20}: the upper corresponding to the double-stranded RNA and the lower formed by an unstructured conformation of the RNA. The intensity of the lower band increased concomitantly with increasing concentrations of the miRNA. The analysis of the intensities of both bands allowed us to quantify the interaction of miR-107 to CUG_{20} as a DC50 (50% dissociation concentration) of 11.6 μM (Fig. R-13 E,G). To confirm specificity, we conducted the experiment with a control RNA lacking complementarity to the CUG_{20} (cRNA). In this case, the experiments showed no shift in the CUG_{20} bands, suggesting that the miR-107 can effectively and specifically interact with the CUG_{20} secondary structures and unfold them (Fig. R-13 F,H). Taken together, these results indicate that miR-107 directly base-pairs to the CUG repeats.

2.3.4. CUG repeats exert an inhibitory effect on DMPK expression mediated by miR-107.

A prediction from luciferase reporter experiments and direct binding is that miR-107 may repress DMPK expression in a DM1 cell context. To confirm this hypothesis 7 day-differentiated DM1 TDMs were treated with agomiR-107. To define the experimental conditions, the toxicity profile of the miR-107 mimic was assessed in these same cells (Fig. R-14 A). We selected 100 nM (first vertical dotted line in Fig. R-14 A) for subsequent experiments, as at this concentration, around 70% of cells remained viable, reaching the TD_{50} concentration at 1000 nM. We found that the expression of DMPK was significantly reduced in DM1 TDMs compared to control TDMs, both at transcript and protein levels, as previously reported (Cerro-Herreros et al., 2021) (Fig. R-14 B-D). Notably, supplementation of miR-107 yielded a significant additional decrease in *DMPK* mRNA in DM1 cells (Fig. R-14 B) that reached 50 % reduction in DMPK protein levels by western blot (Fig. R-14 C,D).

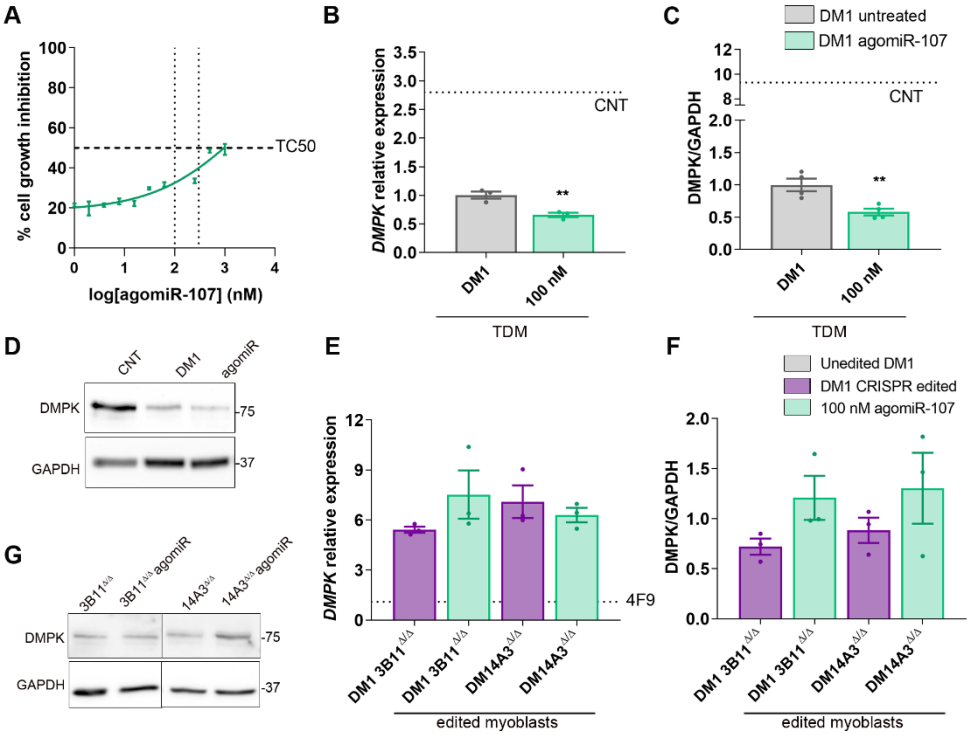

Fig. R-14. CUG repeats exert a repressive effect on DMPK expression mediated by miR-107. (A) Cell growth inhibition assay by MTS/PMS method. DM1 TDM were transfected with agomiR-107 ranging 1 nM to 1 µM (n=4). TC50 (2,106 nM) was obtained using the least-squares non-linear regression model. Vertical dashed lines denote agomiR concentrations used for further studies: 100 and 300 nM. Quantification of *DMPK* transcripts (B,E) or protein (C,D,F,G) in 7-day-differentiated TDM (n=3/4) (B,C,D) and CRISPR-edited myoblasts (E,F,G) untreated or treated with 100 nM agomiR-107 (n=3). *DMPK* transcripts were normalized to the endogenous expression of the mean of *GAPDH* and *GPI*, while DMPK protein was relative to GAPDH expression. The bar graphs show mean±S.E.M. **P<0.01 according to Student's t-test or one-way ANOVA test and post hoc tests when necessary.

To confirm that the downregulation of DMPK in response to miR-107 stems from the direct and functional binding of the miRNA to the CUG sequence within the 3'UTR of *DMPK* and to dismiss the possibility of the miRNA binding to another region of the sequence, we analyzed DMPK expression in edited DM1 immortalized myoblast.

Briefly, using the CRISPR/Cas9 system, DM1 myoblasts (cl5, 4F9) were edited to excise CTG repeats, resulting in a DM1 recovered phenotype (Agtmaal et al., 2017). We observed a strong derepression of DMPK in both edited lines, DM1 3B1Δ/Δ and DM1 4A3Δ/Δ, compared to the isogenic line containing the 2,600 repeats, 4F9, after 7 days of differentiation (Fig. R-14 E-G). The fact that upon repeat excision, DMPK significantly increased revealed a repressor effect of the CTG repeats. This hypothesis was reinforced when treating DM1 and DM1 edited cells with 100 nM agomiR-107. Unlike the substantial decrease observed upon increasing miR-107 levels in DM1 TDMs (Fig. 14 B,C), edited cells were unresponsive to miR-107 levels at the transcript (Fig. R-14 E) or protein levels (Fig. R-14 F,G), which is consistent with our hypothesis that miR-107 regulates DMPK by its interaction with CUG repeats.

2.3.5. miR-107 mediates foci reduction and MBNL1 subcellular localization.

To assess if the inhibitory effect of miR-107 over DMPK has an impact on ribonuclear foci, we proceeded to study this phenotype in DM1 TDM treated with increasing agomiR-107 concentrations by means of fluorescent *in situ* hybridization. To validate our experimental setup, chromomycin, a well-established foci-reducing compound (Ketley et al., 2014), was employed as a positive control, and TDMs from healthy donors were used as a negative control since these cells do not display foci formation. The results demonstrated that there was a significant decrease in the mean number of foci per cell upon miRNA replenishing at 25, 100, or 150 nM (Fig. R-15 A). Concurrently, the proportion of diseased cells lacking foci increased significantly within the concentration range of 25 nM to 250 nM (Fig. R-15 B), demonstrating a robust cellular response to agomiR-107 treatment. Our data demonstrates a specific and concentration-dependent hormetic effect of agomiR-107.

Considering these results, we decided to explore MBNL1 colocalization with the *DMPK* aberrant transcripts. For this, we immunodetected MBNL1 and ribonuclear foci in control, DM1 and DM1 cells treated with increasing concentrations of

agomiR-107. The experiment was performed both in TDM and immortalized myoblasts (Fig. R-15 C,D). Then, we analyzed the colocalization of signals corresponding to ribonuclear foci and MBNL1 (Fig. R-15 E,F). Our data revealed a significantly reduced colocalization of foci with MBNL1 in treated TDM cells upon 100 or 300 nM agomiR treatment. However, no discernible response was noted upon myoblast treatment (Fig. R-15 D).

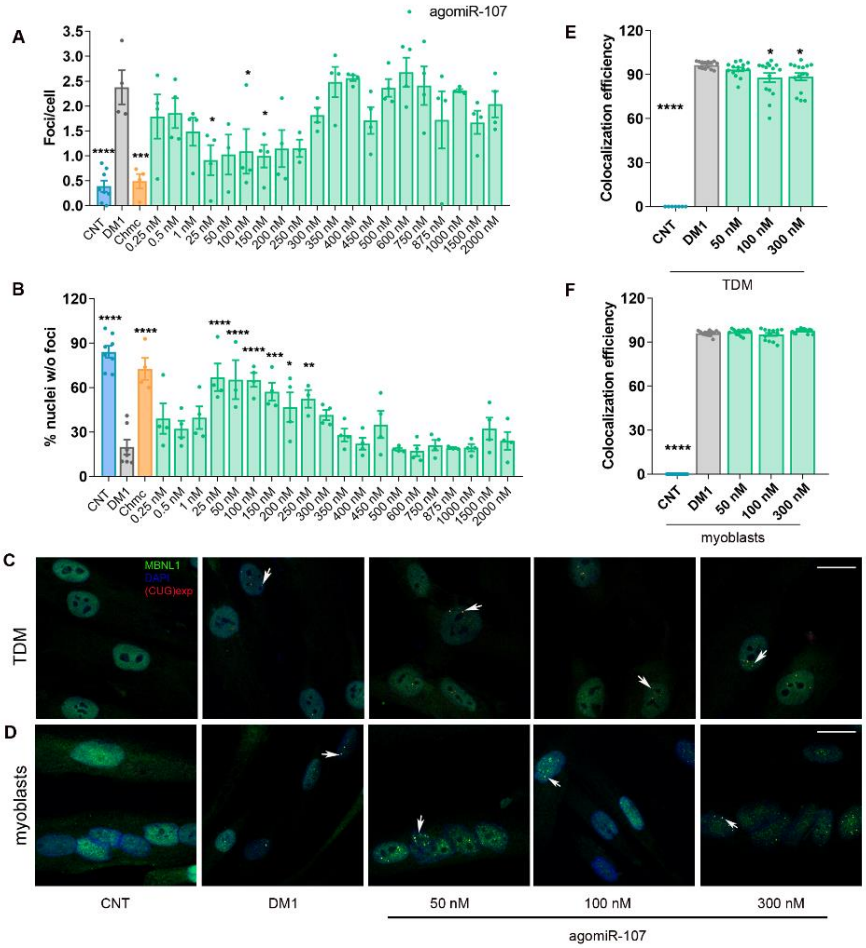

Fig. R-15. Modulating miR-107 levels in DM1 ameliorates foci-related phenotypes. Quantification of foci number per cell (A) and the percentage of nuclei without foci (B) obtained from *in situ* hybridization in CNT and DM1 TDM untreated or treated with the indicated concentrations of miR-107 mimic. 4 μM chromomycin (chmc) was used as a positive control. (C,D) Representative confocal images of MBNL1 (green) immunostaining and fluorescent *in situ* hybridization showing the ribonuclear foci using a CAG probe (red) in control and DM1 TDM (C) or immortalized myoblasts (D) untreated or supplemented with the indicated concentrations of agomiR-107. Nuclei were counterstained with DAPI and white arrows indicate ribonuclear foci. Between 100 and 200 nuclei were analysed per condition. The scale bar equals 20 μm. (E,F) Percentage of colocalization between foci (measured as Cy3 positive pixels) and MBNL1 (FITC positive pixels) and normalized to the total number of pixels in TDM (E) or immortalized myoblasts (F) per image. The bar graphs show mean±S.E.M. *P<0.05, **P<0.01, *** P<0.001, **** P<0.0001 according to a one-way ANOVA test and Tukey's HSD post hoc test when necessary.

The consistent reduction of foci is further supported by the interaction between miR-107 and *DMPK*, which may be causing not only DMPK downregulation but also disruption of ribonuclear foci and release of MBNL1. Interestingly, supplementing TDMs with 300 nM agomiR did not affect the foci but did influence the sequestration of MBNL1 in these structures, suggesting that in the nucleus, miR-107 could bind mutant *DMPK* in competition with other molecules also sequestered by the mutant RNA.

2.3.6. Impaired MSI2>miR-7>autophagy axis in DM1 is restored upon miR-107 replenishment.

To elucidate the intricate molecular dynamics associated with DM1 and the involvement of miR-107 in key components of the MSI2>miR-7>autophagy pathway, we treated DM1 TDM and immortalized myoblasts with 100 and 300 nM agomiR-107 to compensate for the miRNA lack of function caused by its sequestration by mutant *DMPK* transcripts. Firstly, we analyzed MSI2 levels in treated cells (Fig. R-16 A-D), and our data confirmed a decrease in both the protein (Fig. R-16 A-C) and transcript (Fig. R-16 D) levels in the case of TDMs treated with either concentration of mimetic. In the case of immortalized myoblasts, a significant decrease in MSI2 protein (Fig. R-

16 A,C) was observed at both concentrations of agomiR-107 tested, but the effect could not be observed at the RNA level (Fig. R-16 D).

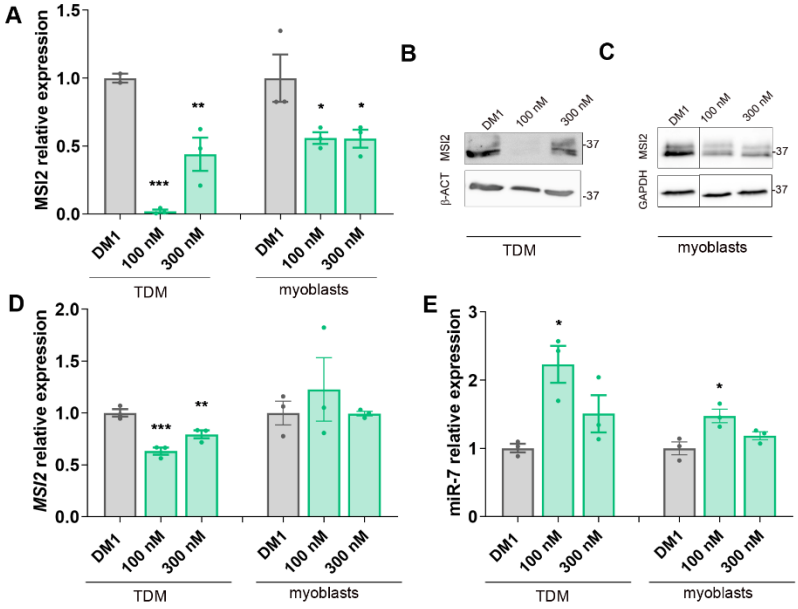

Fig. R-16. AgomiR-7 treatment in DM1 cells restores MSI2 and miR-7 levels. Quantification (A) and representative blots (B,C) of MSI2 protein in 7-day-differentiated TDM and immortalized myoblasts treated with miR-107 mimic at the indicated concentrations (n=3). Quantification of MSI2 transcripts (D) and relative miR-7 (E) levels by RT-qPCR in the same experimental conditions as in (A). miR-7 quantification is relative to endogenous U1 and U6 levels, and *MSI2* transcripts were normalized to endogenous expression of the mean of *GAPDH* and *GPI*. Asterisks indicate statistically significant differences between untreated DM1 cells and the conditions indicated in the graphs. The bar graphs show mean±S.E.M. *P<0.05, **P<0.01, *** P<0.001, according to one-way ANOVA test and Tukey's HSD post hoc test when necessary.

Then, we assessed miR-7 levels (Fig. R-16 E), which are expected to increase upon MSI2 repression since miR-7 biogenesis is inhibited by MSI2 through its binding to the terminal loop of pri-mir-7-1 (Kumar et al., 2017). Treatment with 100 nM agomiR-107 significantly increased miR-7 expression in TDMs and myoblasts, indicating a positive modulation of miR-7. However, no effect was detected when cells were

supplemented with the highest dose of miRNA mimic. Notably, miR-7 increase and MSI2 reduction correlated negatively.

To assess the role of miR-107 in autophagy, we determined several markers previously reported to be dysregulated in DM1 condition and directly involved in the upregulation of this pathway (Bargiela et al., 2019; Sabater-Arcis et al., 2020, 2021). Thus, we supplemented DM1 TDM with miR-107 mimic at 100 or 300 nM. The administration of 100 nM agomiR-107 demonstrated a compelling rescue of the autophagic phenotype in TDMs, as evidenced by the nuanced responses observed in ATG4, ATG7, and P62 proteins (Fig. R-17 A-F). Upon treatment, both ATG4 (Fig. R-17 A,B) and ATG7 (Fig. R-17 C,D) exhibited a reduction towards control-like levels, indicating a reduction of autophagy, influencing the dynamics of autophagosome formation and subsequent cellular degradation. According to these data, the mimetic action of 100 nM agomiR-107 led to the upregulation of P62 levels (Fig. R-17 E,F). The concurrent elevation of P62, known for its role in shuttling ubiquitinated cargo to autophagosomes (Bjørkøy et al., 2009), implies a modulation of cargo recognition and clearance and suggests a potential disruption in the degradation process. However, at 300 nM condition, no significant effects were detected, underlining the importance of finding an effective dose in treatments.

Complementing protein quantifications, we performed the LysoTracker staining, which allows the visualization of lysosomes, a key indicator of autophagic activity (Raben et al., 2009) (Fig. R-17 G). In control healthy cells, minimal red LysoTracker staining was observed, aligning with the expected outcome, as healthy cells typically exhibit well-regulated and basal autophagic levels. This observation contrasts with the heightened autophagy observed in cells derived from DM1 patients. Treatment with agomiR-107 revealed a noteworthy reduction in red staining, mainly at 100 nM, indicating a decrease in lysosomal activity. This observation is consistent with the diminished autophagic activity indicated by changes in ATG4, ATG7, and P62 levels, collectively reinforcing the potential therapeutic relevance of miR-107 modulation in pathogenesis.

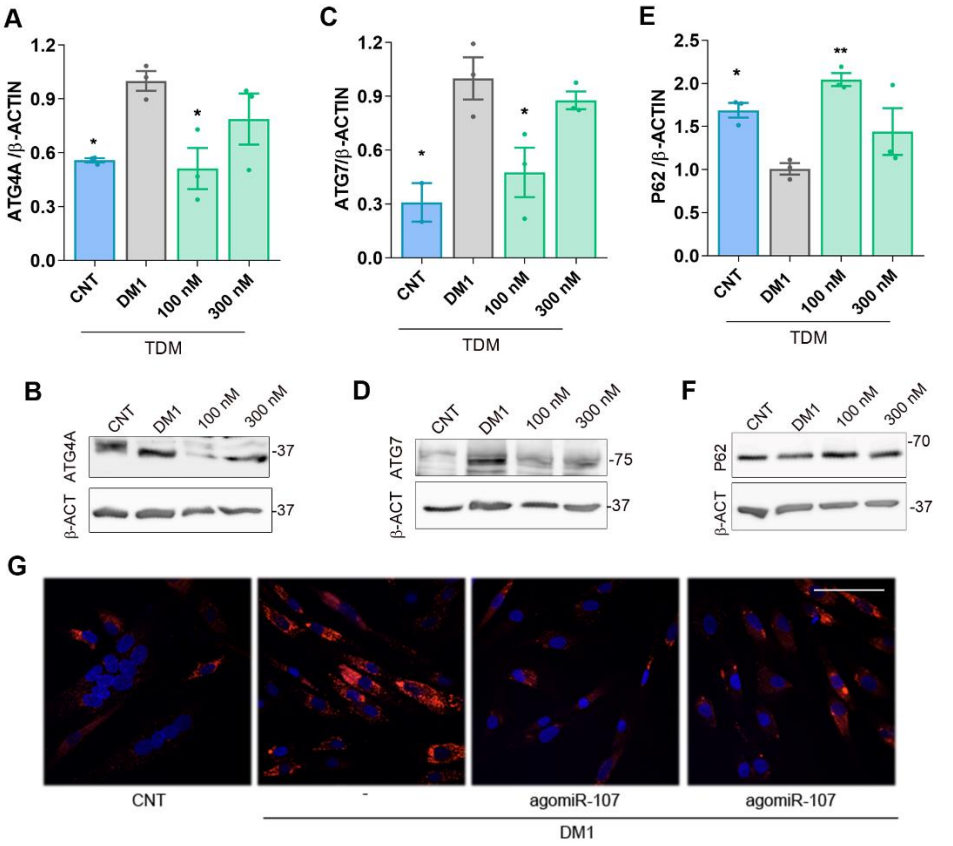

Fig. R-17. Replenishing miR-107 in DM1 TDMs restores autophagic pathway activity. Quantification (A,C,E) and representative blots (B,D,F) of immunoreactive bands with indication of molecular weight sizes to the right in kDa. ATG4A (A,B), ATG7 (C,D), and P62 (E,F) were immunodetected in control (CNT) and DM1 TDMs untreated or treated with the indicated concentrations of agomiR-107 (n=3) and differentiated for 7-days. Proteins were normalized to endogenous expression of β -ACT. (G) Representative confocal images of LysoTracker staining (red) in the same experimental conditions as in A-F. Nuclei were counterstained with DAPI. Scale bar 100 μm. All comparisons were performed against untreated DM1 cells. The bar graphs show mean±S.E.M. *P<0.05, **P<0.01 according to one-way ANOVA test and Tukey's HSD post hoc test when necessary.

2.3.7. Supplementation with agomiR-107 improves fusion index and diameter in cellular models.

To further explore the therapeutic potential of miR-107 modulation in the context of DM1, we investigated its impact on the fusion index and diameter of DM1 cellular models. These parameters measured the differentiation capacity of the cells and were assessed through immunofluorescent staining for the desmin protein, which provides crucial insights into the differentiation status of the affected cells (X. Peng et al., 2015; Yablonka-Reuveni & Nameroff, 1990) (Fig. R-18 A,B).

Both in TDMs and myoblasts from patients, treatment with agomiR-107 notably increased the fusion index, which rose by 20% to 40% in TDMs and by 10% to 20% in myoblasts (Fig. R-18 C,D). Concurrently, the relative diameter of the myocytes increased significantly post-treatment. When analyzed, diameter data demonstrated that this phenotype strongly recovered upon agomiR supplement, exhibiting around a 2-fold increase in both muscular cell lines and at both tested concentrations of miRNA mimic (Fig. R-18 E,F).

The observed enhancement in the fusion index and diameter following agomiR-107 treatment suggests a potential structural and functional rescue in the differentiation of DM1 cellular models. The increase in fusion index indicates improved cellular fusion and myotube formation, which are crucial for muscle development and regeneration. These findings align with our previous results, emphasizing the multifaceted benefits of miR-107 modulation in mitigating the pathological features associated with DM1.

In conclusion, the modulation of miR-107 levels is a promising avenue for therapeutic intervention, demonstrating its potential to ameliorate both molecular and cellular aspects of DM1 pathology. These results underscore the relevance of miR-107 in the context of DM1 and warrant further exploration of its therapeutic applications in muscle and autophagy-related disorders.

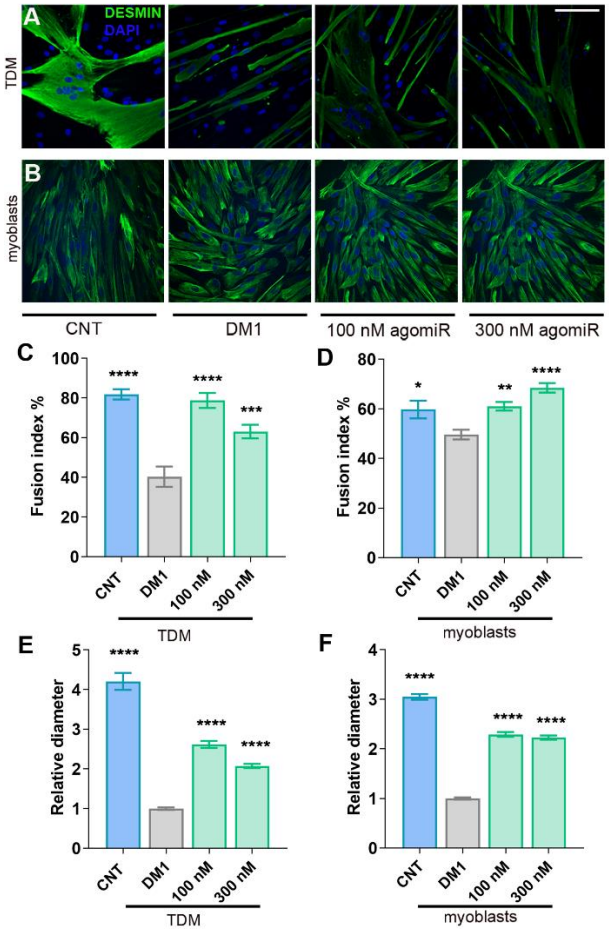

Fig. R-18. Replenishing miR-107 promotes muscle cell differentiation in DM1 cells. Representative confocal microscopy images of immunofluorescence using an anti-Desmin antibody (green) in CNT and DM1 TDM (A), or myoblasts (B). The DM1 lines were treated with 100 or 300 nM agomiR-107 for 48 h. In all cases, cells were differentiated for 7 days. Nuclei were counterstained with DAPI. The scale bar equals 100 µm. Quantification of fusion index (C,D) and myotube diameter (E,F) in TDMs (C,E) and myoblast (D,F). The bar graphs show mean±S.E.M. *P<0.05, **P<0.01, ***P<0.001, **** P<0.0001 according to one-way ANOVA test and Tukey's HSD post hoc test when necessary.

2.4. DISCUSSION

The results presented in this study shed light on the intricate molecular mechanisms underlying DM1 pathogenesis, with a particular focus on the dysregulation of miR-107. Our findings provide compelling evidence that the expanded CUG repeats in *DMPK* transcripts sequester miR-107 in the nucleus, impairing its function and resulting in dysregulation of its cytoplasmic targets, including MSI2 and DMPK, which is repressed by this miRNA (Fig. R-19).

Previous studies proposed the existence of miRNAs capable of binding to CUG repeats within the 3'UTR region of the *DMPK* gene. Computational analyses identified the potential binding to expanded CUG repeats contained in *DMPK* of some miR-15b/16 family members, including miR-107 (Gambardella et al., 2010; Hon & Zhang, 2007) that contain complementary AGCAGCA sequences in their seed regions. We performed differential gene expression analysis that revealed an imbalance in the regulation of miR-107 targets, with a significant upregulation of predicted targets in DM1 samples compared to controls. These data, together with those derived from DSF and EMSA assays, denoted that miR-107 is being retained by a direct base-pairing in the nucleus with mutant DMPK transcripts, similar to the depletion observed over some RNA-binding proteins such as MBNLs (Fardaei et al., 2001) (Fig. R-30 A). Thus, the deficit of miR-107 repressor activity in the cytoplasm, caused by its retention in the nucleus, may contribute to the disease's pathological hallmarks. These results align with those that suggested miR-107 and miR-103 preferentially bound to the mutant DMPK transcripts (Gambardella et al., 2010). Indeed, miR-107 can be regarded as a competitor of MBNL1 for CUG binding, as revealed by the effect of miR-107 supplementation on nuclear RNA and MBNL1 foci. Subsequently, because MBNL1 is required for RNA foci formation (Pettersson et al., 2014), it is possible that mutant *DMPK* transcripts get translocated to the cytoplasm and get repressed by miR-107 or degraded by unidentified mechanisms (Fig. R-19 B).

Our results using a luciferase reporter system indicated that, in the cytoplasm, miR-107 is regulating DMPK expression via RISC complexes according to the canonical mechanism of posttranscriptional regulation (Michlewski & Cáceres, 2019). Moreover, this effect was observed on DMPK independently of the number of CUG repeats, evidencing that DMPK is a target of miR-107 in non-pathological conditions as well (Fig. 8 B). Interestingly when CTG repeats were removed from *DMPK* using the CRISPR-Cas9 technique, DMPK levels turned unresponsive to miR-107 supplementation unlike to that observed in DM1 myotubes. This confirms that both the binding (nucleus) and regulatory effects (cytoplasm) occur due to the base-pairing between miR-107 and CUG repeats reinforcing miR-107 as a negative regulator of DMPK expression and possibly an anti-DM1 molecule as, in the nucleus, its presence releases key factors in the DM1 pathogenic hallmark such as MBNL1. Globally, mutant *DMPK* transcripts in the nucleus may function as miRNA sponges, sequestering miR-107 and potentially disrupting their regulatory functions in the cytoplasm. Given the established role of miRNAs in transcript regulation, the sequestration of miRNAs by *DMPK*, exemplified by miR-107, may initiate a cascade of dysregulation within the pathways they govern. Moreover, restoring miR-107 levels through agomiR-107 holds therapeutic promise in mitigating the molecular and cellular abnormalities associated with DM1.

The consequences of miR-107 sequestration in DM1 extend beyond its direct interaction with *DMPK* transcripts, impacting downstream pathways implicated in muscle homeostasis. *In vivo* studies showed that after suspending mouse hind limbs for seven days and inducing muscle atrophy, the expression of miR-107 was decreased. In contrast, when mice were exposed to endurance exercise, miR-107 was upregulated, suggesting the implication of this miRNA in muscle plasticity (S. Zhang & Chen, 2018). Similar results were reported by Safdar et al. after studying miR-107 expression in quadriceps femoris from mice that underwent endurance exercise (Safdar et al., 2009). Reduced availability of miR-107 leads to the derepression of its targets, including MSI2, whose upregulation in DM1 contributes to the activation of pro-atrophic pathways and exacerbates disease phenotypes

(Sabater-Arcis et al., 2023). Replenishment of miR-107 led to decreased expression of MSI2 and an increased expression of miR-7 that accentuates the interconnections in the miR-107>MSI2>miR-7>autophagic pathway, which is consistent with our previous studies (Sabater-Arcis et al., 2020, p. 202, 2021, 2023) and provides a potential therapeutic strategy for DM1 (Fig. R-19 C).

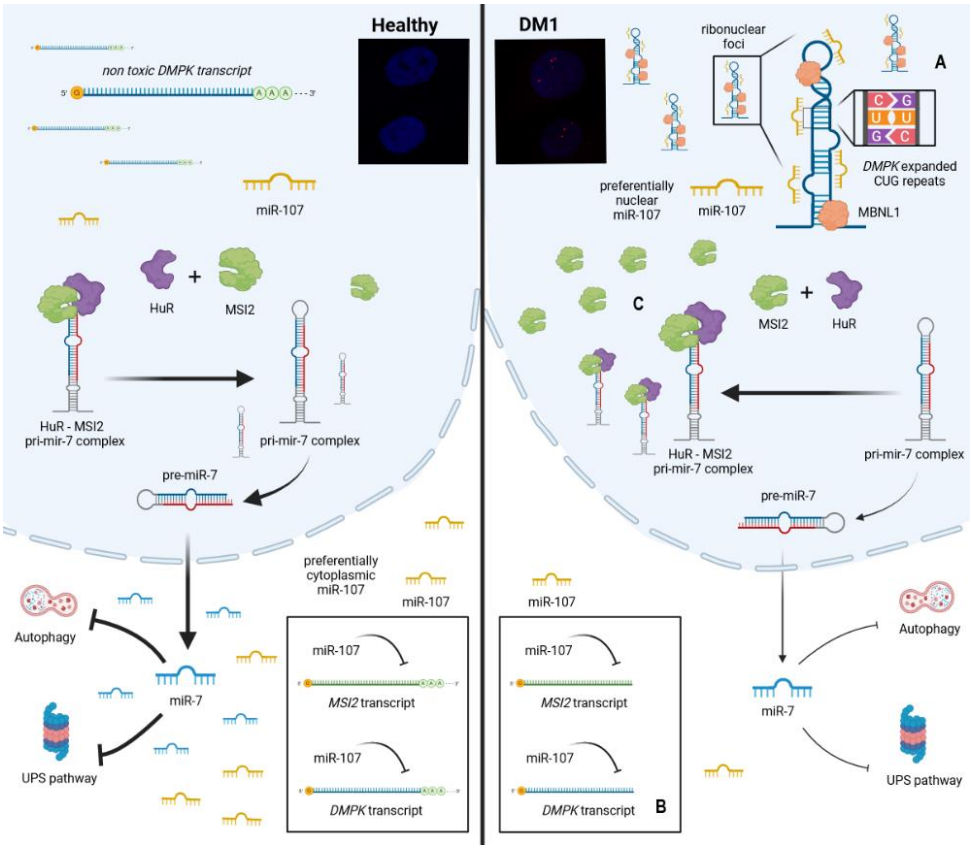

Fig. R-19. Schematic representation of the model of miR-107 dysregulation implications in the MSI2>miR-7>autophagy axis in DM1. (A) In DM1, the sequestration of miR-107 within ribonuclear foci formed by the expanded CUG repeats in *DMPK* transcript, as with other molecules such as MBNL1, results in the preferential localization of this miRNA within the nucleus, a phenomenon not observed in healthy cells. This disparity in subcellular localization hampers the ability of miR-107 to repress its targets in the cytoplasm, thereby leading to their overexpression, including MSI2. (B) *DMPK* is also among the targets of miR-107, and their interaction may stimulate the translocation of mutant *DMPK* transcripts to the cytoplasm, where miR-107 acts as a repressor promoting its degradation. (C) The heightened expression of MSI2 in DM1 facilitates the formation of the pri-miR-7-MSI2-HuR complex, which impedes miR-7 biogenesis by inhibiting the maturation of pre-miR-7. Consequently, this culminates in diminished levels of miR-7 in DM1, which fails to sufficiently repress autophagy and the UPS, thus exacerbating the characteristic imbalance of muscle homeostasis in DM1 by amplifying these catabolic pathways. In contrast, in healthy conditions without ribonuclear foci, miR-107 operates within the cytoplasm to suppress MSI2 expression, ultimately resulting in normal levels of miR-7 capable of inhibiting autophagy and the UPS system. Figure created with BioRender.com

miRNAs impact a wide range of biological processes. So, the reduction and subcellular relocalization of miR-107 to the nucleus due to its sequestration by mutant *DMPK* is expected to impact several pathways involved in DM1. Our findings strengthen prior evidence of hyperactive autophagy processes in DM1 (Loro et al., 2010; Morriss et al., 2018; Sabater-Arcis et al., 2020). Particularly, these disruptions were ameliorated upon replenishing miR-107. This suggests that miR-107 sequestration increases muscle impairment, at least partly through the MSI2>miR-7 pathway. This underscores the potential benefit of targeting miR-107 in rescuing typical disease phenotypes, such as fusion index and myotube diameter, in DM1. However, our results suggest a decrease in miR-107 levels under DM1 conditions that could be contributing to the lack of miRNA function caused by its sequestration in CUG repeats. In the last years, it become apparent that miRNA regulators themselves are subject to sophisticated control by a range of mechanisms, including miRNA gene transcription, miRNA processing, RNA editing of miRNAs, and regulation of miRNA function (Krol et al., 2007). Specifically, the pri-mir-107 sequence is encoded within an intron of the *PANK1* gene, and the promoter

regulating pri-mir-107 expression was described to be epigenetically regulated (K. H. Lee et al., 2009). The pathological implications of epigenetics in DM1 is gaining more and more strength (Visconti et al., 2021). Thus, it cannot be ruled out that epigenetic defects could be contributing to miR-107 downregulation.

Overall, these observations and the results obtained in the current study suggest that miR-107 is involved in muscle maintenance. Hence, in DM1, miR-107 sequestration in RNA foci by expanded CUG might affect the DM1 landscape. By elucidating the interaction between miR-107 and expanded CUG repeats in DMPK transcripts, we shed light on a novel aspect of DM1 pathogenesis. These findings underscore the therapeutic potential of targeting miR-107 and its downstream pathways, offering new avenues for developing targeted therapies for DM1.

CHAPTER 3:

THERAPEUTIC POTENTIAL OF OLEIC ACID SUPPLEMENTATION IN MYOTONIC DYSTROPHY MUSCLE CELLS MODELS

Published on May 2024 DOI: 10.1186/s40659-024-00496-z

3.1. BACKGROUND

Myotonic dystrophy type 1 (DM1) is a degenerative rare genetic disease with a prevalence of 1/2100 (Johnson et al., 2021). Most symptoms are neuromuscular, including muscle weakness (myopathy), muscle stiffness and trouble relaxing muscles (myotonia), and progressive muscle wasting (atrophy), but DM1 is characteristically multisystemic and also affects the heart, the brain, and the smooth musculature (André et al., 2018; Smith & Gutmann, 2016). DM1 is caused by the pathological expansion of the CTG trinucleotide in the 3´-UTR of the *DM1 protein kinase* (*DMPK*) gene. The pathogenicity is linked to the mutant transcripts that form insoluble hairpins with U-U mismatches, named ribonuclear foci, that sequester RNA-binding proteins of the Muscleblind-like family (MBNL) (Miller et al., 2000). These proteins regulate mRNA metabolism, including alternative splicing and polyadenylation (Batra et al., 2014; Konieczny et al., 2014).

Different pathways have been described that contribute to muscle atrophy in DM1, such as AKT-GSK3β (Jones et al., 2012; C. Wei et al., 2018), TWEAK/Fn14 (Gladman et al., 2015), AMPK/mTORC1 (Brockhoff et al., 2017), and PKC (Kuyumcu-Martinez et al., 2007; G. S. Wang et al., 2009). However, in recent years, increased autophagy has gained prominence as an alteration contributing to muscle wasting (Bargiela et al., 2015, 2019; Loro et al., 2010; Morriss et al., 2018; Sabater-Arcis et al., 2020). Pathological activation of autophagy and apoptosis was proved in DM1 myotubes and a *Drosophila* model and was linked to the DM1 atrophic phenotype (Bargiela et al., 2015; Loro et al., 2010). Additionally, miR-7 was reported as a critical autophagy repressor by direct translational silencing of critical autophagy genes, namely *ATG7*, *ULK2*, and *ATG4A* (Gu et al., 2017). Different works demonstrated that miR-7 was downregulated in DM1 model samples and patient muscle biopsies. Inhibition of miR-7 activity in control myotubes induced atrophic phenotypes similar to those observed in DM1. In contrast, supplementation of miR-7 by a mimetic in DM1 muscle cells restored basal levels of autophagy and improved muscle atrophy and

cell differentiation capacity (Sabater-Arcis et al., 2020). Therefore, miR-7 is a relevant target for modulating atrophic phenotypes in DM1.

miR-7 biogenesis is regulated by Musashi 2 (MSI2) and Hu R antigen (HuR). MSI2, an RNA-binding protein, binds to the pri-mir-7 terminal loop through the HuR protein, inhibiting its processing by Drosha. Consequently, miR-7 biogenesis is inhibited by MSI2/HuR complex (Choudhury et al., 2013). MSI2 was recently reported to be upregulated in DM1 samples, thus leading to excessive miR-7 inhibition (Sabater-Arcis et al., 2021). Considering these data, we hypothesized that modulation of MSI2 to regulate miR-7 offered an opportunity to recover atrophic phenotypes in DM1.

Kumar et al. 2017 demonstrated that oleic acid (OA), a natural monounsaturated fatty acid produced by plants and animal cells, binds to MSI2 at its N-terminal RNA recognition motif 1 (RRM1), producing an allosteric conformational change in the protein that prevents it from binding to pri-mir-7-1. Thus, OA treatment in HeLa cells enhanced miR-7 biogenesis (Kumar et al., 2017). Several studies have demonstrated the importance of OA in human health and diseases (Kumar et al., 2017). For example, OA modulates several physiological functions and has been suggested as a beneficial therapy for inflammatory, immune, and cardiovascular diseases (Duarte et al., 2016; Q. Wang et al., 2022). In the same way, some published studies have evaluated the effects of OA in muscle (Abreu et al., 2016; Watanabe et al., 2020), reporting fatty acids' ability to modulate skeletal muscle proliferation and differentiation (Lipina & Hundal, 2017; G. Zhang et al., 2012). Specifically, OA was demonstrated to regulate the differentiation of satellite stem cells and the growth and maturation of myotubes (Abreu et al., 2016). Additionally, OA promotes the differentiation of L6 myoblasts (Hurley et al., 2006) and C2C12 myoblasts (K. H. Lee et al., 2009; Tan et al., 2021).

Here, we report low OA levels in different DM1 cells, which contributes to the miR-7 deficit through its reduced repression on MSI2 and participates in cell differentiation alteration. Furthermore, OA supplement to DM1 myoblast was sufficient to restore

different phenotypes related to the MSI2-regulated autophagy. Finally, we propose SCD1 deficiency could contribute to decreased OA levels. Globally, MSI2 inhibition through OA would be a therapeutic strategy to increase endogenous miR-7 and therefore, inhibit the processes of muscle atrophy and impaired differentiation. Taken together, we describe a new mechanism contributing to muscle dysfunction in DM1.

3.2. MATERIAL AND METHODS

Lipid extraction and analytical method for the estimation of OA concentration

$1x10^6$ cells were seeded in a Petri plate (n= 3 to 6). After differentiation and OA treatment, cells were resuspended in 225 µL of methanol (15518534, Thermo Fisher Scientific, Waltham, Massachusetts, USA) at 4ºC. Cells lysis was performed for 20 s vortex three times, followed by 1 min in liquid nitrogen. Samples were kept on ice during thawing and were subjected to sonication (3x 10 s 0.55 cycle 60% amplitude). Then, samples were incubated under agitation for 1 h at 4ºC with 750 µL of cold methyl-tert-butyl ether (MTBE) (143312, Panreac Applichem ITW Reagents, Barcelona, Spain). After that, 750 µL of a solution of 0.1% $C_2H_7NO_2$ (10714391, Thermo Fisher Scientific, Waltham, Massachusetts, USA) was added to each sample and vortexed, followed by a 10 min incubation at room temperature (RT). Samples were centrifuged at 10,000 x *g* for 5 min at 4ºC to separate the two phases. The upper phase, containing apolar lipids, was transferred to a new tube and dried in a vacuum centrifuge. The pellet was dissolved in 100 µL of methanol. The volume of the lower phase containing polar proteins was measured, and four volumes of cold methanol were added and incubated for 1 h at -20ºC and then centrifuged at 13,000 x *g* for 10 min at 4ºC. The pellet was resuspended in 100 µL of RIPA buffer (10230544, Thermo Fisher Scientific, Waltham, Massachusetts, USA) plus protease and phosphatase inhibitor cocktails (4906837001, Roche Applied Science, Indianapolis, IN, USA). Total protein was determined in the Tecan Infinite M200 pro

plate reader by using a BCA protein assay and BSA as protein standard (10741395, Thermo Fisher Scientific Pierce, Grand Island, NY, USA).

The OA concentration was determined using a liquid chromatography-mass spectrometry (LC/MS) system (ACQUITY TQD, Waters, MA, USA). The chromatographic separation was performed using an ACQUITY UPLC C18 Kinetex column (Phenomenex, particle size 1.7 µm; 2.1 mm X 100 mm). The mobile phase was in isocratic mode MeOH: $CHCl_3$: H2O (1:1:0.04). The flow rate used was 0.2 mL/min. The mass spectrometer was equipped with a Z-spray electrospray ionization source, and the samples were analyzed with the following conditions: capillary: 3 KV, cone: 40 V, extractor: 5 V, RF Lens: 0.3 V, source temperature: 120 °C, desolvation temperature: 300 °C, cone gas: 25 L/h, desolvation gas: 650 L/h. MS1 parameters were: LM resolution: 13; HM resolution: 13; ion energy: 1. MS2 parameters were: LM resolution: 13; HM resolution: 13; ion energy: 1; multiplier: 650 V. Spectra were acquired in negative ionization selected reaction monitoring (SRM) mode with an inter-channel delay of Spectra of 0.050 s. OA concentration was normalized to the total protein in each sample.

Cell lines and culture conditions

Transdifferentiated myoblast (TDM) and immortalized myoblast were obtained from the Institute of Myology, Paris, and were cultured as previously described (Arandel et al., 2017). Briefly, skin and skeletal muscle biopsies were obtained from a DM1-affected female and a healthy male donor (Table R-2). Primary fibroblasts from skin biopsies of DM1 and control donors (Table R-2) were immortalized by hTERT induction and transduced to conditionally express MyoD (hereafter referred to as primary transdifferentiated myotubes, pTDM) and cultured as previously described (Bargiela et al., 2019). All experiments were carried out in 7-day differentiated cells except the experiment in which the fusion index was determined in control cells at 0, 4, 7, and 10 days of differentiation. For fatty acid supplementation, cells were treated with 0.5 or 2 µM of OA, or 2 µM EA (01008 and E4637, respectively, Sigma

Aldrich, San Luis, Missouri, USA), dissolved in 1% DMSO, that also served as vehicle-only control, for 24 h in opti-MEM (31985070, Thermo Fisher Scientific, Waltham, Massachusetts, USA). After fatty acid treatment, cells were supplemented with differentiation medium for 7 days. To treat cells with LXR (T 0901317, Tocris Bio-Techne, Bristol, UK), 1 x 10^6 TDM DM1 cells were seeded in a petri plate, and differentiation medium was added after 24 h. At day 4 of differentiation, LXR was added at a final concentration of 5 µM or 10 µM in 0.8% de DMSO for 72h. On day 7 cells were collected for OA determination.

Sample ID	Cell type	Condition	CTG repeats	Age	Sex	Ref.
TDM	Immortalized fibroblast	CNT	-	25	male	(Arandel et al., 2017)
TDM	Immortalized fibroblast	DM1	1300	11	female	(Arandel et al., 2017)
Immortalized myoblast	Immortalized myoblast	CNT	-	25	male	(Arandel et al., 2017)
Immortalized myoblast	Immortalized myoblast	DM1	1300	11	female	(Arandel et al., 2017)
pTDM 819	Primary fibroblast	CNT	-	48	female	(Bargiela et al., 2019)
pTDM 988	Primary fibroblast	CNT	-	unknown	female	(Bargiela et al., 2019)
pTDM 966	Primary fibroblast	DM1	1000	33	male	(Bargiela et al., 2019)
pTDM 973	Primary fibroblast	DM1	333	46	male	(Bargiela et al., 2019)

Table R-2. Characteristics of the cell lines used in this study.

Toxicity assay

DM1 TDMs were seeded in 96-well plates (1x10^5 cells/well). After 24h, cells were treated with LXR as described (concentrations ranging from 0.1 µM to 80 µM). Cell viability was measured after 7 days of differentiation. Briefly, 20 µL of MTS/PMS (CellTiter 96® Aqueous Non-Radioactive Cell Proliferation Assay, Promega, Madison, WI) was added to each well with 80 µL of differentiated medium. Cells were

incubated for 4 h at 37 °C with 5% CO2, and absorbance at 490 nm was measured using an Infinity Pro M200 plate reader. Four biological replicates were performed for each condition.

Immunofluorescent methods

Cells were seeded in 24-well plates ($3x10^5$ cells/well) and were transdifferentiated for 7 days to carry out immunodetection of DESMIN, LC3B, and MF-20. After 24 h of the corresponding treatment, cells were fixed with 4% paraformaldehyde (PFA) for 15 min at RT. Immunodetection of Desmin was carried out with mouse anti-DESMIN (1:50, ab8470, Abcam, Cambridge, UK), goat biotin-conjugated anti-mouse-IgG (1:200, Sigma-Aldrich, San Luis, Missouri, USA) and Streptavidin Fluorescein (1:200, SA-5001-1, Vector laboratories, Newark, California, USA. For LC3B immunostaining rabbit anti-LC3B (1:3000, 51520, Abcam, Cambridge, UK) and goat anti-rabbit-IgG (H+L) Alexa Fluor Plus 594 (1:200; Invitrogen, Carlsbad, CA, USA) were used. Immunodetections were performed as previously described (Sabater-Arcis et al., 2021). Images were obtained with an LSM800 confocal microscope (Zeiss, Jena, Germany) at 200x magnification.

The fusion index was defined as the proportion of nuclei contained within myotubes (>2 myonuclei) relative to the overall count of nuclei in each condition. The mean count of nuclei per myotube was ascertained by analyzing over 250 nuclei taken randomly from Desmin-positive cells (5-7 micrographs). The diameter of myotubes was gauged at 5 points, spanning the entire length of the tube. Fifty myotubes were scrutinized for each distinctive experimental setup. Quantitative analysis was executed using the ImageJ software (NIH). LC3 puncta quantifications were performed using the Ifdotmeter software (Rodríguez-Arribas et al., 2016). We conducted image analyses on myotubes stained with LC3. Briefly, the quantification of LC3 dots or puncta was executed on 15–20 images for each specific condition. The aggregate count of LC3 dots per image was adjusted in proportion to the entire area encompassing all the observed myotubes within each image. Measurement of

the myotube area was carried out using the ImageJ software. Data were expressed as the number of LC3 dots/µm2.

In the case of MF20, immunostaining was performed as DESMIN, but the mouse anti-MHC MF20 was used(1:20, MYH1E, Developmental Studies Hybridoma Bank, Douglas, USA).

For LysoTracker staining, cells were incubated for 30 min at 37°C with 100 nM of LysoTracker RED-DND99 (12090146, Invitrogen, Carlsbad, CA, USA), washed with PBS 1x and fixed with 4% PFA for 15 min. After three washes with PBS 1x, cells were mounted in Vectashield (Vector Laboratories, London, UK) with 2 µg/ml DAPI (4', 6-diamidino-2-phenylindole). Images were acquired in an LSM800 confocal microscope (Zeiss) at 400x magnification.

Western blotting

Protein extraction, quantification, and immunodetection were performed as described in (Sabater-Arcis et al., 2020, 2021). Membranes were incubated O/N with the corresponding primary antibody dilutions: mouse anti-β-ACTIN (1:5000, A5441, Sigma-Aldrich, San Luis, Missouri, USA), goat horseradish peroxidase (HRP)-conjugated anti-GAPDH (1:3500, sc-365062, Santa Cruz, Dallas, Texas), rabbit anti-ATG4A (1:1000, #7613, Cell Signaling, Danvers, Massachusetts, USA), rabbit anti-LC3B (1:3000, 51520, Abcam, Cambridge, UK), rabbit anti-MSI2 antibody (1:1000, EP1305Y, Abcam, Cambridge, UK), mouse anti-P62 (1:1000, 65416, Abcam, Cambridge, UK), mouse anti-P21 (1:2000, #2946, Cell Signaling, Danvers, Massachusetts, USA), mouse anti-SCD1 (1:1000, 19862, Abcam, Cambridge, UK). After three washes with 1x PBS-T, membranes were incubated for 1 h at RT with the corresponding secondary antibody dilutions: goat HRP-conjugated anti-rabbit-IgG (1:3500, A0545, Sigma-Aldrich, San Luis, Missouri, USA) or goat HRP-conjugated anti-mouse-IgG (1:5000, B7264, Sigma-Aldrich, San Luis, Missouri, USA). Images were acquired with an ImageQuant LAS 4000 or AMERSHAM ImageQuant 800 (GE Healthcare) and were quantified using ImageJ software (NIH).

RNA extraction and Real-Time Quantitative Reverse Transcription PCR (qRT-PCR)

According to the manufacturer's instructions, total RNA from 1 x 10^6 cells was extracted from each experimental replicate using the miRNeasy mini kit (217004, QIAGEN, Hilden, Germany). For miRNA determinations, 2 µL of 5 ng/µL samples were reverse-transcribed with miRCURY LNA RT kit (339340, Qiagen, Hilden, Germany). miR-7 expression was quantified using specific miRCURY LNA miRNA PCR primers (339340, Qiagen, Hilden, Germany) and was normalized to *U1* or *U6* small nuclear RNA (snRNA) (339306, Qiagen, Hilden, Germany) according to the manufacturer's recommendations. For analyses of relative expression of genes, one microgram of total RNA was digested with DNase I and reverse-transcribed with SuperScript II (18068015 and 18064014, respectively, Invitrogen, Carlsbad, CA, USA) using random hexanucleotides (11277081001, Sigma-Aldrich, San Luis, Missouri, USA). qRT-PCR was performed using 2 ng of cDNA template with 5x HOT FIREPol EvaGreen qPCR mix plus (ROX) (08-24-000S, Solis BioDyne, Tartu, Estonia) and specific primers. Gene expression was normalized to *GAPDH* and *GPI*. The primers used were: *GAPDH* (fwd CATCTTCCAGGAGCGAGATC; rev GTTCACACCCATGACGAACAT), *GPI* (fwd CAGGGCATCATCTGGGACAT; rev TCTTAGCCAGCTGCTTTCCC) and *MSI2* (fwd GCAGACCTCACCAGATAGCCTT; rev AAGCCTCTGGAGCGTTTCGTAG); *HMGR* (fwd TGCTTG CCGAGCCTAATGAAAG; rev AGAGCGTTCGTGGGTCCATC); *FAS* (fwd AAGGCTTTCGTGGGTCCATC; rev GATGCCAATTACGAAGCAGTTG); *PGC1-α* (fwd CCAAAGGATGCGCTCTCGTTCA; rev CGGTGTCTGTAGTGGCTTGACT); *RNF145* (fwd GCAGGTTGTTCATCGGGCATTC; rev GGCTTACAGCACGGAAGTGTTTC); *ABCA1* (fwd CAGGCTACTACCTGACCTTGGT; rev CTGCTCTGAGAAACACTGTCCTC); and *SCD1* (fwd TGTGGTGAAGTTGATGTGCCAGC; fwd CCTGGTTTCACTTGGAGCTGTG)

qRT-PCRs were performed in a Step One Plus PCR system (Applied Biosystems, Foster City, CA, USA). Three experimental replicates and three repeats per biological sample were performed. Expression levels were normalized to the mean of

reference genes using the comparative cycle threshold (Ct) method ($2^{-\Delta\Delta C}$) (Livak & Schmittgen, 2001).

Statistical analyses

Graphical outputs from statistical analyses used GraphPad Prism 9 software. In all experiments, we assumed that all parameters followed a normal distribution to compare normalized data means. For comparisons of two conditions, a two-tailed Student's t-test ($\alpha = 0.05$) was applied with Welch's correction when necessary. For comparisons of more conditions, one-way ANOVA ($\alpha = 0.05$) was applied, and Tukey's HSD post hoc test when necessary. The correlation was measured with Pearson's correlation coefficient.

3.3. RESULTS

3.3.1. A marked reduction of OA levels is detected in DM1 *in vitro*.

We previously proposed that MSI2 overexpression contributed to wasting phenotypes through repressing miR-7 biogenesis that hyperactivated muscle autophagy (Sabater-Arcis et al., 2021). Considering the previously described impact of OA in MSI2 function during miR-7 maturation (Kumar et al., 2017), we tested the hypothesis that OA deficits could impinge on miR-7 levels in DM1 by quantifying OA by mass spectrometry in different DM1 muscle cells.

Firstly, we measured OA in DM1 fibroblasts expressing 1300 CTG repeats and transdifferentiated by doxycyclin-induced MyocddsD expression into multinucleated myotubes (hereafter referred to as transdifferentiated myotubes, TDM) for 7 days (Fig. R-20 A). The results showed a 40-fold reduction in OA in DM1 TDMs compared to healthy controls. The same determination was performed on DM1 and control immortalized myoblasts at 0 and 7 days of differentiation. In this case, OA levels were halved compared to controls after 7 days of differentiation with no preexisting differences at day 0 (Fig. R-20 B). Finally, OA levels were analysed in two primary fibroblast cell lines from DM1 patients and two unaffected donors,

transdifferentiated for 7 days into myotubes (hereafter referred to as primary transdifferentiated myotubes; pTDM; Fig. R-20 C). In this case, more than 6 and 2-fold reduction was observed in lines 973 and 966, respectively, compared to controls. Thus, we confirmed a significant reduction in OA levels in four cell lines derived from 3 DM1 patients (note TDM and immortalized myoblasts from the same donor; Table R-2) compared to their corresponding controls.

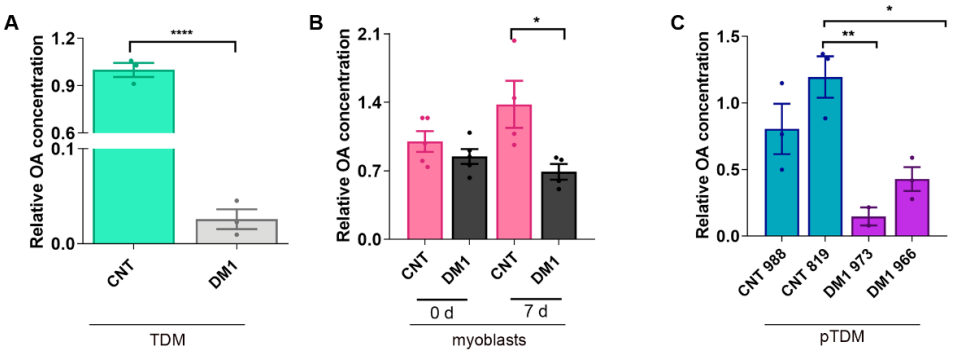

Fig. R-20. OA levels are decreased in DM1 cells. OA levels were quantified by LC/MS in (A) healthy controls (CNT) and DM1 TDM, (B) undifferentiated (0 d) and differentiated (7 d) myoblasts obtained from a DM1 patient and unaffected control, and (C) two DM1 (973 and 966) and two control pTDM (988 and 819) transdifferentiated for 7-day into myotubes. In A) and C), OA values are shown relative to levels in control muscle cells, and in b) are relative to CNT myotubes prior to differentiation. The bar graphs show mean±S.E.M. *P<0.05, **P<0.01, **** P<0.0001 according to Student's t-test. In all cases, experimental replicates were n=3-4.

3.3.2. OA derepresses miR-7 biogenesis with stable MSI2 levels.

The binding of OA to the N-terminus of MSI2 causes an allosteric change that prevents MSI2 binding to the HuR-MSI2-pri-miR-7-1 complex, thereby derepressing miR-7 biogenesis (Kumar et al., 2017). Having confirmed the abnormally low levels of OA in DM1 cells, we hypothesized that OA supplementation would enhance miR-7 levels by partially interfering with MSI2-mediated repression. TDM and immortalized myoblasts were grown in a medium supplemented with 0.5 or 2 μM

OA. To confirm the efficacy of the treatment, OA was determined in cells after exposure to the highest dose of the fatty acid. For TDMs, the increase in OA levels in cells at 0 and 7 days of differentiation was 1.57 and 1.50 μM, respectively. This variation was slightly higher for immortalized myoblasts treated in parallel, reaching 2.08 and 2.02 μM, thus confirming the effectiveness of the treatment. Exposure of DM1 cells to 0.5 or 2 μM OA demonstrated that MSI2 transcript and protein levels were not significantly affected by treatment (Fig. R-21 A-E). However, we observed a significant increase in miR-7 expression in TDMs at both concentrations tested and at the highest concentration in the case of immortalized myoblasts (Fig. R-21 F), consistent with the OA´s allosteric role upon binding MSI2. In all cases, miR-7 expression upon OA treatment reached values similar to those detected in CNT cells. These results reinforce the deleterious effect of increased MSI2 in DM1 where, in addition to being upregulated (Sabater-Arcis et al., 2021), its inhibitory activity on miR-7 maturation from pri-miR-7-1 synergizes with the abnormally low levels of OA we detect in DM1 cell lines.

It was previously described that MSI2 overexpression was sufficient to reduce P21 levels and that its inhibition had the opposite effect over P21 (H. Zhang et al., 2014; Zhou et al., 2020). Therefore, to confirm that inhibiting MSI2 regulatory activity by OA affected its targets, we quantified the levels of P21 in TDM and immortalized myotubes exposed to an OA-enriched medium (Fig. R-21 G-J). The results showed that P21 was significantly reduced in DM1 cells, as expected under conditions where MSI2 is hyperactivated. Upon OA treatment of DM1 TDMs, P21 was derepressed, reaching levels similar to controls. Furthermore, in the case of immortalized myotubes, where P21 levels in DM1 cells were around 5-fold lower than in controls, a significant two- to three-fold increase over untreated DM1 was observed after OA treatment.

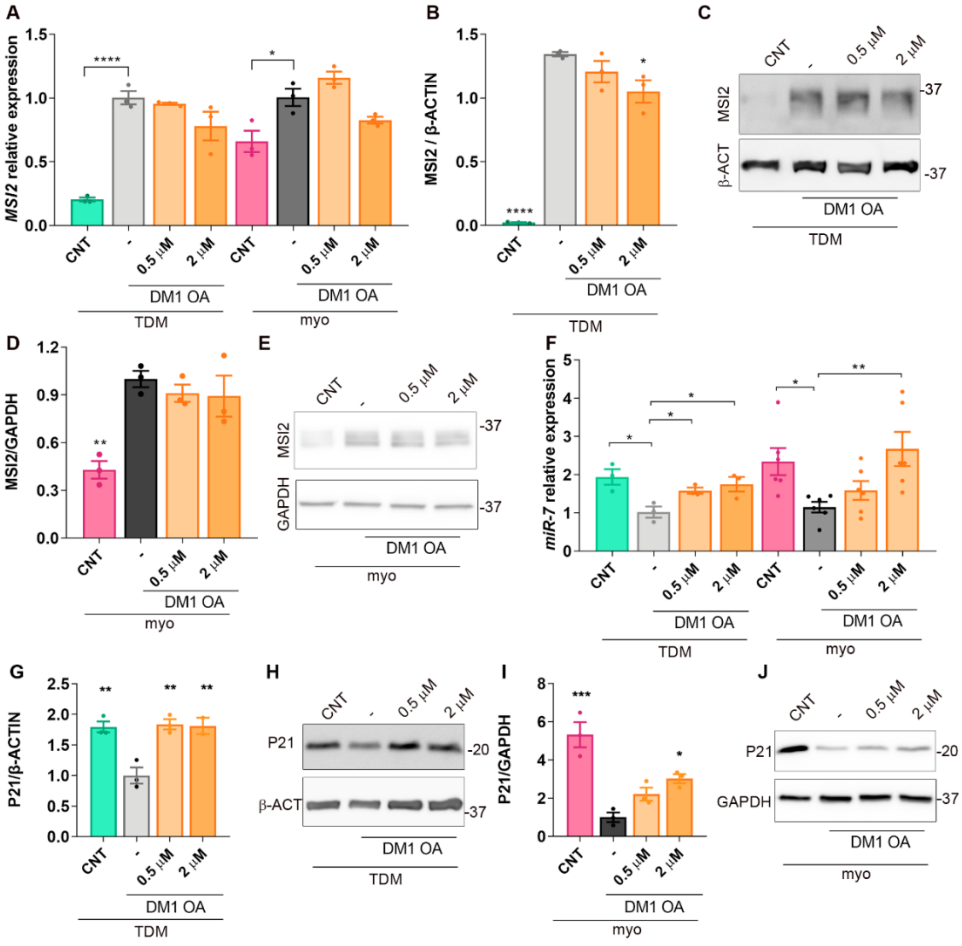

Fig. R-21. Inhibition of MSI2 activity by OA increases levels of MSI2 targets. Quantification of *MSI2* transcripts (A) or protein (B-E) in 7-day-differentiated TDM (B,C) and immortalized myoblasts (D,E) treated with 1% DMSO as vehicle (-) or OA at the indicated concentrations (n=3). Representative western blots are also shown (C,E). (F) The same samples as in (A) were used to determine relative miR-7 levels by RT-qPCR. (G-J) Quantification of P21 relative levels by western blot in the indicated conditions. *MSI2* transcripts were normalized to endogenous expression of the mean of *GAPDH* and *GPI*. miR-7 quantification is relative to endogenous *U1* and *U6* levels. Asterisks indicate statistically significant differences between DM1 cells treated with DMSO (-) and the conditions indicated in the graphs. The bar graphs show mean±S.E.M. *P<0.05, **P<0.01, **** P<0.0001 according to one-way ANOVA test.

3.3.3. Excessive muscle autophagy in DM1 is restored upon OA treatment.

It was previously demonstrated that abnormally low levels of miR-7 in DM1 muscle cells contribute to the pathological increase in autophagy and that its modulation was sufficient to impact this catabolic pathway (Sabater-Arcis et al., 2020). Therefore, after confirming the de-repression of miR-7 biogenesis upon OA treatment, we investigated autophagy status in OA-treated TDM and immortalized myoblasts by staining the cells with LysoTracker. This acidotropic dye marks the acidic cellular compartments, namely, lysosomes and autophagolysosomes. Compared to control counterparts, we confirmed a stronger signal indicative of autophagy overactivation in DM1 cells. Notably, a substantial signal reduction was detected in cells that underwent OA treatment at either 0.5 or 2 µM (Fig. R-22 A-H), despite still being higher than that in control cells. Additionally, LC3-I and LC3 conjugated to membrane-bound phosphatidylethanolamine (LC3-II) were detected by immunofluorescence. DM1 cells (TDM and immortalized myoblasts) showed a strong signal with a punctate pattern corresponding to LC3-II in autophagosomes (ref) (Fig. 22 I-P). In healthy controls, the signal was less intense, more diffuse, and predominantly cytoplasmatic, indicating the presence of soluble LC3-I, and reduced autophagic levels. In OA-treated DM1 cells, the signal lost intensity, and the presence of dots dropped notably. We quantified LC3-II dots per unit of area in each experimental condition (Fig. R-22 Q,R). Results revealed a significant 5 and 4-fold increase in the presence of LC3-II in DM1 TDM and immortalized myoblasts, respectively, compared to their corresponding controls that significantly dropped in OA-treated cells, reaching levels similar to those in control cells at the highest tested OA dose.

Complementary to the immunofluorescence assessment of autophagosome-associated and soluble LC3 (LC3-II/LC3-I ratio), we quantified their levels by western blot. Results confirmed the overactivation of the pathway in DM1 TDM as well as in DM1 myoblasts, and the LC3-II/LC3-I ratio was restored to close to normal when cells were cultured at the highest OA dose (Fig. R-22 S,T). Importantly, this

reduction was in a dose-dependent manner in the case of TDM, where no effect was detected in cells treated with 0.5 μM OA, but a substantial drop in the ratio was observed upon OA treatment at the highest dose. When DM1 myoblasts were supplemented, the parameter was reduced to almost half the values in untreated cells, with a slight difference between both concentrations of OA tested.

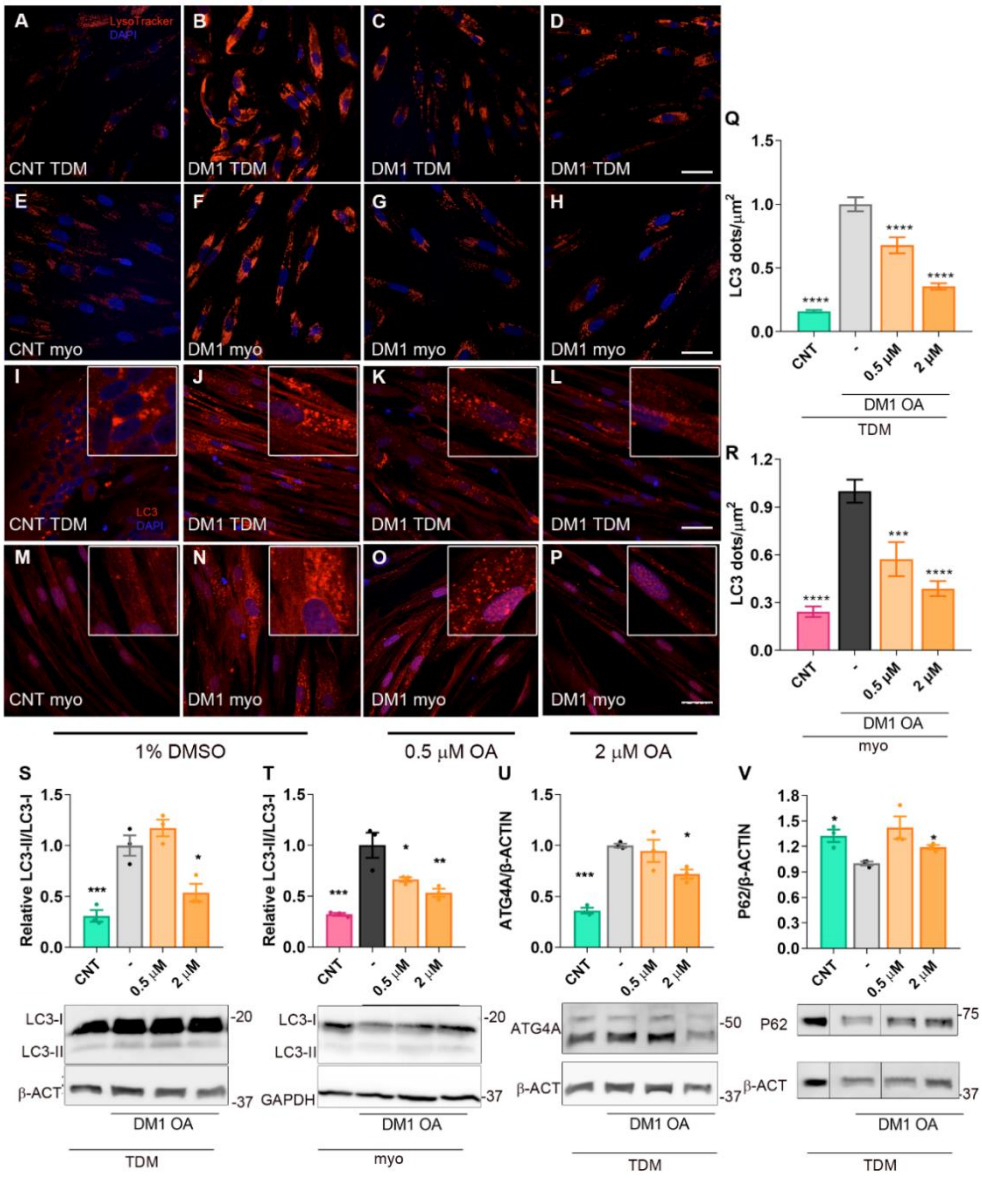

Fig. R-22. OA represses autophagy in DM1. Representative confocal images of LysoTracker staining (red, A-H) and LC3 immunodetection (red, I-P) in TDM (A-D, I-L) and immortalized myoblasts (E-H, M-P) treated for 24 h with 1% DMSO or OA at a final concentration of 0.5 or 2 μM and differentiated for 7 days. (Q, R) Quantification of LC3 puncta per square micrometer (n=20 to 25 images per condition) in TDM (Q) and immortalized myoblasts (R). (S-V) Quantification and representative western blots of immunoreactive bands for LC3 in control and DM1 TDM (S) or immortalized myoblasts (T). (U,V) Representative western blots, with indication of molecular weight sizes to the right in kDa and quantification of total ATG4 and P62 in protein extracts from healthy control (CNT), DM1 TDM untreated or treated with the indicated concentrations and differentiated for 7 days. DM1 cells were treated with 1% DMSO as a control (-) or 0.5 or 2 μM OA for 24 h (n=3). Each condition was compared to DM1 cells treated with 1% DMSO. The scale bar equals 20 μm. Nuclei were counterstained with DAPI. The bar graphs show mean±S.E.M. *P<0.05, **P<0.01, ***P< 0.001, and ****P< 0.0001 according to one-way ANOVA test.

To confirm the effect of OA supplementation on this pathway, we additionally evaluated ATG4A, which, besides being directly involved in the autophagic pathway, is translationally repressed by miR-7 (Gu et al., 2017). Results showed that ATG4 was overexpressed (3-fold) in DM1 TDM, and protein levels significantly decreased upon OA treatment at the highest dose (Fig. R-22 U). Finally, we evaluated the impact of OA treatment on the P62 scaffold protein (Fig. R-22 V). Low levels of autophagic activity lead to the accumulation of P62, as autophagy itself degrades the protein (Bjørkøy et al., 2009; Rusten & Stenmark, 2010). Our results confirm the significant reduction of this protein in DM1 TDM cells and its increase toward control-like amounts upon supplementing OA in the cell medium.

3.3.4. OA supplementation enhances DM1 muscle cell differentiation.

Given the background linking OA to cell proliferation and differentiation (Tan et al., 2021; Watanabe et al., 2020; G. Zhang et al., 2012), we proposed that its low levels could be one of the reasons why DM1 model cells have differentiation defects, as previously reported (André et al., 2018; Arandel et al., 2017; Sabater-Arcis et al., 2020). To test this hypothesis, the different cell lines (Table R-2) were exposed to 0.5 or 2 μM of OA and stained for Desmin, a marker of myotubes. Then, the fusion index

and diameter of 7-day-differentiated myotubes were determined. In immortalized healthy myoblasts and TDMs, we determined the fusion index and myotube diameter in parallel at differentiation times of 0, 4, 7, and 10 days. Results demonstrated a similar evolution of the fusion index in both lines with an exponential increase until 7 days of differentiation, where values close to 100% were reached and remained stable until day 10. Regarding the myotube diameter, we observed an increase in the values of this parameter as days of differentiation increased, while for TDMs at day 10, a marked drop ($p>0.0001$) in this parameter was observed compared to the previous time point, 7 days (Fig. R-23 A-J).

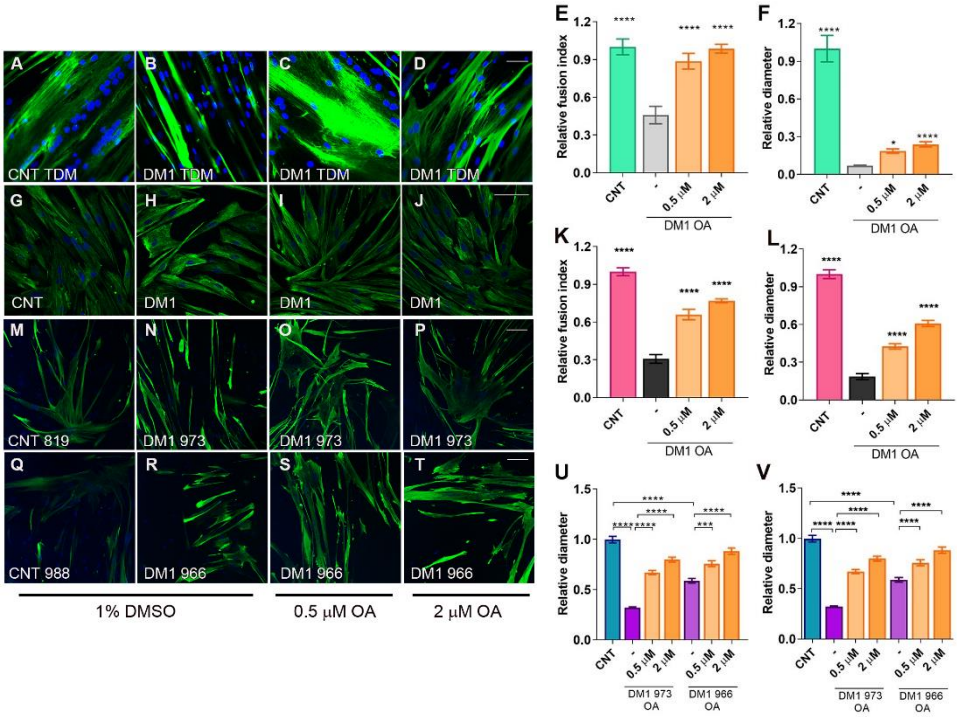

Fig. R-23. OA treatment promotes muscle cell differentiation parameters in DM1 cells. Representative confocal microscopy images of immunofluorescence using an anti-Desmin antibody (green) in CNT and DM1 TDM (A-D), immortalized myoblasts (G-J), and the indicated control (M and Q) and DM1 pTDMs (N-P and R-T). The DM1 lines were treated with 1% DMSO, 0.5, or 2 µM of OA for 24 h. CNT cells were treated with 1% DMSO. In all cases, cells were differentiated for 7 days. Nuclei were counterstained with DAPI. The scale bar equals 100 µm. Fusion index (E,K,U) and myotube diameter (F,L,V) were obtained for each cell line (n=10 to 15 images per condition). All comparisons were made against DM1 cells treated with the vehicle (- in the graphs). The bar graphs show mean±S.E.M. *P<0.05, ***P<0.001, **** P<0.0001 according to one-way ANOVA test.

Overall, these results demonstrate that under our experimental conditions, at 7 days of differentiation, both myoblasts and TDMs behave similarly in terms of their differentiation profile. In all cases, the treatment was found to improve the phenotypes significantly. Specifically, for TDM (Fig. R-23 A-F), DM1 cells showed their fusion capacity reduced to less than half of that observed in control cells, which, upon OA treatment, reached values similar to those in the control condition (Fig. R-23 E). As for myotube diameter, also reduced in DM1 TDM, this parameter improved by 2 to 4 times upon OA supplementation compared to untreated DM1 TDM (Fig. R-23 F). However, the size of the cells was still significantly smaller than control TDMs, and the rescue was far from complete. Results were reproduced when the experiment was carried out in DM1 immortalized myoblasts (Fig. R-23 G-L) and DM1 pTDMs (Fig. R-23 M-V). In pTDM, although both fusion index and diameter phenotypes were milder than in the other cell lines, they still significantly ameliorated upon OA treatment.

We also performed MF20 immunofluorescence in TDMs as a marker of late differentiation of myotubes (Chal & Pourquié, 2017). The analysis of the images revealed a pronounced defect in the terminal differentiation of DM1 cells, as no stained cells were detected with an anti-MF20 antibody. However, following treatment with OA, this value increased in a dose-dependent manner, reaching 60% in cells treated with the highest concentration of OA, with values even exceeding

those obtained for control cells (Fig. R-24 A-E). Similar to fusion index and diameter, OA treatment was sufficient to improve this phenotype significantly.

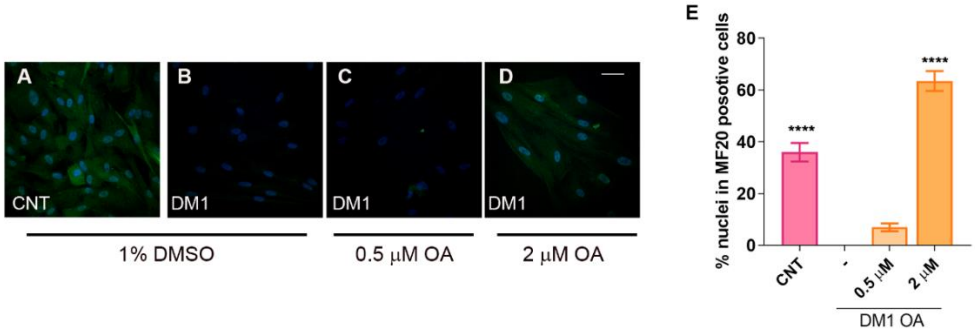

Fig. R-24. MF20 immunostaining in OA-treated TDMs (A-D) Representative confocal micrographs of MF20 immunostaining (green) in 7-day-differentiated control or DM1 TDMs treated with the indicated compounds and concentrations. (E) Quantification of the percentage of nuclei within MF20-positive cells in each condition. Nuclei were stained with DAPI. Scale bar: 40 μm. All data were compared to cells treated with DMSO (-). The bar graphs show the mean±SEM; $P < 0.0001$, according to the one-way ANOVA test.

3.3.5. DM1 muscle cell differentiation rescue by OA is specific.

To ascertain whether the phenotype reversal is specific to OA supplementation and not attributable to a general deficit of fatty acids, we assessed the impact of supplementing the medium with elaidic acid (EA). The EA fatty acid is a *trans*-isoform of OA with the same molecular weight, similar refractive index, and molar aqueous solubility, but its ω-9 double bond is *trans* rather than *cis* (Mensink, 2005), and cannot interfere with MSI2 activity (Clingman et al., 2014). In fact, it has been demonstrated that OA binds directly to MSI2 with an inhibition constant of 1.2 μM. However, this parameter could not be obtained for EA as its interaction with MSI2 is minimal when tested at similar concentrations to those used with OA (Clingman et al., 2014; Kumar et al., 2017). Additionally, recent results have elucidated the tridimensional structure of the interaction between MSI2 and OA (Yeh et al., 2023). Thus, EA is an appropriate control to demonstrate the specificity of the OA

treatment. For that purpose, we treated DM1 lines with 2 µM EA, the highest concentration at which the OA effect was studied. We immunodetected DESMIN with a specific antibody in the four available DM1 patient-derived lines in which we demonstrated that OA supplementation was sufficient to improve both fusion capacity and cell size significantly. Notably, no significant differences were detected in either parameter between cells treated with DMSO and 2 µM of EA (Fig. R-25 A-J).

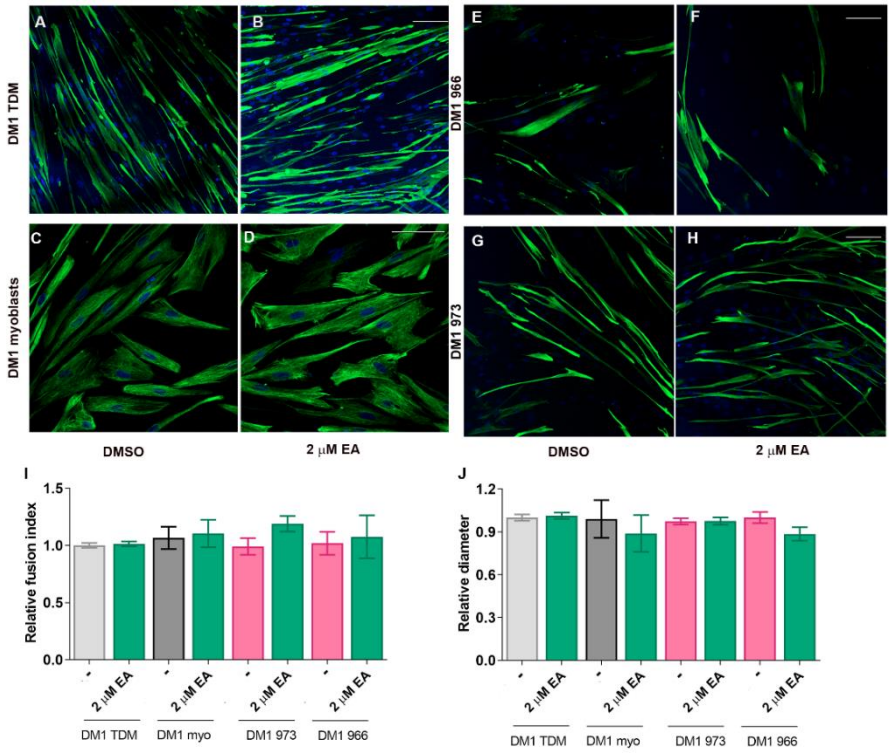

Fig. R-25. The OA isoschizomer EA fails to rescue DM1 muscle cell differentiation defects. Representative immunofluorescence stainings of Desmin (green) in 7-day-differentiated DM1 TDMs (A,B), DM1 immortalized myoblasts (C,D), and two lines of primary fibroblast transdifferentiated into myotubes (E,F, and G,H) treated with 1% DMSO (A,C,E,G) or 2 µM EA (B,D,F,H). Two parameters were analyzed for each condition, the fusion index (I) and the myotube diameter (J), shown relative to the DMSO condition. Nuclei were stained in blue (DAPI). The scale bar equals 100 µm. The bar graphs show mean±S.E.M. No significant differences were detected according to a Student's t-test.

Effects of EA were characterized at the molecular level in DM1 TDMs and immortalized myoblasts differentiated for 7 days. First, treatment with the OA isoschizomer EA did not affect MSI2 protein levels (Fig. R-26 A-D). Nevertheless, as was the case after OA treatment, there was a possibility that EA was hindering the interaction of MSI2 with its targets. However, we confirmed that both miR-7 and P21 levels remained unchanged after exposure of both cell lines to EA-supplemented medium (Fig. R-26 E-I). Consistent with these results, we also detected no effect on the autophagy marker LC3-II/LC3-I ratio, which was sensitive to OA treatment of DM1 muscle cells (Fig. R-26 J-M). Our results confirm that MSI2 inhibition is OA-specific, which is in line with results obtained by independent groups that showed that the affinity of EA for MSI2 was much lower than that of its isoschizomer, OA (Clingman et al., 2014).

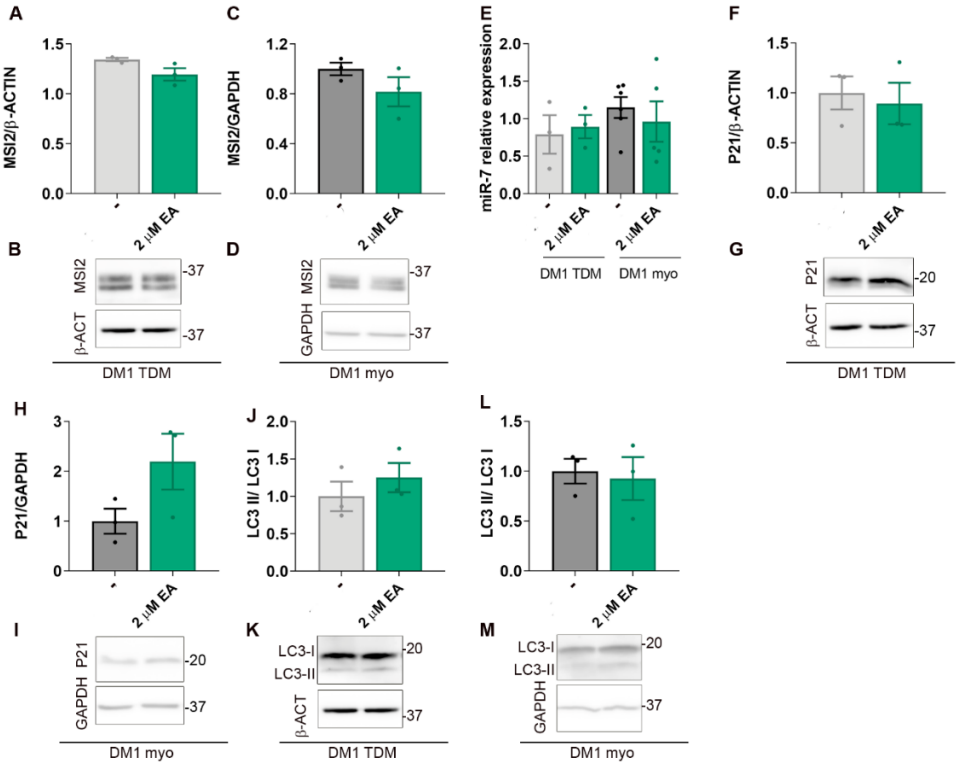

Fig. R-26. EA fails to inhibit several MSI2-related molecular functions. (A-D) Quantification and representative blots of immunoreactive bands for MSI2 in protein extracts from DM1 TDMs (B,C) or immortalized myoblasts (D,E) supplemented for 24 h with 1% DMSO or 2 μM EA. (E) Quantification of the relative expression of miR-7 relative to endogenous U1 and U6 levels (n=3-5) in DM1 TDMs and immortalized myoblasts treated for 24 h with 1% DMSO or 2 μM EA and differentiated for 7 days**.** *MSI2* transcripts were normalized to endogenous expression of the mean of *GAPDH* and *GPI* (n=3). (F-M) Quantification and representative blots of P21 levels and LC3-II/LC3-I ratio in DM1 TDMs (F,G,J, K) or immortalized myoblasts (H,I,L,M) in the same experimental conditions as in (A-D) (n=3). The bar graphs show mean±S.E.M. No significant differences were detected according to a Student's t-test between DMSO and EA-treated cells.

Additionally, we evaluated the expression of *peroxisome proliferator-activator receptor γ coactivator 1-α* (*PGC1α*), whose expression depends on OA levels in skeletal muscle (Lim et al., 2013) and those of *fatty acid synthase* (*FAS,* also known as *FASN*) and *3-hydroxy-2-methylglutaryl-CoA reductase* (*HMGR*) whose upregulation occurs after EA supplementation in HuH-7 hepatic cells (Shao & Ford, 2014).

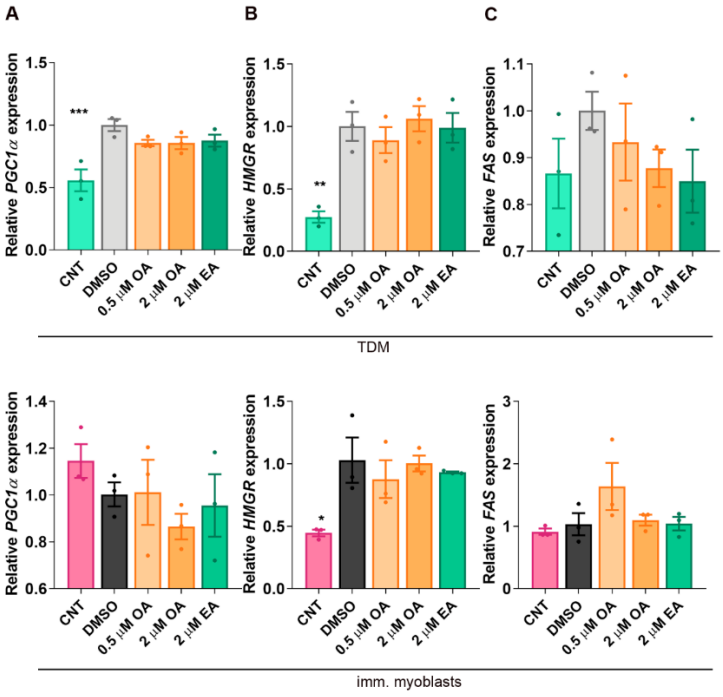

Fig. R-27. The OA isoschizomer EA fails to rescue DM1 muscle cell differentiation defects. Representative immunofluorescence stainings of Desmin (green) in 7-day-differentiated DM1 TDMs (A,B), DM1 immortalized myoblasts (C,D), and two lines of primary fibroblast transdifferentiated into myotubes (E,F, and G,H) treated with 1% DMSO (A,C,E,G) or 2 µM EA (B,D,F,H). Two parameters were analyzed for each condition, the fusion index (I) and the myotube diameter (J), shown relative to the DMSO condition. Nuclei were stained in blue (DAPI). The scale bar equals 100 µm. The bar graphs show mean±S.E.M. No significant differences were detected according to a Student's t-test.

However, the data showed that the expression of these genes remained stable after supplementation of the medium with either OA or EA (Fig. R-27). This suggests that the OA effect at the concentrations tested in DM1 cells may be due specifically to its interaction with MSI2 and not to other canonical pathways related to lipogenesis and fatty acid oxidation where similar *in vitro* experiments use concentrations up to 250-fold higher than those used in this work (Granados et al., 2011).

3.6. SCD1 expression is strongly repressed in DM1 muscle cells.

Having confirmed the deficit of OA in DM1 muscle cells and the therapeutic potential of its supplementation, we investigated the causes that could be contributing to its deficit. Unlike other fatty acids that come exclusively from the diet, OA can be synthesized *de novo* by stearoyl-CoA desaturase 1 (SCD1) from stearic acid (Piccinin et al., 2019). To assess the hypothesis that endogenous production of OA is impaired in DM1 cells, we quantified this enzyme's levels in the cell lines in which we had previously confirmed OA deficit. The results demonstrated a decrease of more than 14-fold in DM1 TDMs compared to controls (Fig. R-28 A,B); this reduction was also significant in immortalized myoblasts although milder than in the previous case (2-fold reduction) (Fig. R-28 C,D). Finally, in the case of pTDM, the enzyme was strongly reduced (between four and six times) in patient-derived pTDM when compared to lines 988. However, no significant differences were detected when comparing cells derived from patients to those from controls 819 (Fig. R-28 E,F).

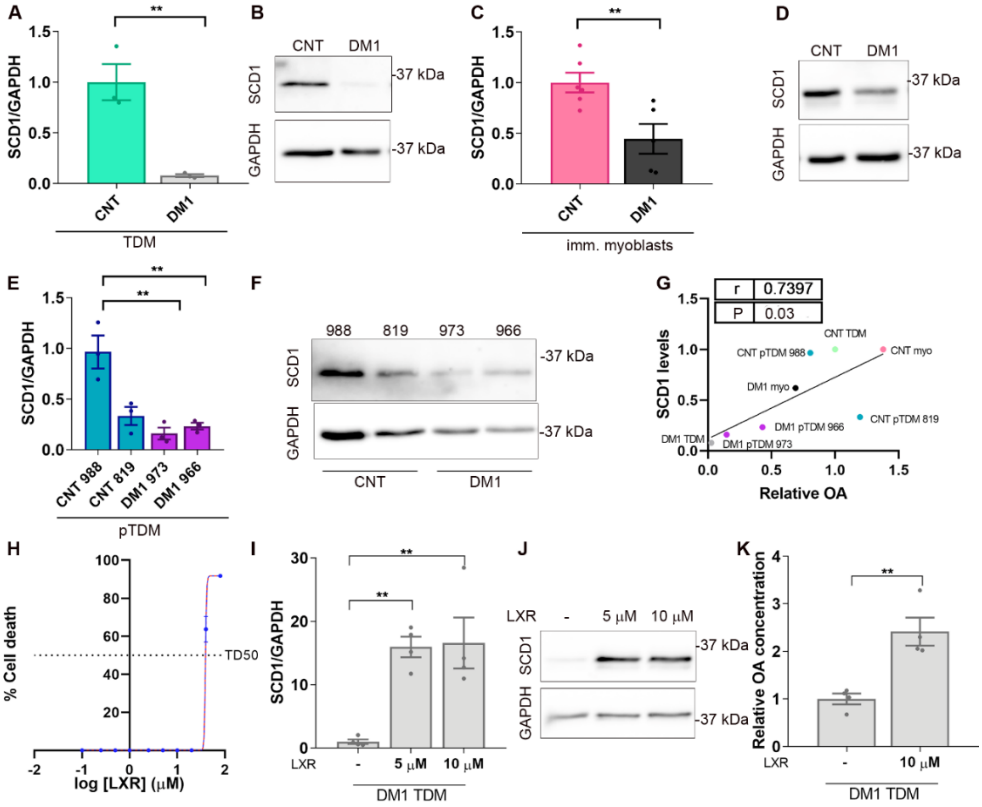

Fig. R-28. Expression of the critical OA synthesis enzyme SCD1 is reduced in DM1 cells. (A-F) Quantification and representative immunoblots of SCD1 in control and DM1 TDMs (A,B) immortalized myoblasts (C,D), and in two different lines of control (988 and 819) and DM1 (973 and 966) pTDMs. (G) Pearson's correlations between the relative SCD1 protein levels and OA levels in control and DM1 TDM (CNT/DM1 TDM), immortalized myoblasts (CNT/DM1 myo) or primary transdifferentiated myoblasts (CNT/DM1 pTDM). (H) Cell growth inhibition assay by 3-(4,5-dimethylthiazol-2-yl)-5-(3-carboxymethoxy-phenyl)-2-(4-sulfophenyl)-2H-tetrazolium, inner salt (MTS) method. 7-day-differentiated DM1 TDM were treated with a range of concentrations of LXR (n = 4). TD50 (39.03 μM) was obtained using the least-squares non-linear regression model. (I,J) Determination of relative SCD1 levels in DM1 TDM supplemented with 5 or 10 μM LXR. (K) Quantification of OA levels by LC/MS in LXR-treated DM1 TDM. In all cases, cells were differentiated for 7 days. Protein was normalized to endogenous GAPDH. The bar graphs show mean±S.E.M. **P<0.01 according to a Student's t-test. In all cases, 3<n<6.

Consistently, the relative expression of SCD1 protein and OA levels correlated positively and significantly in all the DM1 muscular cell lines (r=0.74, p=0.03) (Fig. R-28 G). To confirm that the OA deficit in DM1 conditions was at least partially due to SCD1 deficiency, we proceeded to supplement the medium of the cells with a liver X receptor (LXR) agonist. LXR is a nuclear receptor and transcription factor that directly and positively regulates SCD1 (Piccinin et al., 2021; Yao et al., 2016). First, we evaluated the toxicity of this compound in DM1 TDM differentiated for 7 days to establish a safe range of working concentrations (Fig. R-28 H). It was determined that the TD50 was 39.03 µM. Thus, we proceeded to supplement the cells with 5 or 10 µM LXR. After treatment, SCD1 levels were determined, and its activation was confirmed by detecting a more than 15-fold increase regardless of the LXR dose. Similar results were observed both at protein and mRNA levels (Fig. R-28 I,J). SCD1 activation correlated with a more than 2-fold increase in OA levels in DM1 TDM (Fig. R-28 K).

As controls, we quantified transcripts of *ATP binding cassette subfamily A member 1* (*ABCA1*), *ring finger protein 145* (*RNF145*), and *FAS*, also regulated by LXR transcription factor and involved in the metabolism of cholesterol (Fig. R-29) (B. Wang & Tontonoz, 2018). At the tested doses, the LXR agonist was sufficient to induce *ABCA1* and *RNF145* expression. However, no effect on *FAS* transcripts was detected, supporting the idea that response to LXR-agonist treatment was dose-dependent and did not have broad effects at the tested concentrations.

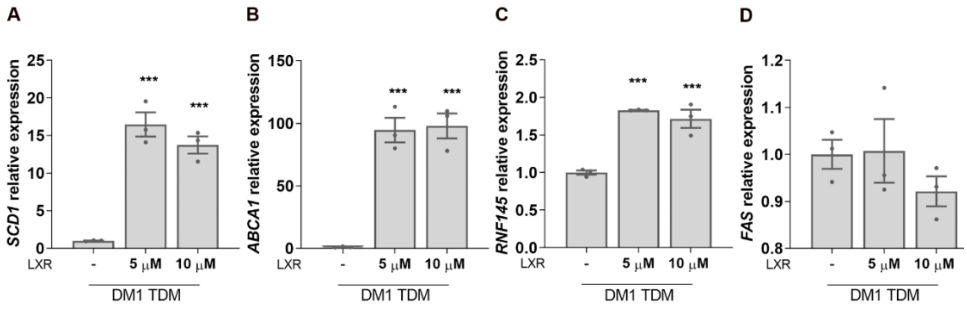

Fig. R-29. Quantification by RT-qPCR of the relative expression of (A) *SCD1*, (B) *ABCA1*, (C) *RNF15*, and (D) *FAS* in DM1 TDM treated with the indicated concentrations of LXR agonist. Gene expression was normalized to *GAPDH,* and *GPI* expression. Three independent experiments with three technical replicates from each biological sample were performed. The bar graphs show the mean ± SEM *** P<0.001 according to the one-way ANOVA test.

Together, these results demonstrate that a deficit in SCD1 enzyme levels contributes to low levels of OA present in DM1 muscle cells.

3.4. DISCUSSION

We have previously demonstrated that miR-7 is downregulated in DM1 and that MSI2 overexpression contributes to this reduction (Sabater-Arcis et al., 2020, 2021). OA inhibits the RNA-binding ability of the MSI1 and MSI2 proteins by interacting with their N-terminal RNA recognition motif (RRM1) and inducing an allosteric change to the MSI conformation, thus preventing binding to target RNAs, including miR-7 biogenesis precursors (Clingman et al., 2014). Indeed, HeLA cell treatment with OA was sufficient to induce mature miR-7 production due to the inhibitory role of OA on MSI2 activity (Kumar et al., 2017). Determination of OA levels in DM1 myotubes demonstrated a marked deficit of OA levels. Therefore, two seemingly independent contributions exist to reducing mir-7 levels and enhancing its pathological effects. On the one hand, the overexpression of MSI2 in DM1 and, on the other hand, the deficit of OA potentiates the inhibitory activity of MSI2 on miR-7. Altered OA levels have been linked to pathologies of many different etiologies, such as Alzheimer's disease (Amtul et al., 2011), cardiovascular disease (Perdomo et al., 2015), or cancer (Navarro-Tito et al., 2010). There are more than 150 clinical trials for various pathologies in which OA is being assessed as therapy (*Search for: Other Terms: Oleic Acid | Card Results | ClinicalTrials.Gov*, n.d.). Thus, we report the reduced OA levels and its therapeutic potential in myotonic dystrophy.

Our results suggest a defect in OA biosynthesis as the leading cause of its low levels. OA reaches cells supplied from the diet or is endogenously produced from the

desaturation of stearic acid by the SCD1 enzyme that converts saturated fatty acids into their monounsaturated counterparts by introducing a double bond between positions 9 and 10 of the carbon chain (Stevenson et al., 2016). Independent studies observed that SCD1 levels increase during myogenesis when satellite cells differentiate into myotubes (Pinheiro, 2012), reducing stearic acid levels while OA levels increase. These data are consistent with ours, where the defective muscle differentiation observed in DM1 myoblasts (Sabater-Arcis et al., 2020) could be related to the abnormally low levels of SCD1 and reduced OA. Indeed, OA levels in myoblasts at 0 days of differentiation showed no differences between healthy and DM1 cells. However, after 7 days in the differentiation medium, OA levels in DM1 cells dropped by half compared to controls. Interestingly, differences in OA levels between control and DM1 were higher in fibroblast-derived cells compared to myoblasts. Additionally, in all cases, OA levels correlated with SCD1 reduction in these cell types. Moreover, it is worth mentioning that SCD1 is a short-lived multispanning ER membrane protein reported to be ubiquitously degraded by the ubiquitin-proteasome system (UPS). An abnormal increase in UPS activity was described in skeletal and cardiac muscle from DM300 and DMSXL model mice (Huguet et al., 2012; Vignaud et al., 2010). Consistent with these observations, studies in human myoblasts from DM1 patients confirmed abnormal overexpression of UPS-related genes (Arandel et al., 2017). It was also demonstrated that miR-7 regulates UPS in these cells as supplementation of DM1 muscle cells with a miR-7 mimic repressed UPS while treatment of control cells with an antagomiR promoted UPS-related gene expression (Sabater-Arcis et al., 2020). Thus, considering our results, the overactivated UPS system may promote the degradation of SCD1 over its synthesis, leading to fatty acid dysregulation. In addition, OA supplementation enhances miR-7 biogenesis, which impacts UPS by inhibiting its activity. All this may translate into a decrease in SCD1 degradation through the UPS pathway, generating a regulatory loop that improves the alterations generated by the DM1 pathological conditions (Fig. R-30). DM1 is classified as a spliceopathy, and it is reasonable to speculate that besides a reduced expression of SCD1, the enzyme has lower activity

due to defective alternative splicing regulation. However, this hypothesis is invalidated by the fact that only one isoform of *SCD1* has been described (Cunningham et al., 2022).

Interestingly, several independent studies reported a very tight and complex regulation of *SCD1* gene expression in response to hormonal factors. DM1-related changes in insulin signaling have been reported in ~30 clinical studies, and insulin resistance is a key phenotype (Nieuwenhuis et al., 2019) due to, at least partially, the aberrant regulation of *insulin receptor* (*INSR*) splicing (López-Martínez et al., 2020). In addition, serum leptin and glucagon levels in DM1 patients are pathologically increased (Stojanovic et al., 2010; Suzuki, 1981). Specifically, insulin is a potent activator of SCD1 transcription (Mauvoisin et al., 2007), while leptin was reported to inhibit SCD1 expression (Casimir & Ntambi, 1996). Additionally, regulation of SCD1 expression by leptin is of particular interest because *in vivo* the role of insulin seems to be subordinate to that of leptin, thus suggesting a crosstalk between the two signaling pathways (Mauvoisin et al., 2010). Similarly, glucagon has also been described as an inhibitor of SCD1 transcription, possibly due to a direct inhibition of the insulin-stimulating effects (Lefevre et al., 1999). Deficient insulin signaling contributes to mTOR/AKT downregulation in DM1, which may fail to activate *sterol regulatory element binding protein 1c* (*SREBP-1C*), a direct transcriptional regulator of fatty acids synthesis genes (G. Chen et al., 2004; Costa et al., 2023; Ozimski et al., 2021). This hypothesis is supported by our results, where we observed that adding an LXR agonist to DM1 cells is sufficient to restore OA levels. Globally, it is likely that defects in the aberrant splicing of *INSR* contribute to SCD1 downregulation in DM1. Moreover, it cannot be ruled out that the induction of *SCD1* expression is the only reason that rescues OA levels since LXR is not specific to SCD1 but activates other genes, including those involved in the cholesterol metabolism such as *ABCA1* or *RNF145*, an integral cell membrane protein that exports of excess cholesterol from cells (Y. Liu & Tang, 2012; B. Wang & Tontonoz, 2018). *ABCA1* expression has been shown to respond to OA levels themselves (H. Song et al., 2023), raising the possibility that the strong increase in *ABCA1* levels may stem from a direct effect by

LXR and indirectly by the rise in OA in comparison to the more modest increases in expression for *SCD1* and *RNF15* whose transcription is also regulated by LXR.

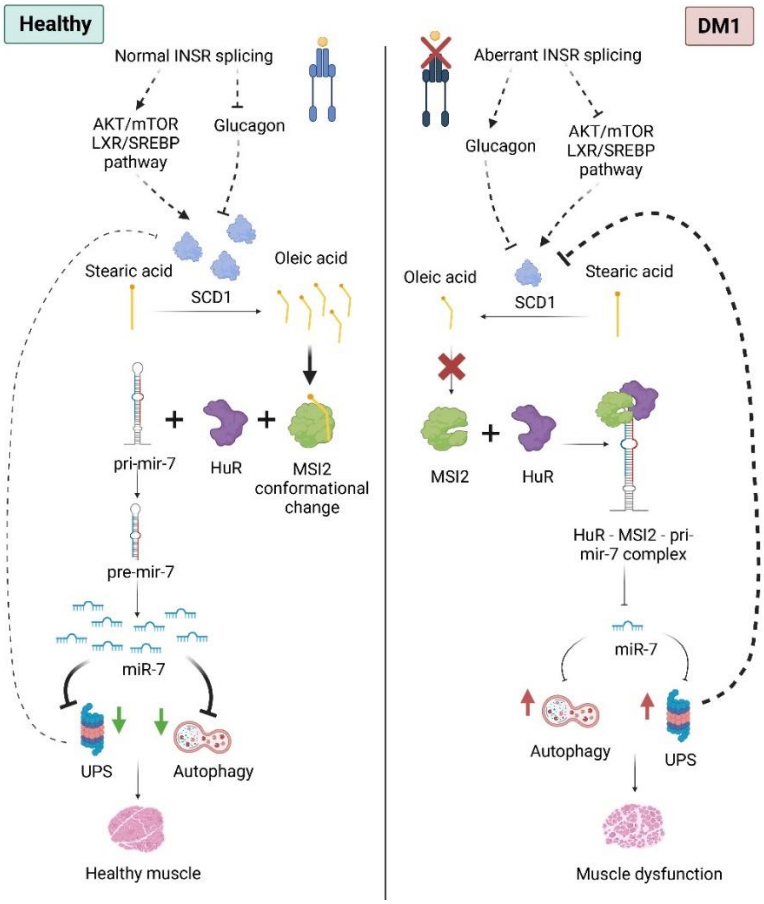

Fig. R-30. Schematic representation of the involvement of OA in DM1. Reduced levels of SCD1 in DM1, possibly promoted by high UPS activity and/or aberrant *INSR* splicing, lead to a deficit of OA. Low OA levels allow the binding of the MSI2-HuR complex to pri-mir-7, thereby inhibiting the generation of the mature miR-7, which derepresses autophagy and UPS leading to the characteristic imbalance of muscle homeostasis of DM1 by potentiating these catabolic pathways. On the other hand, high OA levels release HuR-MSI2 complexes from the pri-mir-7 precursors, allowing normal levels of the miRNA and repression on autophagy and UPS. Figure created with BioRender.com.

OA supplementation has been shown to promote myoblast cell proliferation and differentiation *in vitro* (Briolay et al., 2013; Hurley et al., 2006; J. H. Lee et al., 2009). DM1 myotubes have strongly altered these parameters. However, we observed a complete reversal of differentiation after OA treatment of the cells. This pronounced effect may be due to the sum of the effect of OA on cell differentiation and the MSI2>miR-7 axis, whose modulation by different strategies we have previously observed results in significant improvements in cell differentiation-related parameters (Sabater-Arcis et al., 2020, 2021). As determined by Desmin immunodetection, it is interesting to note that OA treatment led to an increase in myotube fusion capacity and myotube diameter comparable to values previously obtained when MSI2 was silenced by gapmer antisense oligonucleotides or inhibited by the small molecule Ro 08-2750 (Sabater-Arcis et al., 2021). However, in previous work, we reported no effect on the diameter upon miR-7 supplementation by mimetics (Sabater-Arcis et al., 2020). These results suggest that while there is a clear link in DM1 pathology between MSI2 and miR-7, MSI2 may also contribute to pathology independently of miR-7. As shown, MSI2 down-regulates P21, which is a well-known inhibitor of the cell cycle and can arrest its progression in G1/S and G2/M transitions by inhibiting CDK4,6/cyclin-D and CDK2/cyclin-E, respectively (Karimian et al., 2016). At this point, it is important to highlight the relationship between levels OA and P21, likely mediated by the activity of MSI2. Specifically, in TDM, we observed that treatment with OA increased P21 to levels similar to those observed in control cells. However, although significant in immortalized myoblasts, the increase in P21 did not reach the levels observed in healthy cells. These findings are consistent with the results obtained for the fusion index achieved by cells upon supplementation with OA. In aggregate, these findings suggest a correlation between OA levels, P21 expression, and cellular differentiation outcomes. Thus, it is possible that de-repression of P21 after OA treatment is sufficient to enhance terminal differentiation of myotubes, thus promoting an increase in myotubes size.

Cell membrane integrity has been studied in different murine models and DM1 patient biopsies. The authors concluded that the membranes in skeletal muscle,

heart, and brain from DM1 tissue do not exhibit compromised membrane integrity (González-Barriga et al., 2015). In animals, cell membranes consist of various lipid species, classified into three main classes: glycerophospholipids, sphingolipids, and cholesterol. The presence of OA in the phospholipids of the cell membrane can regulate its structure and modify its biophysical properties. Additionally, OA plays a role in stabilizing the bilayer structure and regulating the proteins embedded within the membrane (Lopez et al., 2014). It is possible that the OA deficit observed in DM1, which may be partly attributed to a defect in its biosynthesis, is not sufficient to negatively impact the structure or activity of affected individuals' cell membranes. However, considering that the presence of OA in the organism is derived from both endogenous biosynthesis and dietary intake (Bourre et al., 2004), it is possible that the dietary source is enough to maintain membrane integrity while not adequately interacting with MSI2. Further research is needed to explore the precise mechanisms underlying these observations and their implications in DM1.

GENERAL DISCUSSION

The debilitating effects of muscle atrophy in DM1 significantly impair quality of life and are often a contributing factor to premature mortality in DM1, making it a critical area of investigation. Recent research highlighted the significant role of the MSI2>miR-7>autophagy axis in DM1 pathogenesis. MSI2 is overexpressed in DM1 cell models and patient biopsies, which in turn reduces the expression levels of miR-7. The inhibition of miR-7 biogenesis contributes to the dysregulation of autophagy due to deficient repression of key autophagy genes (Sabater-Arcis et al., 2020, 2021). In this study, we demonstrate the crucial role of MSI2 in DM1, particularly in muscle atrophy progression, and the cause of its overexpression, the sequestration of miR-107 in *DMPK* transcripts. We also revealed a deficiency in OA metabolism in DM1 cell lines and investigated the modulation of miR-7 biogenesis through OA supplementation.

Notably, studies using the HSA^{LR} mouse model reported that although reflective of DM1 symptoms like myotonia and muscle weakness, the HSA^{LR} does not exhibit the severe muscle atrophy observed in humans (Crawford Parks et al., 2020). This discrepancy, potentially caused by the lack of MSI2>miR-7>autophagy axis activation, made the HSA^{LR} mice a perfect model to prove the implications of MSI2 in muscle atrophy. Our results demonstrated that Msi2 overexpression by rAVV in skeletal muscle led to a significant reduction in miR-7 and increased autophagy and muscle degeneration. In fact, demonstrating *in vivo* that Msi2 overexpression produces atrophic phenotypes indicates that MSI2 is both necessary and sufficient to induce increased autophagy and muscle damage characteristic of atrophy in a DM1 context. This observation provides a suitable explanation for the absence of muscle atrophy in the HSA^{LR} mouse model: the lack of Msi2 overexpression prevents a reduction in miR-7 levels, thus maintaining the balance.

Independent studies demonstrated that in a healthy context, MSI2 function is related to myogenesis, and the repression of miR-7 biogenesis by MSI2 enables muscular differentiation, likely via autophagy regulation (R. Wang et al., 2024; W. Yang et al., 2022). For the effective differentiation, basal levels of autophagy are

required, which subsequently decrease as myogenesis progresses (Cho et al., 2014; Fortini, Ferretti, et al., 2016). Indeed, overactivation of autophagy, such as with rapamycin treatment, impedes proper differentiation (Fortini, Iorio, et al., 2016). The importance of balanced autophagy regulation becomes evident when considering both the absence and overexpression of Msi2. Msi2 knock-out mice exhibit impaired muscle regeneration and atrophy, due to dysregulated autophagy (Furuichi et al., 2023; R. Wang et al., 2024). Indeed, MSI2 is highly expressed in stem cells and maintains their pluripotency by regulating autophagy (Wuebben et al., 2012). Thus, while a certain degree of autophagy is necessary for maintaining stem cell integrity, cellular homeostasis and correct muscle differentiation, excessive autophagy is detrimental and leads to muscle atrophy. In DM1, the situation is reversed, while basal MSI2 levels repressing miR-7 are physiological, MSI2 overexpression in DM1 leads to insufficient miR-7 levels and, consequently excessive autophagy, resulting in muscle atrophy. Thus, understanding and regulating MSI2's impact on the autophagy pathway could offer potential therapeutic strategies for DM1 and other autophagy-related disorders.

According to our results, a significant factor contributing to MSI2 overexpression in DM1 is the sequestration of miR-107 by CUG expansions in the mutant *DMPK* RNA. This sequestration reduces the availability of miR-107, releasing repression on MSI2 and resulting in its overexpression. This mechanism underscores the complexity of molecular interactions in DM1, where CUG expansions interfere with MBNL1 function but also contribute to disease pathology through miRNA dysregulation. However, in the HSA^{LR} mouse, we did not observe alterations in the MSI2>miR-7>autophagy axis. Notably, the murine miR-107 is identical to the human and it is also predicted to bind CTG expansions, suggesting a similar mechanism could occur. Nevertheless, this transgenic model has limitations. In DM1 patients, the CUG expansion RNA is found in the entire muscle tissue from the onset of differentiation as *DMPK* is also expressed in satellite cells (Ganassi & Zammit, 2022), whereas, in the HSA^{LR} mouse, the expansions are expressed under the control of the *ACTA1* gene. Evidence supports that in human satellite cells, *ACTA1* expression

remains low and relatively unchanged until day 12 of differentiation, with a significant increase observed only by day 16 (Stern-Straeter et al., 2011). This delay could imply a mosaic expression of the repeats in the mouse muscle, with a higher expression in differentiated and mature muscle cells, while less differentiated satellite cells would exhibit lower expression levels. Mouse myoblasts could, therefore, integrate into the diseased muscle expressing normal Msi2 levels, whereas human counterparts might already express high MSI2 from the begining. Considering additional epigenetics processes, this could explain the apparent inability of the *HSA* transgene to replicate the ability of mutant *DMPK* transcripts to sequestrate miR-107. Alternatively, the availability of miR-107-binding sites in CUG repeat expansions may be limited if, for example, mouse Mbnl1 binding to CUG is stronger than human MBNL1 or the relative abundance/stoichiometry of Mbnl1 to CUG binding sites prevents further binding to miR-107 causing the differences observed between the mouse model and the human cells.

Beyond MSI2 regulation of miR-7 biogenesis, this miRNA could be regulated by several other RBPs, such as QKI or SF2/ASF, which complicates the regulatory landscape of MSI2>miR-7>autophagy axis modulation. This opens the possibility of the alteration of some of these RBPs in the HSA^{LR}, which could overshadow MSI2 regulation, leading to unaltered miR-7 levels in the mouse model. SF2/ASF, a prototypical splicing factor encoded by the *SFRS1* gene, has been demonstrated to play a critical role in pri-miRNA processing. Specifically, SF2/ASF promotes the maturation of miR-7 by directly binding to pri-miR-7 and enhancing Drosha cleavage, functioning independently of its splicing role. This interaction forms a negative feedback loop where mature miR-7 downregulates SFRS1 expression at the translational level, indicating a complex regulatory mechanism coordinating splicing and miRNA-mediated gene repression (H. Wu et al., 2010). Additionally, QKI proteins, particularly two nuclear isoforms, QKI-5 and QKI-6, suppress miR-7 expression in glial cells by inhibiting the processing of primary miR-7 to its mature form. These preferentially nuclear isoforms prevent miR-7 export to the cytoplasm. Consequently, the depletion of QKI proteins leads to elevated miR-7 levels, affecting

downstream signaling pathways such as EGFR expression and ERK activation (Y. Wang et al., 2013).

miR-107 binding to CUG repeats may also have dual implications. On the one hand, miR-107 sequestration could potentially mitigate some symptoms by competing with MBNL1 and partially preserving its function. On the other hand, although the binding predictions for miR-107 to MBNL1 have not been experimentally supported, this interaction suggests a possible direct regulation of MBNL1 by miR-107. Thus, if not sequestered, MBNL1 inhibition might exacerbate DM1 pathology. Understanding the exact role of miR-107 in this context could provide deeper insights into DM1 mechanisms. Indeed, the sequestration of miR-107 by mutant *DMPK* transcripts further complicates the pathology of DM1. miR-107 affects several pathways implicated in DM1 beyond the MSI2>miR-7>autophagy axis. miR-107 targets several key genes involved in muscle differentiation and maintenance, such as PTEN and CDK6 (Ahonen et al., 2019; Feng et al., 2012; S. Wang et al., 2019). The dysregulation of these targets due to miR-107 sequestration could also contribute to the symptoms of DM1.

For instance, it has been suggested that PTEN overexpression is one of the causes leading to the downregulation of PI3K/AKT pathway that was linked to multiple cellular processes implicated in DM1, such as apoptosis, autophagy, and excessive ubiquitin-proteasome activity (Egerman & Glass, 2014; Morriss et al., 2018; Ozimski et al., 2021; Parks et al., 2017; Stitt et al., 2004). AKT, in turn, inhibits the activity of GSK3β, hyperactivated in DM1 (Jones et al., 2012) and is associated with the altered expression of skeletal muscle genes like MEF2 and MAPK (Dionyssiou et al., 2013), both crucial for muscle cell differentiation, maintenance and proliferation. Thus, despite the overexpression of Staufen 1 (STAU) being described as a possible cause of PTEN upregulation, it could be a combinatory effect involving miR-107 regulation of PTEN (Ozimski et al., 2021; Parks et al., 2017; F. Tian et al., 2019). Our results demonstrate that restoration of miR-107 levels through agomiR-107 improves fusion index and myotube diameter, potentially by means of PTEN downregulation

subsequently inhibiting GSK3β. In fact, GSK3β is the target of Tideglusib, a drug candidate to treat DM1 (Lutz et al., 2023). Additionally, dysregulation of AKT due to PTEN upregulation also affects the AKT/mTOR pathway, leading to FOXOs translocation into the nucleus. FOXO1 and FOXO3 are transcription factors directly related to the expression of atrogenes such as MuRF1 and Atrogin-1 (Sandri et al., 2004). Our findings strengthen prior evidence of hyperactive autophagy processes in DM1 (Loro et al., 2010; Morriss et al., 2018; Sabater-Arcis et al., 2020, 2021). Particularly, these disruptions were ameliorated upon replenishing miR-107. This suggests that miR-107 sequestration leads to increased muscle impairment, primarily through the MSI2>miR-7 pathway but with a potential PTEN>AKT>FOXO pathway contribution.

Another interesting target validated for miR-107 is CDK6 (Ahonen et al., 2019; Feng et al., 2012). In a typical differentiation cascade, increased p21 and diminished CDK6 expression prompt G1 cell cycle exit and subsequent cellular differentiation. However, in DM1, the dysregulation of this process is evident. Heightened MSI2 levels contribute to reduced p21 expression (Sabater-Arcis et al., 2021), compounded by the upregulation of CDK6. MSI2>p21 dysregulation likely stems from the sequestration of miR-107 by mutant *DMPK* transcripts, as we have suggested in our study. The comparison of early differentiation programs in isogenic cDM1 myoblasts with and without 2,600 CTG repeat further supports the findings involving CDK6 (André et al., 2019; Costa et al., 2023), emphasizing the impact of CUG expansions on the dysregulation of miR-107 and its downstream targets.

It is well known that exercise has a beneficial effect on skeletal muscle by modulating the autophagy process (Botella et al., 2024; da Rocha et al., 2020). Besides, exercise has also been linked to disease related phenotypic rescue in the DM1 mouse model (Sharp et al., 2019). In parallel, exercise has been found to increase miR-107 expression. Safdar *et al*. reported a 56% increase in miR-107 expression following acute endurance exercise in mice and independent studies have also shown that mice with high exercise capacity exhibit significant

upregulation of miR-107, which in addition enhances insulin sensitivity (Safdar et al., 2009; Tung et al., 2019). These observations suggest a possible connection between the improvement in autophagy and the rise in miR-107 expression. Exercise could potentially decrease autophagic activity through the elevation of miR-107 levels and the modulation of the MSI2>miR-7>autophagy pathway, where increased miR-107 may reduce MSI2 levels, affecting miR-7 and subsequently leading to the normalization of autophagic activity.

The findings of this study underscore that the MSI2>miR-7>autophagy axis operates independently of the alterations in MBNL1 typically associated with DM1 pathology. Instead, this pathway is directly influenced by the expanded CUG repeats present in the *DMPK* transcripts. The direct interaction between the expanded repeats and miR-107, suggests a distinct pathological mechanism that contributes to muscle dysfunction separate from the splicing disruptions caused by MBNL1 sequestration. Nonetheless, these pathways could interact downstream of its triggering events. For example, previous studies demonstrated that autophagy inhibition with chloroquine increases MBNL proteins and reduces ribonuclear foci (Bargiela et al., 2019). Another potential point of convergence could be the competition of MBNL and miR-107 for CUG binding sites, however, this possible influence of miR-107 on MBNL levels does not preclude them from being two pathways that act in parallel in DM1 pathogenesis.

Therapeutic modulation of the miR-107>MSI2>miR-7>autophagy axis presents a promising strategy for DM1 treatment particularly because independent studies demonstrated that OA can inhibit MSI2's binding to its targets, promoting miR-7 biogenesis (Kumar et al., 2017). Thus, OA supplementation appears as a new approach to regulate miR-7 levels and autophagy, thus improving muscle homeostasis, at least in cell models of disease.

In addition to the primary focus on the MSI2>miR-7>autophagy axis, our findings underscore the significant role of metabolic regulation involving SCD1 and its

impact with OA in DM1 pathology. The regulation of SCD1 by insulin signalling pathways is particularly relevant, given the characteristic insulin resistance observed in DM1 patients. Insulin resistance disrupts the AKT/mTOR/SREBP1/LXR signalling pathway, which is crucial for the activation of SCD1 expression. This is consistent with our studies where LXR increased SCD1 levels (G. Chen et al., 2004; Mauvoisin et al., 2007; Yao et al., 2016; Yu et al., 2015). Consequently, disruption in glucose metabolism likely contributes to the decreased expression of SCD1 observed in DM1 cells, compounding the metabolic dysregulation characteristic of this disease.

Interestingly, while *in vivo* studies have not yet demonstrated a deficiency in OA, likely due to its daily intake through diet, the dysregulation of SCD1 could be a critical concern. SCD1 is regulated by the UPS, which is hyperactive in DM1 (Kato et al., 2006). The heightened activity of the UPS in DM1 could accelerate the degradation of SCD1, further contributing to the lipid metabolism disturbances observed in DM1. This potential dysregulation of SCD1 in patients, despite adequate dietary OA, suggests that further investigations should not only focus on OA supplementation but also on understanding the underlying mechanisms of this regulatory loop involving OA, miR-7, and SCD1 and the consequences of SCD1 dysregulation. For example, it is known that SCD1 is involved in membrane fluidity regulation (Angelucci et al., 2018), which in fact provides new hypothesis for old studies. Concretely, the altered fatty acid composition, with low linoleic acid (C18:2) and an increased palmitic acid (C16:0), that have been reported in erythrocyte membranes, mononuclear cells, and blood plasma of DM1 patients could be due to the SCD1 alteration (Antoku et al., 1985). SCD1 also plays a protective role in muscle cells regulating insulin signalling, as evidenced by research showing that SCD1 inhibition produces insulin resistance by regulating AKT in L6 myoblasts (Pinnamaneni et al., 2006). Then, it is possible that a regulatory feedback loop occurs in which SCD1 regulates insulin signalling and the insulin pathway also regulates SCD1, emphasising their interdependent relationship. Moreover, OA's ability to increase

adiponectin levels, an insulin-sensitizing hormone, could help alleviate insulin resistance in DM1 patients (Daniele et al., 2011).

In conditions presenting metabolic dysregulation, as occurs in cell models of DM1, OA has demonstrated the potential to improve insulin sensitivity and reduce endoplasmic reticulum (ER) stress (X. Liu et al., 2019). Studies have shown that OA can prevent palmitate-induced insulin resistance in skeletal muscle by modulating lipid composition and preventing ER expansion and stress (G. Peng et al., 2011). Additionally, OA ameliorates type 2 diabetes mellitus by improving insulin sensitivity, inflammation, and regulating glucose and lipid metabolism (Miklankova et al., 2022). OA treatment also upregulates the expression of myosin heavy chain 1 (MyHC1), a marker of type 1 muscle fibers, which upregulation is associated with increased mitochondrial mass and enhanced oxidative metabolism, indicating a potential role in muscle endurance and fatigue resistance (Watanabe et al., 2020). Moreover, OA was found to exert benefits by affecting mitochondrial function, reducing adipose tissue inflammation, and modulating macrophage activation, thereby improving metabolic outcomes in obese mice (W. Li et al., 2021).

In conclusion, the miR-107>MSI2>miR-7>autophagy axis is a critical pathway in DM1 pathogenesis. Dysregulation of this axis contributes to the abnormal autophagy and muscle atrophy observed in DM1. The sequestration of miR-107 by the expanded CUG repeats elucidates a complex regulatory mechanism involving mutant *DMPK* transcripts acting as a sponge. The disruption of miR-107's cellular distribution and function produces the overexpression of Msi2 in DM1, and highlights its crucial role in autophay regulation. Additionally, the novel finding of impaired OA metabolism due to reduced SCD1 underscores a new dimension of metabolic dysfunction contributing to DM1 pathology. Therapeutic strategies aimed at modulating MSI2 and miR-7 levels, as well as addressing miR-107 sequestration, hold promise for treating DM1, and future research should focus on understanding the complex molecular interactions of these key players.

CONCLUSIONS

Considering the results presented in this doctoral thesis, the following conclusions can be derived:

1. The sustained overexpression of Msi2 in HSA^{LR} mouse models significantly promotes autophagy and muscle atrophy. These data highlight MSI2 as a crucial regulator of autophagy and muscle pathology in DM1, providing a potential target for therapeutic intervention.
2. Mutant *DMPK* transcripts act as a sponge for miR-107, sequestering it within the nucleus. Nuclear retention of miR-107 disrupts its normal cellular distribution and impairs its ability to regulate target gene expression post-transcriptionally in the cytoplasm.
3. The sequestration of miR-107 by expanded CUG repeats contributes to MSI2 overexpression in DM1. This finding extends the pathological MSI2>miR-7>autophagy axis to include miR-107 (miR-107>MSI2>miR-7>autophagy), further elucidating the complex molecular mechanisms underlying muscle atrophy in DM1.
4. miR-107 is identified as a potential therapeutic target for restoring normal levels of MSI2, autophagy, and related pathways.
5. The miR-107>MSI2>miR-7>autophagy axis is triggered independently of the MBNL1/CELF1 and its associated missplicings. This indicates that the miR-107>MSI2>miR-7>autophagy pathway functions in parallel with the alternative splicing changes induced by MBNL1 sequestration, highlighting distinct and concurrent mechanisms contributing to the pathogenesis of DM1.
6. Impairment in oleic acid metabolism has been identified in DM1 muscle cell models for the first time, and it is originated, at least partially, from reduced SCD1. This metabolic dysfunction may contribute to the disease pathogenesis through the crucial role of SCD1 in muscle homeostasis.
7. Reduced OA levels observed *in vitro* synergizes with the overexpression of MSI2. Since OA allosterically inhibits MSI2 binding to its molecular targets, lower OA levels exacerbate the MSI2>miR-7>autophagy axis. This synergy

could further explain the atrophy phenotype observed in DM1, suggesting that targeting fatty acid metabolism could be a novel therapeutic approach.

REFERENCES

Abreu, P., Pinheiro, C. H. J., Vitzel, K. F., Vasconcelos, D. A. A., Torres, R. P., Fortes, M. S., Marzuca-Nassr, G. N., Mancini-Filho, J., Hirabara, S. M., & Curi, R. (2016). Contractile function recovery in severely injured gastrocnemius muscle of rats treated with either oleic or linoleic acid. *Experimental Physiology*, *101*(11), 1392–1405. https://doi.org/10.1113/EP085899

Agtmaal, E. L. van, André, L. M., Willemse, M., Cumming, S. A., Kessel, I. D. G. van, Broek, W. J. A. A. van den, Gourdon, G., Furling, D., Mouly, V., Monckton, D. G., Wansink, D. G., & Wieringa, B. (2017). CRISPR/Cas9-Induced (CTG·CAG)n Repeat Instability in the Myotonic Dystrophy Type 1 Locus: Implications for Therapeutic Genome Editing. *Molecular Therapy : The Journal of the American Society of Gene Therapy*, *25*(1), 24–43. https://doi.org/10.1016/J.YMTHE.2016.10.014

Ahonen, M. A., Haridas, P. A. N., Mysore, R., Wabitsch, M., Fischer-Posovszky, P., & Olkkonen, V. M. (2019). miR-107 inhibits CDK6 expression, differentiation, and lipid storage in human adipocytes. *Molecular and Cellular Endocrinology*, *479*, 110–116. https://doi.org/10.1016/J.MCE.2018.09.007

Ambrose, K. K., Ishak, T., Lian, L. H., Goh, K. J., Wong, K. T., Ahmad-Annuar, A., & Thong, M. K. (2017). Deregulation of microRNAs in blood and skeletal muscles of myotonic dystrophy type 1 patients. *Neurology India*, *65*(3), 512–517. https://doi.org/10.4103/NEUROINDIA.NI_237_16

Amtul, Z., Westaway, D., Cechetto, D. F., & Rozmahel, R. F. (2011). Oleic Acid Ameliorates Amyloidosis in Cellular and Mouse Models of Alzheimer's Disease. *Brain Pathology*, *21*(3), 321. https://doi.org/10.1111/J.1750-3639.2010.00449.X

André, L. M., Ausems, C. R. M., Wansink, D. G., & Wieringa, B. (2018). Abnormalities in Skeletal Muscle Myogenesis, Growth, and Regeneration in Myotonic Dystrophy. *Frontiers in Neurology*, *9*(MAY). https://doi.org/10.3389/FNEUR.2018.00368

André, L. M., Cruchten, R. T. P. van, Willemse, M., Bezstarosti, K., Demmers, J. A. A., Agtmaal, E. L. van, Wansink, D. G., & Wieringa, B. (2019). Recovery in the Myogenic Program of Congenital Myotonic Dystrophy Myoblasts after Excision of the Expanded (CTG) n Repeat. *International Journal of Molecular Sciences*, *20*(22). https://doi.org/10.3390/IJMS20225685

Angelucci, C., D'Alessio, A., Iacopino, F., Proietti, G., Di Leone, A., Masetti, R., & Sica, G. (2018). Pivotal role of human stearoyl-CoA desaturases (SCD1 and 5) in breast cancer progression: Oleic acid-based effect of SCD1 on cell migration and a novel pro-cell survival role for SCD5. *Oncotarget*, *9*(36), 24364–24380. https://doi.org/10.18632/oncotarget.25273

Anglister, L., McMahan, U. J., & Marshall, R. M. (1985). Basal lamina directs acetylcholinesterase accumulation at synaptic sites in regenerating muscle. *The Journal of Cell Biology*, *101*(3), 735–743. https://doi.org/10.1083/JCB.101.3.735

Antoku, Y., Sakai, T., Goto, I., Iwashita, H., & Kuroiwa, Y. (1985). Fatty acid compositions of erythrocytes, mononuclear cells and blood plasma of patients with myotonic dystrophy. *Journal of the Neurological Sciences*, *71*(2–3), 387–393. https://doi.org/10.1016/0022-510X(85)90077-2

Antonio, M. D., Dogan, C., Hamroun, D., Mati, M., Zerrouki, S., Eymard, B., Katsahian, S., & Bassez, G. (2016). Unravelling the myotonic dystrophy type 1 clinical spectrum: A systematic registry-based study with implications for disease classification. *Revue Neurologique*, *172*(10), 572–580. https://doi.org/10.1016/J.NEUROL.2016.08.003

Aparicio-Puerta, E., Gómez-Martín, C., Giannoukakos, S., Medina, J. M., Scheepbouwer, C., García-Moreno, A., Carmona-Saez, P., Fromm, B., Pegtel, M., Keller, A., Marchal, J. A., & Hackenberg, M. (2022). sRNAbench and sRNAtoolbox 2022 update: Accurate miRNA and sncRNA profiling for model and non-model organisms. *Nucleic Acids Research*, *50*(W1), W710–W717. https://doi.org/10.1093/NAR/GKAC363

Arandel, L., Espinoza, M. P., Matloka, M., Bazinet, A., Diniz, D. D. D., Naouar, N., Rau, F., Jollet, A., Edom-Vovard, F., Mamchaoui, K., Tarnopolsky, M., Puymirat, J., Battail, C., Boland, A., Deleuze, J. F., Mouly, V., Klein, A. F., & Furling, D. (2017). Immortalized human myotonic dystrophy muscle cell lines to assess therapeutic compounds. *Dis Model Mech*, *10*(4), 487–497. https://doi.org/dmm.027367 [pii] 10.1242/dmm.027367

Artero, R., Prokop, A., Paricio, N., Begemann, G., Pueyo, I., Mlodzik, M., Perez-Alonso, M., & Baylies, M. K. (1998). The muscleblind gene participates in the organization of Z-bands and epidermal attachments of Drosophila muscles and is regulated by Dmef2. *Developmental Biology*, *195*(2), 131–143. https://doi.org/10.1006/DBIO.1997.8833

Ashizawa, T., Gagnon, C., Groh, W. J., Gutmann, L., Johnson, N. E., Meola, G., Moxley, R., Pandya, S., Rogers, M. T., Simpson, E., Angeard, N., Bassez, G., Berggren, K. N., Bhakta, D., Bozzali, M., Broderick, A., Byrne, J. L. B., Campbell, C., Cup, E., … Winblad, S. (2018). Consensus-based care recommendations for adults with myotonic dystrophy type 1. *Neurology. Clinical Practice*, *8*(6), 507–520. https://doi.org/10.1212/CPJ.0000000000000531

Ashizawa, T., & Sarkar, P. S. (2011). Myotonic dystrophy types 1 and 2. *Handbook of Clinical Neurology*, *101*, 193–237. https://doi.org/10.1016/B978-0-08-045031-5.00015-3

Barclay, R. D., Burd, N. A., Tyler, C., Tillin, N. A., & Mackenzie, R. W. (2019). The Role of the IGF-1 Signaling Cascade in Muscle Protein Synthesis and Anabolic Resistance in Aging Skeletal Muscle. *Frontiers in Nutrition*, *6*. https://doi.org/10.3389/FNUT.2019.00146

Bareja, A., Holt, J. A., Luo, G., Chang, C., Lin, J., Hinken, A. C., Freudenberg, J. M., Kraus, W. E., Evans, W. J., & Billin, A. N. (2014). Human and mouse skeletal muscle stem cells: Convergent and divergent mechanisms of myogenesis. *PloS One*, *9*(2). https://doi.org/10.1371/JOURNAL.PONE.0090398

Bargiela, A., Cerro-Herreros, E., Fernandez-Costa, J. M., Vilchez, J. J., Llamusi, B., & Artero, R. (2015). Increased autophagy and apoptosis contribute to muscle atrophy in a myotonic dystrophy type 1 Drosophila model. *Dis Model Mech*, *8*(7), 679–690. https://doi.org/8/7/679 [pii] 10.1242/dmm.018127

Bargiela, A., Sabater-Arcis, M., Espinosa-Espinosa, J., Zulaica, M., Munain, A. L. D., & Artero, R. (2019). Increased Muscleblind levels by chloroquine treatment improve myotonic dystrophy type 1 phenotypes in in vitro and in vivo models. *Proceedings of the National Academy of Sciences of the United States of America*, *116*(50), 25203–25213. https://doi.org/10.1073/PNAS.1820297116

Bargiela, A., Ten-Esteve, A., Martí-Bonmatí, L., Sevilla, T., Perez Alonso, M., & Artero, R. (2023). Quantitative magnetic resonance imaging assessment of muscle composition in myotonic dystrophy mice. *Scientific Reports*, *13*(1), 503. https://doi.org/10.1038/s41598-023-27661-w

Bartolomé, A. R., Martín, V. P., González, C. D., & Miranda, M. R. (2022). [Cognitive impairment in myotonic dystrophy type 1 (Steinert's disease)]. *Semergen*, *48*(3), 208–213. https://doi.org/10.1016/J.SEMERG.2022.01.013

Batra, R., Charizanis, K., Manchanda, M., Mohan, A., Li, M., Finn, D. J., Goodwin, M., Zhang, C., Sobczak, K., Thornton, C. A., & Swanson, M. S. (2014). Loss of MBNL leads to disruption of developmentally regulated alternative polyadenylation in RNA-mediated disease. *Molecular Cell*, *56*(2), 311–322. https://doi.org/10.1016/J.MOLCEL.2014.08.027

Begemann, G., Paricio, N., Artero, R., Kiss, I., Pérez-Alonso, M., & Mlodzik, M. (1997). Muscleblind, a gene required for photoreceptor differentiation in Drosophila, encodes novel nuclear Cys3His-type zinc-finger-containing

proteins. *Development (Cambridge, England)*, *124*(21), 4321–4331. https://doi.org/10.1242/DEV.124.21.4321

Bennett, C. G., Riemondy, K., Chapnick, D. A., Bunker, E., Liu, X., Kuersten, S., & Yi, R. (2016). Genome-wide analysis of Musashi-2 targets reveals novel functions in governing epithelial cell migration. *Nucleic Acids Research*, *44*(8), 3788–3800. https://doi.org/10.1093/NAR/GKW207

Bentzinger, C. F., Maltzahn, J. V., & Rudnicki, M. A. (2010). Extrinsic regulation of satellite cell specification. *Stem Cell Research and Therapy*, *1*(3), 1–9. https://doi.org/10.1186/SCRT27/FIGURES/1

Bhakta, D., Lowe, M. R., & Groh, W. J. (2004). Prevalence of structural cardiac abnormalities in patients with myotonic dystrophy type I. *American Heart Journal*, *147*(2), 224–227. https://doi.org/10.1016/j.ahj.2003.08.008

Bigot, A., Klein, A. F., Gasnier, E., Jacquemin, V., Ravassard, P., Butler-Browne, G., Mouly, V., & Furling, D. (2009). Large CTG repeats trigger p16-dependent premature senescence in myotonic dystrophy type 1 muscle precursor cells. *The American Journal of Pathology*, *174*(4), 1435–1442. https://doi.org/10.2353/AJPATH.2009.080560

Bjørkøy, G., Lamark, T., Pankiv, S., Øvervatn, A., Brech, A., & Johansen, T. (2009). Monitoring autophagic degradation of p62/SQSTM1. *Methods in Enzymology*, *452*(C), 181–197. https://doi.org/10.1016/S0076-6879(08)03612-4

Bolger, A. M., Lohse, M., & Usadel, B. (2014). Trimmomatic: A flexible trimmer for Illumina sequence data. *Bioinformatics (Oxford, England)*, *30*(15), 2114–2120. https://doi.org/10.1093/BIOINFORMATICS/BTU170

Botella, J., Shaw, C. S., & Bishop, D. J. (2024). Autophagy and Exercise: Current Insights and Future Research Directions. *International Journal of Sports Medicine*, *45*(03), 171–182. https://doi.org/10.1055/a-2153-9258

Bourre, J. M., Dumont, O., & Durand, G. (2004). Dose-effect of dietary oleic acid: Oleic acid is conditionally essential for some organs. *Reproduction, Nutrition, Development*, *44*(4), 371–380. https://doi.org/10.1051/RND:2004042

Briolay, A., Jaafar, R., Nemoz, G., & Bessueille, L. (2013). Myogenic differentiation and lipid-raft composition of L6 skeletal muscle cells are modulated by PUFAs. *Biochimica et Biophysica Acta*, *1828*(2), 602–613. https://doi.org/10.1016/J.BBAMEM.2012.10.006

Brockhoff, M., Rion, N., Chojnowska, K., Wiktorowicz, T., Eickhorst, C., Erne, B., Frank, S., Angelini, C., Furling, D., Rüegg, M. A., Sinnreich, M., & Castets, P. (2017). Targeting deregulated AMPK/mTORC1 pathways improves muscle function in myotonic dystrophy type I. *The Journal of Clinical Investigation*, *127*(2), 549–563. https://doi.org/10.1172/JCI89616

Brook, J. D., McCurrach, M. E., Harley, H. G., Buckler, A. J., Church, D., Aburatani, H., Hunter, K., Stanton, V. P., Thirion, J. P., Hudson, T., Sohn, R., Zemelman, B., Snell, R. G., Rundle, S. A., Crow, S., Davies, J., Shelbourne, P., Buxton, J., Jones, C., … Housman, D. E. (1992). Molecular basis of myotonic dystrophy: Expansion of a trinucleotide (CTG) repeat at the 3' end of a transcript encoding a protein kinase family member. *Cell*, *68*(4), 799–808. https://doi.org/10.1016/0092-8674(92)90154-5

Careccia, G., Mangiavini, L., & Cirillo, F. (2023). Regulation of Satellite Cells Functions during Skeletal Muscle Regeneration: A Critical Step in Physiological and Pathological Conditions. *International Journal of Molecular Sciences 2024, Vol. 25, Page 512*, *25*(1), 512. https://doi.org/10.3390/IJMS25010512

Casimir, D. A., & Ntambi, J. M. (1996). cAMP Activates the Expression of Stearoyl-CoA Desaturase Gene 1 during Early Preadipocyte Differentiation. *Journal of Biological Chemistry*, *271*(47), 29847–29853. https://doi.org/10.1074/JBC.271.47.29847

Cerro-Herreros, E., González-Martínez, I., Moreno, N., Espinosa-Espinosa, J., Fernández-Costa, J. M., Colom-Rodrigo, A., Overby, S. J., Seoane-Miraz, D., Poyatos-García, J., Vilchez, J. J., Munain, A. L. de, Varela, M. A., Wood, M. J., Pérez-Alonso, M., Llamusí, B., & Artero, R. (2021). Preclinical characterization of antagomiR-218 as a potential treatment for myotonic dystrophy. *Molecular Therapy. Nucleic Acids*, *26*, 174–191. https://doi.org/10.1016/J.OMTN.2021.07.017

Cerro-Herreros, E., González-Martínez, I., Moreno-Cervera, N., Overby, S., Pérez-Alonso, M., Llamusí, B., & Artero, R. (2020). Therapeutic Potential of AntagomiR-23b for Treating Myotonic Dystrophy. *Molecular Therapy - Nucleic Acids*, *21*, 837–849. https://doi.org/10.1016/j.omtn.2020.07.021

Cerro-Herreros, E., Sabater-Arcis, M., Fernandez-Costa, J. M., Moreno, N., Perez-Alonso, M., Llamusi, B., & Artero, R. (2018). miR-23b and miR-218 silencing increase Muscleblind-like expression and alleviate myotonic dystrophy phenotypes in mammalian models. *Nat Commun*, *9*(1), 2482. https://doi.org/10.1038/s41467-018-04892-4

Chal, J., & Pourquié, O. (2017). Making muscle: Skeletal myogenesis in vivo and in vitro. *Development (Cambridge, England)*, *144*(12), 2104–2122. https://doi.org/10.1242/DEV.151035

Charlet-B, N., Savkur, R. S., Singh, G., Philips, A. V., Grice, E. A., & Cooper, T. A. (2002). Loss of the muscle-specific chloride channel in type 1 myotonic dystrophy due to misregulated alternative splicing. *Molecular Cell*, *10*(1), 45–53. https://doi.org/10.1016/S1097-2765(02)00572-5

Chau, A., & Kalsotra, A. (2015). Developmental insights into the pathology of and therapeutic strategies for DM1: Back to the basics. *Developmental Dynamics : An Official Publication of the American Association of Anatomists*, *244*(3), 377–390. https://doi.org/10.1002/DVDY.24240

Chen, G., Liang, G., Ou, J., Goldstein, J. L., & Brown, M. S. (2004). Central role for liver X receptor in insulin-mediated activation of Srebp-1c transcription and stimulation of fatty acid synthesis in liver. *Proceedings of the National Academy of Sciences of the United States of America*, *101*(31), 11245–11250. https://doi.org/10.1073/PNAS.0404297101

Chen, K., Gao, P., Li, Z., Dai, A., Yang, M., Chen, S., Su, J., Deng, Z., & Li, L. (2022). Forkhead Box O Signaling Pathway in Skeletal Muscle Atrophy. *The American Journal of Pathology*, *192*(12), 1648–1657. https://doi.org/10.1016/J.AJPATH.2022.09.003

Chen, K. Y., Pan, H., Lin, M. J., Li, Y. Y., Wang, L. C., Wu, Y. C., & Hsiao, K. M. (2007). Length-dependent toxicity of untranslated CUG repeats on Caenorhabditis elegans. *Biochemical and Biophysical Research Communications*, *352*(3), 774–779. https://doi.org/10.1016/J.BBRC.2006.11.102

Cho, Y. H., Han, K. M., Kim, D., Lee, J., Lee, S. H., Choi, K. W., Kim, J., & Han, Y. M. (2014). Autophagy regulates homeostasis of pluripotency-associated proteins in hESCs. *Stem Cells (Dayton, Ohio)*, *32*(2), 424–435. https://doi.org/10.1002/STEM.1589

Choi, J., Dixon, D. M., Dansithong, W., Abdallah, W. F., Roos, K. P., Jordan, M. C., Trac, B., Lee, H. S., Comai, L., & Reddy, S. (2016). Muscleblind-like 3 deficit results in a spectrum of age-associated pathologies observed in myotonic dystrophy. *Scientific Reports 2016 6:1*, *6*(1), 1–10. https://doi.org/10.1038/srep30999

Choudhury, N. R., Alves, F. de L., Andrés-Aguayo, L. de, Graf, T., Cáceres, J. F., Rappsilber, J., & Michlewski, G. (2013). Tissue-specific control of brain-enriched miR-7 biogenesis. *Genes & Development*, *27*(1), 24–38. https://doi.org/10.1101/GAD.199190.112

Cisco, L. A., Sipple, M. T., Edwards, K. M., Thornton, C. A., & Lueck, J. D. (2024). Verapamil mitigates chloride and calcium bi-channelopathy in a myotonic dystrophy mouse model. *The Journal of Clinical Investigation*, *134*(1). https://doi.org/10.1172/JCI173576

Clingman, C. C., Deveau, L. M., Hay, S. A., Genga, R. M., Shandilya, S. M., Massi, F., & Ryder, S. P. (2014). Allosteric inhibition of a stem cell RNA-binding protein by an intermediary metabolite. *Elife*, *3*. https://doi.org/10.7554/eLife.02848

Costa, A., Cruz, A. C., Martins, F., & Rebelo, S. (2023). Protein Phosphorylation Alterations in Myotonic Dystrophy Type 1: A Systematic Review. *International Journal of Molecular Sciences*, *24*(4). https://doi.org/10.3390/IJMS24043091

Cox, D. C., Guan, X., Xia, Z., & Cooper, T. A. (2020). Increased nuclear but not cytoplasmic activities of CELF1 protein leads to muscle wasting. *Human Molecular Genetics*, *29*(10), 1729–1744. https://doi.org/10.1093/HMG/DDAA095

Cragle, C. E., MacNicol, M. C., Byrum, S. D., Hardy, L. L., Mackintosh, S. G., Richardson, W. A., Gray, N. K., Childs, G. V., Tackett, A. J., & MacNicol, A. M. (2019). Musashi interaction with poly(A)-binding protein is required for activation of target mRNA translation. *The Journal of Biological Chemistry*, *294*(28), 10969–10986. https://doi.org/10.1074/JBC.RA119.007220

Crawford Parks, T. E., Marcellus, K. A., Péladeau, C., Jasmin, B. J., & Ravel-Chapuis, A. (2020). Overexpression of Staufen1 in DM1 mouse skeletal muscle exacerbates dystrophic and atrophic features. *Human Molecular Genetics*, *29*(13), 2185–2199. https://doi.org/10.1093/hmg/ddaa111

Creugny, A., Fender, A., & Pfeffer, S. (2018). Regulation of primary microRNA processing. *FEBS Letters*, *592*(12), 1980–1996. https://doi.org/10.1002/1873-3468.13067

Cunningham, F., Allen, J. E., Allen, J., Alvarez-Jarreta, J., Amode, M. R., Armean, I. M., Austine-Orimoloye, O., Azov, A. G., Barnes, I., Bennett, R., Berry, A., Bhai, J., Bignell, A., Billis, K., Boddu, S., Brooks, L., Charkhchi, M., Cummins, C., Fioretto, L. D. R., … Flicek, P. (2022). Ensembl 2022. *Nucleic Acids Research*, *50*(D1), D988–D995. https://doi.org/10.1093/NAR/GKAB1049

da Rocha, A. L., Pinto, A. P., Morais, G. P., Marafon, B. B., Rovina, R. L., Veras, A. S. C., Teixeira, G. R., Pauli, J. R., de Moura, L. P., Cintra, D. E., Ropelle, E. R., Rivas, D. A., & da Silva, A. S. R. (2020). Moderate, but Not Excessive, Training Attenuates Autophagy Machinery in Metabolic Tissues. *International*

Journal of Molecular Sciences, *21*(22), Article 22. https://doi.org/10.3390/ijms21228416

Daniele, A., Rosa, A. D., Cristofaro, M. D., Monaco, M. L., Masullo, M., Porcile, C., Capasso, M., Tedeschi, G., Oriani, G., & Costanzo, A. D. (2011). Decreased concentration of adiponectin together with a selective reduction of its high molecular weight oligomers is involved in metabolic complications of myotonic dystrophy type 1. *European Journal of Endocrinology*, *165 6*(6), 969–975. https://doi.org/10.1530/EJE-11-0537

Dastidar, S., Ardui, S., Singh, K., Majumdar, D., Nair, N., Fu, Y., Reyon, D., Samara, E., Gerli, M. F. M., Klein, A. F., De Schrijver, W., Tipanee, J., Seneca, S., Tulalamba, W., Wang, H., Chai, Y. C., In't Veld, P., Furling, D., Tedesco, F. S., … VandenDriessche, T. (2018). Efficient CRISPR/Cas9-mediated editing of trinucleotide repeat expansion in myotonic dystrophy patient-derived iPS and myogenic cells. *Nucleic Acids Research*, *46*(16), 8275–8298. https://doi.org/10.1093/nar/gky548

Delfini, M. C., Celle, M. D. L., Gros, J., Serralbo, O., Marics, I., Seux, M., Scaal, M., & Marcelle, C. (2009). The timing of emergence of muscle progenitors is controlled by an FGF/ERK/SNAIL1 pathway. *Developmental Biology*, *333*(2), 229–237. https://doi.org/10.1016/J.YDBIO.2009.05.544

Denli, A. M., Tops, B. B. J., Plasterk, R. H. A., Ketting, R. F., & Hannon, G. J. (2004). Processing of primary microRNAs by the Microprocessor complex. *Nature*, *432*(7014), 231–235. https://doi.org/10.1038/NATURE03049

Dewald, Z., Chembazhi, U. V., Gupta, A., & Kalsotra, A. (2021). Altered drug metabolism and increased susceptibility to fatty liver disease in an inducible liver-specific mouse model of myotonic dystrophy. *bioRxiv*. https://doi.org/10.1101/2021.04.06.438688

Dionyssiou, M. G., Nowacki, N. B., Hashemi, S., Zhao, J., Kerr, A., Tsushima, R. G., & McDermott, J. C. (2013). Cross-talk between glycogen synthase kinase 3β (GSK3β) and p38MAPK regulates myocyte enhancer factor 2 (MEF2) activity in skeletal and cardiac muscle. *Journal of Molecular and Cellular Cardiology*, *54*(1), 35–44. https://doi.org/10.1016/J.YJMCC.2012.10.013

Dixon, D. M., Choi, J., El-Ghazali, A., Park, S. Y., Roos, K. P., Jordan, M. C., Fishbein, M. C., Comai, L., & Reddy, S. (2015). Loss of muscleblind-like 1 results in cardiac pathology and persistence of embryonic splice isoforms. *Scientific Reports*, *5*. https://doi.org/10.1038/SREP09042

Dong, P., Xiong, Y., Hanley, S. J. B., Yue, J., & Watari, H. (2017). Musashi-2, a novel oncoprotein promoting cervical cancer cell growth and invasion, is

negatively regulated by p53-induced miR-143 and miR-107 activation. *Journal of Experimental & Clinical Cancer Research : CR*, *36*(1). https://doi.org/10.1186/S13046-017-0617-Y

Dong, W., Chen, X., Wang, M., Zheng, Z., Zhang, X., Xiao, Q., & Peng, X. (2019). Mir-206 partially rescues myogenesis deficiency by inhibiting CUGBP1 accumulation in the cell models of myotonic dystrophy. *Neurological Research*, *41*(1), 9–18. https://doi.org/10.1080/01616412.2018.1493963

Du, H., Cline, M. S., Osborne, R. J., Tuttle, D. L., Clark, T. A., Donohue, J. P., Hall, M. P., Shiue, L., Swanson, M. S., Thornton, C. A., & Ares, M. (2010). Aberrant alternative splicing and extracellular matrix gene expression in mouse models of myotonic dystrophy. *Nature Structural & Molecular Biology 2010 17:2*, *17*(2), 187–193. https://doi.org/10.1038/nsmb.1720

Duarte, M. K. R. N., Araújo, J. N. G. D., Duarte, V. H. R., Oliveira, K. M. D., Oliveira, J. M. D., Carioca, A. A. F., Bortolin, R. H., Rezende, A. A., Hirata, M. H., Hirata, R. D., Waitzberg, D. L., Lima, S. C. V. C., Luchessi, A. D., & Silbiger, V. N. (2016). The relationship of the oleic acid level and ECHDC3 mRNA expression with the extent of coronary lesion. *Lipids in Health and Disease*, *15*(1). https://doi.org/10.1186/S12944-016-0312-6

Duggimpudi, S., Kloetgen, A., Maney, S. K., Münch, P. C., Hezaveh, K., Shaykhalishahi, H., Hoyer, W., McHardy, A. C., Lang, P. A., Borkhardt, A., & Hoell, J. I. (2018). Transcriptome-wide analysis uncovers the targets of the RNA-binding protein MSI2 and effects of MSI2's RNA-binding activity on IL-6 signaling. *Journal of Biological Chemistry*, *293*(40), 15359–15369. https://doi.org/10.1074/jbc.ra118.002243

Ebralidze, A., Wang, Y., Petkova, V., Ebralidse, K., & Junghans, R. P. (2004). RNA leaching of transcription factors disrupts transcription in myotonic dystrophy. *Science (New York, N.Y.)*, *303*(5656), 383–387. https://doi.org/10.1126/science.1088679

Echenne, B., & Bassez, G. (2013). Congenital and infantile myotonic dystrophy. *Handbook of Clinical Neurology*, *113*, 1387–1393. https://doi.org/10.1016/B978-0-444-59565-2.00009-5

Egerman, M. A., & Glass, D. J. (2014). Signaling pathways controlling skeletal muscle mass. *Critical Reviews in Biochemistry and Molecular Biology*, *49*(1), 59–68. https://doi.org/10.3109/10409238.2013.857291

Fardaei, M., Larkin, K., Brook, J. D., & Hamshere, M. G. (2001). In vivo co-localisation of MBNL protein with DMPK expanded-repeat transcripts. *Nucleic Acids Research*, *29*(13), 2766. https://doi.org/10.1093/NAR/29.13.2766

Fardaei, M., Rogers, M. T., Thorpe, H. M., Larkin, K., Hamshere, M. G., Harper, P. S., & Brook, J. D. (2002). Three proteins, MBNL, MBLL and MBXL, co-localize in vivo with nuclear foci of expanded-repeat transcripts in DM1 and DM2 cells. *Human Molecular Genetics*, *11*(7), 805–814. https://doi.org/10.1093/HMG/11.7.805

Feng, L., Xie, Y., Zhang, H., & Wu, Y. (2012). miR-107 targets cyclin-dependent kinase 6 expression, induces cell cycle G1 arrest and inhibits invasion in gastric cancer cells. *Medical Oncology (Northwood, London, England)*, *29*(2), 856–863. https://doi.org/10.1007/S12032-011-9823-1

Fernandez-Costa, J. M., & Artero, R. (2010). A conserved motif controls nuclear localization of Drosophila Muscleblind. *Molecules and Cells*, *30*(1), 65–70. https://doi.org/10.1007/S10059-010-0089-9

Fernandez-Costa, J. M., Garcia-Lopez, A., Zuniga, S., Fernandez-Pedrosa, V., Felipo-Benavent, A., Mata, M., Jaka, O., Aiastui, A., Hernandez-Torres, F., Aguado, B., Perez-Alonso, M., Vilchez, J. J., Munain, A. L. de, & Artero, R. D. (2013). Expanded CTG repeats trigger miRNA alterations in Drosophila that are conserved in myotonic dystrophy type 1 patients. *Hum Mol Genet*, *22*(4), 704–716. https://doi.org/dds478 [pii] 10.1093/hmg/dds478

Fernandez-Costa, J. M., Llamusi, M. B., Garcia-Lopez, A., & Artero, R. (2011). Alternative splicing regulation by Muscleblind proteins: From development to disease. *Biological Reviews of the Cambridge Philosophical Society*, *86*(4), 947–958. https://doi.org/10.1111/J.1469-185X.2011.00180.X

Fernández-Garibay, X., Ortega, M. A., Cerro-Herreros, E., Comelles, J., Martínez, E., Artero, R., Fernández-Costa, J. M., & Ramón-Azcón, J. (2021). Bioengineered in vitro 3D model of myotonic dystrophy type 1 human skeletal muscle. *Biofabrication*, *13*(3). https://doi.org/10.1088/1758-5090/ABF6AE

FLORINI, J. R., EWTON, D. Z., & COOLICAN, S. A. (1996). Growth hormone and the insulin-like growth factor system in myogenesis. *Endocrine Reviews*, *17*(5), 481–517. https://doi.org/10.1210/EDRV-17-5-481

Florini, J. R., & Magri, K. A. (1989). Effects of growth factors on myogenic differentiation. *The American Journal of Physiology*, *256*(4 Pt 1). https://doi.org/10.1152/AJPCELL.1989.256.4.C701

Fortini, P., Ferretti, C., Iorio, E., Cagnin, M., Garribba, L., Pietraforte, D., Falchi, M., Pascucci, B., Baccarini, S., Morani, F., Phadngam, S., Luca, G. D., Isidoro, C., & Dogliotti, E. (2016). The fine tuning of metabolism, autophagy and differentiation during in vitro myogenesis. *Cell Death & Disease*, *7*(3). https://doi.org/10.1038/CDDIS.2016.50

Fortini, P., Iorio, E., Dogliotti, E., & Isidoro, C. (2016). Coordinated Metabolic Changes and Modulation of Autophagy during Myogenesis. *Frontiers in Physiology*, *7*, 237. https://doi.org/10.3389/fphys.2016.00237

Franco-Romero, A., & Sandri, M. (2021). Role of autophagy in muscle disease. *Molecular Aspects of Medicine*, *82*. https://doi.org/10.1016/J.MAM.2021.101041

Fritegotto, C., Ferrati, C., Pegoraro, V., & Angelini, C. (2017). Micro-RNA expression in muscle and fiber morphometry in myotonic dystrophy type 1. *Neurological Sciences : Official Journal of the Italian Neurological Society and of the Italian Society of Clinical Neurophysiology*, *38*(4), 619–625. https://doi.org/10.1007/S10072-017-2811-2

Frontera, W. R., & Ochala, J. (2015). Skeletal Muscle: A Brief Review of Structure and Function. *Behavior Genetics*, *45*(2), 183–195. https://doi.org/10.1007/S00223-014-9915-Y/FIGURES/5

Fugier, C., Klein, A. F., Hammer, C., Vassilopoulos, S., Ivarsson, Y., Toussaint, A., Tosch, V., Vignaud, A., Ferry, A., Messaddeq, N., Kokunai, Y., Tsuburaya, R., Grange, P. D. L., Dembele, D., Francois, V., Precigout, G., Boulade-Ladame, C., Hummel, M. C., Munain, A. L. D., … Charlet-Berguerand, N. (2011). Misregulated alternative splicing of BIN1 is associated with T tubule alterations and muscle weakness in myotonic dystrophy. *Nature Medicine 2011 17:6*, *17*(6), 720–725. https://doi.org/10.1038/nm.2374

Fukunaga, R. (2023). miRNAs/Small Noncoding RNAs. In R. A. Bradshaw, G. W. Hart, & P. D. Stahl (Eds.), *Encyclopedia of Cell Biology (Second Edition)* (pp. 454–464). Academic Press. https://doi.org/10.1016/B978-0-12-821618-7.00096-1

Furuichi, Y., Furutani, A., Tamura, K., Manabe, Y., & Fujii, N. L. (2023). Lack of Musashi-2 induces type IIa fiber-dominated muscle atrophy. *The FASEB Journal*, *37*(9), e23154. https://doi.org/10.1096/fj.202300563R

Galka-Marciniak, P., Urbanek, M. O., & Krzyzosiak, W. J. (2012). Triplet repeats in transcripts: Structural insights into RNA toxicity. *Biological Chemistry*, *393*(11), 1299–1315. https://doi.org/10.1515/HSZ-2012-0218

Gambardella, S., Rinaldi, F., Lepore, S. M., Viola, A., Loro, E., Angelini, C., Vergani, L., Novelli, G., & Botta, A. (2010). Overexpression of microRNA-206 in the skeletal muscle from myotonic dystrophy type 1 patients. *Journal of Translational Medicine*, *8*. https://doi.org/10.1186/1479-5876-8-48

Ganassi, M., & Zammit, P. S. (2022). Involvement of muscle satellite cell dysfunction in neuromuscular disorders: Expanding the portfolio of satellite cell-opathies. *European Journal of Translational Myology*, *32*(1), 10064. https://doi.org/10.4081/ejtm.2022.10064

Gao, K., Oerlemans, R., & Groves, M. R. (2020). Theory and applications of differential scanning fluorimetry in early-stage drug discovery. *Biophysical Reviews*, *12*(1), 85–104. https://doi.org/10.1007/S12551-020-00619-2

Gao, Y., Guo, X., Santostefano, K., Wang, Y., Reid, T., Zeng, D., Terada, N., Ashizawa, T., & Xia, G. (2016). Genome Therapy of Myotonic Dystrophy Type 1 iPS Cells for Development of Autologous Stem Cell Therapy. *Molecular Therapy : The Journal of the American Society of Gene Therapy*, *24*(8), 1378–1387. https://doi.org/10.1038/MT.2016.97

García-Cruz, I., Muñoz-Negrete, F. J., Benito-Pascual, B., Arriola-Villalobos, P., Pérez-Bañón, M. D., Alió, J. L., & Mingo-Botín, D. (2023). Ocular findings in a Spanish cohort of myotonic dystrophy type 1. *Graefe's Archive for Clinical and Experimental Ophthalmology = Albrecht von Graefes Archiv Fur Klinische Und Experimentelle Ophthalmologie*, *261*(4), 1109–1114. https://doi.org/10.1007/S00417-022-05875-4

García-López, A., Llamusí, B., Orzáez, M., Pérez-Payá, E., & Artero, R. D. (2011). In vivo discovery of a peptide that prevents CUG-RNA hairpin formation and reverses RNA toxicity in myotonic dystrophy models. *Proceedings of the National Academy of Sciences of the United States of America*, *108*(29), 11866–11871. https://doi.org/10.1073/PNAS.1018213108

García-Puga, M., Saenz-Antoñanzas, A., Fernández-Torrón, R., Munain, A. L. de, & Matheu, A. (2020). Myotonic Dystrophy type 1 cells display impaired metabolism and mitochondrial dysfunction that are reversed by metformin. *Aging*, *12*(7), 6260–6275. https://doi.org/10.18632/AGING.103022

Garibaldi, M., Nicoletti, T., Bucci, E., Fionda, L., Leonardi, L., Morino, S., Tufano, L., Alfieri, G., Lauletta, A., Merlonghi, G., Perna, A., Rossi, S., Ricci, E., Alonso Perez, J., Tartaglione, T., Petrucci, A., Pennisi, E. M., Salvetti, M., Cutter, G., … Antonini, G. (2022). Muscle magnetic resonance imaging in myotonic dystrophy type 1 (DM1): Refining muscle involvement and implications for clinical trials. *European Journal of Neurology*, *29*(3), 843–854. https://doi.org/10.1111/ene.15174

Gates, D. P., Coonrod, L. A., & Berglund, J. A. (2011). Autoregulated splicing of muscleblind-like 1 (MBNL1) Pre-mRNA. *The Journal of Biological Chemistry*, *286*(39), 34224–34233. https://doi.org/10.1074/JBC.M111.236547

Geetha-Loganathan, P., Nimmagadda, S., Scaal, M., Huang, R., & Christ, B. (2008). Wnt signaling in somite development. *Annals of Anatomy = Anatomischer Anzeiger : Official Organ of the Anatomische Gesellschaft*, *190*(3), 208–222. https://doi.org/10.1016/J.AANAT.2007.12.003

Gladman, J. T., Mandal, M., Srinivasan, V., & Mahadevan, M. S. (2013). Age of Onset of RNA Toxicity Influences Phenotypic Severity: Evidence from an Inducible Mouse Model of Myotonic Dystrophy (DM1). *PLoS ONE*, *8*(9), e72907. https://doi.org/10.1371/journal.pone.0072907

Gladman, J. T., Yadava, R. S., Mandal, M., Yu, Q., Kim, Y. K., & Mahadevan, M. S. (2015). NKX2-5, a modifier of skeletal muscle pathology due to RNA toxicity. *Human Molecular Genetics*, *24*(1), 251. https://doi.org/10.1093/HMG/DDU443

Goers, E. S., Purcell, J., Voelker, R. B., Gates, D. P., & Berglund, J. A. (2010). MBNL1 binds GC motifs embedded in pyrimidines to regulate alternative splicing. *Nucleic Acids Research*, *38*(7), 2467–2484. https://doi.org/10.1093/NAR/GKP1209

González-Barriga, A., Kranzen, J., Croes, H. J. E., Bijl, S., Broek, W. J. A. A. V. D., Kessel, I. D. G. V., Engelen, B. G. M. V., Deutekom, J. C. T. V., Wieringa, B., Mulders, S. A. M., & Wansink, D. G. (2015). Cell Membrane Integrity in Myotonic Dystrophy Type 1: Implications for Therapy. *PLoS ONE*, *10*(3). https://doi.org/10.1371/JOURNAL.PONE.0121556

Gramegna, L. L., Giannoccaro, M. P., Manners, D. N., Testa, C., Zanigni, S., Evangelisti, S., Bianchini, C., Oppi, F., Poda, R., Avoni, P., Lodi, R., Liguori, R., & Tonon, C. (2018). Mitochondrial dysfunction in myotonic dystrophy type 1. *Neuromuscular Disorders : NMD*, *28*(2), 144–149. https://doi.org/10.1016/J.NMD.2017.10.007

Granados, N., Amengual, J., Ribot, J., Palou, A., & Bonet, M. L. (2011). Distinct effects of oleic acid and its trans-isomer elaidic acid on the expression of myokines and adipokines in cell models. *British Journal of Nutrition*, *105*(8), 1226–1234. https://doi.org/10.1017/S0007114510004885

Gregory, R. I., Chendrimada, T. P., Cooch, N., & Shiekhattar, R. (2005). Human RISC couples microRNA biogenesis and posttranscriptional gene silencing. *Cell*, *123*(4), 631–640. https://doi.org/10.1016/J.CELL.2005.10.022

Gu, D. na, Jiang, M. jie, Mei, Z., Dai, J. juan, Dai, C. yun, Fang, C., Huang, Q., & Tian, L. (2017). microRNA-7 impairs autophagy-derived pools of glucose to suppress pancreatic cancer progression. *Cancer Letters*, *400*, 69–78. https://doi.org/10.1016/J.CANLET.2017.04.020

Ha, M., & Kim, V. N. (2014). Regulation of microRNA biogenesis. *Nature Reviews Molecular Cell Biology 2014 15:8*, *15*(8), 509–524. https://doi.org/10.1038/nrm3838

Hale, M. A., Richardson, J. I., Day, R. C., McConnell, O. L., Arboleda, J., Wang, E. T., & Berglund, J. A. (2018). An engineered RNA binding protein with improved splicing regulation. *Nucleic Acids Research*, *46*(6), 3152–3168. https://doi.org/10.1093/NAR/GKX1304

Hamel, J. I. (2022). Myotonic Dystrophy. *Continuum (Minneapolis, Minn.)*, *28*(6), 1715–1734. https://doi.org/10.1212/CON.0000000000001184

Harley, H. G., Brook, J. D., Rundle, S. A., Crow, S., Reardon, W., Buckler, A. J., Harper, P. S., Housman, D. E., & Shaw, D. J. (1992). Expansion of an unstable DNA region and phenotypic variation in myotonic dystrophy. *Nature*, *355*(6360), 545–546. https://doi.org/10.1038/355545A0

Haro, M. de, Al-Ramahi, I., Gouyon, B. D., Ukani, L., Rosa, A., Faustino, N. A., Ashizawa, T., Cooper, T. A., & Botas, J. (2006). MBNL1 and CUGBP1 modify expanded CUG-induced toxicity in a Drosophila model of myotonic dystrophy type 1. *Human Molecular Genetics*, *15*(13), 2138–2145. https://doi.org/10.1093/HMG/DDL137

Higham, C. F., Morales, F., Cobbold, C. A., Haydon, D. T., & Monckton, D. G. (2012). High levels of somatic DNA diversity at the myotonic dystrophy type 1 locus are driven by ultra-frequent expansion and contraction mutations. *Human Molecular Genetics*, *21*(11), 2450–2463. https://doi.org/10.1093/HMG/DDS059

Hildebrandt, R. P., Moss, K. R., Janusz-Kaminska, A., Knudson, L. A., Denes, L. T., Saxena, T., Boggupalli, D. P., Li, Z., Lin, K., Bassell, G. J., & Wang, E. T. (2023). Muscleblind-like proteins use modular domains to localize RNAs by riding kinesins and docking to membranes. *Nature Communications*, *14*(1), 3427. https://doi.org/10.1038/s41467-023-38923-6

Hintze, S., Mensel, R., Knaier, L., Schoser, B., & Meinke, P. (2021). CTG-Repeat Detection in Primary Human Myoblasts of Myotonic Dystrophy Type 1. *Frontiers in Neuroscience*, *15*. https://doi.org/10.3389/FNINS.2021.686735

Ho, T. H., Charlet-B, N., Poulos, M. G., Singh, G., Swanson, M. S., & Cooper, T. A. (2004). Muscleblind proteins regulate alternative splicing. *The EMBO Journal*, *23*(15), 3103–3112. https://doi.org/10.1038/SJ.EMBOJ.7600300

Ho, T. H., Savkur, R. S., Poulos, M. G., Mancini, M. A., Swanson, M. S., & Cooper, T. A. (2005). Colocalization of muscleblind with RNA foci is separable from

mis-regulation of alternative splicing in myotonic dystrophy. *Journal of Cell Science*, *118*(Pt 13), 2923–2933. https://doi.org/10.1242/JCS.02404

Holt, I., Jacquemin, V., Fardaei, M., Sewry, C. A., Butler-Browne, G. S., Furling, D., Brook, J. D., & Morris, G. E. (2009). Muscleblind-like proteins: Similarities and differences in normal and myotonic dystrophy muscle. *The American Journal of Pathology*, *174*(1), 216–227. https://doi.org/10.2353/AJPATH.2009.080520

Holt, I., Mittal, S., Furling, D., Butler-Browne, G. S., Brook, J. D., & Morris, G. E. (2007). Defective mRNA in myotonic dystrophy accumulates at the periphery of nuclear splicing speckles. *Genes to Cells : Devoted to Molecular & Cellular Mechanisms*, *12*(9), 1035–1048. https://doi.org/10.1111/J.1365-2443.2007.01112.X

Hon, L. S., & Zhang, Z. (2007). The roles of binding site arrangement and combinatorial targeting in microRNA repression of gene expression. *Genome Biology*, *8*(8), R166. https://doi.org/10.1186/GB-2007-8-8-R166

Hsu, S. D., Lin, F. M., Wu, W. Y., Liang, C., Huang, W. C., Chan, W. L., Tsai, W. T., Chen, G. Z., Lee, C. J., Chiu, C. M., Chien, C. H., Wu, M. C., Huang, C. Y., Tsou, A. P., & Huang, H. D. (2011). miRTarBase: A database curates experimentally validated microRNA-target interactions. *Nucleic Acids Research*, *39*(Database issue). https://doi.org/10.1093/NAR/GKQ1107

Hu, M., Ge, M. R., Li, H. X., Zhang, B., & Li, G. (2022). Identification of DAPK1 as an autophagy-related biomarker for myotonic dystrophy type 1. *Frontiers in Genetics*, *13*. https://doi.org/10.3389/FGENE.2022.1022640/FULL

Huang, H. Y., Lin, Y. C. D., Cui, S., Huang, Y., Tang, Y., Xu, J., Bao, J., Li, Y., Wen, J., Zuo, H., Wang, W., Li, J., Ni, J., Ruan, Y., Li, L., Chen, Y., Xie, Y., Zhu, Z., Cai, X., … Huang, H. D. (2022). miRTarBase update 2022: An informative resource for experimentally validated miRNA–target interactions. *Nucleic Acids Research*, *50*(D1), D222. https://doi.org/10.1093/NAR/GKAB1079

Hubbard, J. I. (1973). Microphysiology of vertebrate neuromuscular transmission. *Physiological Reviews*, *53*(3), 674–723. https://doi.org/10.1152/PHYSREV.1973.53.3.674

Huguet, A., Medja, F., Nicole, A., Vignaud, A., Guiraud-Dogan, C., Ferry, A., Decostre, V., Hogrel, J. Y., Metzger, F., Hoeflich, A., Baraibar, M., Gomes-Pereira, M., Puymirat, J., Bassez, G., Furling, D., Munnich, A., & Gourdon, G. (2012). Molecular, physiological, and motor performance defects in DMSXL mice carrying >1,000 CTG repeats from the human DM1 locus. *PLoS Genetics*, *8*(11). https://doi.org/10.1371/JOURNAL.PGEN.1003043

Hurley, M. S., Flux, C., Salter, A. M., & Brameld, J. M. (2006). Effects of fatty acids on skeletal muscle cell differentiation in vitro. *The British Journal of Nutrition*, *95*(3), 623–630. https://doi.org/10.1079/BJN20051711

Huxley, A. F. (1975). The origin of force in skeletal muscle. *Ciba Foundation Symposium*, *31*, 271–290. https://doi.org/10.1002/9780470720134.CH15

Ikeda, K. S., Iwabe-Marchese, C., França, M. C., Nucci, A., & Carvalho, K. M. de. (2016). Myotonic dystrophy type 1: Frequency of ophthalmologic findings. *Arquivos de Neuro-Psiquiatria*, *74*(3), 183–188. https://doi.org/10.1590/0004-282X20150218

Inoguchi, Y., Inoguchi, T., Eto, T., Masakado, M., Suehiro, S., Yamauchi, T., & Umeda, F. (2022). Relationship between serum indirect bilirubin levels and skeletal muscle mass in older male and female patients with type 2 diabetes. *PloS One*, *17*(11). https://doi.org/10.1371/JOURNAL.PONE.0276976

Irion, U. (2012). Drosophila muscleblind codes for proteins with one and two tandem zinc finger motifs. *PloS One*, *7*(3). https://doi.org/10.1371/JOURNAL.PONE.0034248

Jiang, L., Xue, S., Xu, J., Fu, X., Wei, J., & Zhang, C. (2022). Prognostic value of Musashi 2 (MSI2) in cancer patients: A systematic review and meta-analysis. *Frontiers in Oncology*, *12*. https://doi.org/10.3389/FONC.2022.969632

Jiang, P., Zhang, T., Wu, B., Li, X., Fu, M., & Xu, B. (2023). Musashi-2 (MSI2) promotes neuroblastoma tumorigenesis through targeting MYC-mediated glucose-6-phosphate dehydrogenase (G6PD) transcriptional activation. *Medical Oncology (Northwood, London, England)*, *40*(11). https://doi.org/10.1007/S12032-023-02199-Z

Jiang, X., Tan, J., Wen, Y., Liu, W., Wu, S., Wang, L., Wangou, S., Liu, D., Du, C., Zhu, B., Xie, D., & Ren, C. (2019). MSI2-TGF-β/TGF-β R1/SMAD3 positive feedback regulation in glioblastoma. *Cancer Chemotherapy and Pharmacology*, *84*(2), 415–425. https://doi.org/10.1007/s00280-019-03892-5

Johnson, N. E., Butterfield, R. J., Mayne, K., Newcomb, T., Imburgia, C., Dunn, D., Duval, B., Feldkamp, M. L., & Weiss, R. B. (2021). Population Based Prevalence of Myotonic Dystrophy Type 1 Using Genetic Analysis of State-wide Blood Screening Program. *Neurology*, 10.1212/WNL.0000000000011425. https://doi.org/10.1212/WNL.0000000000011425

Jones, K., Wei, C., Iakova, P., Bugiardini, E., Schneider-Gold, C., Meola, G., Woodgett, J., Killian, J., Timchenko, N. A., & Timchenko, L. T. (2012). GSK3β mediates muscle pathology in myotonic dystrophy. *Journal of Clinical Investigation*. https://doi.org/10.1172/JCI64081

Kajdasz, A., Niewiadomska, D., Sekrecki, M., & Sobczak, K. (2022). Distribution of alternative untranslated regions within the mRNA of the CELF1 splicing factor affects its expression. *Scientific Reports*, *12*(1). https://doi.org/10.1038/S41598-021-03901-9

Kalsotra, A., Xiao, X., Ward, A. J., Castle, J. C., Johnson, J. M., Burge, C. B., & Cooper, T. A. (2008). A postnatal switch of CELF and MBNL proteins reprograms alternative splicing in the developing heart. *Proceedings of the National Academy of Sciences of the United States of America*, *105*(51), 20333–20338. https://doi.org/10.1073/PNAS.0809045105/SUPPL_FILE/ST11.XLS

Kanadia, R. N., Urbinati, C. R., Crusselle, V. J., Luo, D., Lee, Y. J., Harrison, J. K., Oh, S. P., & Swanson, M. S. (2003). Developmental expression of mouse muscleblind genes Mbnl1, Mbnl2 and Mbnl3. *Gene Expression Patterns*, *3*(4), 459–462. https://doi.org/10.1016/S1567-133X(03)00064-4

Karimian, A., Ahmadi, Y., & Yousefi, B. (2016). Multiple functions of p21 in cell cycle, apoptosis and transcriptional regulation after DNA damage. *DNA Repair*, *42*, 63–71. https://doi.org/10.1016/J.DNAREP.2016.04.008

Kato, H., Sakaki, K., & Mihara, K. (2006). Ubiquitin-proteasome-dependent degradation of mammalian ER stearoyl-CoA desaturase. *Journal of Cell Science*, *119*(Pt 11), 2342–2353. https://doi.org/10.1242/JCS.02951

Ketley, A., Chen, C. Z., Li, X., Arya, S., Robinson, T. E., Granados-Riveron, J., Udosen, I., Morris, G. E., Holt, I., Furling, D., Chaouch, S., Haworth, B., Southall, N., Shinn, P., Zheng, W., Austin, C. P., Hayes, C. J., & Brook, J. D. (2014). High-content screening identifies small molecules that remove nuclear foci, affect MBNL distribution and CELF1 protein levels via a PKC-independent pathway in myotonic dystrophy cell lines. *Human Molecular Genetics*, *23*(6), 1551–1562. https://doi.org/10.1093/HMG/DDT542

Kino, Y., Washizu, C., Kurosawa, M., Oma, Y., Hattori, N., Ishiura, S., & Nukina, N. (2015). Nuclear localization of MBNL1: Splicing-mediated autoregulation and repression of repeat-derived aberrant proteins. *Human Molecular Genetics*, *24*(3), 740–756. https://doi.org/10.1093/HMG/DDU492

Klionsky, D. J., Abdelmohsen, K., Abe, A., Abedin, M. J., Abeliovich, H., Acevedo Arozena, A., Adachi, H., Adams, C. M., Adams, P. D., Adeli, K., Adhihetty, P. J., Adler, S. G., Agam, G., Agarwal, R., Aghi, M. K., Agnello, M., Agostinis, P.,

Aguilar, P. V., Aguirre-Ghiso, J., … Zughaier, S. M. (2016). Guidelines for the use and interpretation of assays for monitoring autophagy (3rd edition). *Autophagy*, *12*(1), 1–222. https://doi.org/10.1080/15548627.2015.1100356

Klionsky, D. J., Petroni, G., Amaravadi, R. K., Baehrecke, E. H., Ballabio, A., Boya, P., Pedro, J. M. B.-S., Cadwell, K., Cecconi, F., Choi, A. M. K., Choi, M. E., Chu, C. T., Codogno, P., Colombo, M. I., Cuervo, A. M., Deretic, V., Dikic, I., Elazar, Z., Eskelinen, E.-L., … Pietrocola, F. (2021). Autophagy in major human diseases. *The EMBO Journal*, *40*(19). https://doi.org/10.15252/EMBJ.2021108863

Koehorst, E., Ballester-lopez, A., Arechavala-gomeza, V., Martínez-piñeiro, A., & Nogales-gadea, G. (2020). The Biomarker Potential of miRNAs in Myotonic Dystrophy Type I. *Journal of Clinical Medicine*, *9*(12), 1–18. https://doi.org/10.3390/JCM9123939

Koike, H., Manabe, I., & Oishi, Y. (2022). Mechanisms of cooperative cell-cell interactions in skeletal muscle regeneration. *Inflammation and Regeneration 2022 42:1*, *42*(1), 1–11. https://doi.org/10.1186/S41232-022-00234-6

Konieczny, P., Stepniak-Konieczna, E., & Sobczak, K. (2014). MBNL proteins and their target RNAs, interaction and splicing regulation. *Nucleic Acids Research*, *42*(17), 10873–10887. https://doi.org/10.1093/NAR/GKU767

Koscianska, E., Witkos, T. M., Kozlowska, E., Wojciechowska, M., & Krzyzosiak, W. J. (2015). Cooperation meets competition in microRNA-mediated DMPK transcript regulation. *Nucleic Acids Research*, *43*(19), 9500. https://doi.org/10.1093/NAR/GKV849

Krol, J., Fiszer, A., Mykowska, A., Sobczak, K., Mezer, M. de, & Krzyzosiak, W. J. (2007). Ribonuclease dicer cleaves triplet repeat hairpins into shorter repeats that silence specific targets. *Molecular Cell*, *25*(4), 575–586. https://doi.org/10.1016/J.MOLCEL.2007.01.031

Kudinov, A. E., Karanicolas, J., Golemis, E. A., & Boumber, Y. (2017). Musashi RNA-Binding Proteins as Cancer Drivers and Novel Therapeutic Targets. *Clinical Cancer Research : An Official Journal of the American Association for Cancer Research*, *23*(9), 2143–2153. https://doi.org/10.1158/1078-0432.CCR-16-2728

Kumar, S., Velasco, A. D. R., & Michlewski, G. (2017). Oleic Acid Induces MiR-7 Processing through Remodeling of Pri-MiR-7/Protein Complex. *Journal of Molecular Biology*, *429*(11), 1638–1649. https://doi.org/10.1016/J.JMB.2017.05.001

Kurogoushi, R., Hasegawa, T., Akazawa, Y., Iwata, K., Sugimoto, A., Yamaguchi-Ueda, K., Miyazaki, A., Narwidina, A., Kawarabayashi, K., Kitamura, T., Nakagawa, H., Iwasaki, T., & Iwamoto, T. (2021). Fibroblast growth factor 2 suppresses the expression of C-C motif chemokine 11 through the c-Jun N-terminal kinase pathway in human dental pulp-derived mesenchymal stem cells. *Experimental and Therapeutic Medicine*, *22*(6). https://doi.org/10.3892/ETM.2021.10791

Kuyumcu-Martinez, N. M., Wang, G. S., & Cooper, T. A. (2007). Increased steady-state levels of CUGBP1 in myotonic dystrophy 1 are due to PKC-mediated hyperphosphorylation. *Mol Cell*, *28*(1), 68–78.

Lala, V., Zubair, M., & Minter, D. A. (2024). Liver Function Tests. In *StatPearls*. StatPearls Publishing. http://www.ncbi.nlm.nih.gov/books/NBK482489/

Lan, L., Xing, M., Kashipathy, M., Douglas, J., Gao, P., Battaile, K., Hanzlik, R., Lovell, S., & Xu, L. (2020). Crystal and solution structures of human oncoprotein Musashi-2 N-terminal RNA recognition motif 1. *Proteins*, *88*(4), 573. https://doi.org/10.1002/PROT.25836

Lan, X. Q., Deng, C. J., Wang, Q. Q., Zhao, L. M., Jiao, B. W., & Xiang, Y. (2024). The role of TGF-β signaling in muscle atrophy, sarcopenia and cancer cachexia. *General and Comparative Endocrinology*, *353*. https://doi.org/10.1016/J.YGCEN.2024.114513

Lau, J. K., Sy, R. W., Corbett, A., & Kritharides, L. (2015). Myotonic dystrophy and the heart: A systematic review of evaluation and management. *International Journal of Cardiology*, *184*(1), 600–608. https://doi.org/10.1016/J.IJCARD.2015.03.069

Lee, J. E., & Cooper, T. A. (2009). Pathogenic mechanisms of myotonic dystrophy. *Biochemical Society Transactions*, *37*(Pt 6), 1281–1286. https://doi.org/10.1042/BST0371281

Lee, J. H., Cho, A. R., & Lee, Y. J. (2021). Relationship between Serum Alkaline Phosphatase and Low Muscle Mass Index Among Korean Adults: A Nationwide Population-Based Study. *Biomolecules*, *11*(6). https://doi.org/10.3390/BIOM11060842

Lee, J. H., Tachibana, H., Morinaga, Y., Fujimura, Y., & Yamada, K. (2009). Modulation of proliferation and differentiation of C2C12 skeletal muscle cells by fatty acids. *Life Sciences*, *84*(13–14), 415–420. https://doi.org/10.1016/J.LFS.2009.01.004

Lee, K. H., Lotterman, C., Karikari, C., Omura, N., Feldmann, G., Habbe, N., Goggins, M. G., Mendell, J. T., & Maitra, A. (2009). Epigenetic Silencing of MicroRNA miR-107 Regulates Cyclin-Dependent Kinase 6 Expression in Pancreatic Cancer. *Pancreatology*, *9*(3), 293. https://doi.org/10.1159/000186051

Lefevre, P., Diot, C., Legrand, P., & Douaire, M. (1999). Hormonal regulation of stearoyl coenzyme-A desaturase 1 activity and gene expression in primary cultures of chicken hepatocytes. *Archives of Biochemistry and Biophysics*, *368*(2), 329–337. https://doi.org/10.1006/ABBI.1999.1315

Lewis, J. E., Brameld, J. M., Hill, P., Barrett, P., Ebling, F. J. P., & Jethwa, P. H. (2015). The use of a viral 2A sequence for the simultaneous over-expression of both the vgf gene and enhanced green fluorescent protein (eGFP) in vitro and in vivo. *Journal of Neuroscience Methods*, *256*, 22–29. https://doi.org/10.1016/J.JNEUMETH.2015.08.013

Li, M., Li, A. Q., Zhou, S. L., Lv, H., Wei, P., & Yang, W. T. (2020). RNA-binding protein MSI2 isoforms expression and regulation in progression of triple-negative breast cancer. *Journal of Experimental & Clinical Cancer Research : CR*, *39*(1). https://doi.org/10.1186/S13046-020-01587-X

Li, M., Zhuang, Y., Batra, R., Thomas, J. D., Li, M., Nutter, C. A., Scotti, M. M., Carter, H. A., Wang, Z. J., Huang, X.-S., Pu, C. Q., Swanson, M. S., & Xie, W. (2020). HNRNPA1-induced spliceopathy in a transgenic mouse model of myotonic dystrophy. *Proceedings of the National Academy of Sciences*, *117*(10), 5472–5477. https://doi.org/10.1073/pnas.1907297117

Li, W., Zeng, H., Xu, M., Huang, C., Tao, L., Li, J., Zhang, T., Chen, H., Xia, J., Li, C., & Li, X. (2021). Oleanolic Acid Improves Obesity-Related Inflammation and Insulin Resistance by Regulating Macrophages Activation. *Frontiers in Pharmacology*, *12*, 697483–697483. https://doi.org/10.3389/FPHAR.2021.697483/FULL

Li, Y., Li, S., & Wu, H. (2022). Ubiquitination-Proteasome System (UPS) and Autophagy Two Main Protein Degradation Machineries in Response to Cell Stress. *Cells*, *11*(5). https://doi.org/10.3390/CELLS11050851

Liao, Q., Zhang, Y., He, J., & Huang, K. (2022). Global Prevalence of Myotonic Dystrophy: An Updated Systematic Review and Meta-Analysis. *Neuroepidemiology*, *56*(3), 163–173. https://doi.org/10.1159/000524734

Lim, J. H., Gerhart-Hines, Z., Dominy, J. E., Lee, Y., Kim, S., Tabata, M., Xiang, Y. K., & Puigserver, P. (2013). Oleic acid stimulates complete oxidation of fatty acids through protein kinase A-dependent activation of SIRT1-PGC1α

complex. *The Journal of Biological Chemistry*, *288*(10), 7117–7126. https://doi.org/10.1074/JBC.M112.415729

Lima, J. E. de, & Relaix, F. (2021). Master regulators of skeletal muscle lineage development and pluripotent stem cells differentiation. *Cell Regeneration 2021 10:1*, *10*(1), 1–13. https://doi.org/10.1186/S13619-021-00093-5

Lin, X., Miller, J. W., Mankodi, A., Kanadia, R. N., Yuan, Y., Moxley, R. T., Swanson, M. S., & Thornton, C. A. (2006). Failure of MBNL1-dependent post-natal splicing transitions in myotonic dystrophy. *Human Molecular Genetics*, *15*(13), 2087–2097. https://doi.org/10.1093/HMG/DDL132

Lipina, C., & Hundal, H. S. (2017). Lipid modulation of skeletal muscle mass and function. *Journal of Cachexia, Sarcopenia and Muscle*, *8*(2), 190–201. https://doi.org/10.1002/JCSM.12144

Liu, X., Zeng, X., Chen, X., Luo, R., Li, L., Wang, C., Liu, J., Cheng, J., Lu, Y., & Chen, Y. (2019). Oleic acid protects insulin-secreting INS-1E cells against palmitic acid-induced lipotoxicity along with an amelioration of ER stress. *Endocrine*, *64*(3), 512–524. https://doi.org/10.1007/S12020-019-01867-3

Liu, Y., & Tang, C. (2012). Regulation of ABCA1 Functions by Signaling Pathways. *Biochimica et Biophysica Acta*, *1821*(3), 522. https://doi.org/10.1016/J.BBALIP.2011.08.015

Livak, K. J., & Schmittgen, T. D. (2001). Analysis of relative gene expression data using real-time quantitative PCR and the 2(-Delta Delta C(T)) Method. *Methods (San Diego, Calif.)*, *25*(4), 402–408. https://doi.org/10.1006/METH.2001.1262

Lopez, S., Bermudez, B., Paz, S. M.-D. L., Jaramillo, S., Varela, L. M., Ortega-Gomez, A., Abia, R., & Muriana, F. J. G. (2014). Membrane composition and dynamics: A target of bioactive virgin olive oil constituents. *Biochimica et Biophysica Acta (BBA) - Biomembranes*, *1838*(6), 1638–1656. https://doi.org/10.1016/J.BBAMEM.2014.01.007

López-Martínez, A., Soblechero-Martín, P., De-La-puente-ovejero, L., Nogales-Gadea, G., & Arechavala-Gomeza, V. (2020). An Overview of Alternative Splicing Defects Implicated in Myotonic Dystrophy Type I. *Genes*, *11*(9), 1–27. https://doi.org/10.3390/GENES11091109

Loro, E., Rinaldi, F., Malena, A., Masiero, E., Novelli, G., Angelini, C., Romeo, V., Sandri, M., Botta, A., & Vergani, L. (2010). Normal myogenesis and increased apoptosis in myotonic dystrophy type-1 muscle cells. *Cell Death*

Differ, *17*(8), 1315–1324. https://doi.org/cdd201033 [pii] 10.1038/cdd.2010.33

Lutz, M., Levanti, M., Karns, R., Gourdon, G., Lindquist, D., Timchenko, N. A., & Timchenko, L. (2023). Therapeutic Targeting of the GSK3β-CUGBP1 Pathway in Myotonic Dystrophy. *International Journal of Molecular Sciences*, *24*(13), 10650. https://doi.org/10.3390/ijms241310650

Lyu, C. C., Meng, Y., Che, H. Y., Suo, J. L., He, Y. T., Zheng, Y., Jiang, H., Zhang, J. B., & Yuan, B. (2023). MSI2 Modulates Unsaturated Fatty Acid Metabolism by Binding FASN in Bovine Mammary Epithelial Cells. *Journal of Agricultural and Food Chemistry*, *71*(50), 20359–20371. https://doi.org/10.1021/ACS.JAFC.3C07280/SUPPL_FILE/JF3C07280_SI_001.PDF

Ma, P., Han, W., Meng, C., Tan, X., Liu, P., & Dong, L. (2022). LINC02389/miR-7-5p Regulated Cisplatin Resistance of Non-Small-Cell Lung Cancer via Promoting Oxidative Stress. *Analytical Cellular Pathology (Amsterdam)*, *2022*. https://doi.org/10.1155/2022/6100176

MacNicol, M. C., Cragle, C. E., McDaniel, F. K., Hardy, L. L., Wang, Y., Arumugam, K., Rahmatallah, Y., Glazko, G. V., Wilczynska, A., Childs, G. V., Zhou, D., & MacNicol, A. M. (2017). Evasion of regulatory phosphorylation by an alternatively spliced isoform of Musashi2. *Scientific Reports*, *7*(1). https://doi.org/10.1038/S41598-017-11917-3

Mahadevan, M. S., Yadava, R. S., Yu, Q., Balijepalli, S., Frenzel-Mccardell, C. D., Bourne, T. D., & Phillips, L. H. (2006). Reversible model of RNA toxicity and cardiac conduction defects in myotonic dystrophy. *Nature Genetics*, *38*(9), 1066–1070. https://doi.org/10.1038/NG1857

Maltzahn, J. V., Bentzinger, C. F., & Rudnicki, M. A. (2011). Wnt7a-Fzd7 signalling directly activates the Akt/mTOR anabolic growth pathway in skeletal muscle. *Nature Cell Biology*, *14*(2), 186–191. https://doi.org/10.1038/NCB2404

Mankodi, A., Logigian, E., Callahan, L., McClain, C., White, R., Henderson, D., Krym, M., & Thornton, C. A. (2000). Myotonic dystrophy in transgenic mice expressing an expanded CUG repeat. *Science (New York, N.Y.)*, *289*(5485), 1769–1772. https://doi.org/10.1126/SCIENCE.289.5485.1769

Mankodi, A., Takahashi, M. P., Jiang, H., Beck, C. L., Bowers, W. J., Moxley, R. T., Cannon, S. C., & Thornton, C. A. (2002). Expanded CUG repeats trigger aberrant splicing of ClC-1 chloride channel pre-mRNA and hyperexcitability

of skeletal muscle in myotonic dystrophy. *Molecular Cell*, *10*(1), 35–44. https://doi.org/10.1016/S1097-2765(02)00563-4

Martorell, L., Gámez, J., Cayuela, M. L., Gould, F. K., McAbney, J. P., Ashizawa, T., Monckton, D. G., & Baiget, M. (2004). Germline mutational dynamics in myotonic dystrophy type 1 males: Allele length and age effects. *Neurology*, *62*(2), 269–274. https://doi.org/10.1212/WNL.62.2.269

Matalkah, F., Jeong, B., Sheridan, M., Horstick, E., Ramamurthy, V., & Stoilov, P. (2022). The Musashi proteins direct post-transcriptional control of protein expression and alternate exon splicing in vertebrate photoreceptors. *Communications Biology*, *5*(1). https://doi.org/10.1038/S42003-022-03990-W

Mateus, T., Martins, F., Nunes, A., Herdeiro, M. T., & Rebelo, S. (2021). Metabolic Alterations in Myotonic Dystrophy Type 1 and Their Correlation with Lipin. *International Journal of Environmental Research and Public Health*, *18*(4), 1–22. https://doi.org/10.3390/IJERPH18041794

Mathieu, J., Allard, P., Potvin, L., Prévost, C., & Begin, P. (1999). A 10-year study of mortality in a cohort of patients with myotonic dystrophy. *Neurology*, *52*(8), 1658–1662. https://doi.org/10.1212/WNL.52.8.1658

Mauvoisin, D., Prévost, M., Ducheix, S., Arnaud, M. P., & Mounier, C. (2010). Key role of the ERK1/2 MAPK pathway in the transcriptional regulation of the Stearoyl-CoA Desaturase (SCD1) gene expression in response to leptin. *Molecular and Cellular Endocrinology*, *319*(1–2), 116–128. https://doi.org/10.1016/J.MCE.2010.01.027

Mauvoisin, D., Rocque, G., Arfa, O., Radenne, A., Boissier, P., & Mounier, C. (2007). Role of the PI3-kinase/mTor pathway in the regulation of the stearoyl CoA desaturase (SCD1) gene expression by insulin in liver. *Journal of Cell Communication and Signaling*, *1*(2), 113–125. https://doi.org/10.1007/S12079-007-0011-1

McCarthy, J. J., & Esser, K. A. (2010). Anabolic and catabolic pathways regulating skeletal muscle mass. *Current Opinion in Clinical Nutrition and Metabolic Care*, *13*(3), 230–235. https://doi.org/10.1097/MCO.0B013E32833781B5

McPherron, A. C., Lawler, A. M., & Lee, S. J. (1997). Regulation of skeletal muscle mass in mice by a new TGF-beta superfamily member. *Nature*, *387*(6628), 83–90. https://doi.org/10.1038/387083A0

Mensink, R. P. (2005). Metabolic and health effects of isomeric fatty acids. *Current Opinion in Lipidology*, *16*(1), 27–30. https://doi.org/10.1097/00041433-200502000-00006

Meola, G. (2013). Clinical aspects, molecular pathomechanisms and management of myotonic dystrophies. *Acta Myologica*, *32*(3), 154.

Meola, G. (2014). Myotonic dystrophy is not only a disease affecting the muscles, it is also a CNS disorder. *European Journal of Neurology*, *21*(2), 183–184. https://doi.org/10.1111/ENE.12247

Meola, G., & Cardani, R. (2015). Myotonic dystrophies: An update on clinical aspects, genetic, pathology, and molecular pathomechanisms. *Biochimica et Biophysica Acta (BBA) - Molecular Basis of Disease*, *1852*(4), 594–606. https://doi.org/10.1016/J.BBADIS.2014.05.019

Merien, A., Tahraoui-Bories, J., Cailleret, M., Dupont, J. B., Leteur, C., Polentes, J., Carteron, A., Polvèche, H., Concordet, J. P., Pinset, C., Jarrige, M., Furling, D., & Martinat, C. (2021). CRISPR gene editing in pluripotent stem cells reveals the function of MBNL proteins during human in vitro myogenesis. *Human Molecular Genetics*, *31*(1), 41–56. https://doi.org/10.1093/HMG/DDAB218

Michalowski, S., Miller, J. W., Urbinati, C. R., Paliouras, M., Swanson, M. S., & Griffith, J. (1999). Visualization of double-stranded RNAs from the myotonic dystrophy protein kinase gene and interactions with CUG-binding protein. *Nucleic Acids Research*, *27*(17), 3534–3542. https://doi.org/10.1093/NAR/27.17.3534

Michlewski, G., & Cáceres, J. F. (2019). Post-transcriptional control of miRNA biogenesis. *RNA*, *25*(1), 1. https://doi.org/10.1261/RNA.068692.118

Miele, L., Perna, A., Dajko, M., Zocco, M. A., Magistris, A. D., Nicoletti, T. F., Biolato, M., Marrone, G., Liguori, A., Maccora, D., Valenza, V., Rossi, S., Riso, V., Natale, D. D., Gasbarrini, A., Grieco, A., & Silvestri, G. (2021). Clinical characteristics of metabolic associated fatty liver disease (MAFLD) in subjects with myotonic dystrophy type 1 (DM1). *Digestive and Liver Disease : Official Journal of the Italian Society of Gastroenterology and the Italian Association for the Study of the Liver*, *53*(11), 1451–1457. https://doi.org/10.1016/J.DLD.2020.12.010

Miklankova, D., Markova, I., Hüttl, M., Stankova, B., & Malinska, H. (2022). The Different Insulin-Sensitising and Anti-Inflammatory Effects of Palmitoleic Acid and Oleic Acid in a Prediabetes Model. *Journal of Diabetes Research*, *2022*, 1–14. https://doi.org/10.1155/2022/4587907

Miller, J. W., Urbinati, C. R., Teng-Umnuay, P., Stenberg, M. G., Byrne, B. J., Thornton, C. A., & Swanson, M. S. (2000). Recruitment of human muscleblind proteins to (CUG)(n) expansions associated with myotonic dystrophy. *The EMBO Journal*, *19*(17), 4439–4448. https://doi.org/10.1093/EMBOJ/19.17.4439

Mitsui, T., & Ohshima, H. (2012). Theory of muscle contraction mechanism with cooperative interaction among crossbridges. *Biophysics (Nagoya-Shi, Japan)*, *8*, 27–39. https://doi.org/10.2142/BIOPHYSICS.8.27

Mooers, B. H. M., Logue, J. S., & Berglund, J. A. (2005). The structural basis of myotonic dystrophy from the crystal structure of CUG repeats. *Proceedings of the National Academy of Sciences of the United States of America*, *102*(46), 16626–16631. https://doi.org/10.1073/PNAS.0505873102

Morales, F., Couto, J. M., Higham, C. F., Hogg, G., Cuenca, P., Braida, C., Wilson, R. H., Adam, B., Valle, G. D., Brian, R., Sittenfeld, M., Ashizawa, T., Wilcox, A., Wilcox, D. E., & Monckton, D. G. (2012). Somatic instability of the expanded CTG triplet repeat in myotonic dystrophy type 1 is a heritable quantitative trait and modifier of disease severity. *Human Molecular Genetics*, *21*(16), 3558–3567. https://doi.org/10.1093/HMG/DDS185

Morissette, M. R., Cook, S. A., Buranasombati, C., Rosenberg, M. A., & Rosenzweig, A. (2009). Myostatin inhibits IGF-I-induced myotube hypertrophy through Akt. *American Journal of Physiology - Cell Physiology*, *297*(5). https://doi.org/10.1152/ajpcell.00043.2009

Morriss, G. R., Rajapakshe, K., Huang, S., Coarfa, C., & Cooper, T. A. (2018). Mechanisms of skeletal muscle wasting in a mouse model for myotonic dystrophy type 1. *Human Molecular Genetics*, *27*(16), 2789–2804. https://doi.org/10.1093/HMG/DDY192

Mukund, K., & Subramaniam, S. (2020). Skeletal muscle: A review of molecular structure and function, in health and disease. *Wiley Interdisciplinary Reviews. Systems Biology and Medicine*, *12*(1). https://doi.org/10.1002/WSBM.1462

Muraine, L., Bensalah, M., Dhiab, J., Cordova, G., Arandel, L., Marhic, A., Chapart, M., Vasseur, S., Benkhelifa-Ziyyat, S., Bigot, A., Butler-Browne, G., Mouly, V., Negroni, E., & Trollet, C. (2020). Transduction Efficiency of Adeno-Associated Virus Serotypes After Local Injection in Mouse and Human Skeletal Muscle. *Human Gene Therapy*, *31*(3–4), 233–240. https://doi.org/10.1089/HUM.2019.173

Navarro-Tito, N., Soto-Guzman, A., Castro-Sanchez, L., Martinez-Orozco, R., & Salazar, E. P. (2010). Oleic acid promotes migration on MDA-MB-231 breast

cancer cells through an arachidonic acid-dependent pathway. *The International Journal of Biochemistry & Cell Biology*, *42*(2), 306–317. https://doi.org/10.1016/J.BIOCEL.2009.11.010

Nguyen, D. T. T., Lu, Y., Chu, K. L., Yang, X., Park, S. M., Choo, Z. N., Chin, C. R., Prieto, C., Schurer, A., Barin, E., Savino, A. M., Gourkanti, S., Patel, P., Vu, L. P., Leslie, C. S., & Kharas, M. G. (2020). HyperTRIBE uncovers increased MUSASHI-2 RNA binding activity and differential regulation in leukemic stem cells. *Nature Communications*, *11*(1). https://doi.org/10.1038/S41467-020-15814-8

Nieuwenhuis, S., Okkersen, K., Widomska, J., Blom, P., Hoen, P. A. C. 't, Engelen, B. van, & Glennon, J. C. (2019). Insulin Signaling as a Key Moderator in Myotonic Dystrophy Type 1. *Frontiers in Neurology*, *10*, 1229. https://doi.org/10.3389/FNEUR.2019.01229

O'Brien, J., Hayder, H., Zayed, Y., & Peng, C. (2018). Overview of MicroRNA Biogenesis, Mechanisms of Actions, and Circulation. *Frontiers in Endocrinology*, *9*(AUG). https://doi.org/10.3389/FENDO.2018.00402

Oddo, J. C., Saxena, T., McConnell, O. L., Berglund, J. A., & Wang, E. T. (2016). Conservation of context-dependent splicing activity in distant Muscleblind homologs. *Nucleic Acids Research*, *44*(17), 8352–8362. https://doi.org/10.1093/NAR/GKW735

Okada, C., Yamashita, E., Lee, S. J., Shibata, S., Katahira, J., Nakagawa, A., Yoneda, Y., & Tsukihara, T. (2009). A high-resolution structure of the pre-microRNA nuclear export machinery. *Science (New York, N.Y.)*, *326*(5957), 1275–1279. https://doi.org/10.1126/SCIENCE.1178705

ONO, K., ONO, T., & MATSUMATA, T. (1995). The pathogenesis of decreased aspartate aminotransferase and alanine aminotransferase activity in the plasma of hemodialysis patients: The role of vitamin B6 deficiency. *Clinical Nephrology*, *43*(6), 405–408.

Orengo, J. P., Chambon, P., Metzger, D., Mosier, D. R., Snipes, G. J., & Cooper, T. A. (2008). Expanded CTG repeats within the DMPK 3' UTR causes severe skeletal muscle wasting in an inducible mouse model for myotonic dystrophy. *Proceedings of the National Academy of Sciences of the United States of America*, *105*(7), 2646–2651. https://doi.org/10.1073/PNAS.0708519105/SUPPL_FILE/08519MOVIE1.MPG

Overby, S. J., Cerro-Herreros, E., Espinosa-Espinosa, J., González-Martínez, I., Moreno, N., Fernández-Costa, J. M., Balaguer-Trias, J., Ramón-Azcón, J.,

Pérez-Alonso, M., Møller, T., Llamusí, B., & Artero, R. (2023). BlockmiR AONs as Site-Specific Therapeutic MBNL Modulation in Myotonic Dystrophy 2D and 3D Muscle Cells and HSALR Mice. *Pharmaceutics*, *15*(4). https://doi.org/10.3390/PHARMACEUTICS15041118

Ozimski, L. L., Sabater-Arcis, M., Bargiela, A., & Artero, R. (2021). The hallmarks of myotonic dystrophy type 1 muscle dysfunction. *Biological Reviews of the Cambridge Philosophical Society*, *96*(2), 716–730. https://doi.org/10.1111/BRV.12674

Pacak, C. A., Sakai, Y., Thattaliyath, B. D., Mah, C. S., & Byrne, B. J. (2008). Tissue specific promoters improve specificity of AAV9 mediated transgene expression following intra-vascular gene delivery in neonatal mice. *Genetic Vaccines and Therapy*, *6*. https://doi.org/10.1186/1479-0556-6-13

Pang, P. D., Alsina, K. M., Cao, S., Koushik, A. B., Wehrens, X. H. T., & Cooper, T. A. (2018). CRISPR-mediated expression of the fetal Scn5a isoform in adult mice causes conduction defects and arrhythmias. *Journal of the American Heart Association*, *7*(19). https://doi.org/10.1161/JAHA.118.010393

Park, S. M., Deering, R. P., Lu, Y., Tivnan, P., Lianoglou, S., Al-Shahrour, F., Ebert, B. L., Hacohen, N., Leslie, C., Daley, G. Q., Lengner, C. J., & Kharas, M. G. (2014). Musashi-2 controls cell fate, lineage bias, and TGF-β signaling in HSCs. *Journal of Experimental Medicine*. https://doi.org/10.1084/jem.20130736

Parks, T. E. C., Ravel-Chapuis, A., Bondy-Chorney, E., Renaud, J. M., Cŏté, J., & Jasmin, B. J. (2017). Muscle-specific expression of the RNA-binding protein Staufen1 induces progressive skeletal muscle atrophy via regulation of phosphatase tensin homolog. *Human Molecular Genetics*, *26*(10), 1821–1838. https://doi.org/10.1093/HMG/DDX085

Pavićević, D. S., Miladinović, J., Brkušanin, M., Šviković, S., Djurica, S., Brajušković, G., & Romac, S. (2013). Molecular Genetics and Genetic Testing in Myotonic Dystrophy Type 1. *BioMed Research International*, *2013*, 13. https://doi.org/10.1155/2013/391821

Peng, G., Li, L., Liu, Y., Pu, J., Zhang, S., Yu, J., Zhao, J., & Liu, P. (2011). Oleate Blocks Palmitate-Induced Abnormal Lipid Distribution, Endoplasmic Reticulum Expansion and Stress, and Insulin Resistance in Skeletal Muscle. *Endocrinology*, *152*(6), 2206–2218. https://doi.org/10.1210/EN.2010-1369

Peng, X., Shen, X., Chen, X., Liang, R., Azares, A. R., & Liu, Y. (2015). Celf1 regulates cell cycle and is partially responsible for defective myoblast differentiation in myotonic dystrophy RNA toxicity. *Biochimica et Biophysica Acta (BBA) -*

Molecular Basis of Disease, *1852*(7), 1490–1497. https://doi.org/10.1016/J.BBADIS.2015.04.010

Perbellini, R., Greco, S., Sarra-Ferraris, G., Cardani, R., Capogrossi, M. C., Meola, G., & Martelli, F. (2011). Dysregulation and cellular mislocalization of specific miRNAs in myotonic dystrophy type 1. *Neuromuscular Disorders : NMD*, *21*(2), 81–88. https://doi.org/10.1016/J.NMD.2010.11.012

Perdomo, L., Beneit, N., Otero, Y. F., Escribano, Ó., Díaz-Castroverde, S., Gómez-Hernández, A., & Benito, M. (2015). Protective role of oleic acid against cardiovascular insulin resistance and in the early and late cellular atherosclerotic process. *Cardiovascular Diabetology*, *14*(1), 1–12. https://doi.org/10.1186/S12933-015-0237-9/FIGURES/8

Perna, A., Maccora, D., Rossi, S., Nicoletti, T. F., Zocco, M. A., Riso, V., Modoni, A., Petrucci, A., Valenza, V., Grieco, A., Miele, L., & Silvestri, G. (2020). High Prevalence and Gender-Related Differences of Gastrointestinal Manifestations in a Cohort of DM1 Patients: A Perspective, Cross-Sectional Study. *Frontiers in Neurology*, *11*, 394. https://doi.org/10.3389/FNEUR.2020.00394/FULL

Pettersson, O. J., Aagaard, L., Andrejeva, D., Thomsen, R., Jensen, T. G., & Damgaard, C. K. (2014). DDX6 regulates sequestered nuclear CUG-expanded DMPK-mRNA in dystrophia myotonica type 1. *Nucleic Acids Res*, *42*(11), 7186–7200. https://doi.org/10.1093/nar/gku352

Picchio, L., Plantie, E., Renaud, Y., Poovthumkadavil, P., & Jagla, K. (2013). Novel Drosophila model of myotonic dystrophy type 1: Phenotypic characterization and genome-wide view of altered gene expression. *Human Molecular Genetics*, *22*(14), 2795–2810. https://doi.org/10.1093/HMG/DDT127

Piccinin, E., Cariello, M., & Moschetta, A. (2021). Lipid metabolism in colon cancer: Role of Liver X Receptor (LXR) and Stearoyl-CoA Desaturase 1 (SCD1). *Molecular Aspects of Medicine*, *78*. https://doi.org/10.1016/J.MAM.2020.100933

Piccinin, E., Cariello, M., Santis, S. D., Ducheix, S., Sabbà, C., Ntambi, J. M., & Moschetta, A. (2019). Role of Oleic Acid in the Gut-Liver Axis: From Diet to the Regulation of Its Synthesis via Stearoyl-CoA Desaturase 1 (SCD1). *Nutrients*, *11*(10). https://doi.org/10.3390/NU11102283

Pinheiro, C. H. da J. (2012). *Efeito da terapia com células-tronco musculares e células-tronco mesenquimais na regeneração do músculo esquelético:*

Modulação por ácido oléico. https://doi.org/10.11606/T.42.2012.TDE-18092012-091244

Pinnamaneni, S. K., Southgate, R. J., Febbraio, M. A., & Watt, M. J. (2006). Stearoyl CoA desaturase 1 is elevated in obesity but protects against fatty acid-induced skeletal muscle insulin resistance in vitro. *Diabetologia*, *49*(12), 3027–3037. https://doi.org/10.1007/S00125-006-0427-9

Pisani, V., Panico, M. B., Terracciano, C., Bonifazi, E., Meola, G., Novelli, G., Bernardi, G., Angelini, C., & Massa, R. (2008). Preferential central nucleation of type 2 myofibers is an invariable feature of myotonic dystrophy type 2. *Muscle & Nerve*, *38*(5), 1405–1411. https://doi.org/10.1002/MUS.21122

Poussel, M., Thil, C., Kaminsky, P., Mercy, M., Gomez, E., Chaouat, A., Chabot, F., & Chenuel, B. (2015). Lack of correlation between the ventilatory response to CO2 and lung function impairment in myotonic dystrophy patients: Evidence for a dysregulation at central level. *Neuromuscular Disorders : NMD*, *25*(5), 403–408. https://doi.org/10.1016/J.NMD.2015.02.006

Raben, N., Shea, L., Hill, V., & Plotz, P. (2009). Monitoring Autophagy in Lysosomal Storage Disorders. *Methods in Enzymology*, *453*(C), 417. https://doi.org/10.1016/S0076-6879(08)04021-4

Rau, F., Freyermuth, F., Fugier, C., Villemin, J. P., Fischer, M. C., Jost, B., Dembele, D., Gourdon, G., Nicole, A., Duboc, D., Wahbi, K., Day, J. W., Fujimura, H., Takahashi, M. P., Auboeuf, D., Dreumont, N., Furling, D., & Charlet-Berguerand, N. (2011). Misregulation of miR-1 processing is associated with heart defects in myotonic dystrophy. *Nature Structural & Molecular Biology*, *18*(7), 840–845. https://doi.org/10.1038/NSMB.2067

Renna, L. V., Bosè, F., Brigonzi, E., Fossati, B., Meola, G., & Cardani, R. (2019). Aberrant insulin receptor expression is associated with insulin resistance and skeletal muscle atrophy in myotonic dystrophies. *PloS One*, *14*(3). https://doi.org/10.1371/JOURNAL.PONE.0214254

Renna, L. V., Bosè, F., Iachettini, S., Fossati, B., Saraceno, L., Milani, V., Colombo, R., Meola, G., & Cardani, R. (2017). Receptor and post-receptor abnormalities contribute to insulin resistance in myotonic dystrophy type 1 and type 2 skeletal muscle. *PLoS ONE*, *12*(9). https://doi.org/10.1371/JOURNAL.PONE.0184987

Riaz, M., Raz, Y., Moloney, E. B., Putten, M. van, Krom, Y. D., Maarel, S. M. van der, Verhaagen, J., & Raz, V. (2015). Differential myofiber-type transduction preference of adeno-associated virus serotypes 6 and 9. *Skeletal Muscle*, *5*(1). https://doi.org/10.1186/S13395-015-0064-4

Rodríguez-Arribas, M., Pizarro-Estrella, E., Gómez-Sánchez, R., Yakhine-Diop, S. M. S., Gragera-Hidalgo, A., Cristo, A., Pedro, J. M. B.-S., González-Polo, R. A., & Fuentes, J. M. (2016). IFDOTMETER. *Journal of Laboratory Automation*, *21*(2), 246–259. https://doi.org/10.1177/2211068215600650

Rossi, S., Marca, G. D., Ricci, M., Perna, A., Nicoletti, T. F., Brunetti, V., Meleo, E., Calvello, M., Petrucci, A., Antonini, G., Bucci, E., Licchelli, L., Sancricca, C., Massa, R., Rastelli, E., Botta, A., Muzio, A. D., Romano, S., Garibaldi, M., & Silvestri, G. (2019). Prevalence and predictor factors of respiratory impairment in a large cohort of patients with Myotonic Dystrophy type 1 (DM1): A retrospective, cross sectional study. *Journal of the Neurological Sciences*, *399*, 118–124. https://doi.org/10.1016/J.JNS.2019.02.012

Roy, B., Lee, E., Li, T., & Rampersaud, M. (2022). Role of miRNAs in Neurodegeneration: From Disease Cause to Tools of Biomarker Discovery and Therapeutics. *Genes*, *13*(3). https://doi.org/10.3390/GENES13030425

Rusten, T. E., & Stenmark, H. (2010). P62, an autophagy hero or culprit? *Nat Cell Biol*, *12*(3), 207–209. https://doi.org/ncb0310-207 [pii] 10.1038/ncb0310-207

Sabater-Arcis, M., Bargiela, A., Furling, D., & Artero, R. (2020). miR-7 Restores Phenotypes in Myotonic Dystrophy Muscle Cells by Repressing Hyperactivated Autophagy. *Molecular Therapy. Nucleic Acids*, *19*, 278–292. https://doi.org/10.1016/J.OMTN.2019.11.012

Sabater-Arcis, M., Bargiela, A., Moreno, N., Poyatos-Garcia, J., Vilchez, J. J., & Artero, R. (2021). Musashi-2 contributes to myotonic dystrophy muscle dysfunction by promoting excessive autophagy through miR-7 biogenesis repression. *Molecular Therapy. Nucleic Acids*, *25*, 652–667. https://doi.org/10.1016/J.OMTN.2021.08.010

Sabater-Arcis, M., Moreno, N., Sevilla, T., Alonso, M. P., Bargiela, A., & Artero, R. (2023). Msi2 enhances muscle dysfunction in a myotonic dystrophy type 1 mouse model. *Biomedical Journal*, 100667. https://doi.org/10.1016/J.BJ.2023.100667

Safdar, A., Abadi, A., Akhtar, M., Hettinga, B. P., & Tarnopolsky, M. A. (2009). miRNA in the regulation of skeletal muscle adaptation to acute endurance exercise in C57Bl/6J male mice. *PloS One*, *4*(5). https://doi.org/10.1371/JOURNAL.PONE.0005610

Saliminejad, K., Khorshid, H. R. K., Fard, S. S., & Ghaffari, S. H. (2019). An overview of microRNAs: Biology, functions, therapeutics, and analysis methods. *Journal of Cellular Physiology*, *234*(5), 5451–5465. https://doi.org/10.1002/JCP.27486

Salisbury, E., Sakai, K., Schoser, B., Huichalaf, C., Schneider-Gold, C., Nguyen, H., Wang, G. L., Albrecht, J. H., & Timchenko, L. T. (2008). Ectopic expression of cyclin D3 corrects differentiation of DM1 myoblasts through activation of RNA CUG-binding protein, CUGBP1. *Experimental Cell Research*, *314*(11–12), 2266–2278. https://doi.org/10.1016/J.YEXCR.2008.04.018

Sandri, M., Sandri, C., Gilbert, A., Skurk, C., Calabria, E., Picard, A., Walsh, K., Schiaffino, S., Lecker, S. H., & Goldberg, A. L. (2004). Foxo transcription factors induce the atrophy-related ubiquitin ligase atrogin-1 and cause skeletal muscle atrophy. *Cell*, *117*(3), 399–412. https://doi.org/10.1016/S0092-8674(04)00400-3

Sansone, V. A., Gagnon, C., Atalaia, A., Boentert, M., Duboc, D., Falcier, E., Gallais, B., Heatwole, C., Iatomasi, M., Orlikowski, D., Phillips, M., Rao, F., Rogers, M., Schoser, B., & Wijkstra, P. (2015). 207th ENMC Workshop on chronic respiratory insufficiency in myotonic dystrophies: Management and implications for research, 27–29 June 2014, Naarden, The Netherlands. *Neuromuscular Disorders*, *25*(5), 432–442. https://doi.org/10.1016/J.NMD.2015.01.011

Santoro, M., Masciullo, M., Silvestri, G., Novelli, G., & Botta, A. (2017). Myotonic dystrophy type 1: Role of CCG, CTC and CGG interruptions within DMPK alleles in the pathogenesis and molecular diagnosis. *Clinical Genetics*, *92*(4), 355–364. https://doi.org/10.1111/CGE.12954

Santoro, M., Piacentini, R., Masciullo, M., Bianchi, M. L. E., Modoni, A., Podda, M. V., Ricci, E., Silvestri, G., & Grassi, C. (2014). Alternative splicing alterations of Ca2+ handling genes are associated with Ca2+ signal dysregulation in myotonic dystrophy type 1 (DM1) and type 2 (DM2) myotubes. *Neuropathology and Applied Neurobiology*, *40*(4), 464–476. https://doi.org/10.1111/NAN.12076

Savkur, R. S., Philips, A. V., & Cooper, T. A. (2001). Aberrant regulation of insulin receptor alternative splicing is associated with insulin resistance in myotonic dystrophy. *Nature Genetics*, *29*(1), 40–47. https://doi.org/10.1038/NG704

Search for: Other terms: Oleic acid | Card Results | ClinicalTrials.gov. (n.d.). https://clinicaltrials.gov/search?term=oleic%20acid&city=

Seznec, H., Lia-Baldini, A. S., Duros, C., Fouquet, C., Lacroix, C., Hofmann-Radvanyi, H., Junien, C., & Gourdon, G. (2000). Transgenic mice carrying large human genomic sequences with expanded CTG repeat mimic closely the DM CTG repeat intergenerational and somatic instability. *Human*

Molecular Genetics, *9*(8), 1185–1194. https://doi.org/10.1093/HMG/9.8.1185

Shao, F., & Ford, D. A. (2014). Elaidic acid increases hepatic lipogenesis by mediating sterol regulatory element binding protein-1c activity in HuH-7 cells. *Lipids*, *49*(5), 403–413. https://doi.org/10.1007/S11745-014-3883-X

Sharp, L., Cox, D. C., & Cooper, T. A. (2019). Endurance exercise leads to beneficial molecular and physiological effects in a mouse model of myotonic dystrophy type 1. *Muscle & Nerve*, *60*(6), 779–789. https://doi.org/10.1002/mus.26709

Shen, X., Xu, F., Li, M., Wu, S., Zhang, J., Wang, A., Xu, L., Liu, Y., & Zhu, G. (2020). miR-322/-503 rescues myoblast defects in myotonic dystrophy type 1 cell model by targeting CUG repeats. *Cell Death & Disease 2020 11:10*, *11*(10), 1–17. https://doi.org/10.1038/s41419-020-03112-6

Siddall, N. A., McLaughlin, E. A., Marriner, N. L., & Hime, G. R. (2006). The RNA-binding protein Musashi is required intrinsically to maintain stem cell identity. *Proceedings of the National Academy of Sciences of the United States of America*, *103*(22), 8402–8407. https://doi.org/10.1073/PNAS.0600906103

Skoufos, G., Kakoulidis, P., Tastsoglou, S., Zacharopoulou, E., Kotsira, V., Miliotis, M., Mavromati, G., Grigoriadis, D., Zioga, M., Velli, A., Koutou, I., Karagkouni, D., Stavropoulos, S., Kardaras, F. S., Lifousi, A., Vavalou, E., Ovsepian, A., Skoulakis, A., Tasoulis, S. K., … Hatzigeorgiou, A. G. (2024). TarBase-v9.0 extends experimentally supported miRNA–gene interactions to cell-types and virally encoded miRNAs. *Nucleic Acids Research*, *52*(D1), D304–D310. https://doi.org/10.1093/NAR/GKAD1071

Small, E. M., O'Rourke, J. R., Moresi, V., Sutherland, L. B., McAnally, J., Gerard, R. D., Richardson, J. A., & Olson, E. N. (2010). Regulation of PI3-kinase/Akt signaling by muscle-enriched microRNA-486. *Proceedings of the National Academy of Sciences of the United States of America*, *107*(9), 4218–4223. https://doi.org/10.1073/PNAS.1000300107

Smith, C. A., & Gutmann, L. (2016). Myotonic Dystrophy Type 1 Management and Therapeutics. *Curr Treat Options Neurol*, *18*(12), 52. https://doi.org/10.1007/s11940-016-0434-1

Song, H., Yang, R., Zhang, J., Sun, P., Xing, X., Wang, L., Sairijima, T., Hu, Y., Liu, Y., Cheng, H., Zhang, Q., & Li, L. (2023). Oleic acid-induced steatosis model establishment in LMH cells and its effect on lipid metabolism. *Poultry Science*, *102*(1). https://doi.org/10.1016/J.PSJ.2022.102297

Song, K. Y., Guo, X. M., Wang, H. Q., Zhang, L., Huang, S. Y., Huo, Y. C., Zhang, G., Feng, J. Z., Zhang, R. R., Ma, Y., Hu, Q. Z., & Qin, X. Y. (2020). MBNL1 reverses the proliferation defect of skeletal muscle satellite cells in myotonic dystrophy type 1 by inhibiting autophagy via the mTOR pathway. *Cell Death & Disease*, *11*(7). https://doi.org/10.1038/S41419-020-02756-8

Souidi, A., Nakamori, M., Zmojdzian, M., Jagla, T., Renaud, Y., & Jagla, K. (2023). Deregulations of miR-1 and its target Multiplexin promote dilated cardiomyopathy associated with myotonic dystrophy type 1. *EMBO Reports*, *24*(4). https://doi.org/10.15252/EMBR.202256616

Stern-Straeter, J., Bonaterra, G. A., Kassner, S. S., Zügel, S., Hörmann, K., Kinscherf, R., & Goessler, U. R. (2011). Characterization of human myoblast differentiation for tissue-engineering purposes by quantitative gene expression analysis. *Journal of Tissue Engineering and Regenerative Medicine*, *5*(8). https://doi.org/10.1002/TERM.417

Stevenson, J., Huang, E. Y., & Olzmann, J. A. (2016). Endoplasmic Reticulum-Associated Degradation and Lipid Homeostasis. *Annual Review of Nutrition*, *36*, 511–542. https://doi.org/10.1146/ANNUREV-NUTR-071715-051030

Sticht, C., De La Torre, C., Parveen, A., & Gretz, N. (2018). miRWalk: An online resource for prediction of microRNA binding sites. *PLoS ONE*, *13*(10), e0206239. https://doi.org/10.1371/journal.pone.0206239

Stitt, T. N., Drujan, D., Clarke, B. A., Panaro, F., Timofeyva, Y., Kline, W. O., Gonzalez, M., Yancopoulos, G. D., & Glass, D. J. (2004). The IGF-1/PI3K/Akt pathway prevents expression of muscle atrophy-induced ubiquitin ligases by inhibiting FOXO transcription factors. *Molecular Cell*, *14*(3), 395–403. https://doi.org/10.1016/S1097-2765(04)00211-4

Stojanovic, V. R., Peric, S., Lavrnic, D., Popovic, S., Ille, T., Stevic, Z., Basta, I., & Apostolski, S. (2010). Leptin and the metabolic syndrome in patients with myotonic dystrophy type 1. *Acta Neurologica Scandinavica*, *121*(2), 94–98. https://doi.org/10.1111/J.1600-0404.2009.01237.X

Suzuki, H. (1981). Hyperglucagonemia in myotonic dystrophy. *The Journal of Clinical Endocrinology and Metabolism*, *52*(4), 790–795. https://doi.org/10.1210/JCEM-52-4-790

Tahraoui-Bories, J., Mérien, A., González-Barriga, A., Lainé, J., Leteur, C., Polvèche, H., Carteron, A., Lamotte, J. D. D., Nicoleau, C., Polentes, J., Jarrige, M., Gomes-Pereira, M., Ventre, E., Poydenot, P., Furling, D., Schaeffer, L., Legay, C., & Martinat, C. (2023). MBNL-dependent impaired development

within the neuromuscular system in myotonic dystrophy type 1. *Neuropathology and Applied Neurobiology*, *49*(1). https://doi.org/10.1111/NAN.12876

Takada, H. (2018). Lipid Metabolism in Myotonic Dystrophy. *Myotonic Dystrophy: Disease Mechanism, Current Management and Therapeutic Development*, 161–170. https://doi.org/10.1007/978-981-13-0508-5_10

Tan, Y., Jin, Y., Zhao, P., Wu, J., & Ren, Z. (2021). Lipid droplets contribute myogenic differentiation in C2C12 by promoting the remodeling of the acstin-filament. *Cell Death & Disease 2021 12:12*, *12*(12), 1–13. https://doi.org/10.1038/s41419-021-04273-8

Tang, Z. Z., Yarotskyy, V., Wei, L., Sobczak, K., Nakamori, M., Eichinger, K., Moxley, R. T., Dirksen, R. T., & Thornton, C. A. (2012). Muscle weakness in myotonic dystrophy associated with misregulated splicing and altered gating of Ca(V)1.1 calcium channel. *Human Molecular Genetics*, *21*(6), 1312–1324. https://doi.org/10.1093/HMG/DDR568

Taylor, K., Sznajder, L. J., Cywoniuk, P., Thomas, J. D., Swanson, M. S., & Sobczak, K. (2018). MBNL splicing activity depends on RNA binding site structural context. *Nucleic Acids Research*, *46*(17), 9119–9133. https://doi.org/10.1093/NAR/GKY565

Teplova, M., & Patel, D. J. (2008). Structural insights into RNA recognition by the alternative-splicing regulator muscleblind-like MBNL1. *Nature Structural & Molecular Biology*, *15*(12), 1343–1351. https://doi.org/10.1038/NSMB.1519

Thomas, J. D., Oliveira, R., Sznajder, Ł. J., & Swanson, M. S. (2018). Myotonic Dystrophy and Developmental Regulation of RNA Processing. *Comprehensive Physiology*, *8*(2), 509–553. https://doi.org/10.1002/CPHY.C170002

Thornton, C. A. (2014). Myotonic dystrophy. *Neurologic Clinics*, *32*(3), 705–719. https://doi.org/10.1016/J.NCL.2014.04.011

Tian, B., White, R. J., Xia, T., Welle, S., Turner, D. H., Mathews, M. B., & Thornton, C. A. (2000). Expanded CUG repeat RNAs form hairpins that activate the double-stranded RNA-dependent protein kinase PKR. *RNA (New York, N.Y.)*, *6*(1), 79–87. https://doi.org/10.1017/S1355838200991544

Tian, F., Wang, J., Zhang, Z., & Yang, J. (2019). miR-107 modulates chondrocyte proliferation, apoptosis, and extracellular matrix synthesis by targeting PTEN. *International Journal of Clinical and Experimental Pathology*, *12*(2), 488.

Timchenko, L. (2013). Molecular mechanisms of muscle atrophy in myotonic dystrophies. *The International Journal of Biochemistry & Cell Biology*, *45*(10), 2280–2287. https://doi.org/10.1016/J.BIOCEL.2013.06.010

Todd, P. K., Ackall, F. Y., Hur, J., Sharma, K., Paulson, H. L., & Dowling, J. J. (2014). Transcriptional changes and developmental abnormalities in a zebrafish model of myotonic dystrophy type 1. *Disease Models & Mechanisms*, *7*(1), 143–155. https://doi.org/10.1242/DMM.012427

Tung, Y.-T., Hsu, Y.-J., Liao, C.-C., Ho, S.-T., Huang, C.-C., & Huang, W.-C. (2019). Physiological and Biochemical Effects of Intrinsically High and Low Exercise Capacities Through Multiomics Approaches. *Frontiers in Physiology*, *10*, 1201. https://doi.org/10.3389/fphys.2019.01201

Ueki, J., Nakamori, M., Nakamura, M., Nishikawa, M., Yoshida, Y., Tanaka, A., Morizane, A., Kamon, M., Araki, T., Takahashi, M. P., Watanabe, A., Inagaki, N., & Sakurai, H. (2017). Myotonic dystrophy type 1 patient-derived iPSCs for the investigation of CTG repeat instability. *Scientific Reports 2017 7:1*, *7*(1), 1–12. https://doi.org/10.1038/srep42522

Uniewicz, K. A., Ori, A., Xu, R., Ahmed, Y., Wilkinson, M. C., Fernig, D. G., & Yates, E. A. (2010). Differential scanning fluorimetry measurement of protein stability changes upon binding to glycosaminoglycans: A screening test for binding specificity. *Analytical Chemistry*, *82*(9), 3796–3802. https://doi.org/10.1021/AC100188X

Urbańska, K., Stępień, P. W., Nowakowska, K. N., Stefaniak, M., Osial, N., Chorągiewicz, T., Toro, M. D., Nowomiejska, K., & Rejdak, R. (2022). The Role of Dysregulated miRNAs in the Pathogenesis, Diagnosis and Treatment of Age-Related Macular Degeneration. *International Journal of Molecular Sciences*, *23*(14). https://doi.org/10.3390/IJMS23147761

Venneri, M., & Passantino, A. (2023). MiRNA: what clinicians need to know. *European Journal of Internal Medicine*, *113*, 6–9. https://doi.org/10.1016/j.ejim.2023.05.024

Vicente-Crespo, M., Pascual, M., Fernandez-Costa, J. M., Garcia-Lopez, A., Monferrer, L., Miranda, M. E., Zhou, L., & Artero, R. D. (2008). Drosophila muscleblind is involved in troponin T alternative splicing and apoptosis. *PloS One*, *3*(2). https://doi.org/10.1371/JOURNAL.PONE.0001613

Viegas, D., Pereira, C. D., Martins, F., Mateus, T., da Cruz e Silva, O. A. B., Herdeiro, M. T., & Rebelo, S. (2022). Nuclear Envelope Alterations in Myotonic Dystrophy Type 1 Patient-Derived Fibroblasts. *International Journal of Molecular Sciences*, *23*(1), Article 1. https://doi.org/10.3390/ijms23010522

Vignaud, A., Ferry, A., Huguet, A., Baraibar, M., Trollet, C., Hyzewicz, J., Butler-Browne, G., Puymirat, J., Gourdon, G., & Furling, D. (2010). Progressive skeletal muscle weakness in transgenic mice expressing CTG expansions is associated with the activation of the ubiquitin-proteasome pathway. *Neuromuscular Disorders : NMD*, *20*(5), 319–325. https://doi.org/10.1016/J.NMD.2010.03.006

Vihola, A., Bassez, G., Meola, G., Zhang, S., Haapasalo, H., Paetau, A., Mancinelli, E., Rouche, A., Hogrel, J. Y., Laforêt, P., Maisonobe, T., Pellissier, J. F., Krahe, R., Eymard, B., & Udd, B. (2003). Histopathological differences of myotonic dystrophy type 1 (DM1) and PROMM/DM2. *Neurology*, *60*(11), 1854–1857. https://doi.org/10.1212/01.WNL.0000065898.61358.09

Visconti, V. V., Centofanti, F., Fittipaldi, S., Macrì, E., Novelli, G., & Botta, A. (2021). Epigenetics of Myotonic Dystrophies: A Minireview. *International Journal of Molecular Sciences*, *22*(22). https://doi.org/10.3390/IJMS222212594

Visconti, V. V., Macrì, E., D'Apice, M. R., Centofanti, F., Massa, R., Novelli, G., & Botta, A. (2023). In Cis Effect of DMPK Expanded Alleles in Myotonic Dystrophy Type 1 Patients Carrying Variant Repeats at 5' and 3' Ends of the CTG Array. *International Journal of Molecular Sciences*, *24*(12), 10129–10129. https://doi.org/10.3390/IJMS241210129

Vujnic, M., Peric, S., Popovic, S., Raseta, N., Ralic, V., Dobricic, V., Novakovic, I., & Rakocevic-Stojanovic, V. (2015). Metabolic syndrome in patients with myotonic dystrophy type 1. *Muscle & Nerve*, *52*(2), 273–277. https://doi.org/10.1002/MUS.24540

Wang, B., & Tontonoz, P. (2018). Liver X receptors in lipid signalling and membrane homeostasis. *Nature Reviews Endocrinology 2018 14:8*, *14*(8), 452–463. https://doi.org/10.1038/s41574-018-0037-x

Wang, E. T., Treacy, D., Eichinger, K., Struck, A., Estabrook, J., Olafson, H., Wang, T. T., Bhatt, K., Westbrook, T., Sedehizadeh, S., Ward, A., Day, J., Brook, D., Berglund, J. A., Cooper, T., Housman, D., Thornton, C., & Burge, C. (2019). Transcriptome alterations in myotonic dystrophy skeletal muscle and heart. *Human Molecular Genetics*, *28*(8), 1312–1321. https://doi.org/10.1093/HMG/DDY432

Wang, E. T., Ward, A. J., Cherone, J. M., Giudice, J., Wang, T. T., Treacy, D. J., Lambert, N. J., Freese, P., Saxena, T., Cooper, T. A., & Burge, C. B. (2015). Antagonistic regulation of mRNA expression and splicing by CELF and MBNL proteins. *Genome Research*, *25*(6), 858–871. https://doi.org/10.1101/GR.184390.114

Wang, G. S., Kearney, D. L., Biasi, M. D., Taffet, G., & Cooper, T. A. (2007). Elevation of RNA-binding protein CUGBP1 is an early event in an inducible heart-specific mouse model of myotonic dystrophy. *The Journal of Clinical Investigation*, *117*(10), 2802. https://doi.org/10.1172/JCI32308

Wang, G. S., Kuyumcu-Martinez, M. N., Sarma, S., Mathur, N., Wehrens, X. H. T., & Cooper, T. A. (2009). PKC inhibition ameliorates the cardiac phenotype in a mouse model of myotonic dystrophy type 1. *The Journal of Clinical Investigation*, *119*(12), 3797–3806. https://doi.org/10.1172/JCI37976

Wang, P. Y., Lin, Y. M., Wang, L. H., Kuo, T. Y., Cheng, S. J., & Wang, G. S. (2017). Reduced cytoplasmic MBNL1 is an early event in a brain-specific mouse model of myotonic dystrophy. *Human Molecular Genetics*, *26*(12), 2247–2257. https://doi.org/10.1093/HMG/DDX115

Wang, Q., Liu, R., Chang, M., Zhang, H., Jin, Q., & Wang, X. (2022). Dietary oleic acid supplementation and blood inflammatory markers: A systematic review and meta-analysis of randomized controlled trials. *Critical Reviews in Food Science and Nutrition*, *62*(9), 2508–2525. https://doi.org/10.1080/10408398.2020.1854673

Wang, R., Kato, F., Watson, R. Y., Beedle, A. M., Call, J. A., Tsunoda, Y., Noda, T., Tsuchiya, T., Kashima, M., Hattori, A., & Ito, T. (2024). The RNA-binding protein Msi2 regulates autophagy during myogenic differentiation. *Life Science Alliance*, *7*(5). https://doi.org/10.26508/LSA.202302016

Wang, S., Zhu, W., Xu, J., Guo, Y., Yan, J., Meng, L., Jiang, C., & Lu, S. (2019). Interpreting the MicroRNA-15/107 family: Interaction identification by combining network based and experiment supported approach. *BMC Medical Genetics*, *20*(1), 96. https://doi.org/10.1186/s12881-019-0824-9

Wang, Y., Vogel, G., Yu, Z., & Richard, S. (2013). The QKI-5 and QKI-6 RNA Binding Proteins Regulate the Expression of MicroRNA 7 in Glial Cells. *Molecular and Cellular Biology*, *33*(6), 1233–1243. https://doi.org/10.1128/MCB.01604-12

Ward, A. J., Rimer, M., Killian, J. M., Dowling, J. J., & Cooper, T. A. (2010). CUGBP1 overexpression in mouse skeletal muscle reproduces features of myotonic dystrophy type 1. *Human Molecular Genetics*, *19*(18), 3614–3622. https://doi.org/10.1093/HMG/DDQ277

Watanabe, N., Komiya, Y., Sato, Y., Watanabe, Y., Suzuki, T., & Arihara, K. (2020). Oleic acid up-regulates myosin heavy chain (MyHC) 1 expression and increases mitochondrial mass and maximum respiration in C2C12

myoblasts. *Biochemical and Biophysical Research Communications*, *525*(2), 406–411. https://doi.org/10.1016/J.BBRC.2020.02.099

Wei, C., Stock, L., Valanejad, L., Zalewski, Z. A., Karns, R., Puymirat, J., Nelson, D., Witte, D., Woodgett, J., Timchenko, N. A., & Timchenko, L. (2018). Correction of GSK3β at young age prevents muscle pathology in mice with myotonic dystrophy type 1. *FASEB Journal : Official Publication of the Federation of American Societies for Experimental Biology*, *32*(4), 2073–2085. https://doi.org/10.1096/FJ.201700700R

Wei, P., Li, M., Yang, W., & Zhou, X. (2019). Effect of RNA-binding protein MSI2 deficiency on progression in triple-negative breast cancer via stabilizing TP53INP1. *Journal of Clinical Oncology*, *37*(15_suppl), e12555–e12555. https://doi.org/10.1200/JCO.2019.37.15_suppl.e12555

Wheeler, T. M., Lueck, J. D., Swanson, M. S., Dirksen, R. T., & Thornton, C. A. (2007). Correction of ClC-1 splicing eliminates chloride channelopathy and myotonia in mouse models of myotonic dystrophy. *The Journal of Clinical Investigation*, *117*(12), 3952–3957. https://doi.org/10.1172/JCI33355

Wu, H., Sun, S., Tu, K., Gao, Y., Xie, B., Krainer, A. R., & Zhu, J. (2010). A Splicing-Independent Function of SF2/ASF in MicroRNA Processing. *Molecular Cell*, *38*(1), 67–77. https://doi.org/10.1016/j.molcel.2010.02.021

Wu, T., Hornsby, M., Zhu, L., Yu, J. C., Shokat, K. M., & Gestwicki, J. E. (2023). Protocol for performing and optimizing differential scanning fluorimetry experiments. *STAR Protocols*, *4*(4). https://doi.org/10.1016/J.XPRO.2023.102688

Wuebben, E. L., Mallanna, S. K., Cox, J. L., & Rizzino, A. (2012). Musashi2 is required for the self-renewal and pluripotency of embryonic stem cells. *PloS One*, *7*(4). https://doi.org/10.1371/JOURNAL.PONE.0034827

Yablonka-Reuveni, Z., & Nameroff, M. (1990). Temporal differences in desmin expression between myoblasts from embryonic and adult chicken skeletal muscle. *Differentiation; Research in Biological Diversity*, *45*(1), 21. https://doi.org/10.1111/J.1432-0436.1990.TB00452.X

Yadava, R. S., Foff, E. P., Yu, Q., Gladman, J. T., Kim, Y. K., Bhatt, K. S., Thornton, C. A., Zheng, T. S., & Mahadevan, M. S. (2015). TWEAK/Fn14, a pathway and novel therapeutic target in myotonic dystrophy. *Human Molecular Genetics*, *24*(7), 2035–2048. https://doi.org/10.1093/HMG/DDU617

Yadava, R. S., Mandal, M., Giese, J. M., Rigo, F., Bennett, C. F., & Mahadevan, M. S. (2021). Modeling muscle regeneration in RNA toxicity mice. *Human*

Molecular Genetics, *30*(12), 1111–1130. https://doi.org/10.1093/hmg/ddab108

Yadava, R. S., Mandal, M., & Mahadevan, M. S. (2024). Studying the Effect of MBNL1 and MBNL2 Loss in Skeletal Muscle Regeneration. *International Journal of Molecular Sciences*, *25*(5), 2687. https://doi.org/10.3390/ijms25052687

Yadava, R. S., Yu, Q., Mandal, M., Rigo, F., Bennett, C. F., & Mahadevan, M. S. (2020). Systemic therapy in an RNA toxicity mouse model with an antisense oligonucleotide therapy targeting a non-CUG sequence within the DMPK 3 UTR RNA. *Human Molecular Genetics*, *29*(9), 1440–1453. https://doi.org/10.1093/hmg/ddaa060

Yang, W., Yang, L., Wang, J., Zhang, Y., Li, S., Yin, Q., Suo, J., Ma, R., Ye, Y., Cheng, H., Li, J., Hui, J., & Hu, P. (2022). Msi2-mediated MiR7a-1 processing repression promotes myogenesis. *Journal of Cachexia, Sarcopenia and Muscle*, *13*(1), 728–742. https://doi.org/10.1002/jcsm.12882

Yang, Y. P., Liang, Z. Q., Gu, Z. L., & Qin, Z. H. (2005). Molecular mechanism and regulation of autophagy. *Acta Pharmacologica Sinica*, *26*(12), 1421–1434. https://doi.org/10.1111/J.1745-7254.2005.00235.X

Yao, D. W., Luo, J., He, Q. Y., Xu, H. F., Li, J., Shi, H. B., Wang, H., Chen, Z., & Loor, J. J. (2016). Liver X receptor α promotes the synthesis of monounsaturated fatty acids in goat mammary epithelial cells via the control of stearoyl-coenzyme A desaturase 1 in an SREBP-1-dependent manner. *Journal of Dairy Science*, *99*(8), 6391–6402. https://doi.org/10.3168/JDS.2016-10990

Yedigaryan, L., & Sampaolesi, M. (2021). Therapeutic Implications of miRNAs for Muscle-Wasting Conditions. *Cells*, *10*(11). https://doi.org/10.3390/CELLS10113035

Yeh, D. W., Zhao, X., Siddique, H. R., Zheng, M., Choi, H. Y., Machida, T., Narayanan, P., Kou, Y., Punj, V., Tahara, S. M., Feldman, D. E., Chen, L., & Machida, K. (2023). MSI2 promotes translation of multiple IRES-containing oncogenes and virus to induce self-renewal of tumor initiating stem-like cells. *Cell Death Discovery*, *9*(1). https://doi.org/10.1038/S41420-023-01427-9

Yin, Q., Wang, H., Li, N., Ding, Y., Xie, Z., Jin, L., Li, Y., Wang, Q., Liu, X., Xu, L., Li, Q., Ma, Y., Cheng, Y., Wang, K., Zhong, C., Yu, Q., Tang, W., Chen, W., Yang, W., … Li, J. (2020). Dosage effect of multiple genes accounts for multisystem disorder of myotonic dystrophy type 1. *Cell Research*, *30*(2), 133–145. https://doi.org/10.1038/s41422-019-0264-2

Yoshida, T., & Delafontaine, P. (2020). Mechanisms of IGF-1-Mediated Regulation of Skeletal Muscle Hypertrophy and Atrophy. *Cells 2020, Vol. 9, Page 1970*, *9*(9), 1970. https://doi.org/10.3390/CELLS9091970

Yu, M., Wang, H., Xu, Y., Yu, D., Li, D., Liu, X., & Du, W. (2015). Insulin-like growth factor-1 (IGF-1) promotes myoblast proliferation and skeletal muscle growth of embryonic chickens via the PI3K/Akt signalling pathway. *Cell Biology International*, *39*(8), 910–922. https://doi.org/10.1002/CBIN.10466

Yuan, Y., Compton, S. A., Sobczak, K., Stenberg, M. G., Thornton, C. A., Griffith, J. D., & Swanson, M. S. (2007). Muscleblind-like 1 interacts with RNA hairpins in splicing target and pathogenic RNAs. *Nucleic Acids Research*, *35*(16), 5474–5486. https://doi.org/10.1093/NAR/GKM601

Zacharjasz, J., Sztachera, M., Smuszkiewicz, M., & Piwecka, M. (2024). Micromanaging the neuroendocrine system—A review on miR-7 and the other physiologically relevant miRNAs in the hypothalamic-pituitary axis. *FEBS Letters*. https://doi.org/10.1002/1873-3468.14948

Zammit, P. S., & Beauchamp, J. R. (2001). The skeletal muscle satellite cell: Stem cell or son of stem cell? *Differentiation; Research in Biological Diversity*, *68*(4–5), 193–204. https://doi.org/10.1046/J.1432-0436.2001.680407.X

Zhang, G., Chen, X., Lin, L., Wen, C., & Rao, S. (2012). [Effects of fatty acids on proliferation and differentiation of myoblast]. *Wei Sheng Yan Jiu = Journal of Hygiene Research*.

Zhang, H., Kolb, F. A., Jaskiewicz, L., Westhof, E., & Filipowicz, W. (2004). Single processing center models for human Dicer and bacterial RNase III. *Cell*, *118*(1), 57–68. https://doi.org/10.1016/j.cell.2004.06.017

Zhang, H., Tan, S., Wang, J., Chen, S., Quan, J., Xian, J., Zhang, S. S., He, J., & Zhang, L. (2014). Musashi2 modulates K562 leukemic cell proliferation and apoptosis involving the MAPK pathway. *Experimental Cell Research*, *320*(1), 119–127. https://doi.org/10.1016/j.yexcr.2013.09.009

Zhang, S., & Chen, N. (2018). Regulatory Role of MicroRNAs in Muscle Atrophy during Exercise Intervention. *International Journal of Molecular Sciences*, *19*(2). https://doi.org/10.3390/IJMS19020405

Zhong, B.-H., Ma, Y.-T., Sun, J., Tang, J.-T., & Dong, M. (2024). Transcription factor FOXF2 promotes the development and progression of pancreatic cancer by targeting MSI2. *Oncology Reports*, *52*(1), 93. https://doi.org/10.3892/OR.2024.8752

Zhou, L., Sheng, W., Jia, C., Shi, X., Cao, R., Wang, G., Lin, Y., Zhu, F., Dong, Q., & Dong, M. (2020). Musashi2 promotes the progression of pancreatic cancer through a novel ISYNA1-p21/ZEB-1 pathway. *Journal of Cellular and Molecular Medicine*, *24*(18), 10560–10572. https://doi.org/10.1111/jcmm.15676